uOttawa

L'Université canadienne
Canada's university

FACULTÉ DES ÉTUDES SUPÉRIEURES ET POSTOCTORALES

u Ottawa

L'Université canadienne
Canada's university

FACULTY OF GRADUATE AND POSDOCTORAL STUDIES

Suhuai Liu
AUTEUR DE LA THÈSE / AUTHOR OF THESIS

Ph.D. (Chemistry)
GRADE / DEGREE

Department of Chemistry
FACULTÉ, ÉCOLE, DÉPARTEMENT / FACULTY, SCHOOL, DEPARTMENT

Novel *C*-Linked Antifreeze Glycoprotein (AFGP) Analogues as Potent Recrystallization Inhibitors: Preparation, Assessment and *In Vitro* Studies

TITRE DE LA THÈSE / TITLE OF THESIS

Robert Ben
DIRECTEUR (DIRECTRICE) DE LA THÈSE / THESIS SUPERVISOR

CO-DIRECTEUR (CO-DIRECTRICE) DE LA THÈSE / THESIS CO-SUPERVISOR

EXAMINATEURS (EXAMINATRICES) DE LA THÈSE / THESIS EXAMINERS

France-Isabelle Auzanneau

André Beauchemin

William Ogilvie

William Willmore

Gary W. Slater
LE DOYEN DE LA FACULTÉ DES ÉTUDES SUPÉRIEURES ET POSTDOCTORALES /
DEAN OF THE FACULTY OF GRADUATE AND POSTDOCORAL STUDIES

Novel *C*-Linked Antifreeze Glycoprotein (AFGP) Analogues as Potent Recrystallization Inhibitors: Preparation, Assessment and *In Vitro* Studies

Suhuai Liu

Thesis submitted to the
Faculty of Graduate & Postdoctoral Studies
University of Ottawa
in partial fulfillment of the requirements for the
Ph.D. degree in the
Ottawa-Carleton Chemistry Institute

Candidate	Supervisor
Suhuai Liu	Professor Robert N. Ben

Your file Votre référence
ISBN: 978-0-494-18593-3
Our file Notre référence
ISBN: 978-0-494-18593-3

ABSTRACT

Antifreeze glycoproteins (AFGPs) are a subclass of biological antifreezes found primarily in the plasma of Teleost fish inhabiting in sub-zero temperature environments. These compounds have the ability to inhibit the growth and recrystallization of ice, thus ensuring the survival of these organisms in subzero environments. This characteristic property is highly desirable for medical and commercial applications. However, the limited bioavailability and the inherent instability of native AFGPs have precluded their commercialization. Consequently, rationally designed *C*-linked AFGP analogues are very attractive. This work describes the preparation of stable *C*-linked AFGP analogues and the evaluation of their antifreeze-specific activities. The *in vitro* behaviors of AFGP8 and *C*-linked AFGP analogues are also described.

A new series of *C*-linked AFGP analogues was prepared to evaluate the functions of the length and rigidity of the side chain between the carbohydrate moiety and the polypeptide backbone, the acetamide group in the galactosamine residue, and the polypeptide backbone. *C*-linked AFGP analogues containing three and four methylene groups in the side chain were prepared using an olefin cross-metathesis (OCM) method. *C*-linked AFGP analogues containing a *C*-glycosylated L-serine residue were prepared using a catalytic asymmetric hydrogenation (CAH) strategy. A neoglycopolymer with the polymeric chain composed of alternating ethylene groups and cyclopentane rings was prepared using the ring-opening metathesis polymerization (ROMP).

The new series of *C*-linked AFGP analogues was evaluated for their antifreeze-specific activities, including thermal hysteresis (TH) and recrystallization inhibition (RI). Although no TH activity was displayed in any analogues, some analogues demonstrated potent RI activity. These examples with tailored RI and TH activities suggest that it is possible to design AFGP analogues for different applications.

The behaviors of AFGP8 and two *C*-linked AFGP analogues with potent RI activity were studied *in vitro*. High concentration AFGP8 demonstrated significant toxic effects to human liver and kidney cells at both physiological and cryogenic temperatures. In contrast, *C*-linked AFGP analogues did not show any cytotoxicity in human cell lines under the same conditions. A caspase-3/7 assay and an independent fluorescence apoptosis assay verified that the cytotoxicity

caused by AFGP8 was due to the induction of apoptosis, while *C*-linked AFGP analogues could inhibit the activation of caspase 3 and 7. In addition, an internalization study demonstrated that both AFGP8 and the *C*-linked AFGP analogues shared the same cellular uptake mode and intracellular pathway.

The cytotoxicity of AFGP8 may limit its applications in the biological systems. In contrast, our *C*-linked AFGP analogues are not cytotoxic and can inhibit the activation of caspase 3 and 7. In addition, since they have no TH activity, no detrimental ice spicules will be formed. Therefore, these *C*-linked AFGP analogues have an advantage for being used as cryoprotectants for cell preservation.

ACKNOWLEDGEMENTS

There are many people who I would like to thank for their help during my graduate study. First I would like to thank my supervisor, Professor Robert Ben for his support during the last five years. His insightful ideas, broad knowledge and enthusiasm in science deeply impress me. I also appreciate all the encouragement and friendship from him.

I would also like to thank the defense committee members, Dr. France-Isabelle Auzanneau, Dr. William Willmore, Dr. André Beauchemin and Dr. William Ogilvie for providing me with suggestions for the improvement of my thesis. Next, I would like to thank all the past and current members in Dr. Ben's group: Dr. Wenjun Wang for showing me how to perform cell culture and the biological work; Ms. Jessica Jackman, a very talent undergraduate student, for helping me with the cytotoxicity study; Ms. Nicole LeGrand, Mr. Gianni Lorello and Ms. Hajra Khan, another three undergraduate students, whom I had the pleasure to work with during this study; Dr. Madhusudhan Purushotham, Dr. Nobert Owino and Dr. Anastasia Murphy for all the discussion and help; Mr. Frank Cease, Mr. Vincent Bouvet, Ms. Elisabeth von Moos, Ms, Indira Thapa, Mr. Paul Czechura and Mr. Roger Tam for the good time spending together with me in the laboratory. I also want to specially thank for Ms. Jennifer Chaytor and Ms. Alexandra Plagia for spending time on helping me to correct my thesis.

Many people from different labs in the Department of Chemistry and Biology also helped me during this work. I would like to thank Mr. Jay Conrad and Prof. Fogg for helping me to prepare the Grubbs' catalyst; Prof. Sayari, Prof. Goto, Prof. Moon and Prof. Martin for letting me use their facilities. I would also like to thank the people working in the NMR and MS facilities. Especially, I would like to thank Dr. Robert Monette at NRC Canada for his help with the confocal microscopy study.

Many institutions including American Chemistry Society, National Institutes of Health, NSERC, Canada Research Chair Program and A/F Protein Inc. supported this work financially. I would also like to thank University of Ottawa and Binghamton University (S. U. N. Y.) for providing me with scholarships during my graduate study.

Most of all, I would like to thank my parents for always believing in me. Their love, support and encouragement are very important for me to complete this study.

TABLE OF CONTENTS

LIST OF FIGURES

LIST OF SCHEMES

LIST OF TABLES

LIST OF ABBREVIATIONS

Ac	Acetyl
AFP(s)	Antifreeze protein(s)
AFGP(s)	Antifreeze glycoprotein(s)
Apaf-1	Apoptotic-protease activating factor 1
Asn	Asparagine
br	broad
Bn	Benzyl
Boc	*tert*-Butyloxycabonyl
Bz	Benzoyl
CAH	Catalytic asymmetric hydrogenation
Caspases	Cysteine-type aspartic acid-specific proteases
Cbz	benzyloxycarbonyl
CD	Circular dichroism
CIDOCD	Cryopreservation-induced delayed-onset cell death
d	doublet
DAST	Diethylaminosulfurtrifluoride
DCC	Dicyclohexylcarbodiimide
dd	doublet of doublets
DEAD	Diethylazodicarboxylate
DEVD	L-aspartyl-L-glutamyl-L-valyl-L-aspartyl
DIPEA	Diisopropylethylamine
DIS	Dynamic ice-shaping
DISC	Death-inducing signaling complex
DMAP	4-Dimethylamino pyridine
DMF	*N*,*N*-Dimethyl formamide
DMSO	Dimethyl sulfoxide
DPPA	Diphenylphosphorylazide
dt	doublet of triplets
FADD	Fas-associated death domain

Fmoc	9-Fluorenylmethoxycarbonyl
Fmoc-OSu	Fmoc-succinimide
GalNAc	*N*-Acetyl-galactosamine
HBTU	2-(1H-Benzotriazole-1-yl)-1,1,3,3-tetramethyluronium hexafluorophosphate
HOBt	*N*-Hydroxybenzotriazole
Hz	Hertz
kDa	kiloDalton
m	multiplet
M^+	Parent molecular ion
MALDI	Matrix-assisted laser desorption ionization
Me	Methyl
MEM	Minimum essential media
MLGS	Mean largest grain size
mOsmol	milliOsmolars
MS	Mass spectrometry
MTT	Methylthiazolydiphenyl-tetrazolium bromide
NHC	*N*-Heterocyclic carbene
NIS	*N*-Iodosuccinimide
OCM	Olefin cross-metathesis
OD	Optical density
PBS	Phosphate-buffered saline
PCC	Pyridinium chlorochromate
Pd/C	Palladium on carbon
Pfp	Pentaflourophenyl
PI	Propidium iodide
PPII	Polyproline type II
ppm	parts per million
PS	Polystyrene
PTSA	*p*-toluenesulphonic acid
PVP	Polyvinylpyrrolidone

RI	Recrystallization inhibition
ROMP	Ring-opening metathesis polymerization
s	singlet
SEM	Standard error of the mean
SPPS	Solid-phase peptide synthesis
SAR	Structure-activity relationship
t	triplet
TBDMS	*tert*-Butyldimethylsilyl
Tf	trifluoromethanesulfonyl
TFA	Trifluoroacetic acid
TH	Thermal hysteresis
Thr	Threonine
TMG	Tetramethylguanidine
TMSOTf	Trimethylsilyltrifluoromethane sulphonate
TMU	1,1,3,3-Tetramethylurea
TNBS	2,4,6-Trinitrobenzenesulfonic acid
UW solution	University of Wisconsin solution

Chapter 1 Introduction to Biological Antifreezes

1.1 Classification of Biological Antifreezes

Biological antifreezes are protein-based compounds that are found in a wide range of organisms. The physiological significance of these compounds is to ensure survival in a supercooled environment. The first biological antifreezes to be isolated were antifreeze glycoproteins (AFGPs) from Antarctic Notothenioids by DeVries and Wohlschlag in 1969.[1] Since this time, several other types of antifreeze compounds have been discovered in different species of polar and near polar fish,[2] invertebrates (insects[3] and arthropods[4]), plants,[5] fungi and bacteria.[6] Up to now, the most thoroughly studied antifreezes are those isolated from Teleost fish living in both Antarctic and Arctic regions.

The average temperature of seawater where these Teleost fish are found is around -1.9 °C. This decreased freezing point arises due to the colligative freezing point depression of osmotically active solutes dissolved in seawater (approximately 1000 milliosmolar or mOsM, concentration of osmolytes). Fish living in this environment are hyposmotic to seawater and the osmolytes (such as sodium chloride, urea, and free amino acids) present in their bodies only account for a 0.8 °C freezing point depression. Biological antifreezes afford additional freezing point depression to Teleost fish extending their freezing point to about -2.0 to -2.1 °C. The mechanism by which this occurs is different than a colligatively acting substance. The average concentration of biological antifreezes in Teleost fish is about 30 mg/mL.[7] However, their colligative osmotic concentration is very low due to their high molecular mass (2.6-33 kDa) and can only result about 0.002 °C freezing point depression according to the colligative property alone. The efficiency of biological antifreezes is due to their unique ability to inhibit the growth of ice crystals by changing their shape and growing mode.

Figure 1.1 shows the freezing points of the solutions of sodium chloride, biological antifreeze (AFGP3-5), a small carbohydrate (galactose, structural components of AFGPs) and a protein, lysozyme.[2a] At low concentrations, AFGPs are slightly more effective than sodium chloride in decreasing the freezing point of water. However, AFGPs are about 500 times more active than sodium chloride when considered on a molal basis. The addition of sodium chloride to an AFGP

solution shows a strictly additive effect on the freezing point depression, which implies that the small osmolyte has no interaction with AFGP. Since AFGPs are composed of carbohydrates and proteins, the freezing point depression ability of galactose and a regular protein, lysozyme, was studied and compared to that of AFGPs. Both compounds showed very limited activity verifying that AFGPs' potent freezing point depression ability comes from their distinct structural features rather than the sugar, peptide moieties or their high molecular weight.

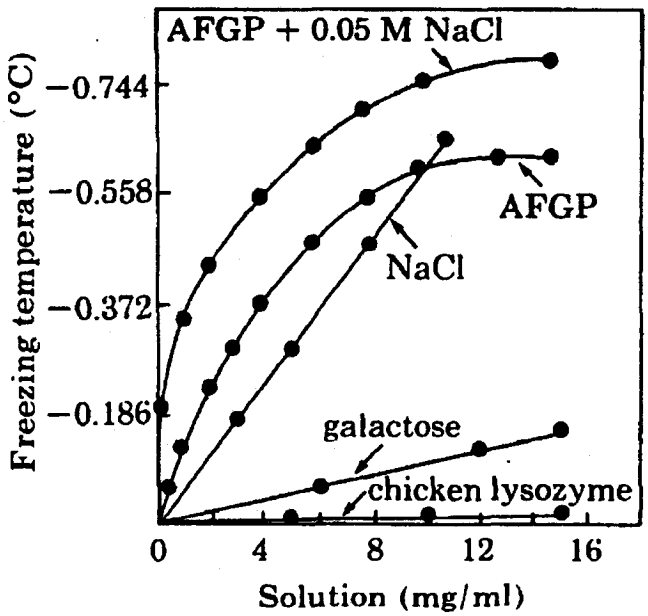

Figure 1.1 Freezing temperatures of solutions of sodium chloride, galactose, lysozyme (14.5 kDa), a mixture of AFGP3-5 and mixtures of AFGP3-5 with sodium chloride.[2a]

1.1.1 Antifreeze Proteins (AFPs)

Based on the structural difference, biological antifreezes are classified into two major categories: antifreeze proteins (AFPs, without saccharides) and antifreeze glycoproteins (AFGPs, with saccharides).[8]

Table 1.1 Structural features and natural resources of AFPs.[8]

Category	Type I AFP	Type II AFP	Type III AFP	Type IV AFP
Key properties	Single α-helix, L-alanine rich	Globular with 5 disulfide bonds	Globular protein with flat surface, 8 β strands	Helical bundle
Conformation				
Molecular mass (kDa)	3.3-4.5	11-24	6.5	12
Natural resources	Right-eyed flounders; sculpins	Rainbow smelt; sea raven; herring	Wolfish; ocean pout; eel pout	Longhorn sculpin

AFPs are short proteins with diverse structures differing in their primary amino acid sequence, as well as secondary and tertiary structures. Based on their structural features, AFPs are further classified into four types (Table 1.1). Type I AFP is an L-alanine rich (>50%) protein with a near perfect single α helix structure.[9] This protein (3.3-4.5 kDa) molecular mass is the most thoroughly studied AFP. AFP I has three 11 amino acid repeating units, each ending with a L-threonine residue. This allows AFP I to form a hydrophilic face with L-threonine hydroxyl groups aligned along one side of helix. This structure is combined with the hydrophobic face formed by the nonpolar L-alanine residues gives AFP I molecule an overall amphipathic structure.[10]

Type II AFP is a globular protein with mixtures of α helix, β sheets and random coil structures. This 11-24 kDa AFP is mainly composed of L-alanine but also contains an increased ratio of L-cysteines which form 5 disulfide bonds.[11]

Type III AFP is a "flat-faced" globular protein with about 6.5 kDa molecular mass. There is no specific amino acid dominant in its primary structural composition. An NMR study of AFP III from ocean pout indicated that there are 8 β strands with two sheets of three antiparallel strands

and one sheet of two antiparallel strands. The two triple-stranded sheets are arranged orthogonally to each other to form a "β sandwich" structure.[12]

Type IV AFP is a class of newly discovered L-alanine rich AFP with a molecular mass of 12 kDa. It is believed to possess a helical bundle structure.[13]

1.1.2 Antifreeze Glycoproteins (AFGPs)

AFGPs are the second class of biological antifreezes. Compared to the diverse structure of AFPs, AFGPs share a great deal of structural homology among Teleost fish species. The general structure of AFGPs is composed of a tripeptide repeating unit of L-threonine-L-alanine-L-alanine with a β-D-galactopyranosyl-(1,3)-2-acetamido-2-deoxy-α-D-galactopyranose disaccharide unit glycosylated on the β-OH group of each L-threonine (Figure 1.2 A). Based on their molecular mass, AFGPs are classified into eight categories: AFGP1-8. AFGP1 is the longest AFGPs with about 33.7 kDa molecular mass while AFGP8 is the shortest with 2.6 kDa.[1b] Because low molecular mass AFGP8 is the easiest to prepare, most of the synthesized AFGP analogues reported are analogues of AFGP8. High molecular mass AFGP1-5 are more effective in lowering the freezing point of solution than low molecular mass AFGP8. For example, AFGP8 only shows 20% activity compared to the same weight of AFGP1-5, which is only about 5% activity if it is considered on the basis of molar concentrations.[14]

In addition to the size difference, structural variations exist in AFGPs. It has been found that the first L-alanine following the L-threonine can occasionally be substituted by L-proline in some short AFGPs such as AFGP6-8 (Figure 1.2 B).[15] It has also been reported that the L-threonine can be replaced by L-arginine in some polar fish species such as Arctic cods (Figure 1.2 C).[16] It worth mentioning that Teleost AFGPs always exist as mixtures of different isoforms, especially in short AFGP6-8 which can contain homologous glycoproteins with different numbers of L-prolines located in different sequences.[17]

Table 1.2 Classification of antifreeze glycoproteins based on molecular mass.

Category	Molecular mass (kDa)
AFGP1-2	33.7 – 28.8
AFGP3-5	21.5 – 10.5
AFGP6-7	5-3.8
AFGP8	2.6

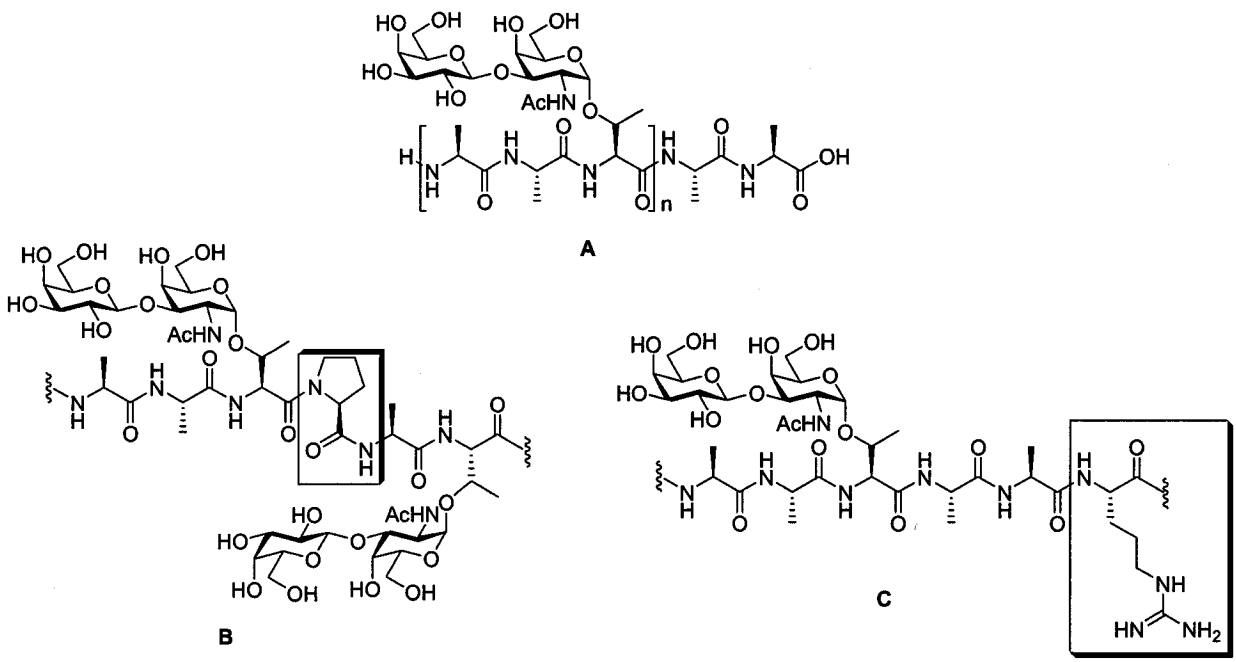

Figure 1.2 Structures of antifreeze glycoproteins found in Teleost fish. **A**: Most common structure of AFGPs, n=4-55; **B**: Structure of AFGPs with L-proline replacing the first L-alanine after L-threonine; **C**: Structure of AFGPs with L-arginine replacing L-threonine.[8]

Previous studies indicated that AFGPs are in the form of left-handed extended 3-fold helices,[18] which is similar to poly-L-proline type II of helical conformation.[19] The hydrophilic disaccharide moieties align on same side of the molecule and the hydrophobic L-alanine methyl groups and acetyl methyl groups in galactosamine align on another side to form an amphipathic structure.[20] However, there were also evidences showing that the conformation of AFGPs in solution phase

was more likely made up of random coil and unfolded structure.[1b, 21] The secondary structure of AFGP has not been fully determined and is still the subject of debate.

1.2 Antifreeze Activity

1.2.1 Thermal Hysteresis (TH)

Thermal hysteresis is the fingerprint property of biological antifreezes and serves as a quantitative indicator for the effectiveness of freezing point depression. Figure 1.3 is a qualitative illustration of the formation of thermal hysteresis. Both the melting and freezing points of pure water are equal to 0 °C. In solutions of some osmolytes such as sodium chloride or glycerol, both melting and freezing points are equally depressed below 0 °C and this is purely a colligative phenomenon. As for biological antifreezes, even the shortest AFGP8 (2600 Dalton) can only exhibit a very small equilibrium freezing point depression due to colligative properties. The colligative freezing point depression of biological antifreeze solution is about 50-500 times less effective compared to the same weight of small osmolyte sodium chloride solution. However, biological antifreezes can depress the freezing point of water in a non-colligative manner without affecting the melting point. This separation between the non-equilibrium freezing point and the equilibrium melting point is referred to as thermal hysteresis. Different from conventional definition, the freezing point of biological antifreeze solution is measured at the temperature when ice starts to grow from a seed ice crystal.

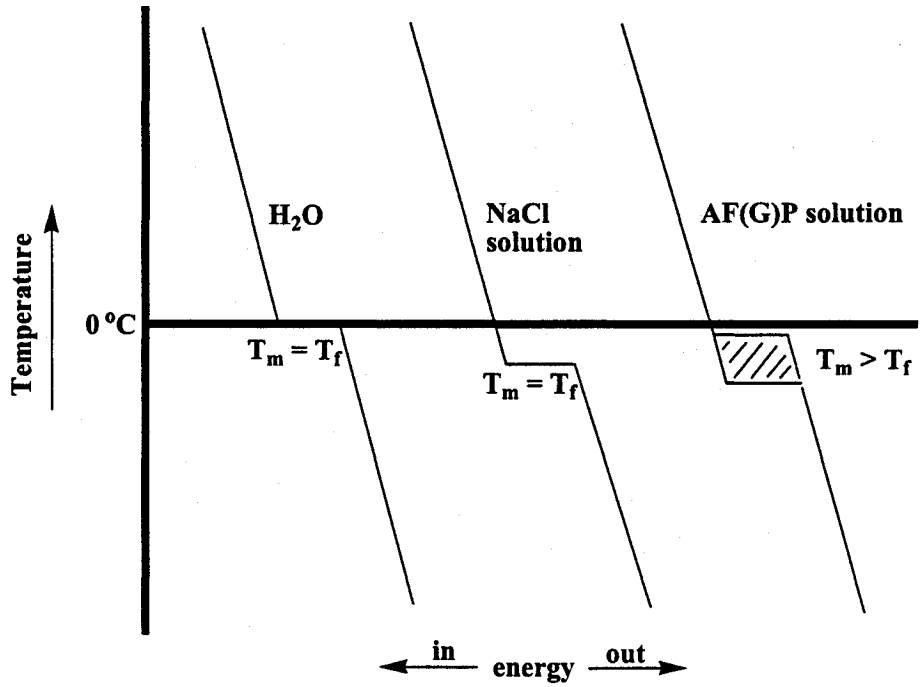

Figure 1.3 Qualitative illustration of thermal hysteresis.

At high concentration of AFGPs, TH activity becomes hyperbolic and eventually forms a plateau when the solution of biological antifreeze saturates. The most saturated AFP solution shows the highest thermal hysteresis about 5-6 °C.[22] The relative efficiency between AFPs and AFGPs were also studied by comparing thermal hysteresis abilities.[23] Type I AFP shows higher activity than AFGPs with similar molecular weight. However, high molecular mass (>10 kDa) AFGPs show higher TH activity than all AFPs.[8]

1.2.2 Dynamic Ice-Shaping

The thermal hysteresis observed in biological antifreeze solution is always accompanied with a modulation of ice crystal morphology to form different shapes. In the case of AFGPs, this is a hexagonal bipyramidal structure at temperatures within the thermal hysteresis gap (Figure 1.4). Under different conditions, ice can exist in polymorphic forms. The most stable form of ice at 1 atm below 0 °C is "Ice I".[8] In pure water, ice crystals grow along a-axes which are parallel to the basal plane; in the solution of biological antifreezes, ice crystal usually grows along c-axis which

is perpendicular to the basal plane. Knight and co-workers used an ice hemisphere etching technique to study the interaction between antifreeze molecules and ice lattices and found that biological antifreeze molecules can selectively bind to specific planes and stop the ice from growing in this direction.[24] Different types of biological antifreezes can bind to different planes of ice crystal as long as the binding sites on the ice plane can match with the binding moieties in antifreeze molecules. In most cases, antifreeze molecules bind to the prism or the second prism plane (such as the pyramidal plane) and cause the seed ice crystal growth to only occur in the basal plane. Binding antifreezes to any non-basal plane of ice seed crystal is sufficient to inhibit its growth and form the hexagonal bipyramidal structure.

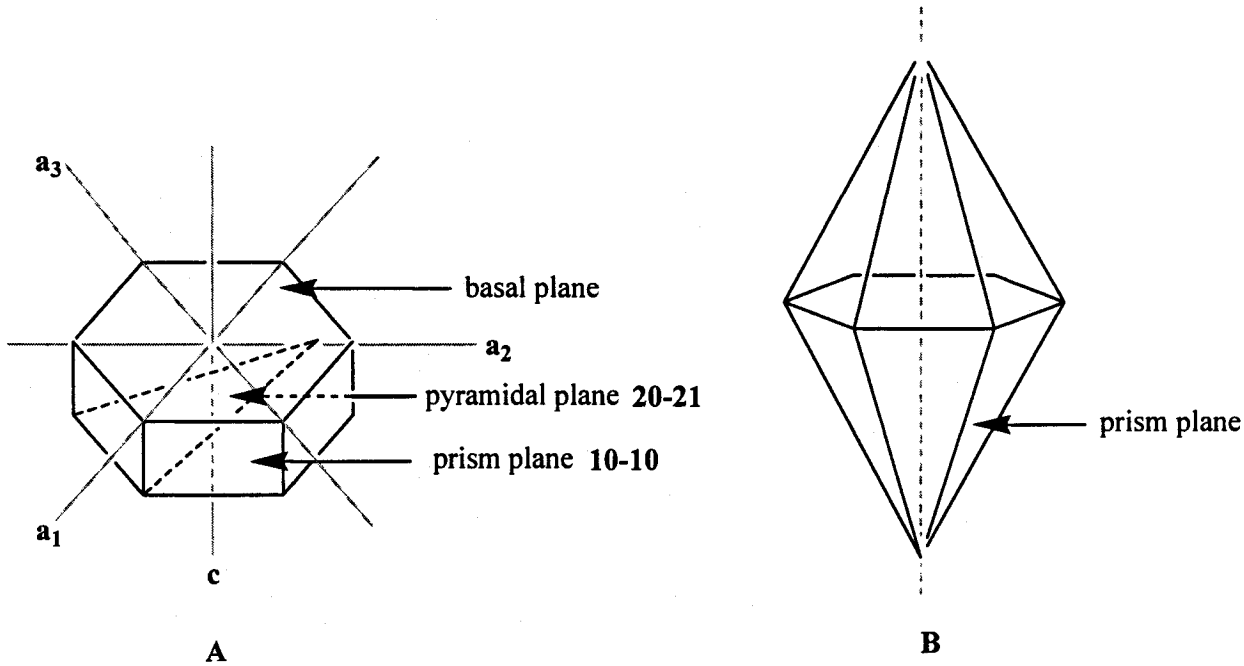

Figure 1.4 Effects of biological antifreezes on modulating the shape of embryonic ice I crystal.

A: hexagonal ice crystal; **B**: hexagonal bipyramidal ice crystal.

At temperatures within the thermal hysteresis gap, biological antifreeze inhibits the growth of seed crystals and changes morphology of the seed crystals to hexagonal bipyramidal (Figure 1.5 A). When the temperature is further decreased to below the TH gap, the seed ice crystals can grow suddenly and swiftly to form a needle-shaped structure (Figure 1.5 B) which cause physical

deformation to cell membranes.[25] Both the needle shape of ice crystals and their rapid growth rate cause most of the cell damage.

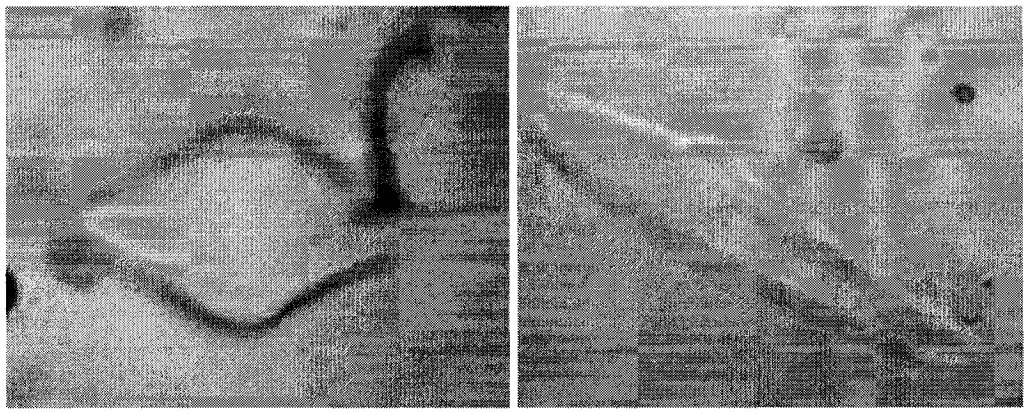

A B

Figure 1.5 Ice crystal growth pattern in AFGP8 solution. **A**: hexagonal bipyramidal ice crystal at temperatures within TH; **B**: needle-shaped ice crystal at temperatures below TH.

1.2.3 Recrystallization Inhibition (RI) of Ice Crystals

Thermal hysteresis is the ability of biological antifreezes to protect Teleost fish from cryoinjury by inhibiting the uncontrolled growth of ice crystals in their body fluid and blood. However, when ice crystals are actually present in the fish body, biological antifreezes still show a protective effect to Teleost fish through a different function, inhibiting ice recrystallization to prevent the formation of large ice crystals (Figure 1.6). Since large ice crystals can cause much more mechanical damage to cell membranes, this recrystallization inhibition ability of biological antifreezes is very important for Teleost fish to survive following partial freezing.[26]

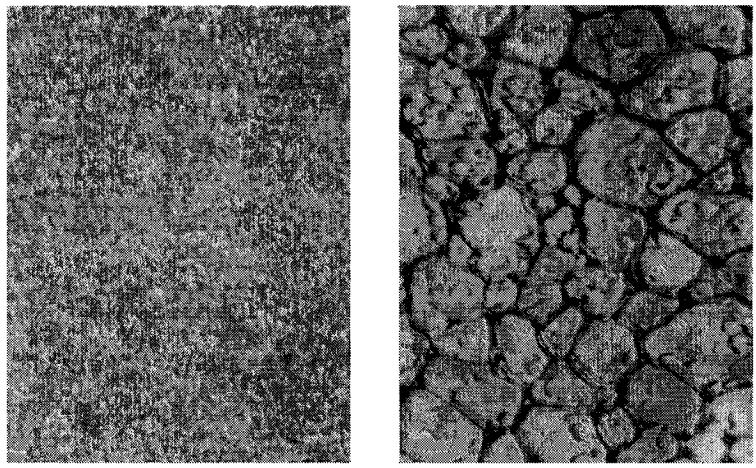

A B

Figure 1.6 Recrystallization inhibition ability of AFGP8 to prevent the formation of large ice crystals. **A**: 10 mg/mL AFGP8 in phosphate-buffered saline (PBS) solution; **B**: PBS solution. (Both pictures with same magnification)

Ice recrystallization occurs during freezing and thawing cycles of a sample and becomes fastest at temperatures slightly below the freezing point. Small ice grains tend to be gradually incorporated (or absorbed) by larger ice grains resulting in a smaller overall number of ice grains. This is a spontaneous process as the overall grain boundary energy decreases. Biological antifreezes have the ability to inhibit ice recrystallization by binding to the ice grain boundary at the ice/water interface and preventing the migration of this solid/liquid interface.[27] It has been reported that the minimum concentration of biological antifreeze showing effective RI activity can be as low as 10^{-12} M,[24c, 28] which is substantially lower than effective TH concentrations. Similarly, it has been demonstrated that thermal hysteresis and recrystallization inhibition are not coupled effects for biological antifreezes.[5b, 29]

Some peptides, which have no TH activity, can inhibit ice recrystallization by simply inhibiting the mobility of the solid/liquid boundary in pure water but show no RI ability when inorganic salts exist in the system.[26] Their recrystallization inhibition ability displayed in water is dependent on and proportional to their concentrations, which is known as the non-specific RI effect.[26, 30] Upon freezing, there is no or very little liquid present and the distribution of these peptides are limited in the grain boundary area and act as barriers for grain boundary migration.

However, the presence of inorganic salts in the system can cause liquid inclusion,[26] which will keep these peptides in solution and show no recrystallization inhibition.

In Summary, thermal hysteresis, dynamic ice-shaping and recrystallization inhibition are the most characteristic properties of biological antifreezes. Thermal hysteresis is usually accompanied by dynamic ice-shaping and can protect organisms by inhibiting the uncontrolled growth of ice crystals at hypothermic temperatures. On the other hand, recrystallization inhibition can help organisms to survive partial frozen by preventing the formation of harmful large ice crystals.

1.3 Mechanism of Action

1.3.1 General Mechanism

The mechanism of antifreeze-specific property at the macroscopic level is an adsorption-inhibition process (Figure 1.7).[24b, 31] It has been found that biological antifreeze molecules can tightly bind to the ice growing surface. Additional water molecules cannot be added to the ice surface which has been attached with antifreeze molecules. Therefore, ice only grows between these areas resulting in a highly curved ice growth front. Since the water-ice interfacial energy is inversely proportional to the sphere radius,[2b] this curved ice surface is not favorable for ice to increase in size. Ice growth therefore stops unless the temperature is further depressed. This localized (high curvature of ice growth front) freezing point depression is also known as Kelvin effect.[32]

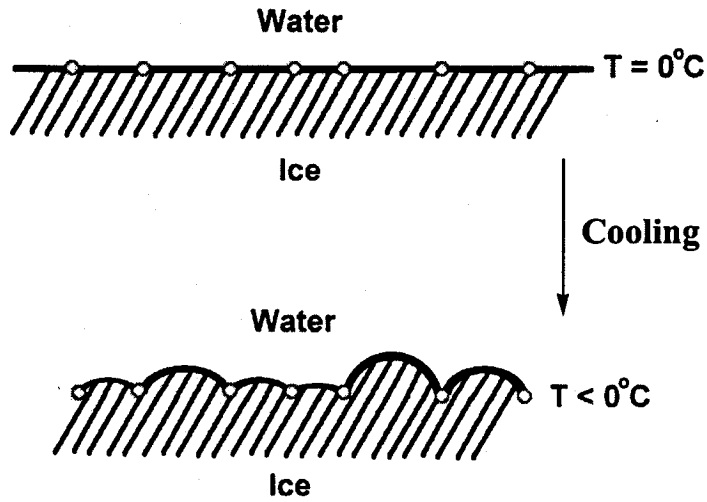

Figure 1.7 Adsorption of biological antifreezes leads to inhibit ice crystal growth.

The detailed binding mechanism between biological antifreezes and the ice lattice is not clear. Knight and DeVries proposed that the binding of antifreezes to the ice surface is irreversible.[24b] This is based on the assumption that multiple numbers of hydrogen bonds form between the antifreezes and ice lattice, and the possibility that all hydrogen bonds are released simultaneously is very low.[33] Subsequent studies show evidence that contradict the irreversible binding hypothesis.[34] In addition, a concentration dependent mechanism was proposed by Wen and Laursen to explain the controversial reports. At low concentrations, the binding of biological antifreezes to ice is reversible. At high concentrations, antifreeze molecules can tightly pack together through efficient van der Waals contact between the hydrophobic moieties. This cooperative interaction between antifreeze molecules makes their binding with ice lattice more effective and difficult to diffuse.[34b]

At the molecular level, the role of hydrophobic and hydrophilic interactions in the binding of biological antifreezes with ice lattices is also in debate. The hydrophilic effect involves hydrogen bonding between the polar hydroxyl groups on biological antifreezes and periodic water molecules in ice crystal lattice.[33, 35] Although the existence of diverse structural features of biological antifreezes cannot exclude the possibility that all antifreezes adopt a similar overall

three-dimensional conformation to interact with ice crystals, it has been found that different types of antifreezes can bind to different ice planes.[24a] For example, AFGPs isolated from Notothenioids were found to bind to the prism plane {10-10} of ice crystals and type I AFP isolated from Winter flounder can bind to the pyramidal plane {20-21}(Figure 1.4).[24a] It is easy to understand this difference if considering the structural differences between AFGPs and type I AFP. The hydrogen bonding moiety in AFGPs is a hydroxyl group on the disaccharide which attaches to every L-threonine of L-threonine-L-alanine-L-alanine tripeptide repeating unit. In type I AFP, the hydrogen bonding site is the hydroxyl group of L-threonine in every eleven amino acid repeat. The length of the periodic binding units in AFGPs and type I AFP have a good lattice match with ice crystal's prism and pyramidal planes, respectively.[24a]

Recently, the hydrophobic effect involved in explaining the binding mechanism of biological antifreezes to the ice/water interface has received a lot of attention. The β-methyl groups on L-threonine residues have been proven to be an important structure for type I AFP to interact with ice lattice via hydrophobic effects.[10,36] The methyl groups on L-alanine residues and the *N*-acetyl methyl groups on galactosamine residues in AFGPs are found to form the hydrophobic phase of the amphipathic conformation, which is crucial for their antifreeze-specific activity.[20]

1.3.2 Structure-Activity Relationship Studies of AFPs

Type I AFP has a near perfect single α-helix structure. The relatively simple structure has made it the most thoroughly studied AFP. Originally, type I AFP was considered to bind to the ice lattice through its periodic spaced polar L-threonine side chain through hydrogen bonding.[9a, 24a] Later studies show more evidence that hydrophobic interactions are more important for its binding with the ice lattice.[10, 36] A structure-activity relationship study of type I AFP from Winter flounder and its analogues shows that the β-methyl groups in L-threonine residues are necessary for activity.[10] Haymet and co-workers used site-directed mutagenesis to vary the four hypothesized hydrogen bonding sites in this AFP from L-threonine to L-serine and the resulting analogue showed no detected thermal hysteresis and no interaction with ice lattices using an ice hemisphere test. Replacing L-threonine with L-serine is not likely to change the α-helical conformation of the original AFP, and L-serine still has hydrogen bonding hydroxyl groups to

bind to the ice/water interface. However, replacing some or all L-threonine residues with L-valine shows no change in the ability to inhibit ice growth. This supports that the β-methyl in L-threonine is more important than the hydroxyl group for antifreeze activity. The hydrophobic phase comprised of the β-methyl groups is more likely to interact with the ice/water interface instead of the hydrophilic phase of the polar β-hydroxyl groups on L-threonines.

Another well-studied AFP is type III AFP. Yang and co-workers[37] determined the structure of a type III AFP isolated from the ocean pout using high resolution X-ray crystallography. The surface planarity was analyzed using an automated algorithm and the ice-binding surface of this globular protein was identified. 67% of the surface is non-polar solvent-accessible surface area. The conformation of type III AFP prohibits the tight packing of polar side chains on the observed ice-binding surface.[2c] The authors predicted that a flat surface is required for AFP binding with ice lattices and the driving force for this binding is van der waals surface complementarity instead of hydrogen bonding. Currently, no detailed mechanism has been reported to explain the binding of type II and type IV AFP to ice lattices due to our limited knowledge of their structure.

1.3.3 Structure-Activity Relationship Studies of AFGPs

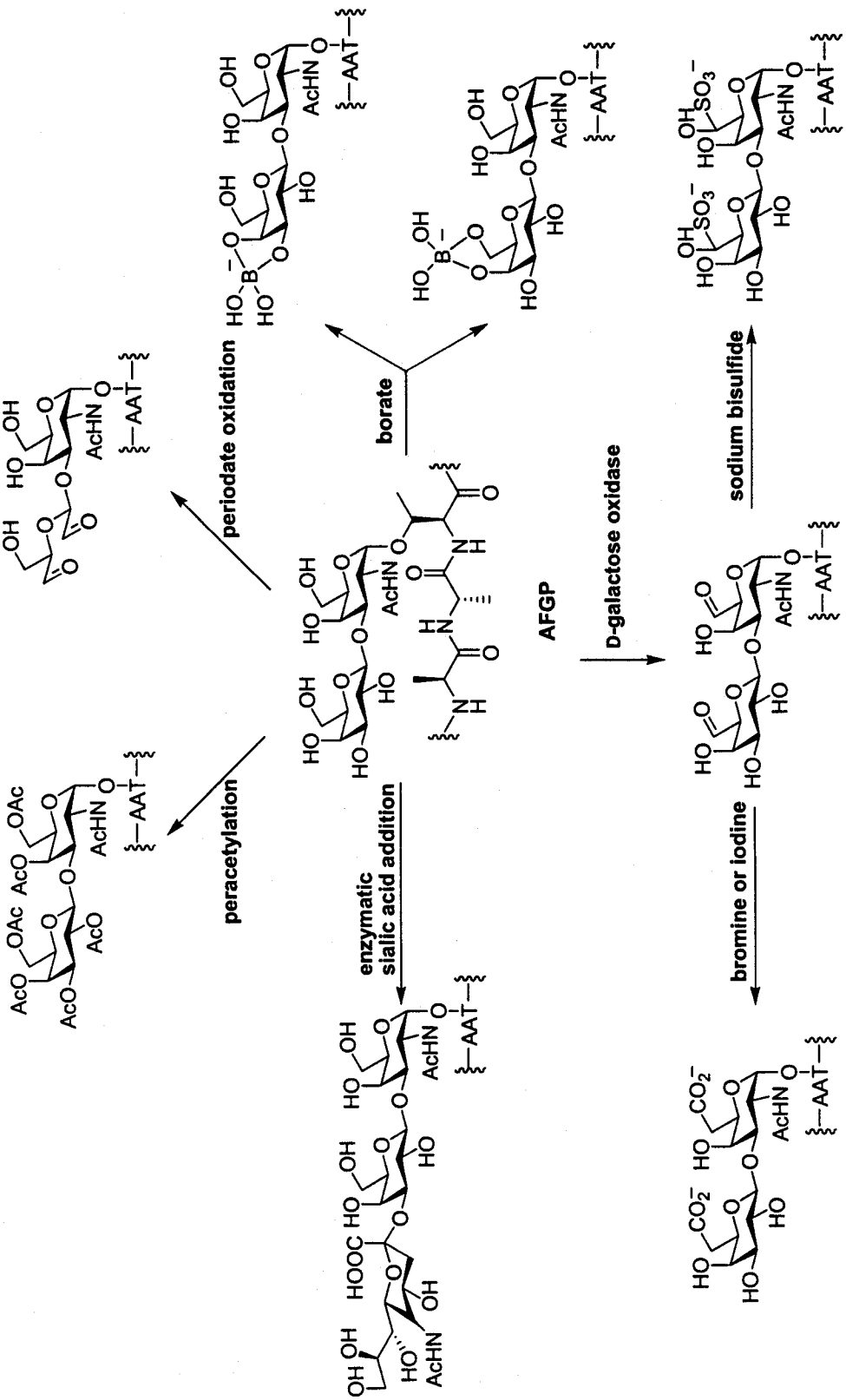

Scheme 1.1 Structural modification on disaccharide residues.[38]

Early structural modification of the disaccharide moiety of AFGP verified the importance of the hydroxyl groups with specific orientation for antifreeze activities (Scheme 1.1).[38] Feeney and co-workers performed the structure-activity relationship (SAR) study of AFGP by chemically modifying the native glycopeptides. Removing all hydroxyl groups on the disaccharide residues by peracetylation caused loss of all TH activity. Periodate oxidation of the terminal galactose residues or formation of a borate adduct with cis hydroxyl groups on the terminal galactose residues also caused complete lost of activity.[39] Introducing sialic acid on the C3 oxygen of the galactose residues showed no thermal hysteresis, suggesting the importance of the C3 hydroxyl group. However, as described by Nishimura, the loss of thermal hysteresis may also be due to the fact that the bulky sialic acid can change AFGPs' specific functional conformation or simply interfere with the binding with the ice/water interface.[20] C6 hydroxyl groups do not appear to be necessary for antifreeze activity. Oxidizing these hydroxyl groups to aldehydes using D-galactose oxidase did not cause any change in activity. However, negatively charged groups such as carboxylate or sulfide anion are not favored for antifreeze activity.[40]

A detailed SAR study of AFGPs by Nishimura and co-workers also pointed out the importance of hydrophobic interaction for antifreeze activity.[20] Unlike the previous SAR studies, Nishimura independently synthesized a series of AFGP analogues using a diphenylphosphorylazide (DPPA)-promoted polymerization of unprotected glycopeptide macromonomer.[20, 41] Although the study didn't rule out the contribution of hydroxyl groups on disaccharide residues to keep an overall functional conformation for AFGPs to interact with the ice/water interface, some hydrophobic functional groups, such as the *N*-acetyl methyl groups on galactosamine residues and the β-methyl groups of L-threonine residues, also behave as crucial structural motifs for antifreeze activity (Table 1.3). It is proposed that AFGPs have an amphipathic helix structure which is similar to that of type I AFP. However, a simple helical conformation is not guaranteed for antifreeze activity as the helical analogue without β-methyl groups shows no thermal hysteresis and hexagonal bipyramidal ice shape. It is believed that both the hydrophilic phase with specific hydroxyl group orientation and hydrophobic phase comprised of the methyl groups from galactosamine and L-alanine residues are necessary for AFGPs' antifreeze activity. The study showed that the α-glycosidic configuration of the disaccharide to L-threonine and the relative hydroxyl group configuration are important for TH activity, as β-glycosidic linkage and lactose analogues almost showed no activity. Interestingly, the

galactosamine monosaccharide showed only slightly reduced activity, which implies that galactosamine is a key structural motif for TH activity.

Table 1.3 Nishimura's AFGP structural-activity relationship study.[20]

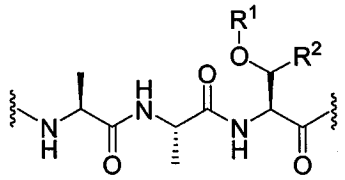

R^1	R^2	Activity
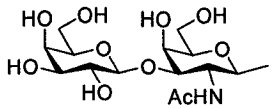	CH_3	No TH
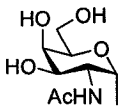	CH_3	Slightly reduced TH
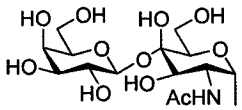	CH_3	Much reduced TH
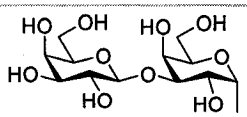	CH_3	No TH
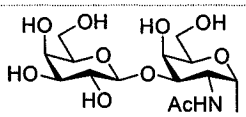	H	No TH

In summary, early studies have identified some important structural moieties in AFGPs for activity. These include the hydroxyl groups[38] and the *N*-acetyl group[20] on the disaccharide residue, the α-configuration of glycoside[20] and the β-methyl group[20] of the L-threonine residue. Evidences indicated that both hydrophilic[33,35] and hydrophobic[10,20,36] interactions might account for the effective binding of AFGPs to certain ice lattices for action. However, unanimous mechanism has not been proposed and further structure-activity relationship studies need to be performed.

1.4 Synthesis of AFGPs and AFGP Analogues

Currently, most AFGPs are isolated and purified from the body fluid and blood of Teleost fish. This process is labor-intensive and time-consuming due to the difficulty in purifying homogeneous antifreezes from the numerous AFGP isoforms in fish bodies. Furthermore, the fact that large amount of fish need to be harvested to isolate small quantity of pure AFGPs[1b] makes this process even less favorable to be used as the major tool to acquire enough analytically pure AFGPs for research study and commercial applications. Preparation of AFGPs using synthetic chemistry is a plausible alternative to circumvent these problems. However, the total synthesis of AFGPs is also a challenging project. AFPs can be easily prepared using either chemical protein synthesis or molecular biology methods such as molecular cloning.[12, 42] However, these methods cannot be directly applied in the preparation of AFGPs because of the presence of the disaccharide moiety in glycoproteins.

1.4.1 Synthesis of *O*-Linked AFGP Analogues

Before the first successful synthesis of natural AFGPs, there were several reports describing the preparation of AFGP analogues. These analogues had either one or more structural variations to the native AFGPs and all of these analogues shared the common structural feature of a C-O glycosidic bond linkage between sugar and amino acid moieties. They are therefore called *O*-linked AFGP analogues.

There have been two major strategies reported to prepare glycopeptides: convergent glycosylation of properly protected peptides and stepwise assembly of glycosylated amino acids as building blocks, either in solution or on solid phase.

Anderson and co-workers reported the preparation of the core tripeptide repeating unit of AFGPs using a convergent method (Scheme 1.2).[43] Benzoyl protected galactose bromide **1** was used as the glycosyl donor to couple with a benzyl-protected galactoside **2** to construct disaccharide **3** using silver triflate as catalyst. After converting the anomeric substituent from *O*-allyl **3** to *O*-1-propenyl **4**, and then to hydroxyl **5**, the glycosyl chloride **6** was prepared by treating **5** with Vilsmeier reagent. A protected tripeptide unit L-alanine-L-threonine-L-alanine **7** is then directly glycosylated with the disaccharide residue **6** to get the protected glycosylated

tripeptide. The final core tripeptide repeating unit of AFGPs **8** was obtained after removing all protecting groups from the disaccharide and tripeptide.

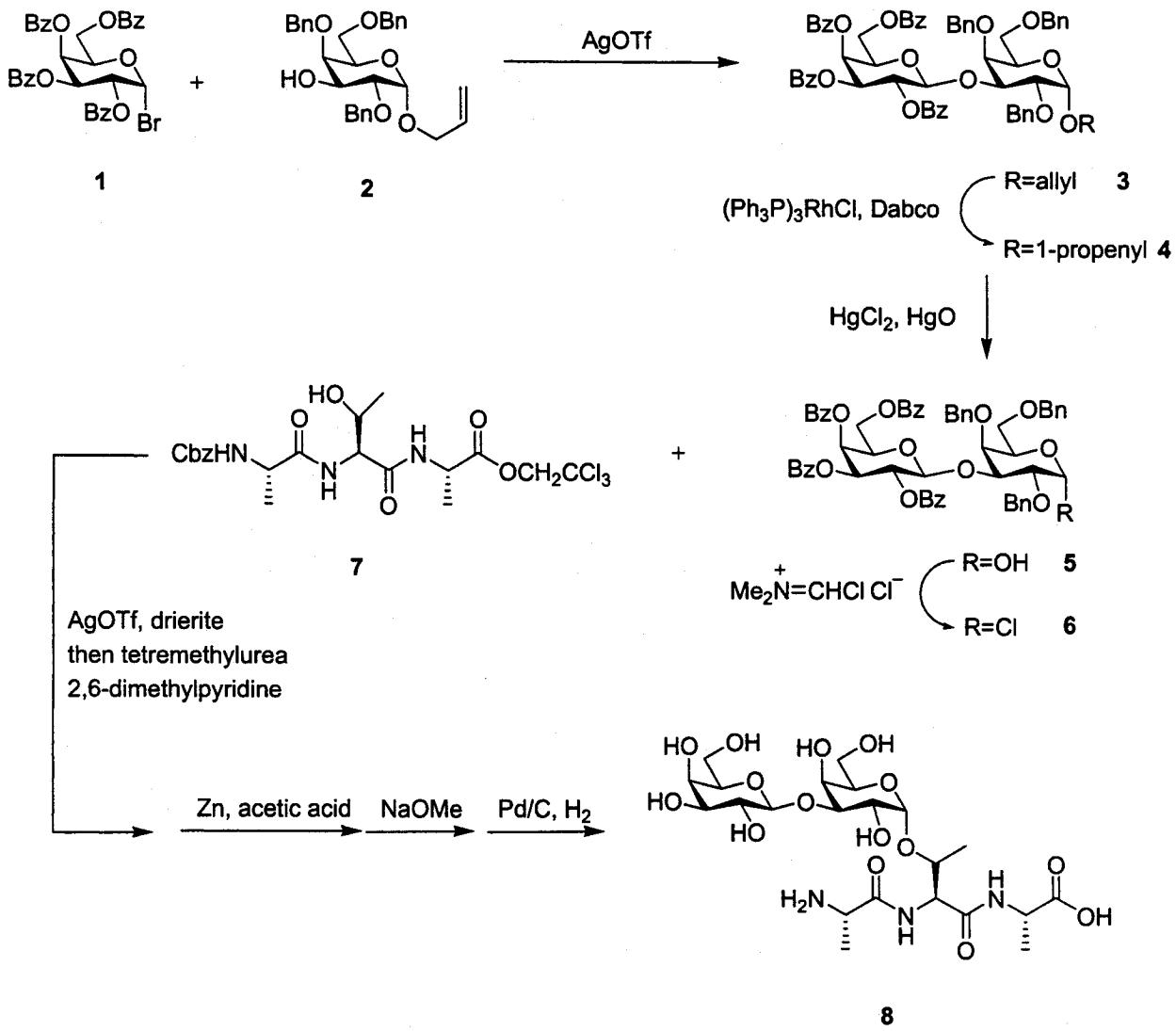

Scheme 1.2 Anderson's convergent strategy to synthesize the core tripeptide repeating unit of AFGPs.[43]

The convergent method is not widely used due to the low solubility of peptides under conditions for glycosylation.[44] Furthermore, the low reactivity of the L-threonine hydroxyl group in the peptide containing more than three amino acid residues limited the use of the convergent strategy in preparing *O*-linked AFGP analogues.[45] Glycosylation of single amino acids to form

building blocks which can be used in the stepwise assembly of peptides is a more reliable strategy to prepare glycopeptides, especially when peptide chain elongation is performed on solid supports. Solid-phase peptide synthesis (SPPS) has shown high efficiency and convenience over solution-phase peptide synthesis.[8] The instability of the C-O glycosidic bond of *O*-linked AFGP analogues to strong acids precludes the use of Boc-chemistry in solid-phase peptide synthesis which involves using HF to cleave glycoproteins from the resin. Therefore, Fmoc (9-fluorenylmethyloxycarbonyl)-chemistry of solid-phase peptide synthesis is widely used in preparing *O*-linked glycopeptides.

Most AFGP analogues were prepared using continuous-flow solid-phase peptide synthesis with Fmoc-chemistry.[46] The first example of applying solid-phase peptide synthesis to AFGP analogue synthesis was reported by Filira and co-workers.[46b] They prepared a series of AFGP analogues with β-linked galactose replacing the α-disaccharide residues in order to mimic the terminal non-reducing galactose residue in native AFGPs (Scheme 1.3). The key strategy was to first synthesize glycosylated L-threonine derivative **11** from galactose pentaacetate **9** and properly protected L-threonine **10** promoted by Lewis acid boron trifluoride ethyl etherate. Following this, the protecting groups were switched to get the Fmoc-protected building block for linear, continuous flow SPPS. After coupling either L-alanine or building block **12** to a Pepsyn KA resin in a stepwise fashion, glycosylated polypeptides were cleaved from the resin with 95% trifluoroacetic acid (TFA) and the protecting groups were removed from galactose moieties to afford AFGP analogues **16**. The length of the oligopeptides ranged from two to seven L-threonine-(β-Gal)-L-alanine-L-alanine tripeptide repeating units.

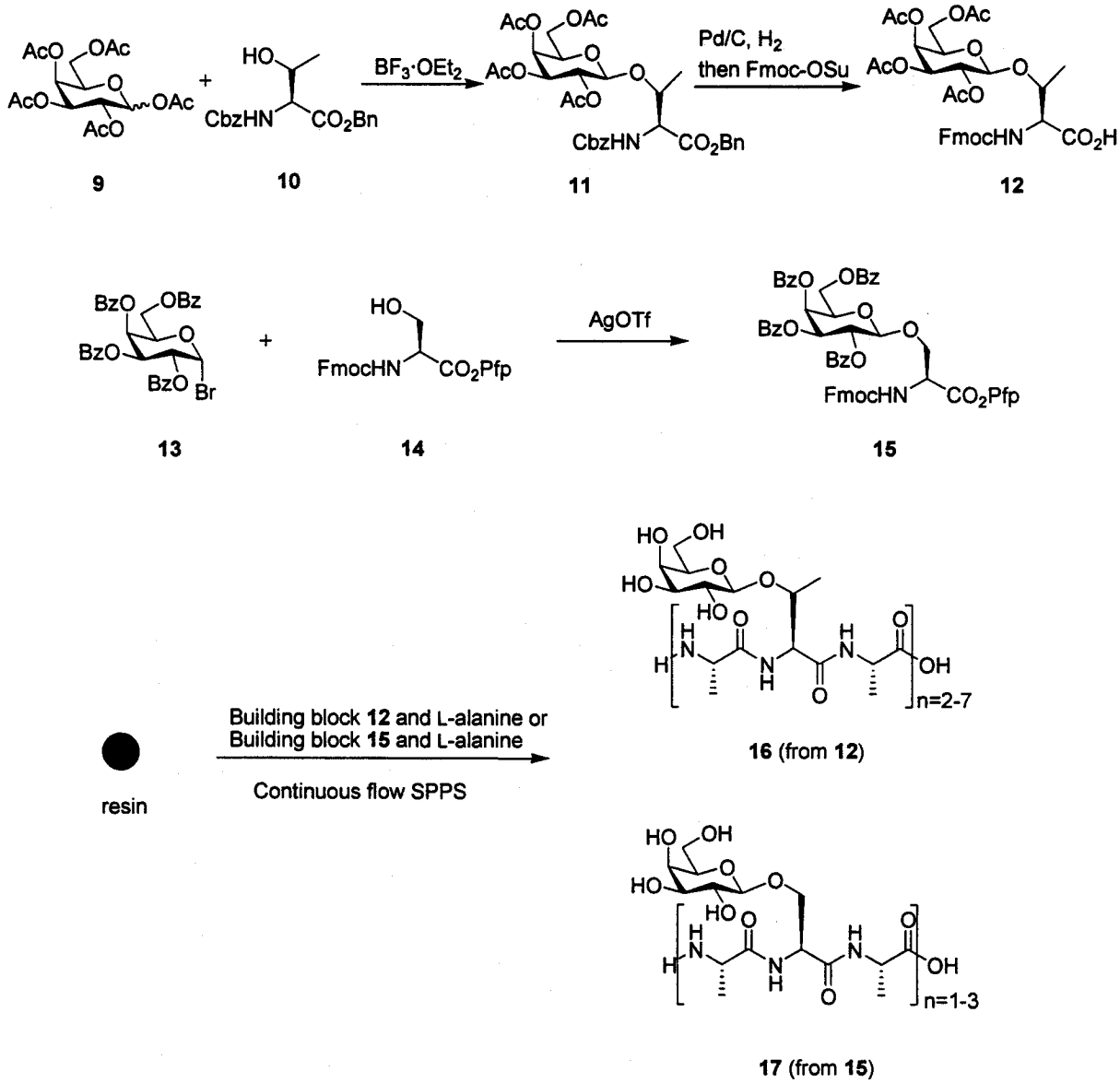

Scheme 1.3 Synthesis of *O*-linked AFGP analogues using continuous flow SPPS.[46]

Meldal and Jensen utilized the same strategy to prepare AFGP analogues with the L-threonine residues in native system replaced by L-serine.[44] An important feature in this study is that the pentafluorophenyl (Pfp) group was used to prepare the glycosylated L-serine building block **15**. The Pfp ester not only functions as a protecting group for the free carboxylic acid in the coupling reaction between galactose bromide **13** and protected L-serine **14**, but also acts as an activating group for the peptide bond forming reaction in SPPS. The polypeptides **17** were built up on

Macrosorb SPR-250 resin with one to three tripeptide repeating units. Later, more *O*-linked AFGP analogues with variant structural mutations were prepared using the same solid-phase peptide synthesis method. This includes the modifications of both the disaccharide and L-threonine moieties. The successful preparation of these compounds proved the feasibility of using Fmoc-chemistry based solid-phase peptide synthesis to prepare AFGP analogues.

1.4.2 Synthesis of Native AFGPs

The first chemical synthesis of native AFGPs was reported by Nishimura and co-workers.[41a] The method involved a diphenylphosphorylazide (DPPA)-promoted polymerization of an unprotected glycotripeptide monomer **26** (Scheme 1.4). The disaccharide residue **22** was prepared in 81% yield by coupling properly protected glycosyl fluoride **20** as a glycosyl acceptor and galactosyl trichloroacetimidate **21** as a glycosyl donor with trimethylsilyltrifluoromethane sulphonate (TMSOTf) as the glycosylation promoter. Then **22** was directly used to glycosylate the protected L-alanine-L-alanine-L-threonine tripeptide **23** with a mixture of cyclopentadienylzirconium dichloride and silver perchlorate as combined promoter to afford disaccharide glycosylated tripeptide as a monomer precursor for polymerization. The fully deprotected monomer **26** was prepared after reducing the 2-azido group in the galactosamine residue and removing all protecting groups from both the disaccharide and peptide moieties. DPPA-catalyzed polymerization afforded mixtures of polypeptides **27** as AFGP analogues with molecular mass ranging from 6000-7300 Dalton, i.e. 10 to 12 tripeptide units. Purification with reverse phase HPLC can offer analytically pure AFGPs for structure-function study.

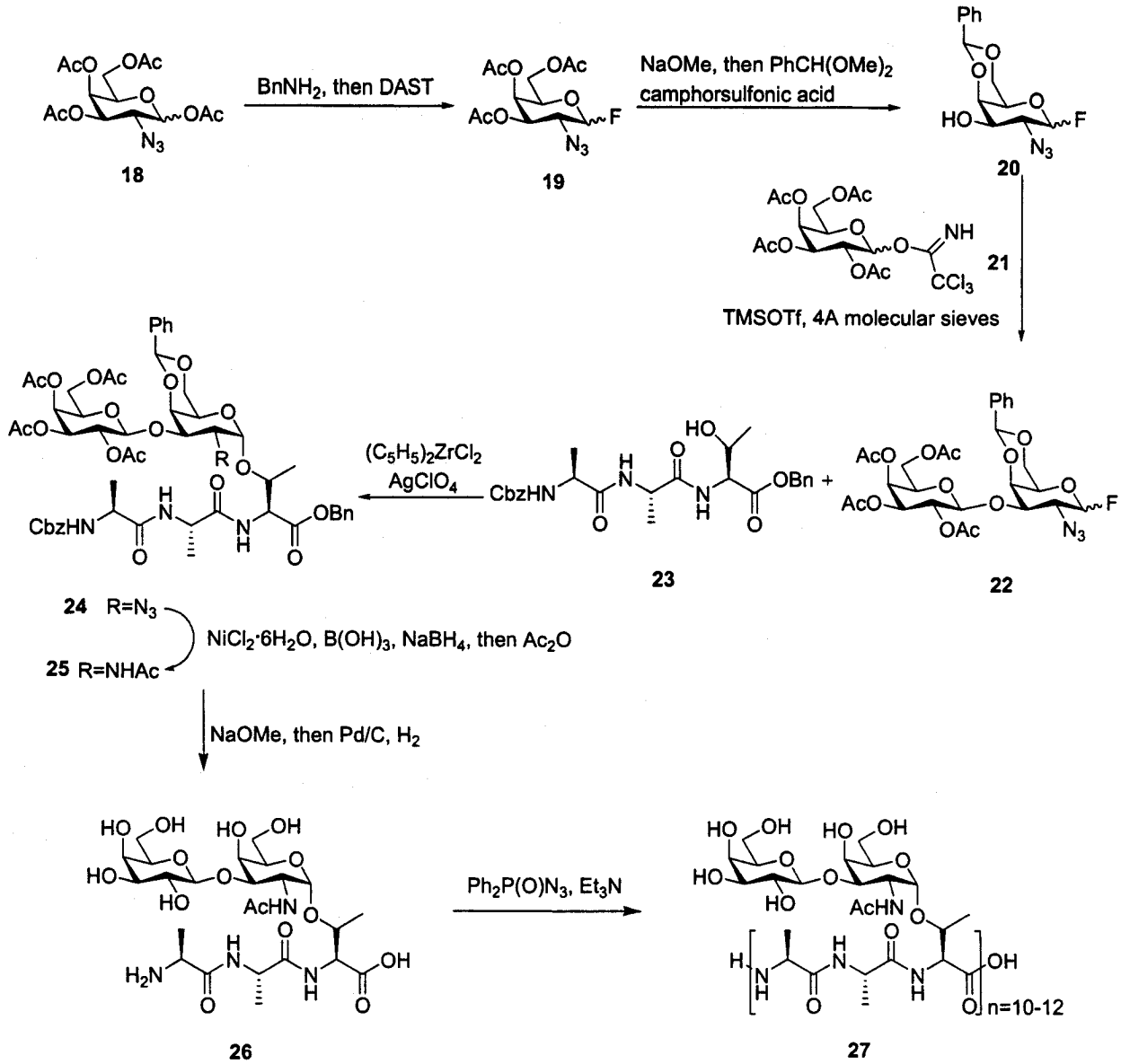

Scheme 1.4 Preparation of AFGPs by using DPPA-promoted polymerization of glycosylated tripeptide residue.[41a]

A different method to prepare native AFGPs was later reported by Chen and co-workers.[47] They utilized the Fmoc-chemistry of solid-phase peptide synthesis to construct polypeptides from a disaccharide-glycosylated L-threonine residue (Scheme 1.5). A monoglycosyl L-threonine conjugate **32** was first prepared by coupling glycosyl selenide **30** with protected L-threonine **31** with silver triflate as a promoter. This glycoconjugate was then coupled with thioglycoside **34** in the presence of *N*-iodosuccinimide (NIS) and TfOH to afford the disaccharide glycosylated L-

threonine in 93% yield. The building block **36** and L-alanine were assembled on a HMP resin with an automatic peptide synthesizer to afford AFGPs **37**. Compared to the DPPA-promoted polymerization method which demands the separation of oligopeptide mixtures, solid-phase peptide chemistry can be used to build up AFGP polypeptide chain with any desired amino acid sequence and any length of interest, which is more flexible for preparing analogues of AFGP to study structure-activity relationships.

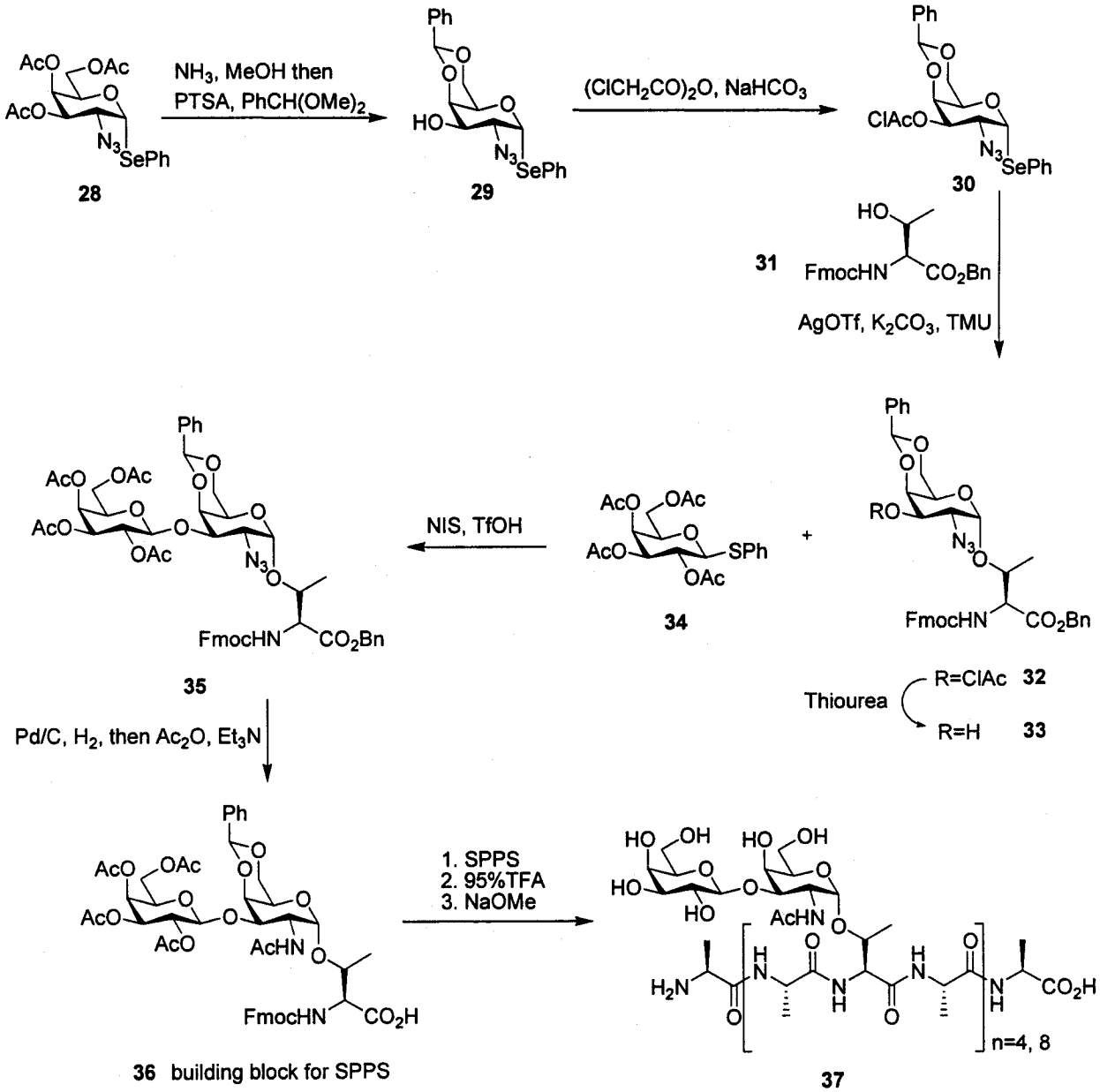

Scheme 1.5 Chen's strategy to prepare AFGPs using SPPS.[47]

1.5 Applications

Biological antifreezes' antifreeze-specific properties render them as having potential applications in different areas.[48] It has been found that biological antifreezes can improve the viability of cells after the freeze-thaw cycle. The detrimental effect of high concentrations of biological antifreezes caused by rapid propagation of needle-shaped ice spicules into cell membranes has been exploited to improve the efficiency of cryosurgery in the destruction of tumor cells. It has also been shown that biological antifreezes can improve the storage of frozen foods by preventing nutrition loss and maintaining the smooth texture.[7]

1.5.1 Hypothermic Storage and Cryogenic Preservation of Cells, Tissues and Organs

Low temperature storage of cells, tissues and organs is always accompanied by decreased viability or reduced biological function. Ice can be formed both extracellularly and intracellularly. Intracellular ice can cause mechanical disruption and is always considered lethal to cells.[49] No studies have shown that the damage caused by the intracellular ice formation can be prevented.[50] Extracellular ice crystals can cause cell damage through two possible mechanisms: the physical injury effect of large ice crystals on cell membranes and cell dehydration caused by the increased osmotic pressure gradient through cell membranes associated with hypertonic stress. Some empirical procedures have been used to improve the recovery of viability. These include the slow and fast freezing protocols. In the slow freezing protocol, the addition of small molecules such as glycerol or dimethyl sulfoxide (DMSO) to cell solutions can increase intracellular osmolality to alleviate the hypertonic stress.[51] In the fast freezing protocol, some non-penetrating polymers such as polyvinylpyrrolidone (PVP) can be used as extracellular cryoprotectants to stabilize cell surface glycoproteins and glycolipids, therefore preventing cell membrane denaturation.[50, 52] However, all these cryoprotectants have limited success and improvement is needed to obtain high recovery of viability after the freeze-thaw cycle. Recently, several reports have shown that biological antifreezes can act as effective cryoprotectants.[53]

Rubinsky and co-workers first reported that biological antifreezes can protect mammalian cell membranes at hypothermic (non-frozen) and cryogenic (frozen) temperatures.[54] Both AFGPs and

AFPs were used in various cells and tissues and demonstrated improved viability after disposing at different temperatures (Table 1.4).[48b] For example, after treating pig oocytes with a solution of AFGPs isolated from Antarctic Notothenioids at 4 °C, oolemma showed improved structural integrity while control cells showed membrane depolarization at low temperatures.[55] Both AFGPs and AFPs also showed a protective effect for whole rat livers' function after either hypothermic or cryogenic storage.[56]

Table 1.4 Biological antifreezes improve the survival of various cells or tissues following low temperature storage.[48b]

Type of cells or tissues	Type of biological antifreeze	Storage temperature	Reference
Fish sperm	AFGP	Cryogenic	57
Carp sperm	AFGP	Cryogenic	58
Mouse embryos	AFGP	Cryogenic	59
Mouse oocytes	AFGP	Cryogenic	60
Rat liver	Type III AFP	Hypothermic	56a
Ram sperm	Type I AFP, AFGP	Cryogenic	61
Pig oocytes	Type I, II, III AFP, AFGP	Cryogenic	62
Bovine oocytes	Type I, II, III AFP	Hypothermic	54
Chimpanzee sperm	Type III AFP	Cryogenic	63
Human oocytes	Type I, III AFP	Hypothermic	64
Human platelets	AFGP	Hypothermic	65

One hypothesis for the improved cell integrity at hypothermic temperatures is that biological antifreezes can block the calcium and potassium ion channels in cell membranes to prevent damage caused by hypothermia. This is supported by the fact that 0.5 mg/mL type I AFP from Winter flounder can inhibit the calcium and potassium current in porcine granulose cells.[66] Another hypothesis for the hypothermic protective effect is that biological antifreezes can protect cell membranes during the phase transition temperature to prevent the leakage of intracellular

contents because cell membranes usually lose the lipid bilayer fluidity after the phase transition from liquid crystal to gel. AFGPs showed the ability to protect the integrity of liposomes, a cell membrane model and prevent the leakage of most liposome contents during phase transition temperature.[67]

In contrast to the protective effects, some studies demonstrated that biological antifreezes can cause damage and toxicity to cells following low temperature incubation.[68] These controversial results indicate that the function of biological antifreezes for cell and tissue cold storage is dependent on the type of cell membranes, type and concentration of biological antifreezes and the storage temperature used. It has been postulated that the physical disruption to cell membranes caused by needle-shaped ice spicules formed below freezing points accounts for the detrimental effects of biological antifreezes.[68e] The rapid ice growth rate in biological antifreeze containing solution is also a factor which can cause more cell damage. Compared to water, it is found that ice crystals grow five times faster at temperatures just below freezing points in antifreeze solution.[69] On the other hand, the recrystallization inhibition ability of biological antifreezes can prevent the formation of more harmful large ice crystals and is the major factor improving cell survival after the freezing-thawing cycle.[48a] However, more studies need to be performed in this area in order to effectively determine biological antifreezes' cold protective function. Current limited knowledge of the mechanism for biological antifreezes interaction with ice lattices and cell membranes is the major obstacle to have a detailed understanding of the controversial effects of biological antifreezes in cryopreservation.

1.5.2 Improving Cryosurgery Efficiency

Cryosurgery is a novel technique in oncology surgeries by employing freezing to destroy undesirable tissues with advantages such as avoidance of a surgical procedure, less overall discomfort, improved cosmesis, quicker recovery and the prospect of overall cost benefits.[70] However, the efficiency of cryosurgery depends on the thermal conditions that targeting tissues experience such as the cooling temperature and cooling rate used in cryosurgical procedures. The survival of the frozen undesirable tissue may lead to complications, such as recurrence of cancer. Previous *in vivo* studies with cells and tissues demonstrated that high concentrations (>5 mg/mL) of biological antifreezes can cause frozen cell destruction and increase the efficacy of

cryosurgery.[71] Using biological antifreezes as adjuvants for cryosurgery is a much easier way to prevent the survival of undesired cells compared to uniformly controlling thermal parameters used in cryosurgery.

1.5.3 Improving Frozen Food Storage

Most problems in frozen food storage, such as the loss of the smooth, creamy texture in ice cream and increased drip (water-holding ability) and nutrition loss in frozen meat after thawing are caused by the large ice crystals that form with inappropriate storage and multiple freezing-thawing procedures. Biological antifreezes are extremely potent ice recrystallization inhibitors and have great potential to be used in the food industry to improve the quality of frozen food. [7, 48] Payne and co-workers were the first to study the effect of antifreezes on frozen meat.[72] In this study, bovine muscle was pre-soaked with either Antarctic cod AFGPs or Winter flounder type I AFP in PBS solution at a concentration of 0.1 mg/mL before freezing at -20 °C for three days. After thawing, samples treated with biological antifreezes showed smaller intracellular space than the control sample that was not soaked in antifreeze solutions. The intracellular space presumably represents the size of ice crystal formed during freezing. Another study of AFGPs in lamb showed similar effects.[73] The AFGP treated sample showed both decreased drip and smaller ice crystals than the control sample.

Given the potential applications in biomedical and food industries, studies on biological antifreezes have recently attracted more attentions. However, more studies need to be performed to understand the mechanism of antifreeze activities at the molecular level and improve the applications of biological antifreezes in variant areas. Especially, it is attractive to develop stable synthetic analogues with potent antifreeze activities to circumvent the limited bioavailability of biological antifreezes and the inherent instability of native AFGPs.

References

1. (a) DeVries, A. L., Wohlschlag, D. E. *Science* **1969**, *163*, 1073-1075.
   (b) DeVries, A. L., Komatsu, S. K., Feeney, R. E. *J. Biol. Chem.* **1970**, *245*, 2901–2908.
2. (a) Feeney, R. E., Burcham, T. S., Yeh, Y. *Annu. Rev. Biophys. Biophys. Chem.* **1986**, *15*, 59-78.
   (b) Yeh, Y., Feeney, R. E. *Chem. Rev.* **1996**, *96*, 601-618.
   (c) Fletcher, G. L, Hew, C. L., Davies, P. L. *Annu. Rev. Physiol.* **2001**, *63*, 359-390.
3. (a) Duman, J. G., Li, N., Verleye, D., Goetz, F. W., Wu, D. W., Andorfer, C. A., Benjamin, T., Parmelee. D. C. *J. Comp. Physiol. B.* **1998**, *168*, 225–232.
   (b) Liou, Y. C., Tocilj, A., Davies, P., Jia, Z. *Nature* **2000**, *406*, 322–325.
   (c) Graether, S. P., Kuiper, M., Gagne, S. M., Walker, V. K., Jia, Z., Skyes, B. D., Davis, P. L. *Nature* **2000**, *406*, 325–328.
   (d) Graham, L. A., Liou, Y. C., Walker, V. K., Davies, P. L. *Nature* **1997**, *388*, 727-728.
4. Duman, J. G. *Annu. Rev. Physiol.* **2001**, *63*, 327–357.
5. (a) Doucet, C. J., Byass, L., Elias, L., Worrall, D., Smallwood, M., Bowles. D. J. *Cryobiology* **2000**, *40*, 218–227.
   (b) Sidebottom, C., Buckley, S., Pudney, S. P., Twigg, S., Jarman, C., Holt, C., Telford, J., McArthur, A., Warrall, D., Hubbard, R., Lillford, P. *Nature* **2000**, *406*, 256.
6. (a) Duman, J. G., Olsen, T. M. *Cryobiology* **1993**, *30*, 322-328.
   (b) Newstead, W. J., Polvi, S., Papish, B., Kendall, E., Saleem, M., Koch, M., Hussain, A., Cutler, A. J., Georges, F. *Biochem. Cell. Biol.* **1994**, *72*, 152-156.
7. Feeney, R. F., Yeh, Y. Trends, *Food, Sci. Technol.* **1998**, *9*, 102-106.
8. Harding, M. M., Anderberg, P. I., Haymet, A. D. J. *Eur. J. Biochem.* **2003**, *270*, 1381-1392.
9. (a) DeVries, A. L., Lin, Y. *Biochim. Biophys. Acta* **1977**, *495*, 388-392.
   (b) Yang, D. S., Sax, M., Chakrabartty, A., Hew C. L. *Nature* **1988**, *333*, 232–237.
10. Haymet, A. D. J., Ward, L. G., Harding, M. *J. Am. Chem. Soc.* **1999**, *121*, 941-948.
11. (a) Slaughter, D., Fletcher, G. L., Ananthanarayanan, V. S., Hew, C. L. *J. Biol. Chem.* **1981**, *256*, 2022-2026.
    (b) Ng, N. F., Trinh, K. Y., Hew, C. L. *J. Biol. Chem.* **1986**, *261*, 15690-15695.
12. Sonnichsen, F. D., Sykes, B. D., Chao, H., Davies, P. L. *Science* **1993**, *259*, 1154-1157.
13. (a) Deng, G. J., Andrews, D. W., Laursen, R. A. *FEBS Lett.* **1997**, *402*, 17-20.

(b) Deng, G. J., Laursen, R. A. *Biochim. Biophys. Acta* **1998**, *1388*, 305-314.

(c) Cheng, C. H. C. *Curr. Opin. Genet. Dev.* **1998**, *8*, 715-720.

14. Wu, Y. L., Banoub, J., Goddard, S. V., Kao, M. H., Fletcher, G. L. *Comp. Biochem. Physiol. B* **2001**, *128*, 265-273.

15. (a) Lin, Y., Duman, J. G., DeVries, A. L. *Biochem. Biophys. Res. Commun.* **1972**, *46*, 87-92.

(b) Geoghegan, K. F., Osuga, D. T., Ahmed, A. I., Yeh, Y., Feeney, R. E. *J. Biol. Chem.* **1980**, *255*, 663-667.

(c) Hew, C. L., Slaughter, D., Fletcher, G. L., Joshi, S. B. *Can. J. Zool.* **1981**, *59*, 2186-2192.

16. (a) O'Grady, S. M., Schrag, J. D., Raymond, J. A., DeVries, A. L. *J. Exp. Zool.* **1982**, *224*, 177-185.

(b) Fletcher, G. L., Hew, C. L., Joshi, S. B. *Can. J. Zool.* **1982**, *60*, 348-355.

(c) Burcham, T. S., Osuga, D. T., Rao, B. N. N., Bush, C. A., Feeney, R. E. *J. Biol. Chem.* **1986**, *261*, 6384-6389.

17. Morris, H. R., Thompson, M. R., Osuga, D. T., Ahmed, A. I., Chan, S. M., Vandenheede, J. R., Feeney, R. E. *J. Biol. Chem.* **1978**, *253*, 5155-5162.

18. (a) Bush, C. A., Feeney, R. E., Osuga, D. T., Ralapati, S., Yeh, Y. *Int. J. Pept. Protein Res.* **1981**, *17*, 125-129.

(b) Franks, F., Morris, E. R. *Biochim, Biophys. Acta* **1978**, *540*, 346-356.

19. Mimura, Y., Yamamoto, Y., Inoue, Y., Chujo, R. *Int. J. Bio. Macromol.* **1992**, *14*, 242-248.

20. Tachibana, Y., Fletcher, G. L., Fujitani, N., Tsuda, S., Monde, K., Nishimura, S. *Angew. Chem. Int. Ed.* **2004**, *43*, 856 –862.

21. (a) Ahmed, A. I., Feeney, R. E., Osuga, D. T., Yeh, Y. *J. Biol. Chem.* **1975**, *250*, 3344-3347.

(b) Tomimatsu, Y., Scherer, J., Yeh, Y., Feeney, R. E. *J. Biol. Chem.* **1976**, *251*, 2290-2298.

(c) Berman, E., Allerhand, A., DeVries, A. L. *J. Biol. Chem.* **1980**, *255*, 4407-4410.

22. Davies, P. L., Baardsnes, J., Kuiper, M. J., Walker, V. K. *Phil. Trans. R. Soc. Lond. B* **2002**, *357*, 927-935.

23. Kao, M. H., Fletcher, G. L., Wang, N. C., Hew, C. L. *Can. J. Zool.* **1986**, *64*, 578-582.

24. (a) Knight, C. A., Cheng, C. C., DeVries, A. L. *Biophys. J.* **1991**, *59*, 409-418.
(b) Knight, C. A., DeVries, A. L. *J. Cryst. Growth* **1994**, *143*, 301-310.
(c) Knight, C. A., DeVries, A. L., Oolman, L. D. *Nature* **1984**, *308*, 295-296.

25. Davies, P. L., Hew, C. L. *FASEB. J.* **1990**, *4*, 2460-2468.

26. Knight, C. L., Wen, D. Y., Laursen, R. A. *Cryobiology* **1995**, *32*, 23-34.

27. Knight, C. L. *Nature* **2000**, *406*, 249-251.

28. Knight, C. L., Hallet, J., DeVries, A. L. *Cryobiology* **1988**, *25*, 55-60.

29. Horwath, K. L., Easton, C. M., Poggioli Jr., G. J., Myers, K., Schnorr, L. *Eur. J. Entomol.* **1996**, *93*, 419-433.

30. Myers, K. L. "Quantification of recrystallization inhibition: an assay for antifreeze protein activity" M.A. Thesis, Binghamton University (S. U. N. Y.) 1999.

31. Ben, R. N. *Chembiochem* **2001**, *2*, 161-166.

32. Wilson, P. W. *Cryoletters* **1993**, *14*, 31-36.

33. Knight, C. A., Driggers, E., DeVries, A. L. *Biophys. J.* **1993**, *64*, 252-259.

34. (a) Hew, C. L., Yang, D. S. C. *Eur. J. Biochem.* **1992**, *203*, 33-42.
(b) Wen, D., Laursen, R. A. *Biophys. J.* **1992**, *63*, 1659-1662.

35. (a) Raymond, J. A., DeVries, A. L. *Proc. Natl. Acad. Sci. USA* **1977**, *74*, 2589-2593.
(b) Wierzbicki, A., Taylor, M. S., Knight, C. A., Madura, J. D., Harrington, J. P., Sikes, C. S. *Biophys. J.* **1996**, *71*, 8-18.

36. Chao, H., Houston, M. E. Jr., Hodges, R. S., Kay, C. M., Sykes, B. D., Loewen, M. C., Davies, P. L., Sonnichsen, F. D. *Biochemistry* **1997**, *36*, 14652-14660.

37. Yang, D. S., Hon, W. C., Bubanko, S., Xue, Y., Seetharaman, J., Hew, C. L., Sicheri, F. *Biophys. J.* **1998**, *74*, 2142-2151.

38. Komatsu, S. K., DeVries, A. L., Feeney, R. E. *J. Biol. Chem.* **1970**, *245*, 2909-2913.

39. Ahmed, A. I., Yeh, Y., Osuga, D. T., Feeney, R. E. *J. Biol. Chem.* **1976**, *251*, 3033-3036.

40. (a) DeVries, A. L. Science 1971, 171, 1152-1155.
(b) Vandenheede, J. R., Ahmed, A. I., Feeney, R. E. *J. Biol. Chem.* **1972**, *247*, 7885-7889.
(c) Osuga, D. T., Feather, M. S., Shah, M. J., Feeney, R. E. *J. Prot. Chem.* **1989**, *8*, 519-528.

41. (a) Tsuda, T., Nishimura, S.-I. *Chem. Commun.* **1996**, *24*, 2779-2780.
(b) Tachibana, Y., Matsubara, N., Nakajima, F., Tsuda, T., Tsuda, S., Monde, K., Nishimura, S. *Tetrahedron* **2002**, *58*, 10213-10224.
(c) Tachibana, Y. Monde, K., Nishimura, S. *Macromolecules* **2004**, *37*, 6771-6779.
42. (a) Worrall, D., Elias, L., Ashford, D., Smallwood, M., Sidebottom, C., Lillford, P., Telford, J., Holt, C., Bowles, D. J. *Science* **1998**, *282*, 115-117.
(b) Fairley, K., Westman, B. J., Pham, L. H., Haymet, A. D. J. Harding, M. M., Mackay, J. P. *J. Biol. Chem.* **2002**, *277*, 24073-24080.
43. Anisuzzaman, A. K. M., Anderson, L., Navia, J. L. *Carbohydr. Res.* **1988**, *174*, 265-278.
44. Meldal, M., Jensen, K. J. *J. Chem. Soc. Chem. Commun.* **1990**, 483-485.
45. Maeji, N. J., Inoue, Y., ChÙjÔ, R. *Carbohydr. Res.* **1986**, *146*, 174-176.
46. (a) Bielfeldt, T., Peters, S., Meldal, M., Bock, K., Paulsen, H. *Angew. Chem. Int. Ed.* **1992**, *31*, 857-859.
(b) Filira, F., Biondi, L., Scolaro, B., Foffani, M. T., Mammi, S., Peggion, E., Rocchi, R. *Int. J. Biol. Macromol.* **1990**, *12*, 41-49.
47. Tseng, P. H., Jiaang, W. T., Chang, M. Y., Chen, S. T. *Chem. Eur. J.* **2001**, *7*, 585-590.
48. (a) Griffith, M., Ewart, K. V. *Biotechnol. Adv.* **1995**, *13*, 375-402.
(b) Fletcher, G. L., Goddard, S. V., Wu, Y. L. *Chemtech* **1999**, *29*, 17-28.
49. (a) Costanzo, J. P., Lee, R. E. Jr., DeVries, A. L., Wang, T., Layne, J. R. Jr. *FASEB. J.* **1995**, *9*, 351-358.
(b) Pegg, D. E. *Semin. Reprod. Med.* **2002**, *20*, 5-13.
50. Meryman, H. T. *Annu. Rev. Biophys. Bioeng.* **1974**, *3*, 341-363.
51. (a) Polge, C., Smith, A. U., Parkes, A. S. *Nature* **1949**, *164*, 666.
(b) Lovelock, J. E., *Biochim. Biophys. Acta* **1953**, *10*, 414-426.
(c) Lovelock, J. E., *Biochim. Biophys. Acta* **1953**, *11*, 28-36.
(d) Lovelock, J. E., Bishop, M. W. H. *Nature* **1959**, *183*, 1394-1395.
52. Meryman, H. T., Hornblower, M. *Cryobiology* **1972**, *9*, 262-267.
53. Wang, J. H. *Cryobiology* **2000**, *41*, 1-9.
54. Rubinsky, B., Arav, A., Fletcher, G. L. *Biochem. Biophys. Res. Commun.* **1991**, *180*, 566-571.

55. Rubinsky, B., Arav, A., Mattioli, M., DeVries, A. L. *Biochem. Biophys. Res. Commun.* **1990**, *173*, 1369-1374.

56. (a) Lee, C. Y., Rubinsky, B., Fletcher, G. L. *Cryoletters* **1992**, *13*, 59-66.

(b) Rubinsky, B., Arav, A., Hong, J. S., Lee, C. Y. *Biochem. Biophys. Res. Commun.* **1994**, *200*, 732-741.

57. Karanova, M. V., Tsvetkova, L. I. *Izv. Akad. Nauk, Ser. Biol.* **1994**, *5*, 818-827.

58. Karanova, M. V., Tsvetkova, L. I., Petropavlov, N. N. *Biofizika* **1997**, *42*, 725-728.

59. Karanova, M. V., Mezhevikina, L. M., Petropavlov, N. N. *Biofizika* **1995**, *40*, 1341-1347.

60. O'Neil, L., Paynter, S. J., Fuller, B. J., Shaw, R. W., DeVries, A. L. *Cryobiology* **1998**, *37*, 59-66.

61. Payne, S. R., Oliver, J. E., Upreti, G. C. *Cryobiology* **1994**, *31*, 180-184.

62. Arav, A., Rubinsky, B., Fletcher, G., Seren, E. *Mol. Reprod. Dev.* **1993**, *36*, 488-493.

63. Younis, A. I., Rooks, B., Khan, S., Gould, K. G. *J. Androl.* **1998**, *19*, 207-214.

64. Itskovitz-Eldor, J., Levron, J., Arav, A., Bar-Ami, S., Stein, D. W., Fletcher, G. L., Rubinsky, B. *Cryoletters* **1993**, *14*, 235-242.

65. Tablin, F., Oliver, A. E., Walker, N. J., Crowe, L. M., Crowe, J. H. *J. Cell. Physiol.* **1996**, *168*, 305-313.

66. Rubinsky, B., Mattioli, M., Arav, A., Barboni, B., Fletcher, G. L. *Am. J. Physiol.* **1992**, *262*, R542-R545.

67. Hayes, L. M., Feeney, R. E., Crowe, L. M., Crowe, J. H., Oliver, A. E. *Proc. Natl. Acad. Sci. U. S. A.* **1996**, *93*, 6835-6840.

68. (a) Hincha, D. K., DeVries, A. L., Schmitt, J. M. *Biochim. Biophys. Acta* **1993**, *1146*, 258-264.

(b) Wang, T., Zhu, Q., Yang, X., Layne, J. R., DeVries, A. L. *Cryobiology* **1994**, *31*, 185-192.

(c) Zhu, Q., Yang, X., Layne, J. R., Jr., DeVries, A. L., Wang, T. *Cryobiology* **1992**, *29*, 783-784.

(d) Mugnano, J. A., Wang, T., Layne, J. R., Jr., DeVries, A. L., Lee, R. E., Jr. *Am. J. Physiol.-Reg. I.* **1995**, 269, R474-R479.

(e) Rubinsky, B., DeVries, A. L. *Cryobiology* **1989**, *26*, 580.

(f) Pegg, D. E. *Cryobiology* **1992**, *29*, 774.

(g) Hansen, T. N., Smith, K. M., Brockbank, K. G. M. *Cryobiology* **1993**, *30*, 646.

(h) Koushafar, H., Pham, L., Lee, C., Rubinsky, B. *Cryobiology* **1997**, *35*, 324.

69. Harrison, K., Hallett, J., Burcham, T. S., Feeney, R. E., Kerr, W. L., Yeh, Y. *Nature* **1987**, *328*, 241-243.

70. (a) Kaufman, C. S., Rewcastle, J. C. *Technol. Cancer Res. Treat.* **2004**, *3*, 165-176.

(b) Seifert, J. K., Junginger, T. *Technol. Cancer Res. Treat.* **2004**, *3*, 151-164.

(c) Maiwand, M. O., Asimakopoulos, G. *Technol. Cancer Res. Treat.* **2004**, *3*, 143-150.

(d) Rees, J., Patel, B., MacDonagh, R., Persad, R. *BJU Int.* **2004**, *93*, 710-714.

(e) Kuflik, E. G. *Dermatol. Surg.* **2004**, *30*, 297-300.

71. (a) Muldrew, K., Rewcastle, J., Donnelly, B. J., Saliken, J. C., Liang, S., Goldie, S., Olson, M., Baissalov R., Sandison, G. *Cryobiology* **2001**, *42*, 182-189.

(b) Koushafar, H., Rubinsky, B. *Urology* **1997**, *49*, 421-425.

(c) Koushafar, H., Pham, L., Lee, C., Rubinsky, B. *J. Surg. Oncol.* **1997**, *66*, 114-121.

(d) Pham, L., Dahiya, R., Rubinsky, B. *Cryobiology* **1999**, *38*, 169-175.

72. Payne, S. R., Sandford, D., Harris, A., Young, O. A. *Meat Sci.* **1994**, *37*, 429-438.

73. Payne, S. R., Young, O. A. *Meat Sci.* **1995**, *41*, 147-155.

Chapter 2 Goals and Objectives

2.1 *C*-Glycosides

Glycoproteins are widely distributed in biological organisms and play important roles in maintaining cell functions.[1] Glycosylation facilitates the folding of proteins to maintain their physiochemical properties.[2] The oligosaccharides of glycoproteins have been identified as important structural moieties that are involved in cell-cell interaction, modulating intercellular trafficking and signaling, and recognition sites for viruses and bacteria.[1] In addition to these important cell functions, glycosylation can increase the thermal and proteolytic stability of glycoproteins.[3] Overall, the critical role that glycoproteins play in the biological recognition process has attracted a great deal of interest from the research community. Scientists are interested in studying the fundamental mechanism involved in the biological recognition process. Furthermore, this study can help develop glycoprotein analogues as carbohydrate-based therapeutic products.[4]

Common glycosidic linkages found in nature include *O*-glycosides and *N*-glycosides. The most popular glycosylation sites on polypeptides are L-threonine (Thr)/L-serine (Ser) in *O*-glycosides and L-asparagine (Asn) in *N*-glycosides. Over 500 *O*-linked and 1000 *N*-linked glycosidic chains are listed in CarbBank[5] (also known as the complex carbohydrate structure database).[6] The most common structures in *O*-linked glycoproteins are GlcNAc-β-Thr/Ser or GalNAc-α-Thr/Ser (which is the case for native AFGPs), and GlcNAc-β-Asn in *N*-linked glycoproteins.[6a] Recently, an unusual glycosidic linkage, a carbon-linked or *C*-linked glycoprotein was reported in human RNase 2, an enzyme involved in the digestion of RNA. The *C*-glycosylation is constructed with an α-D-mannopyranose residue directly linked to the C2 atom on the indole ring of tryptophan (Figure 2.1).[6a, 7]

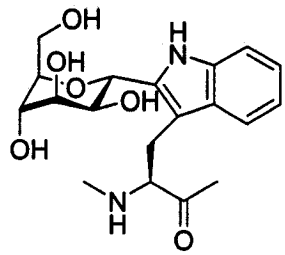

Figure 2.1 Structure of *C*-linked α-D-mannopyranosyl-tryptophan in human RNase 2.[6a,7]

When compared to protein and nucleic acid synthesis, the synthesis of glycoproteins has been a formidable challenge due to the difficulty in preparing complex oligosaccharides. This is due to the fact that the hydroxyl groups on oligosaccharides have similar reactivity and require extensive protecting group manipulation to perform regioselective reactions. In addition, the coupling of carbohydrate moieties with polypeptides needs to be stereoselectively controlled to avoid forming mixtures of α- and β-glycosides.[8] Furthermore, the protecting groups on oligosaccharides need to be compatible with the chemistry employed for polypeptide synthesis.

AFGPs are *O*-linked glycoproteins. Their unique abilities to inhibit ice formation and recrystallization give them potential applications in the biomedical and food industries. However, one structural disadvantage limiting their application is the unstable C-O glycosidic bond. This labile oxygen-linkage is sensitive to a variety of biological and chemical conditions and can be easily hydrolyzed by enzymes, strong acids and bases.[8b] As shown in Scheme 2.1, the glycosidic bond of AFGPs can be readily hydrolyzed under strongly acidic conditions to form an oxocarbenium ion. The *O*-linked L-threonine residue is not stable in highly basic environments either. A β-elimination can cause the detachment of the disaccharide moiety from the polypeptide backbone.

Acid-catalyzed cleavage of AFGPs:

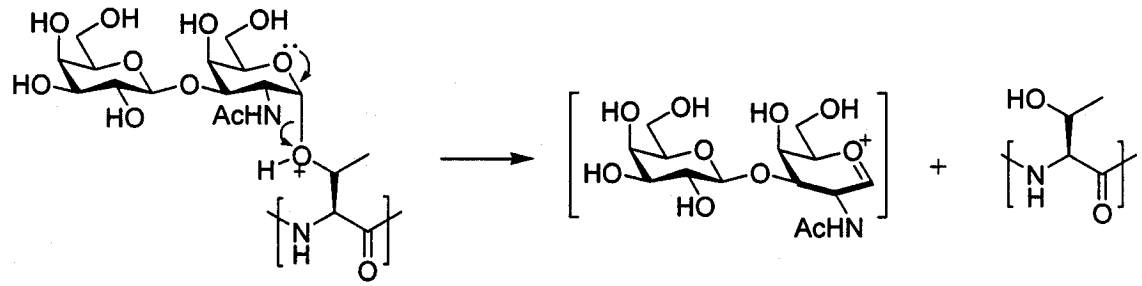

Base-catalyzed cleavage of AFGPs:

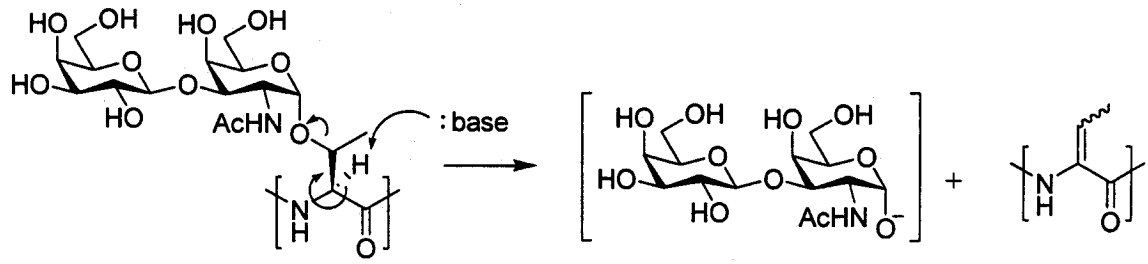

Scheme 2.1 Instability of AFGPs' C-O glycosidic bond in acidic and basic conditions.[8b]

Given the difficulties involved in preparing native glycoproteins and the instability of *O*-glycosides, many efforts have been devoted to the preparation of glycoprotein analogues or mimetics through easily accessible synthetic strategies.[8a] Preparing stable and structurally diverse glycoprotein analogues can not only help to elucidate structural moieties that are crucial for function but also facilitate the exploration of carbohydrate-based therapeutic reagents. Glycoprotein analogues with unusual linkages including *C*-linked, *S*-linked and retro-amide-linked (with the carbonyl carbon connected to the anomeric center) analogues have been made and demonstrated improved stability against cleavage by glycosidases.[8a, 9]

While *S*-glycosides seem to be a reasonable mimic of native *O*-glycosides, the *C*-glycosidic linkage is a dramatic structural change in terms of electronic effects. However, recent studies have shown that *C*-glycoproteins adopted similar solution conformations as their native *O*-linked counterparts and demonstrated comparable or even more potent biological activities.[8a, 10] Kishi and co-workers have performed a series of conformational studies on *C*-pyranoglycosides and compared the results to their native *O*-pyranoglycoside counterparts.[11] The results showed that *C*-pyranosides were capable of adopting similar conformations to *O*-glycosides for both α- and β-

glycans. They also demonstrated the similarity of solution conformations between *O*-linked and *C*-linked oligosaccharides.[12]

The conformational similarities of *C*-glycosides and *O*-glycosides were also verified by studying their receptor-ligand recognition abilities. Kishi demonstrated that the binding affinities of both the H-type II blood group determinant (an *O*-trisaccharide) and its *C*-trisaccharide analogue to the lectin I of *Ulex europaeus* (UEA-I) substrate were almost identical.[12] Vijayan and Kishi also reported the first X-ray crystal structure of *C*-lactose bound to a peanut lectin and observed that the *C*-glycosidic bond in lactose was in the near perfect *exo*-anomeric conformation. Both *C*-lactose and *O*-lactose were found to bind to peanut lectin with the same conformation.[13] Similarly, Glaudemans studied the binding of di-, tri- and tetrasaccharides to three monoclonal antigalactan immunoglobulins, and compared the results with *C*-linked oligosaccharide analogues to understand the hydrogen bonding interactions involved in this process. Both *O*- and *C*-linked oligosaccharides displayed nearly identical affinities to the same proteins and similar ligand-induced tryptophanyl fluorescence changes, which strongly implied that they bound to ligands in nearly identical fashions.[14]

Other studies also confirmed that *C*-glycosides could bind to biological receptors in a similar manner as their native *O*-glycosides.[15] Recently, Franck reported the study of the *C*-glycoside analogue of the immunostimulant α-galactosylceramide (KRN7000), which is an *O*-glycoside with potent antitumor activity (Figure 2.2).[16] The *C*-glycoside analogue was found to be approximately 1000 times more effective than the *O*-glycoside KRN 7000 in reducing the sporozoite levels in mouse livers.

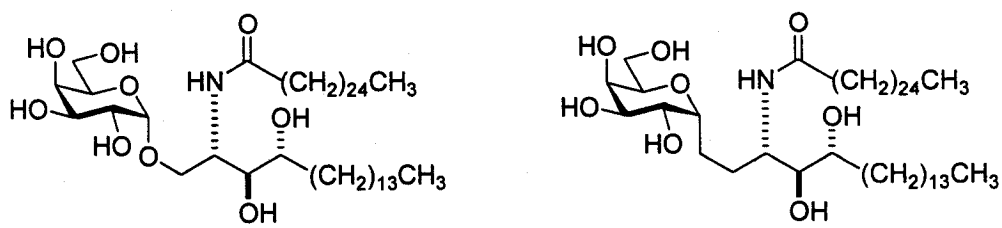

Figure 2.2 Structures of KRN 7000 and its *C*-glycoside analogue.[16]

In summary, previous studies have demonstrated that *C*-linked glycosides have the following characteristics:

1. Improved stability over *O*-linked glycosides against cleavages (chemically and enzymatically).
2. Similar solution conformation to *O*-linked glycosides.
3. Similar binding affinity to the same receptors as *O*-linked glycosides.
4. Similar or enhanced biological activity *in vitro* compared to *O*-linked glycosides.

Given these advantages, it is reasonable to prepare *C*-linked AFGP analogues using an easily accessible synthetic strategy to circumvent the problems of inherent instability and synthetic complexity of native *O*-linked AFGPs. These *C*-linked AFGP analogues can also be used as models for fundamental structure-activity relationship studies.

2.2 Previous Work on *C*-Linked AFGP Analogues: Design, Synthesis and Testing

An AFGP molecule can be considered to be composed of three parts: the disaccharide moiety, the polypeptide backbone moiety and the side chain linker connecting the first two parts (Figure 2.3). All these regions can be modified to form structurally diverse AFGP analogues.

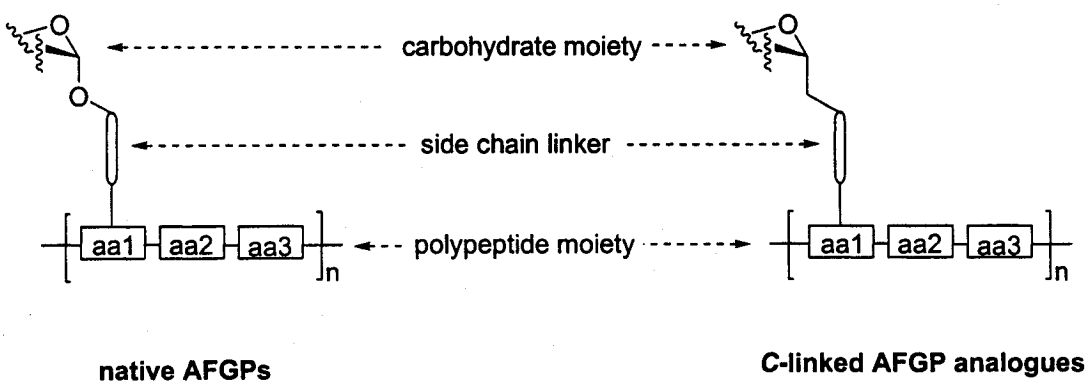

Figure 2.3 Structural comparisons between native *O*-linked AFGPs and their *C*-linked analogues.

Our laboratory has previously explored synthetic routes and successfully prepared a series of *C*-linked AFGP analogues,[17] in which the side chain contains an amide bond connecting the carbohydrate moiety and the polypeptide backbone (Scheme 2.2). This structural modification took advantage of the fact that the L-threonine residues in low molecular mass AFGPs are occasionally replaced by L-arginine, without significant loss of antifreeze-specific activities.[18] In our analogues, the amide bond was used to simulate the guanidine structure in the L-arginine side chain. Although this may seem like a dramatic structural change compared to the native AFGPs, an L-lysine-L-alanine polypeptide was recently reported to display thermal hysteresis activity.[19] For these reasons, either L-lysine or L-ornithine was coupled with *C*-glycosyl carboxylic acids to prepare *C*-linked AFGP analogues.

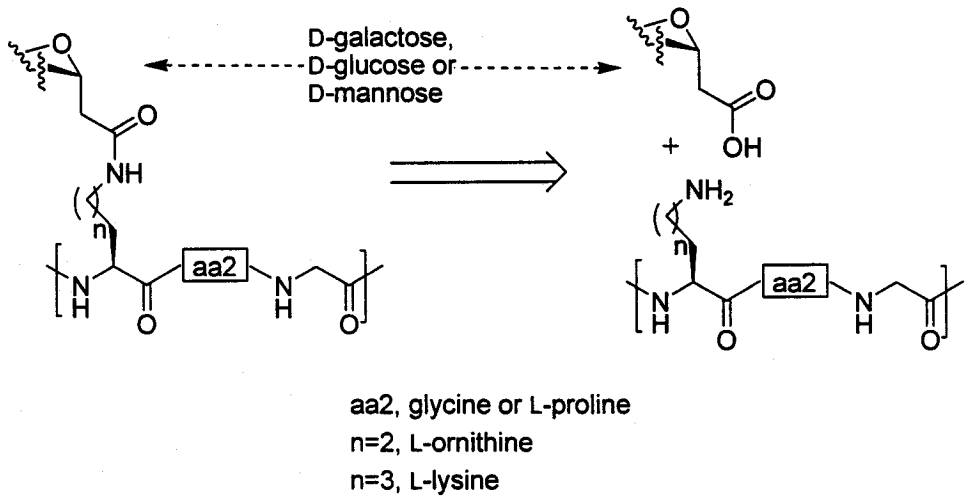

Scheme 2.2 *C*-Linked AFGP analogues prepared in the Ben laboratory.[17]

In addition to the above changes, other structural modifications were implemented. For instance, instead of the disaccharide units in native AFGPs, monosaccharides (including D-galactose, D-glucose and D-mannose) were employed to study how the relative configuration of hydroxyl groups on the pyranose ring might affect antifreeze activities. This structural modification was chosen based on the following reasons. First, replacing disaccharides with monosaccharides can dramatically simplify the synthetic process of AFGP analogues. Secondly and more importantly, the SAR study of AFGPs performed by Feeney demonstrated that the

terminal D-galactose residues are crucial for antifreeze-specific activities.[20] Furthermore, for biologically important oligosaccharide complexes, it has been proposed that the terminal monosaccharide is important for binding to receptors.[21]

In addition to the carbohydrate moiety, structural variations were also made in the other two regions. For example, L-lysine and L-ornithine were each selected as the side chain linker. Although the side chain length of L-lysine and L-ornithine differs by only one methylene group, they can be used as a quick way to study the effect of side chain length on antifreeze-specific activities.

With respect to the polypeptide backbones, the amino acid composition was varied from L-alanine to either glycine or L-proline. At the beginning of this study, glycine was selected to replace L-alanine for constructing polypeptide backbones to avoid any possible racemization of the L-alanine. However, it was later found that the protocol of solid-phase peptide synthesis employed for preparing *C*-linked AFGP analogues resulted in no racemization during coupling sequences. L-Proline was another amino acid used in the preparation of the polypeptides in *C*-linked AFGP analogues. This modification was based upon the fact that in some small native AFGPs, such as AFGP6-AFGP8, it has been found that the first L-alanine after the L-threonine could be occasionally replaced by L-proline. In order to evaluate the effect of this structural feature on antifreeze-specific activities, L-proline was used as one of the components of the polypeptide backbone in some *C*-linked AFGP analogues.

As for the synthetic strategy, both linear (Scheme 2.3)[17b] and convergent (Scheme 2.4)[17a, c] SPPS of *C*-glycosylated AFGP analogues have been utilized by our laboratory. For both strategies, the connection of carbohydrates to amino acids or peptides was accomplished by an amide bond-forming reaction. In the stepwise strategy,[17b] an L-ornithine-glycine-glycine tripeptide unit **39** was first prepared. *C*-Glycosyl acid **38** was then coupled with **39** to give building block **40**, which was assembled on a Wang resin and eventually afforded the *C*-linked AFGP analogue **42**.

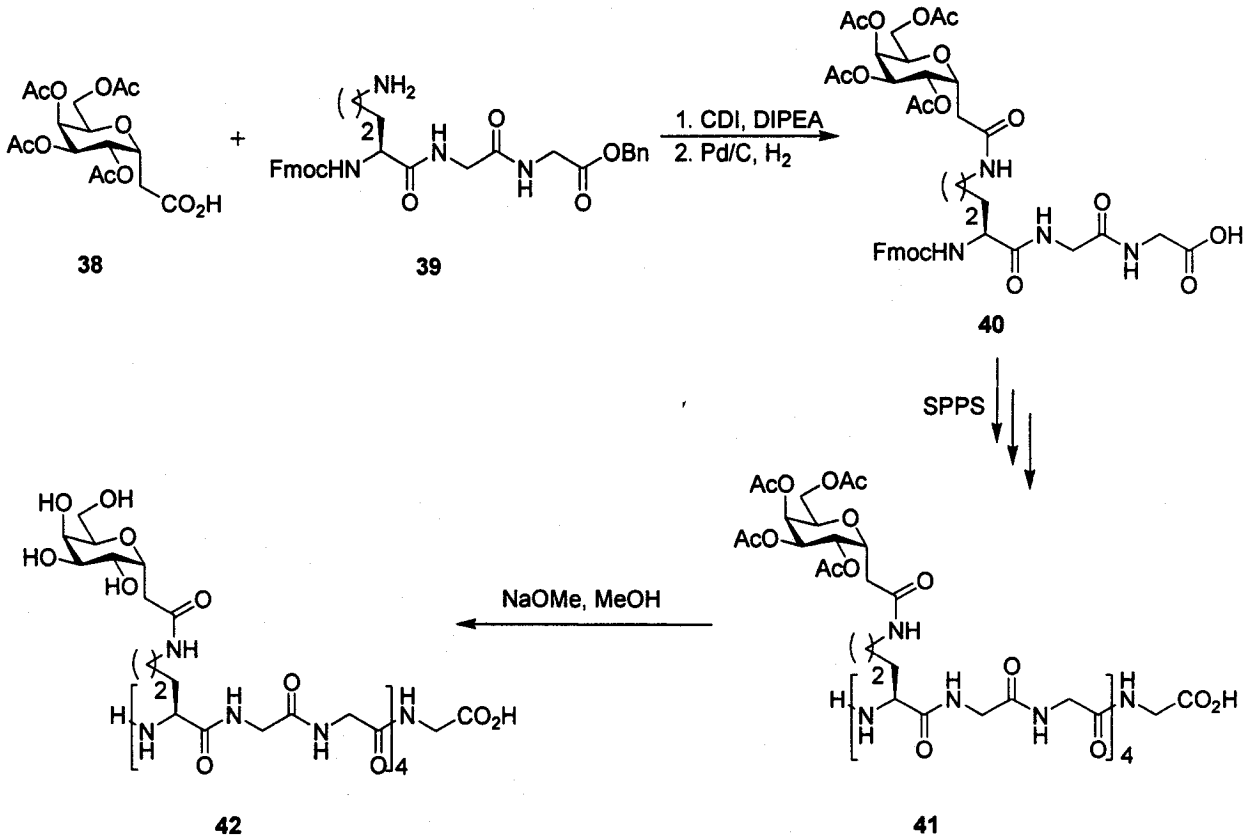

Scheme 2.3 Linear route to prepare *C*-linked AFGP analogues.[17b]

In the convergent strategy,[17a, c] an L-lysine-glycine-glycine tripeptide **43** was used as the building block and assembled to polypeptide **44** on a base-labile HMBA resin. Glycosylation of the ε-amino terminus of L-lysine residues with **38** was performed on the solid support to afford glycopeptide **45**, which after protecting group manipulation furnished analogue **46**.

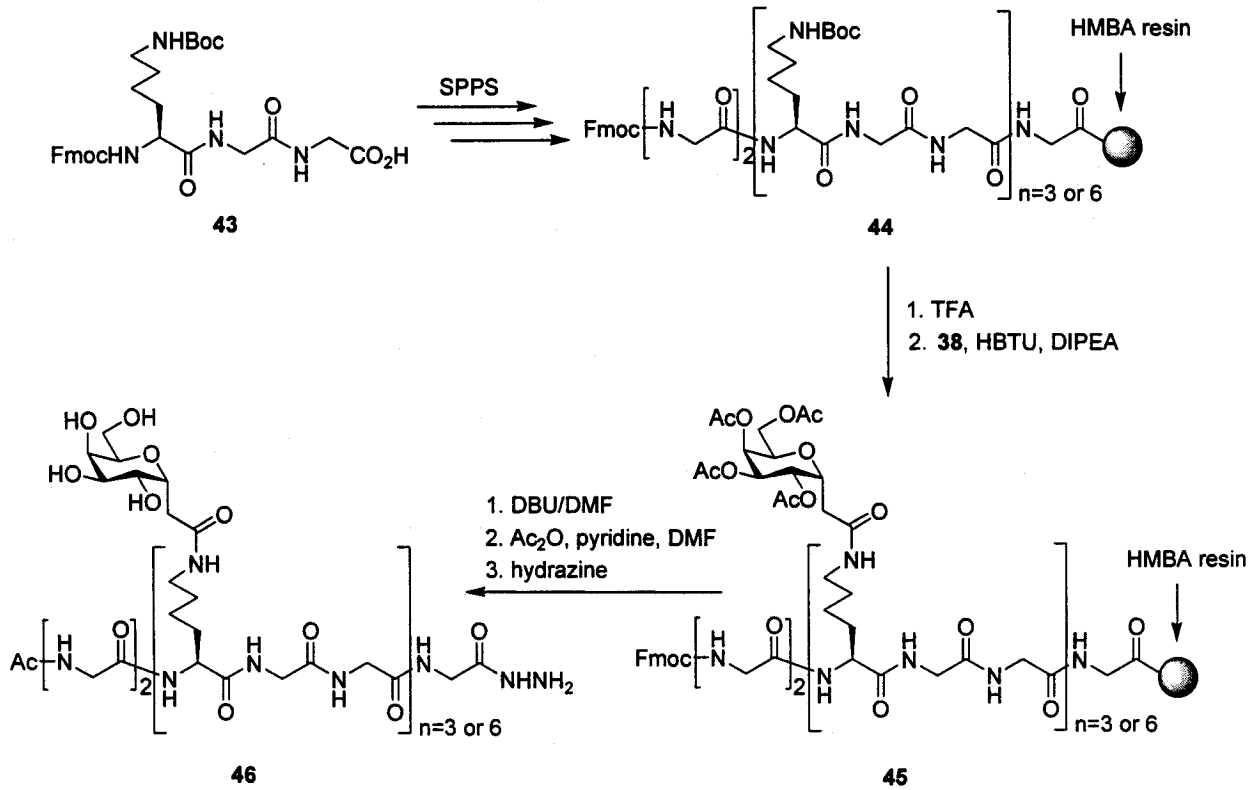

Scheme 2.4 Convergent route to prepare *C*-linked AFGP analogues.[17a,c]

The linear SPPS proved to be a more reliable and efficient method, which afforded AFGP analogues in better chemical yields than the convergent route.[22] In addition, assembling polypeptides in a stepwise fashion allows one to conveniently modify any amino acid residue. This synthetic approach has been employed and a series of *C*-linked AFGP analogues have been successfully prepared (Figure 2.4).[22]

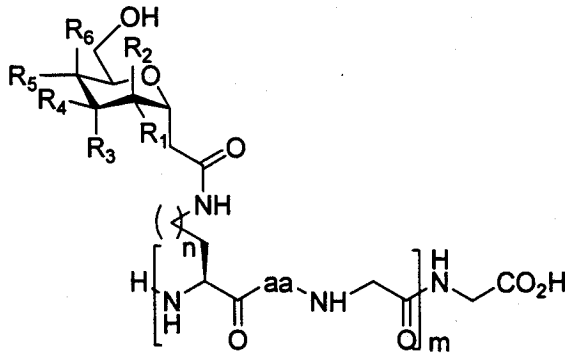

42, aa=glycine; n=2; m=4; R_1, R_4, R_6=OH (D-galactose); R_2, R_3, R_5=H
47, aa=glycine; n=2; m=4; R_1, R_4, R_5=OH (D-glucose); R_2, R_3, R_6=H
48, aa=glycine; n=2; m=4; R_2, R_4, R_5=OH (D-mannose); R_1, R_3, R_6=H

49, aa=L-proline; n=3; m=4; R_1, R_4, R_6=OH (D-galactose); R_2, R_3, R_5=H
50, aa=L-proline; n=3; m=4; R_1, R_4, R_5=OH (D-glucose); R_2, R_3, R_6=H
51, aa=L-proline; n=3; m=4; R_2, R_4, R_5=OH (D-mannose); R_1, R_3, R_6=H

52, aa=glycine; n=3; m=3; R_1, R_4, R_6=OH (D-galactose); R_2, R_3, R_5=H
53, aa=glycine; n=3; m=4; R_1, R_4, R_6=OH (D-galactose); R_2, R_3, R_5=H
54, aa=glycine; n=3; m=6; R_1, R_4, R_6=OH (D-galactose); R_2, R_3, R_5=H
55, aa=glycine; n=3; m=9; R_1, R_4, R_6=OH (D-galactose); R_2, R_3, R_5=H

Figure 2.4 Structure of previously prepared *C*-linked AFGP analogues.[17,22]

The structures of some analogues previously prepared by the Ben laboratory are shown in Figure 2.4. Assessment of antifreeze-specific activities of these *C*-linked AFGP analogues was performed using a nanoliter osmometry assay and a recrystallization inhibition (RI) assay.[22] Analogues **54** and **55**, which are composed of six and nine L-lysine-(D-galactose)-glycine-glycine tripeptide repeating units respectively, displayed weak TH activity of 0.056 °C. However, all other analogues did not display TH or dynamic ice-shaping (DIS) abilities.

In contrast to the above, many analogues displayed very potent recrystallization inhibition (RI) abilities as shown in Figure 2.5. In this figure, the Y-axis represents the mean largest grain size (MLGS). Ice grains are regarded as two dimensions and MLGS is measured as the average size of ice grain surface areas.[23]

D-Galactose was found to be the most effective monosaccharide for RI activity as evidenced by analogues **42** and **47-51**. Analogues **42**, **47** and **48** have the same four L-ornithine-glycine-glycine tripeptide repeating units in the polypeptide backbone but a different monosaccharide on

the L-ornithine residue (D-galactose for analogue **42**, D-glucose for analogue **47** and D-mannose for analogue **48**). Analogue **42** demonstrated the most potent RI activity, which was about 80% as efficient as the native AFGP8 at concentrations around 10^{-6} M (about 0.1 mg/mL) in phosphate-buffered saline (PBS) solution. However, analogues **47** and **48** displayed very limited or no RI activity. In addition, the RI activities of analogues **49-51**, all containing four L-lysine-L-proline-glycine tripeptide repeating units but different monosaccharides (D-galactose for analogue **49**, D-glucose for analogue **50** and D-mannose for analogue **51**), displayed the same trend. With the same concentration in PBS, analogue **49** displayed better RI activity than analogues **50** and **51**. Collectively, these results suggested that the hydroxyl groups at C2 and C4 on the pyranose ring of D-galactose are important for analogues to interact with the ice lattice.

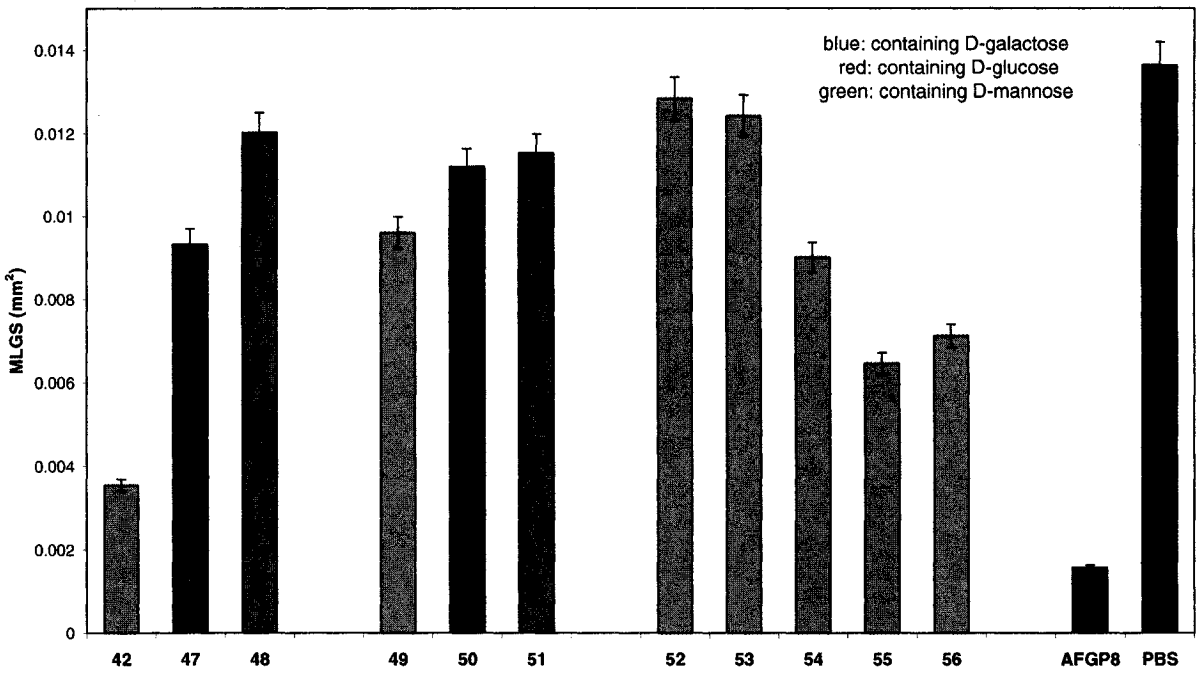

Figure 2.5 RI activity of AFGP8 and previously prepared *C*-linked AFGP analogues (10^{-6} M in PBS).[22]

The effect of the polypeptide length on antifreeze-specific activities was also illustrated by these analogues. Analogue **55** with nine L-lysine-(D-galactose)-glycine-glycine tripeptide repeating units displayed better RI activity than analogues with six (**54**), four (**53**) and three (**52**)

tripeptide repeats. This trend is similar to native AFGPs where larger fractions show more potent thermal hysteresis activity than smaller fractions.[24]

The importance of the carbohydrate concentration on antifreeze-specific activity was studied with the divalent *C*-linked AFGP analogue **56** (Figure 2.6). This analogue possesses two D-galactose residues on the same L-lysine residue in the polypeptide backbone. The total number of D-galactose residues in this analogue is eight. The RI activity of **56** was found to be between that of α-D-galactose monosaccharide analogues with six (**54**) and nine (**55**) tripeptide repeats, indicating that the RI activity of these *C*-linked analogues is proportional to the carbohydrate concentration. In addition, the difference in RI activity between analogues **56** and **55** is very small (about 9%). Both analogues possess similar carbohydrate concentrations but very different polypeptide length (four tripeptide repeats for **56** and nine for **55**). This indicated that the carbohydrate concentration might play a more important role than the polypeptide length in affecting RI activity.

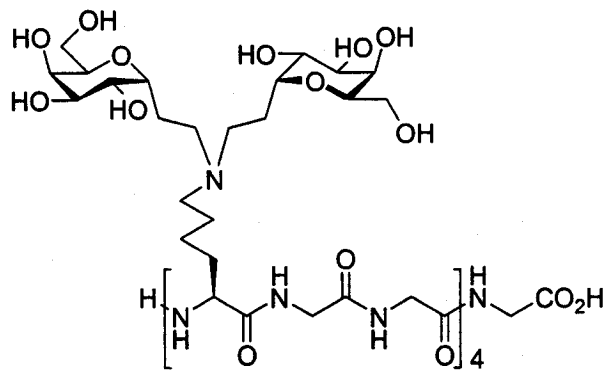

56

Figure 2.6 Structure of divalent *C*-linked AFGP analogue.[22b]

The most surprising result is the difference in RI activities observed in analogues containing L-ornithine and those containing L-lysine. Replacing the L-lysine residue in analogue **53** with L-ornithine resulted in analogue **42** with an eight-fold improvement in RI activity at concentrations around 10^{-6} M (about 0.1 mg/mL) in PBS solution. L-Ornithine has almost the same structure as L-lysine except there is one less methylene in the side chain. This suggested that an optimal side

chain length exists in these *C*-linked AFGP analogues and is important for the RI activity. However, it is necessary to point out that the length may not be the only factor in the side chain that affects RI activity. For instance, the side chain in analogue **42** is much longer than in native AFGPs, which contain an L-threonine side chain with only one methylene group and one oxygen atom. However, analogue **42** still demonstrated comparable RI activity to AFGP8. Therefore, it is reasonable to hypothesize that the relatively rigid amide bond in *C*-linked AFGP analogues such as **42** may also play an important role in RI activity.

Another conclusion drawn from this study is that the TH and RI activities of antifreezes are not necessarily associated with each other, which is in agreement with previously published results.[25] Except for analogues **54** and **55** that displayed weak TH activity (0.06 °C), most *C*-linked AFGP analogues only demonstrated RI activity. However, it seems true that analogues with TH activity always show RI activity. This phenomenon can be explained by the fact that both RI and TH activities require binding of antifreeze molecules to ice lattices. However, in order to display TH activity, the strict match and effective interactions between periodically spaced binding sites on antifreeze molecules and ice lattices are required. Furthermore, the binding needs to be strong enough to prevent ice from growing on the binding sites. On the other hand, RI is considered to be the result of inhibiting ice-water interface migration after the adsorption of antifreeze molecules.[23] The adsorption at the solid-liquid interface may not need to be as effective as the tight binding required for TH activity.

2.3 Research Goals and Objectives

The ultimate goal of this study is to develop stable *C*-linked AFGP analogues that can be used as efficient protecting agents for the cryopreservation of cells, tissues and organs to improve their viability after freezing. To date, the largest freezing point depression of native biological antifreezes is about -5 to -6 °C.[26] However, in the biomedical industry, the temperature employed for cryopreservation is far below this range. For example, cells are usually stored in liquid nitrogen at -196 °C. At temperatures below the thermal hysteresis gap of biological antifreezes, it is well known that ice crystals will form needle-shaped spicules which can exacerbate cellular damage. This destructive effect of biological antifreezes has been used as an adjuvant in

cryosurgery to remove the undesired tumor cells (Section 1.5.2).[27] Therefore, in the field of cryopreservation, thermal hysteresis is not a desirable property. The protecting effects of antifreezes at such low temperatures come from their ability to inhibit recrystallization. Overall, the ideal cryoprotecting agents should possess potent RI activity and no TH ability.

With this in mind, there are two major objectives in this dissertation. The first objective is to develop novel *C*-linked AFGP analogues possessing no TH but potent RI activities and perform structure-activity relationship studies to understand the mechanism of action of these analogues. In addition, in order to facilitate the application of antifreezes in cell cryopreservation, the second objective is to study the *in vitro* cytotoxicity and interactions of AFGP8 and our *C*-linked AFGP analogues.

2.3.1 The Design of New *C*-Linked AFGP Analogues

The major structural modifications made in previously prepared *C*-linked AFGP analogues by our laboratory have centered on the substitution of the disaccharide units and L-alanines in native AFGPs by monosaccharides and glycines, respectively. Since these analogues, especially analogue **42** containing four L-ornithine-(D-galactose)-glycine-glycine tripeptide repeating units, demonstrated comparable RI activity to AFGP8 but very weak or no TH activity, it suggested that the disaccharide and L-alanine residues in native AFGPs are not the essential structural motifs for RI, but are important for TH. For this reason, we have decided to retain these features in subsequent *C*-linked AFGP analogues. Consequently, D-Galactose was used as the carbohydrate moiety and the glycine residues were used instead of L-alanines to prepare the new generation of *C*-linked AFGP analogues.

By preparing and studying the antifreeze-specific activities of the analogues described in this thesis, we hope to better understand the following issues:

1. The effect of the rigid amide bond in the side chain of *C*-linked AFGP analogues.
2. The effect of the side chain length on antifreeze-specific activities.
3. Assess whether a C2-acetamide group in a galactosamine residue of *C*-linked AFGP analogues has any desirable effects for RI activity.

4. The importance of the polypeptide backbone.

2.3.1.1 Investigating the Effect of Side Chain Length and the Potential Role of the Amide Bond in the Side Chain Using *C*-Linked Galactosyl AFGP Analogues 57-59

One of the unanswered questions about previously prepared *C*-linked AFGP analogues is regarding the importance of the amide bond in the side chain for antifreeze-specific activities. Besides the introduction of the amide bond, these analogues possess side chains that are at least four covalent bonds longer than that in the native AFGPs. Given this, it was difficult to evaluate the function of the rigid amide bond or the elongated side chain length because both structural modifications were introduced into analogues at the same time. For this reason, we wish to design a new version of carbon-linked AFGP analogues where the side chain is composed only of methylene groups (Figure 2.7).

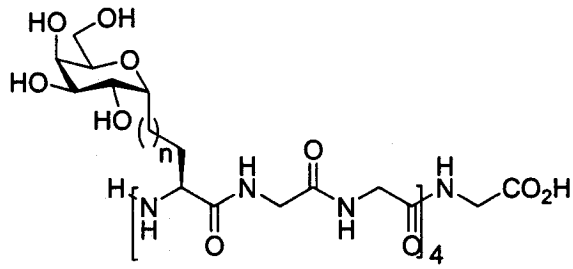

n=1, **57**
n=2, **58**
n=3, **59**

Figure 2.7 Structures of new generation of *C*-linked AFGP analogues **57-59**.

Previous *C*-linked AFGP analogues have indicated the importance of the side chain length. For example, only one carbon-carbon bond difference in the length of the side chain can affect the RI activity dramatically (analogues **42** and **53**). To further verify this observation, we want to vary the length of side chain in the new analogues. As illustrated in Figure 2.7, the length of the side chain in the new generation of *C*-linked AFGP analogues varies from three to five single carbon-carbon bonds (**57-59**). Analogue **57** is particularly attractive as the side chain is only

composed of three covalent bonds, which is approximately the same length as in native AFGPs. In this case, the major side chain difference from native AFGPs in analogue **57** is the oxygen-replaced methylene group. These analogues can clarify whether the side chain length is still an important factor for RI activity when the rigid amide bonds are not present in *C*-linked AFGP analogues.

The methyl group on the L-threonine residue in native AFGPs has been reported to be an important structural motif for TH activity.[28] Since one of the major goals of this study is to develop novel *C*-linked AFGP analogues with no TH but potent RI activities, the methyl group on the L-threonine residue is removed in the new generation of *C*-linked AFGP analogues. Furthermore, this structural modification can simplify the synthesis. Consequently, D-galactose is attached to a carbon-version of the L-serine residue.

Based on the insight from previously prepared *C*-linked AFGP analogues, the length of four tripeptide repeats is sufficient to show RI activity. Therefore, the glycopeptide length of four tripeptide repeats is employed in this study. In addition, this polypeptide length is used to simulate native AFGP8, which has the same number of tripeptide repeating units. The antifreeze-specific activities of the new generation of *C*-linked analogues are compared to AFGP8.

2.3.1.2 Investigating the Role of the C2-Acetamide Group Using *C*-Linked GalNAc Analogue 60

Another important structural motif in native AFGPs that we wish to study is the acetamide group (AcNH-) at the C2 position of the galactosamine residue. In biologically important glycoproteins, *N*-Acetyl-galactosamine is the most common motif as the terminal monosaccharide in oligosaccharide complexes to be connected to either L-serine or L-threonine residues.[6a] Studies by Nishimura[28] suggested that the *N*-acetyl methyl groups are important components for forming the hydrophobic portion of AFGPs' overall amphipathic conformation. In addition, NMR studies have suggested that the nitrogen proton in the acetamide group can form hydrogen bonds with the carbonyl oxygen of the L-threonine residue in the polypeptide backbone, which may have important conformational implications for native AFGPs.[29] Furthermore, although the C2-acetamide group has been proven to be important for TH

activity,[28] there have been no reports about its role in RI activity. For these reasons, the target analogue **60** is designed to use *N*-acetyl-galactosamine (GalNAc) as the carbohydrate moiety (Figure 2.8). The remaining parts of the analogue are maintained as in *C*-galactosyl AFGP analogue **57**. By comparing analogue **60** with analogue **57**, we can find out how the introduction of the acetamide group can affect the antifreeze-specific activities.

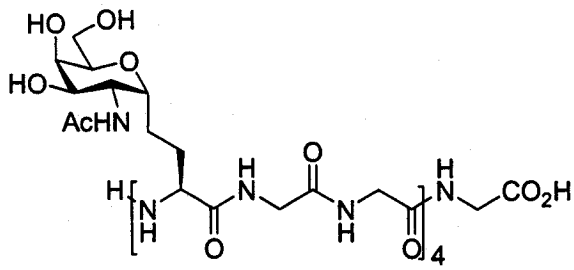

60

Figure 2.8 Structure of *C*-linked GalNAc AFGP Analogue **60**.

2.3.1.3 Investigating the Importance of a Polypeptide Backbone Using *C*-Galactosyl Norbornene Neoglycopolymer 61

The polypeptide backbone is a major structural component of AFGPs. To date, most studies of this structural motif have been focused on the effect of the length of the polypeptide chain on antifreeze-specific activities.[22a, 28] However, native AFGPs isolated from Teleost fish differ not only in their size, but also in their amino acid compositions. For example, in short AFGPs, it has been found that the first L-alanine following the L-threonine in the tripeptide repeat is occasionally replaced by L-proline.[18] The L-threonine can also be substituted by L-arginine in some fish species such as Arctic cods.[18] Despite these structural differences in the polypeptide backbone, similar antifreeze activity is shown for AFGPs of approximately the same size. Therefore, studies need to be performed to determine whether the polypeptide backbone is really necessary for antifreeze activity. The neoglycopolymer **61** (Figure 2.9) will serve as a good analogue for studying the function of the polypeptide backbone. In this analogue, the polymeric chain is composed of alternating ethylene groups and cyclopentane rings, which is derived from a *C*-galactosyl norbornene derivative by ring-opening metathesis polymerization (ROMP).

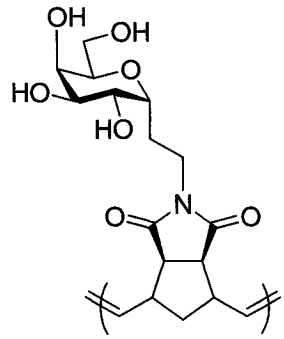

61

Figure 2.9 Structure of *C*-galactosyl norbornene neoglycopolymer **61**.

2.3.2 Studying the *In Vitro* Cytotoxicity and Interactions of AFGP8 and *C*-Linked AFGP Analogues

AFGPs' unique antifreeze-specific activities have rendered them potential candidates for use in a wide variety of applications including the agriculture, food and biomedical industries. To date, most studies on AFGPs have been performed to elucidate important structural motifs and understand the structure-activity relationship so that we can design analogues with more potent functions and improved stability. However, in order to realize their various applications, it is essential to learn whether natural AFGPs and their analogues have any toxic effects because this will prohibit the application of AFGPs.

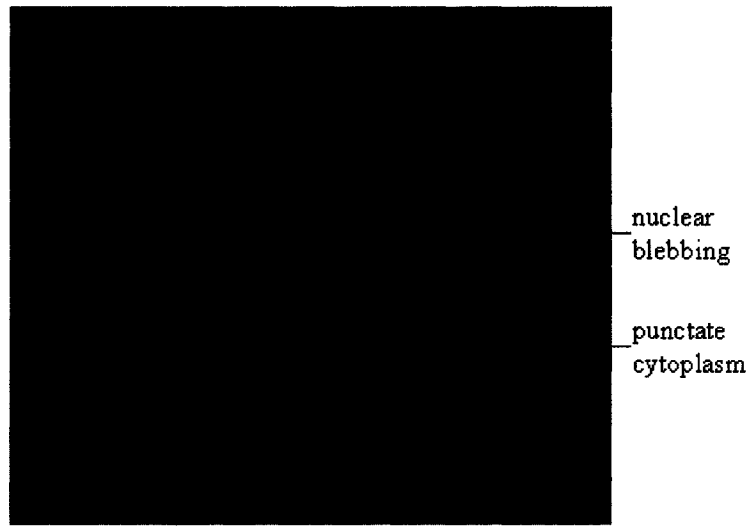

Figure 2.10 Human embryonic liver cells incubated with AFGP8 at 37 °C.

Figure 2.10 is a confocal microscopic image of human embryonic liver cells (WRL68, ATCC) incubated with AFGP8 for 50 minutes at 37 °C. After incubation, human embryonic liver cells displayed some abnormal morphological signs, such as the nuclear blebbing (protrusion on nuclear membrane and chromatin) and punctate structures in the cytoplasm, which are consistent with dying cells. This suggested that AFGP8 might be cytotoxic to human embryonic liver cells. Therefore, we decided to study whether AFGP8 shows any cytotoxic effects to human cells and also investigate the *in vitro* interactions of AFGP8 and *C*-linked AFGP analogues.

In summary, this dissertation will address the following areas:

1. Prepare novel *C*-linked AFGP analogues by chemical synthesis and elucidate important structural features for antifreeze activity. Such structural motifs include the rigid amide bond in previous *C*-linked AFGP analogues, the length of glycoprotein side chain, the C2-acetamide group in the galactosamine residue and the polypeptide backbone.
2. Evaluate the *in vitro* cytotoxicity and interactions of native AFGP8 and *C*-linked AFGP analogues.

The successful fulfillment of this study will improve the current understanding on the mechanism of action of AFGPs and facilitate the development of stable *C*-linked AFGP analogues which can be used as potent recrystallization inhibitors for cell cryopreservation. In addition, this study can help realize other applications of AFGPs and analogues in biomedical science (such as improving the efficiency of cryosurgery) and food industry (such as improving the flavor and reducing the nutritional loss of frozen food).

References

1. (a) Dwek, R. A. *Chem. Rev.* **1996**, *96*, 683-720.
   (b) Varki, A. *Glycobiology* **1993**, *3*, 97-130.
2. (a) Helenius, A. *Mol. Biol. Cell* **1994**, *5*, 253-265.
   (b) Trombetta, E. S., Helenius, A. *Curr. Opin. Struct. Biol.* **1998**, *8*, 587-592.
   (c) Helenius, A., Aebi, M. *Science* **2001**, *291*, 2364-2369.
3. Opdenakker, G., Rudd, P. M., Ponting, C. P., Dwek, R. A. *FASEB J.* **1993**, *7*, 1330-1337.
4. (a) Ritter, T. K., Wong, C.-H. *Angew. Chem. Int. Ed.* **2001**, *40*, 3508-3533
   (b) Nicolaou, K. C., Boddy, C. N. C., Bräse, S., Winssinger, N. *Angew. Chem. Int. Ed.* **1999**, *38*, 2096-2152.
5. http://bssv01.lancs.ac.uk/gig/pages/gag/carbbank.htm.
6. (a) Vliegenthart, J. F. G., Casset, F. *Curr. Opin. Struct. Biol.* **1998**, *8*, 565-571.
   (b) Davis, B. G. *Chem. Rev.* **2002**, *102*, 579-601.
7. (a) Hofsteenge, J., Müller, D. R., de Beer, T., Löffler, A., Richter, W. J., Vliegenthart, J. F. G. *Biochemistry* **1994**, *33*, 13524-13530.
   (b) de Beer, T., Vliegenthart, J. F. G., Löffler, A., Hofsteenge, J. *Biochemistry* **1995**, *34*, 11785-11789.
8. (a) Marcaurelle, L. A., Bertozzi, C. R. *Chem. Eur. J.* **1999**, *5*, 1384-1390.
   (b) Boons, G. J., Hale, K. J. *Organic Synthesis with Carbohydrates*, Blackwell Science: Malden, MA. **2000**, pp. 156-160.
9. (a) Sparks, M. A., Williams, K. W., Whitesides, G. M. *J. Med. Chem.* **1993**, *36*, 778-783.
   (b) Kutterer, K. M. K., Barnes, M. L., Arya, P. *J. Comb. Chem.* **1999**, *1*, 28-31.
10. Kishi, Y. *Pure Appl. Chem.* **1993**, *65*, 771-778.
11. (a) Wu, T.-C., Goekjian, P. G., Kishi, Y. *J. Org. Chem.* **1987**, *52*, 4819-4823.
    (b) Goekjian, P. G., Wu, T.-C., Kang, H.-Y., Kishi, Y. *J. Org. Chem.* **1987**, *52*, 4823-4825.
    (c) Babirad, S. A., Wang, Y., Goekjian, P. G., Kishi, Y. *J. Org. Chem.* **1987**, *52*, 4825-4827.
    (d) Goekjian, P. G., Wu, T.-C., Kishi, Y. *J. Org. Chem.* **1991**, *56*, 6412-6422.
    (e) Haneda, T.; Goekjian, P. G., Kim, S. H., Kishi. Y. *J. Org. Chem.* **1992**, *57*, 490-498.
    (f) Wei, A., Kishi, Y. *J. Org. Chem.* **1994**, *59*, 88-96.

12. Wei, A., Boy, K. M., Kishi, Y. *J. Am. Chem. Soc.* **1995**, *117*, 9432-9436.

13. Ravishankar, R., Surolia, A., Vijayan, M., Lim, S., Kishi, Y. *J. Am. Chem. Soc.* **1998**, *120*, 11297-11303.

14. Wang, J., Kováč, P., Sinaÿ, P., Glaudemans, C. P. J. *Carbohydr. Res.* **1998**, *308*, 191-193.

15. (a) Bertozzi, C., Bednarski, M. *Carbohydr. Res.* **1992**, *223*, 243-253.
(b)Bertozzi, C. R., Cook, D. G., Kobertz, W. R., Gonzalez-Scarano, F., & Bednarski, M. D. *J. Am. Chem. Soc.* **1992**, *114*, 10639-10641.
(c) Nagy, J. O., Wang, P., Gilbert, J. H., Schaefer, M. E., Hill, T. G., Callstrom, M. R., Bednarski, M. D. *J. Med. Chem.* **1992**, *35*, 4501-4502.
(d) Sparks, M. A., Williams, K. W., Whitesides, G. M. *J. Med. Chem.* **1993**, *36*, 778-783.
(e) Weatherman, R. V., Mortell, K. H., Chervenak, M., Kiessling, L. L., Toone, E. J. *Biochem.* **1996**, *35*, 3619-3624.
(f) Weatherman, R. V., Kiessling, L. L. *J. Org. Chem.* **1996**, *61*, 534-538.

16. Yang, G. L., Schmieg, J., Tsuji, M., Franck, R. W. *Angew. Chem. Int. Ed.* **2004**, *43*, 3818-3822.

17. (a) Ben, R. N., Eniade, A. A., Hauer, L. *Org. Lett.* **1999**, *1*, 1759-1762.
(b) Eniade, A., Ben, R. N. *Biomacromolecules* **2001**, *2*, 557-561.
(c) Eniade, A., Murphy, A. V., Landreau, G., Ben, R. N. *Bioconjugate Chem.* **2001**, *12*, 817-823.

18. Harding, M. M., Anderberg, P. I., Haymet, A. D. J. *Eur. J. Biochem.* **2003**, *270*, 1381-1392.

19. Wierzbicki, A., Knight, C. A., Rutland, T. J., Muccio, D. D., Pybus, B. S., Sikes, C. S. *Biomacromolecules* **2000**, *1*, 268-274.

20. (a) Komatsu, S. K., DeVries, A. L., Feeney, R. E. *J. Biol. Chem.* **1970**, *245*, 2909-2913.
(b) Ahmed, A. I., Yeh, Y., Osuga, D. T., Feeney, R. E. *J. Biol. Chem.* **1976**, *251*, 3033-3036.

21. St. Hilaire, P. M., Lowary, T. L., Meldal, M., Bock, K. *J. Am. Chem. Soc.* **1998**, *120*, 13312-13320.

22. (a) Eniade, A., Purushotham, M., Ben, R. N., Wang, J. B., Horwath, K. *Cell Biochem. Biophys.* **2003**, *38*, 115-124.

(b) Murphy, A. V. "Preparation of structurally diverse C-linked antifreeze antifreeze glycoprotein analogues and assessment for antifreeze protein-specific activity" PhD Thesis, Binghamton University (S. U. N. Y.), 2004.

23. Knight, C. L., Wen, D. Y., Laursen, R. A. *Cryobiology* **1995**, *32*, 23-34.
24. Tomczak, M. M., Marshall, C. B., Gilbert, J. A., Davies, P. L. *Biochem. Biophys. Res. Commun.* **2003**, *311*, 1041-1046.
25. (a) Sidebottom, C., Buckley, S., Pudney, S. P., Twigg, S., Jarman, C., Holt, C., Telford, J., McArthur, A., Warrall, D., Hubbard, R., Lillford, P. *Nature* **2000**, *406*, 256.
(b) Horwath, K. L., Easton, C. M., Poggioli Jr., G. J., Myers, K., Schnorr, L. *Eur. J. Entomol.* **1996**, *93*, 419-433.
26. Davies, P. L., Baardsnes, J., Kuiper, M. J, Walker, V. K. *Phil. Trans. R. Soc. Lond. B* **2002**, *357*, 927-935.
27. (a) Muldrew, K., Rewcastle, J., Donnelly, B. J., Saliken, J. C., Liang, S., Goldie, S., Olson, M., Baissalov R., Sandison, G. *Cryobiology* **2001**, *42*, 182-189.
(b) Koushafar, H., Rubinsky, B. *Urology* **1997**, *49*, 421-425.
(c) Koushafar, H., Pham, L., Lee, C., Rubinsky, B. *J. Surg. Oncol.* **1997**, *66*, 114-121.
(d) Pham, L., Dahiya, R., Rubinsky, B. *Cryobiology* **1999**, *38*, 169-175.
28. Tachibana, Y., Fletcher, G. L., Fujitani, N., Tsuda, S., Monde, K., Nishimura, S. *Angew. Chem. Int. Ed.* **2004**, *43*, 856 –862.
29. (a) Yeh, Y., Feeney, R. E. *Chem. Rev.* **1996**, *96*, 601-618.
(b) Mimura, Y., Yamamoto, Y., Inoue, Y., Chujo, R. *Int. J. Bio. Macromol.* **1992**, *14*, 242-248.

Chapter 3 Preparation of *C*-Linked AFGP Analogues

3.1 Strategies for Preparing *C*-Linked AFGP Analogues

Using solid-phase peptide synthesis (SPPS) to assemble amino acids and glycosyl amino acid building blocks in a stepwise fashion has proven to be an efficient and reliable strategy to prepare AFGP analogues.[1] One important feature of this method is that we can perform structural modifications on any specific amino acid residues or building blocks. Two protocols, *tert*-butyloxycarbonyl (Boc) chemistry and 9-fluorenylmethoxycarbonyl (Fmoc) chemistry have been widely used in SPPS.

In the Boc protocol, strong acids such as trifluoroacetic acid (TFA) are used to remove the Boc protecting group to give the free amine for the next coupling reaction. The strongly acidic conditions limit its application to prepare acid-sensitive *O*-linked AFGPs and analogues. In addition, the final cleavage of glycopeptides from resins requires the use of highly dangerous hydrofluoric acid, which can only be performed in specially designed instruments instead of the regular solid-phase synthesizer. However, the special instruments for using hydrofluoric acid are not available in most laboratories, further limiting the use of the Boc protocol. On the other hand, in the Fmoc protocol, the Fmoc protecting group can be easily removed under mild basic conditions. The cleavage of the final polypeptides from resins can be accomplished using TFA. For these reasons, we decided to use the Fmoc chemistry-based SPPS to prepare *C*-linked AFGP analogues **57-60** from *N*-Fmoc protected *C*-glycosyl amino acid building blocks **62-65**, respectively (Scheme 3.1).

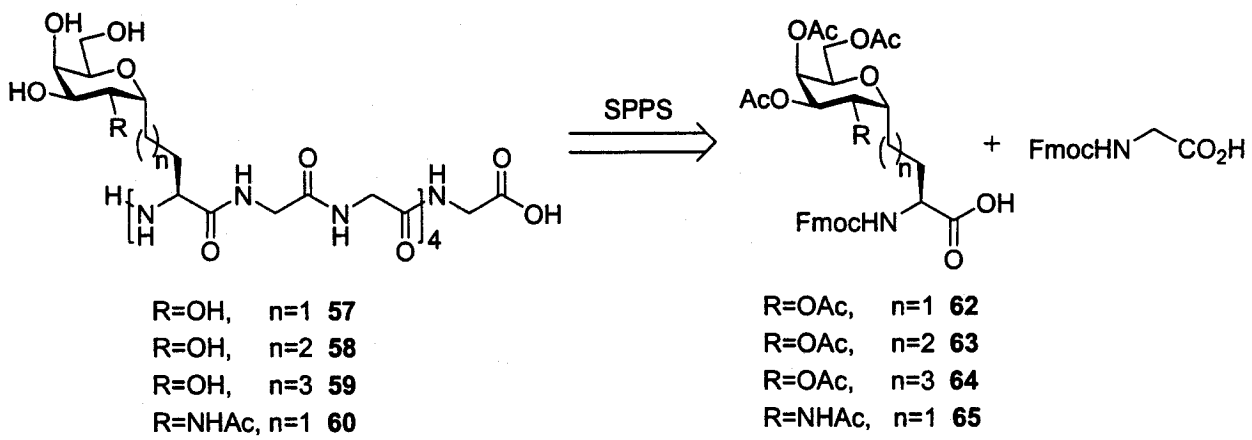

Scheme 3.1 Preparation of *C*-linked AFGP analogues **57-60** by SPPS.

3.1.1 Strategies for Preparing *C*-Glycosyl Amino Acid Derivatives

Several methods have been reported to prepare *C*-linked glycosyl amino acid derivatives and two comprehensive reviews have been published.[2] Bednarski first designed an efficient route to prepare a *β*-*C*-linked glycosyl serine compound (Scheme 3.2).[3] The L-stereocenter of the *α*-amino acid was derived from a chiral Wittig reagent **67**. The key step was the coupling of *C*-galactoside **66** with the amino acid equivalent **67** via Wittig olefination to afford glycoconjugate **68**. The advantage of this method is that the anomeric configuration of glycosides can be preset and is not affected by the subsequent coupling reaction with amino acid equivalents. One drawback of this strategy is that the chiral Wittig reagent **67** needs to be prepared form a serine derivative via five steps and upon coupling with glycoside **66**, it requires additional multi-step manipulations to regenerate the *α*-amino acid structure.

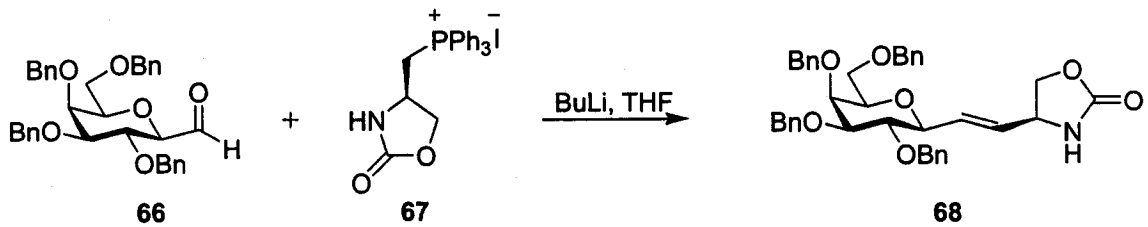

Scheme 3.2 Bednarski's strategy to prepare *C*-glycoconjugates.[3]

Later, Dondoni[4] also demonstrated the feasibility to prepare *C*-glycosyl amino acids using Wittig olefination. Other methods, such as Taylor's strategy of using the Ramberg-Bäcklund rearrangement[5] and Nolen's stereoselective alkylation of Williams' chiral glycine enolate equivalent with a *C*-glycosyl iodide,[6] also demonstrated success in preparing *C*-glycoconjugates. Furthermore, many studies have been performed to explore the feasibility of preparing *C*-glycoconjugates by direct glycosylation. These methods all involve the use of glycosides and chiral amino acid equivalents to stereoselectively form the *C*-linked glycosidic bond at the anomeric center. Toward this end, different intermediates (Figure 3.1), such as glycal **69**,[7] glycosyl pyridyl sulfone **70**[8] and glycosyl trichloroacetimidate **71**,[9] have been used as glycosides for the stereoselective glycosylation.

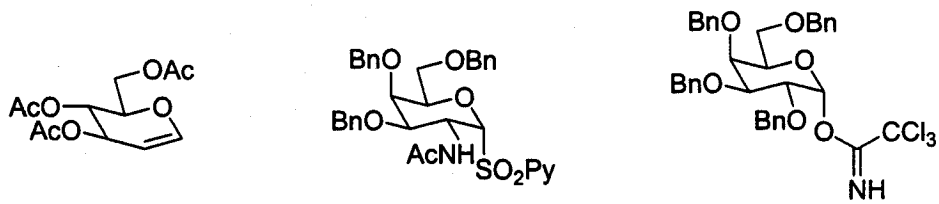

69 **70** **71**

Figure 3.1 Glycosides used in stereoselective glycosylation.[7-9]

Although these strategies, along with many similar published methods,[10] have been employed to prepare *C*-glycosyl amino acids, problems such as low chemical yields and/or low stereoselectivity still exist and limit their application. For example, the harsh reaction conditions for generating enolates in the chiral alkylation strategy restrict the scope of protecting group selection on the carbohydrate moieties.[6] In addition, after glycosylation reactions, additional multi-step manipulations are required to convert chiral amino acid precursors to final products.[3, 6]

In a different strategy, Toone described a novel way to prepare *C*-glycosyl serine derivatives **74** with high efficiency (Scheme 3.3).[11] The key step was the asymmetric hydrogenation of *C*-glycosyl enamide ester **72** by chiral rhodium catalyst **73**. The configuration of the α-carbon in the glycine moiety was controlled by the chirality of alkyl substituents on the DuPHOS residue in the rhodium catalyst. The hydrogenation of *C*-glycosyl enamide ester was highly diastereoselective. *S*-substituted catalysts gave mainly L-amino acid derivatives and *R*-substituted

catalysts gave major D-amino acid products. The high diastereoselectivity of the asymmetric hydrogenation made it possible to prepare *C*-glycosyl amino acids with any desired combination of α, β-glycosides and L, D-amino acids. In addition, the catalysts that were used proved to be compatible with many protecting groups normally used for carbohydrates and amino acids. This strategy was also used to successfully prepare a *C*-linked glycosyl serine analogue of the P^K trisaccharide recognition domain of the glycolipid receptor for shiga and shiga-like toxins.[12]

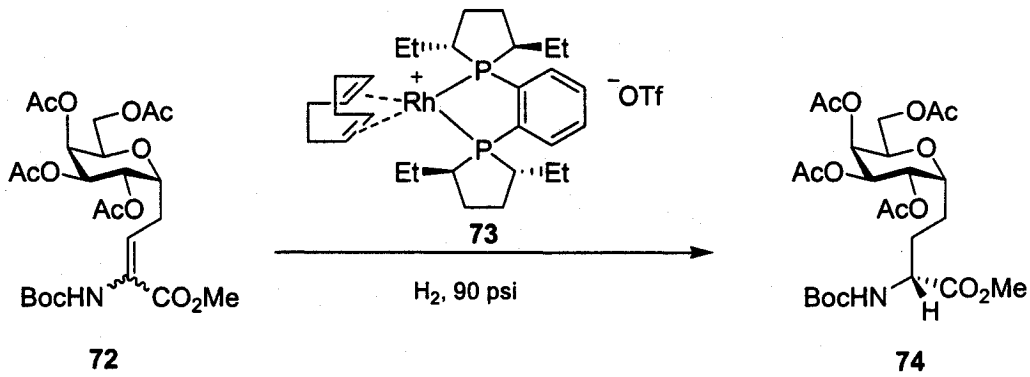

Scheme 3.3 Toone's asymmetric hydrogenation strategy to prepare *C*-glycosyl amino acid derivatives.[11]

More recently, olefin cross-metathesis (OCM) was introduced into carbohydrate synthesis[13] and several examples have shown the conciseness and high efficiency of this method in preparing *C*-linked glycosyl amino acid derivatives.[14] Roy demonstrated the feasibility of applying metathesis to carbohydrate synthesis by coupling racemic allylglycine with allyl glycosides.[14a] Later, Dondoni and Marra reported the success of using OCM to prepare *C*-glycoconjugates with the second generation Grubbs' catalyst (Scheme 3.4).[14b] Vinyloxazolidine **76** was used as the glycine equivalent to react with *C*-glycosyl olefin **75** to afford *C*-glycoconjugate **77**. Cross-metathesis of **76** with different *C*-glycosides was also performed and the best acquired yield was approximately 50%.[14b]

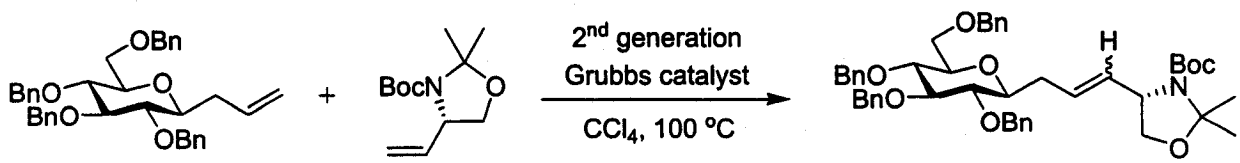

75 76 77

Scheme 3.4 Dondoni and Marra's OCM strategy to prepare *C*-glycoconjugates.[14b]

McGarvey[14c] modified Dondoni and Marra's strategy and improved the efficiency of cross-metathesis reactions. In this method, instead of using amino acid equivalent **76**, properly protected L-amino acid **79** with an olefin-containing side chain was used directly for metathesis (Scheme 3.5). Cross-metathesis of a series of *C*-glycosides **78** with **79** was studied using both the first and second generation of Grubbs' catalysts. The utilization of the second generation Grubbs' catalyst improved the efficiency of cross-metathesis to give *C*-linked glycoconjugates **80** in almost quantitative yields. Furthermore, the metathesis reaction did not introduce any chiral centers into products, which eliminated the diastereoselectivity issue involved in other strategies when preparing *C*-glycoconjugates. The high efficiency of the cross-metathesis reaction, together with the fact that all stereocenters are established at early stages of synthetic sequences, makes OCM an amenable method to prepare *C*-glycosyl amino acid derivatives.

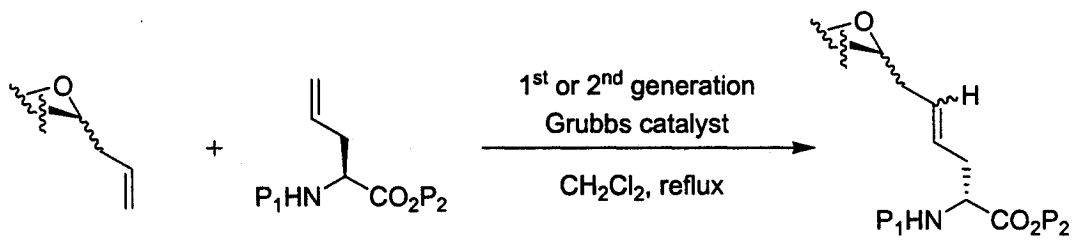

78 79 80

Scheme 3.5 Preparation of *C*-glycosyl amino acid derivatives by olefin cross-metathesis.[14c]

3.1.2 Retrosynthetic Analysis of *C*-Galactosyl Building Blocks 62-64

C-Galactosyl amino acid building blocks **62-64** can be prepared using the olefin cross-metathesis strategy (Scheme 3.6). These building blocks are directly derived from the cross-metathesis products via hydrogenation. Cross-metathesis of vinyl glycine with α-*C*-galactosyl alkene derivatives with different alkenyl substituents on the anomeric carbon can afford desired products with variable side chain lengths between the carbohydrate and glycine moieties. The α-1-*C*-allyl-galactose is the most important *C*-galactosyl alkene, from which we can prepare the other two *C*-galactosides with varying lengths of anomeric alkenyl substituents.

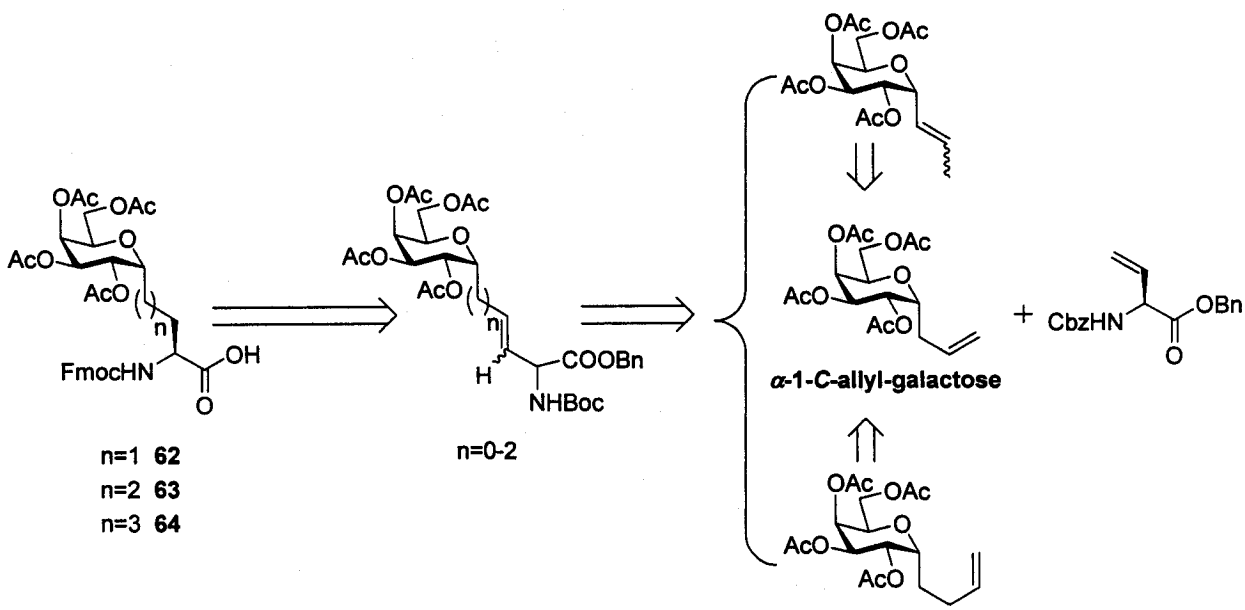

Scheme 3.6 Retrosynthesis of *C*-galactosyl building blocks **62-64**.

3.2 Preparation of *C*-Linked Galactosyl AFGP Analogues 57-59

As outlined in the previous chapter, the SAR study of previously prepared *C*-linked AFGP analogues demonstrated that D-galactose was the best monosaccharide for antifreeze-specific activities. For this reason, D-galactose was used as the carbohydrate moiety in the new generation of *C*-linked AFGP analogues **57-59**. To synthesize the corresponding building blocks

(**62-64**) using olefin cross-metathesis, *C*-linked galactosides containing anomeric alkenyl substituents of variable lengths first needed to be prepared.

3.2.1 Preparation of *C*-Galactosyl Alkenes

The first target *C*-glycosyl alkene was 1-allyl-α-D-galactose derivative **84**, from which both of the other *C*-galactosyl alkenes can be derived. *C*-allylated glycosides have been previously used as important synthons for the preparation of *C*-linked glycoconjugates.[15] These compounds are usually prepared by two strategies: Lewis acid-catalyzed nucleophilic glycosylation to activated glycosides,[16] and radical-mediated addition of allyl-containing agents to anomeric glycosyl radical precursors.[17] The latter is also known as the Keck-type allylation. One problem involved in the strategy of nucleophilic glycosylation was that the products were usually mixtures of α- and β-anomers, that could be difficult to separate by column chromatography. For example, **84** has been previously prepared by boron trifluoride-catalyzed direct allylation of D-galactose pentaacetate **81**. The reaction gave an inseparable mixture **82** with a 4:1 ratio of α:β anomers (Scheme 3.7).[1c,18] The formation of the β-anomer is presumably due to high energy involved in forming the half-chair oxocarbenium intermediate for α-anomer. In addition, the neighboring-group participation[19] also contributes to the formation of the β-anomer. The 2-*O*-acyl protecting group can stabilize the anomeric cation to form a stable acyloxonium ion, which upon the attack of a nucleophile gives the β-anomer. To get pure α-*C*-allylated galactose **84**, the acetate protecting groups on **82** had to be converted to the less polar *tert*-butyldimethylsilyl (TBDMS) groups to form **83**, which could be separated by column chromatography to afford pure α-*C*-allylated glycoside. Then, the TBDMS groups were re-converted to acetates to furnish **84**.

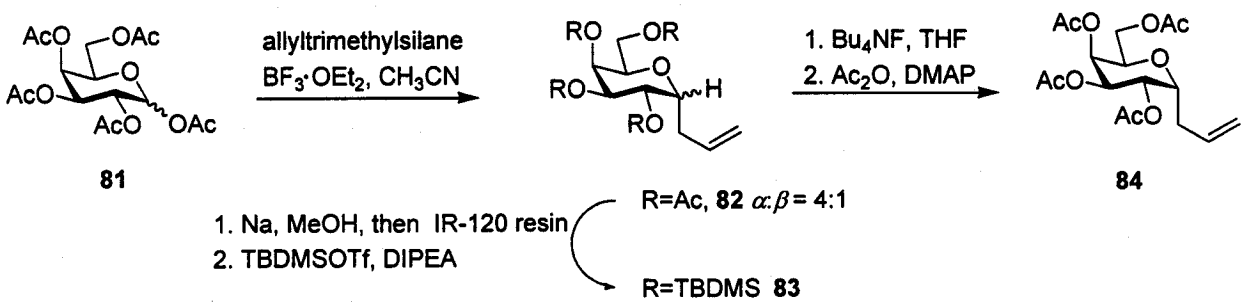

Scheme 3.7 Preparation of *C*-allylated glycosides by Lewis acid-catalyzed glycosylation.[1c,18]

In contrast, the radical-mediated coupling of glycosyl halides with allylic sulfides or sulfones usually affords *C*-glycosides with high stereoselectivity.[17] Glycosyl bromides are good candidates for such reactions because of the labile anomeric C-Br bond, which can by readily cleaved in a homolytic manner to form stable anomeric radicals on glycosides.

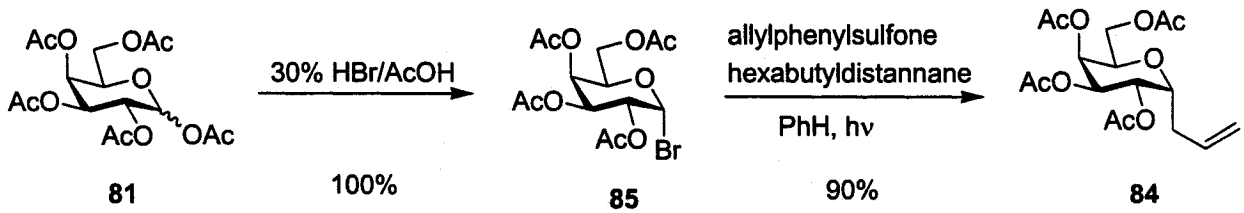

81 100% 85 90% 84

Scheme 3.8 Preparation of α-*C*-allylated galactose **84**.[20]

As illustrated in Scheme 3.8, the synthesis of α-*C*-allylated galactose **84** started from D-galactose pentaacetate **81**. Bromination of **81** with 30% hydrogen bromide in acetic acid solution afforded quantitative yield of bromogalactose **85**. The product was in the form of pure α-anomer as analyzed by ^{1}H NMR. Although both α and β bromination of the oxocarbenium intermediate could occur, the resulting β-anomer is quickly converted to the α-anomer under these reaction conditions, due to the strong endoanomeric effect that favors the thermodynamically more stable α-anomeric configuration.[19]

Trialkylallylstannanes have been used as the allylation reagents in Keck-type reactions.[21] In order to solve the problem of facile allylic rearrangement in substituted allylstannane reagents, Keck used a combination of allyl sulfides and hexabutyldistannane to replace allyl stannanes and successfully extended the application of the reaction.[22] Magnusson was the first to employ this strategy in carbohydrate synthesis.[20] Following Magnusson's procedure, α-*C*-allylated galactose pentaacetate **84** was prepared by a radical-mediated allylation of galactosyl bromide **85** with allyl phenyl sulfone. Both stannane and sulfone reagents were used in stoichiometric amounts, with hexabutyldistannane as an initiator. After initiation, as shown in Scheme 3.9, the stannyl radical could either abstract bromine from substrate **85** or be trapped by the olefin in allyl phenyl sulfone. However, both reaction pathways could lead to the desired allylation product **84**, which was obtained in 90% yield with only the α-anomer observed. This is presumably due to the fact the

axially positioned anomeric radical can be stabilized by the 2-*O*-acyl protecting group through neighboring-group participation.[19] Therefore, the allylation of the anomeric radical gave only the α-anomer product.

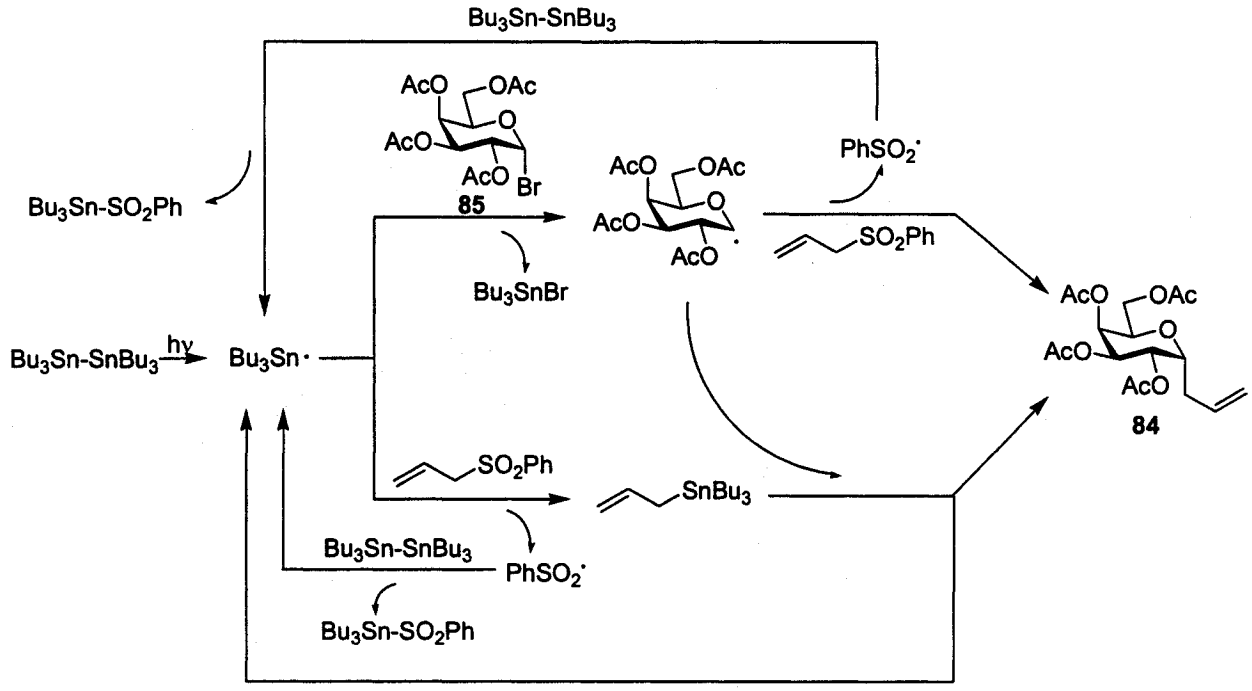

Scheme 3.9 Mechanism of allylation of **85** with hexabutyldistannane and allylphenylsulfone.

C-linked galactosyl alkene **88** containing a 3-butenyl substituent at the anomeric position was prepared from *C*-allylated galactose **84**, in which aldehyde **87** was a key intermediate. Towards this end, alkene **84** was treated with borane followed by hydrogen peroxide under basic conditions to prepare alcohol **86**. However, *in situ* oxidation of the organoboron intermediate was not a clean reaction. Several byproducts were produced and the desired alcohol **86** was isolated in only 16% yield. The poor result was attributed to the basic oxidation conditions, which we hypothesize can cleave the acetate protecting groups on carbohydrates. Consequently, an alternative route was employed that relied on pyridinium chlorochromate (PCC) to directly oxidize the hydroboration product to aldehyde **87** (Scheme 3.10).[23] This two-step reaction sequence proceeded smoothly and aldehyde **87** was obtained in 51% yield. Wittig olefination of

aldehyde **87** with methyltriphenylphosphonium bromide afforded *C*-galactosyl alkene **88** in 70% yield.[24]

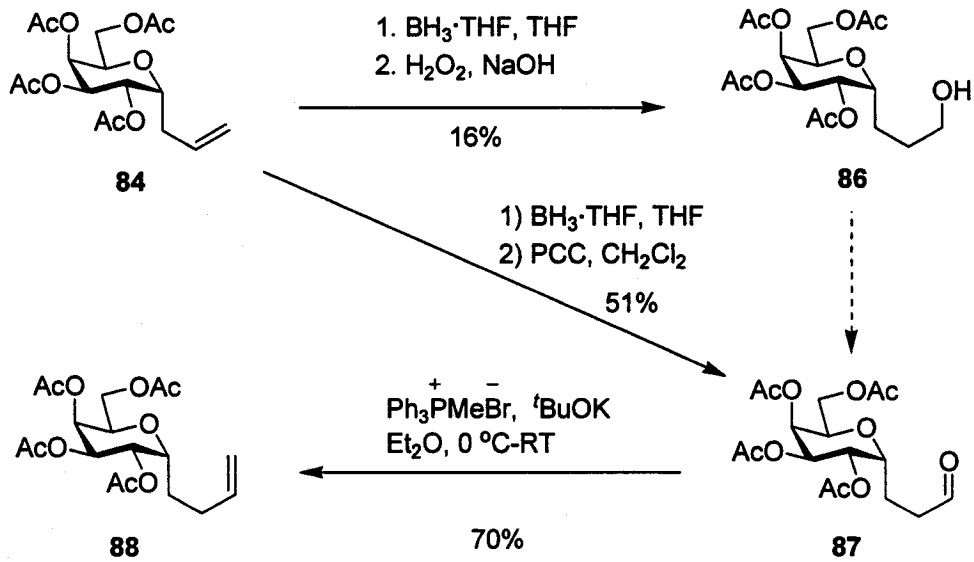

Scheme 3.10 Preparation of *α*-*C*-galactosyl alkene **88**.

C-1-propenyl-galactoside **89** was easily prepared by a palladium-catalyzed isomerization of the carbon-carbon double bond in **84** (Scheme 3.11).[25] Refluxing alkene **84** in the presence of palladium chloride afforded **89** in 49% yield.

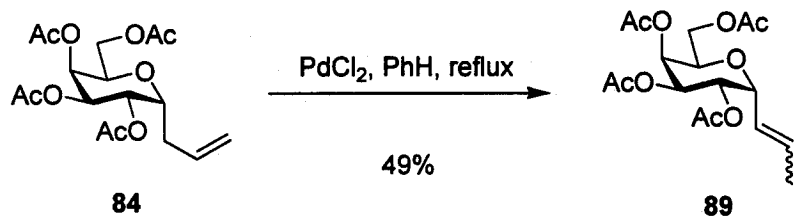

Scheme 3.11 Preparation of *α*-*C*-galactosyl alkene **89**.[25]

3.2.2 Preparation of L-Vinyl Glycine Derivative 95

As outlined in the previous section, L-vinyl glycine derivative **90** was the coupling partner in olefin cross-metathesis to produce the dehydro *C*-galactosyl amino acid derivatives. Two strategies have been reported to prepare β, γ-unsaturated amino acids (Scheme 3.12). L-vinyl glycine derivative **90** can be obtained by pyrolysis of L-methionine sulfoxide **91**, which in turn was derived from protected L-methionine **92**. Pyrolysis of L-methionine sulfoxide was performed by either Kugelrohr distillation[26] or refluxing in xylene.[27] The setbacks of this strategy were the low conversion rate and the racemization at the α-carbon. In lieu of this, a second strategy was to perform an oxidative decarboxylation of protected L-glutamic acid.[28] In this method, vinyl glycine can be prepared in one step from commercially available starting materials. For this reason, the L-vinyl glycine derivative for cross-metathesis with *C*-glycosyl alkenes was prepared using the oxidative decarboxylation strategy (Scheme 3.13).

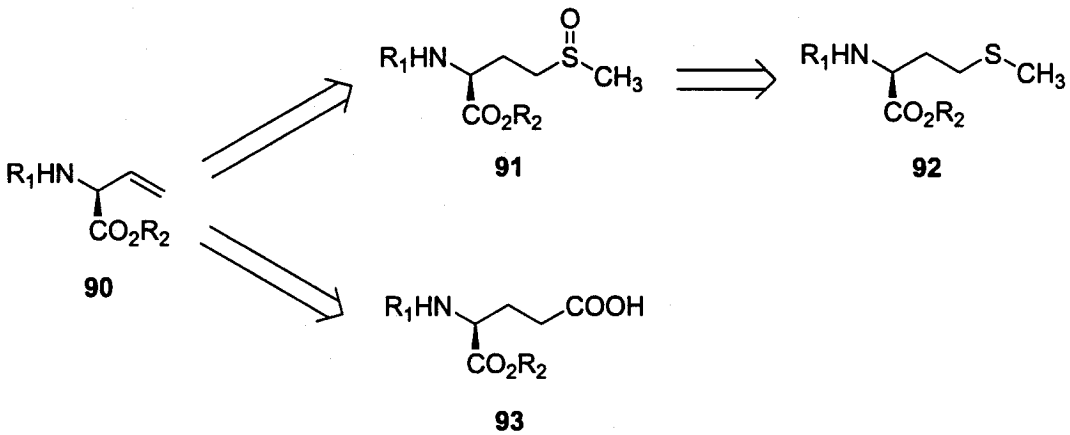

Scheme 3.12 Two strategies for preparing vinyl glycine derivative **90**.[26-28]

N-benzyloxycarbonyl (Cbz) protected L-vinyl glycine benzyl ester **95** was easily acquired using oxidative decarboxylation of orthogonally protected L-glutamic acid **94**.[28] An excess amount of lead tetraacetate was used as the oxidant. In order to avoid forming α, β-dehydro amino acid byproducts, cupric acetate monohydrate was used in catalytic amounts to enhance the decarboxylation rate.

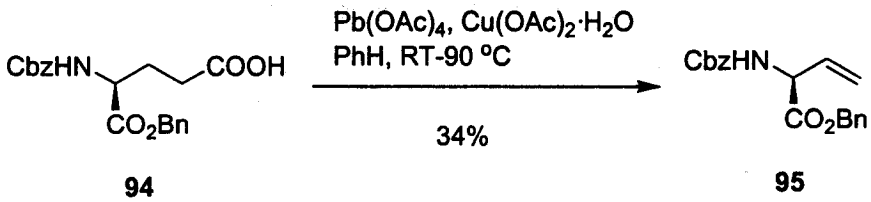

94 **95**

Scheme 3.13 Preparation of L-vinyl glycine **95**.[28]

The decarboxylation of carboxylate acids likely proceeded via a radical-mediated pathway.[28a] The heterogeneous reaction took 15 hours to afford vinyl glycine **95** in 34% yield. The low chemical yield was believed to be due to the competitive consumption of oxidant Pb^{IV} by acetic acid,[28a] which was derived from lead acetate. However, the reaction did not produce significant amounts of byproducts and most of the unconverted L-glutamic acid **94** could be recovered.

3.2.3 Preparation of Building Blocks 62-64 via Olefin Cross-Metathesis

Having both *C*-galactosyl alkenes and a N-Cbz protected L-vinyl glycine benzyl ester in hand, we performed olefin cross-metathesis to construct *C*-linked galactosyl amino acids. These compounds are precursors to the necessary building blocks for SPPS of *C*-linked AFGP analogues.

3.2.3.1 Catalysts Used for Olefin Cross-Metathesis

Grubbs' catalysts have been widely used in olefin cross-metathesis due to their high reactivity, stability to oxygen and humidity and tolerance to a variety of polar functional groups.[29] McGarvey has demonstrated that the first generation Grubbs' catalyst was not compatible with the common protecting groups used on carbohydrates.[14c] Cross-metathesis with amino acid-containing olefins was either unreactive (for acetate-protected carbohydrates) or only produced a moderate yield of desired products (for benzyl-protected carbohydrates).[14c] However, the second generation Grubbs' catalyst can improve the efficiency of cross-metathesis. In the second generation catalyst, a sterically hindered *N*-heterocyclic carbene (NHC) ligand replaces one phosphine ligand from the first generation catalyst (Figure 3.2). The NHC ligand is less labile

than the PCy_3 ligand, but its strong electron donating property can promote the dissociation of the PCy_3 ligand and stabilize the resulting metallacycle intermediate,[30] so as to improve the efficiency of metathesis. Cross-metathesis between carbohydrate-containing and amino acid-containing olefins using the second generation Grubbs' catalyst has been unanimously reported to occur with high yields.[14b-d]

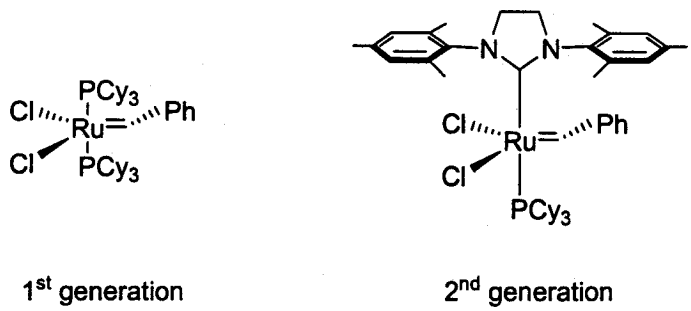

Figure 3.2 The structures of the first and second generation Grubbs' catalysts.

Catalyst **96** (Scheme 3.14) is another version of the second generation Grubbs' catalyst. The NHC ligand in **96** has an unsaturated backbone.[31] It has been demonstrated that **96** has similar efficiency for cross-metathesis compared to the catalyst with a saturated NHC ligand.[30c] Furthermore, the unsaturated NHC ligand can be easily prepared via three steps starting from oxalaldehyde and 2,4,6-trimethylanaline (Scheme 3.14).[32] After exchanging one phosphine ligand of the first generation Grubbs' catalyst with the unsaturated NHC ligand, catalyst **96** can be readily prepared. For these reasons, **96** was employed as the catalyst for cross-metathesis reactions in this study.

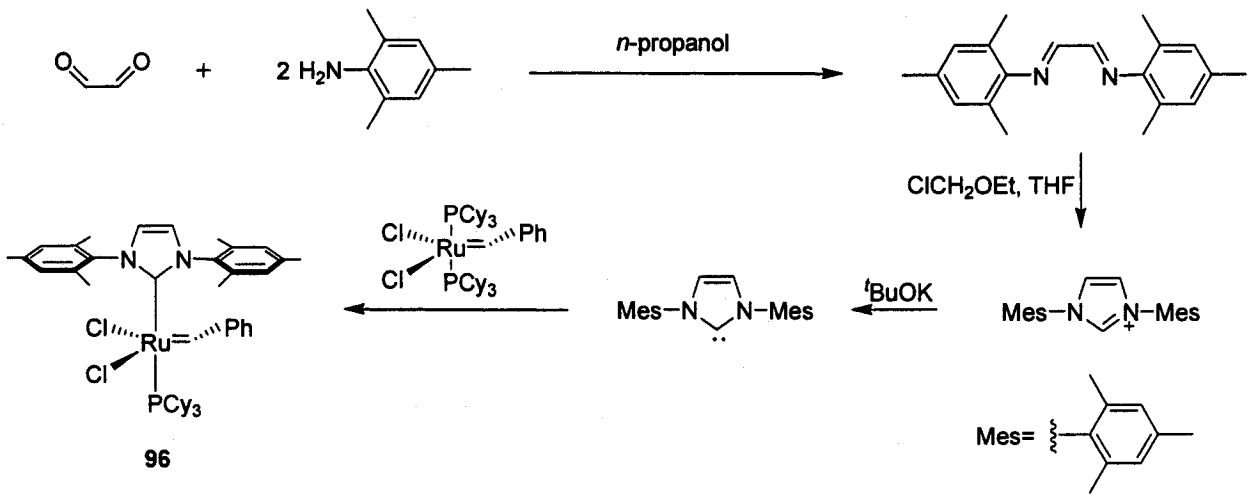

Scheme 3.14 Preparation of catalyst **96**.[32]

3.2.3.2 Olefin Cross-Metathesis

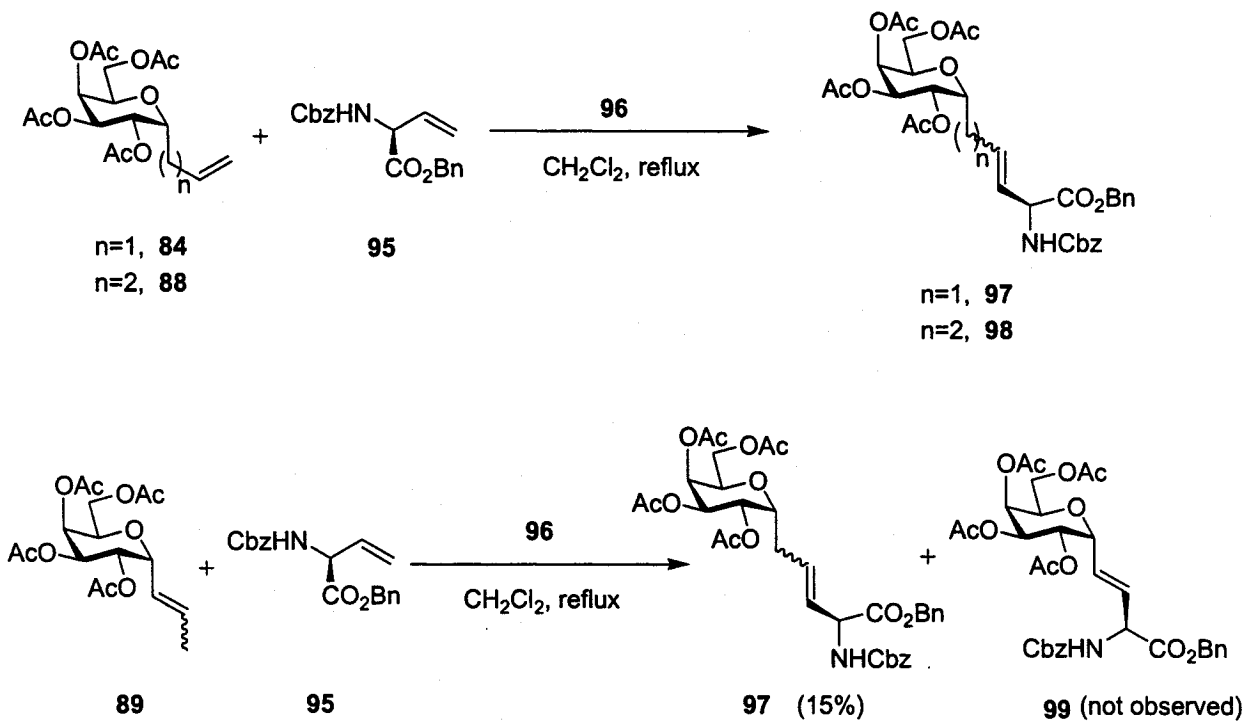

Scheme 3.15 Preparation of **97**, **98**, **99** using olefin cross-metathesis.[14c]

Olefin cross-metathesis reactions between *C*-galactosyl alkenes **84**, **88**, **89** and vinyl glycine **95** were performed following McGarvey's procedure (Scheme 3.15).[14c] A total of 20 mol % ratio

of Grubbs' catalyst was used and added into reaction mixtures in two equal portions at 24 hour intervals. To ensure complete conversion of *C*-galactosyl alkenes to the desired cross-metathesis products, vinyl glycine **95** was used in two fold excess. For alkenes **84** and **88**, the reactions went smoothly and afforded near quantitative yields of the desired products **97** and **98**, respectively.

However, for *C*-galactosyl alkene **89**, the reaction failed to produce the desired cross-metathesis product **99** and instead produced **97** in 15% yield. This result was presumably due to the poor metathesis reactivity of alkene **89**. Based on isolated products, alkene **89** did not undergo self-metathesis or cross-metathesis with vinyl glycine **95** or its homodimer. The formation of compound **97** was surprising, and it might be caused by olefin isomerization[25] of alkene **89** to the more reactive terminal alkene **84** under the employed reaction conditions.

The reduced metathesis reactivity of alkene **89** can be explained in two ways. Firstly, the carbon-carbon double bond in **89** is di-substituted and located much closer to the galactose ring, which can cause significant steric hindrance for olefin metathesis. In addition to steric effects, the carbon-carbon double bond in alkene **89** is directly connected to the electron deficient anomeric carbon, which can decrease the electron density on the olefin so as to reduce its reactivity for metathesis. This effect is further strengthened by the electron-withdrawing acetyl protecting groups on the galactose pyranose ring. Therefore, alkene **89** is not an efficient olefin cross-metathesis partner for both steric and electronic reasons.

In order to improve the selectivity of cross-metathesis and suppress self-metathesis, the two olefins need to differ significantly in their reactivity. Grubbs proposed a general empirical model to predict the selectivity of cross-metathesis based on the structural features of olefins employed.[33] In this model, olefins were classified into four types based on their ability to undergo self-metathesis and the resulting homodimers' ability for secondary metathesis reactions. It has been shown that reactions performed between sterically demanding, electron-deficient olefins and sterically unhindered, electron-rich olefins always gave good selectivity for cross-metathesis products. The same model can be used to analyze the preparation of glycoconjugates **97-99**. Compared to the sterically demanding vinyl glycine **95**, the carbon-carbon double bonds in alkenes **84** and **88** are far away from the bulky galactose pyranose ring and should behave as more reactive olefins for metathesis. However, the carbon-carbon double bond in alkene **89** is

not only sterically hindered but also electron-deficient, which makes it as unreactive as vinyl glycine **95**.

Similar results have been reported by Nolen for preparation of *C*-glucosyl amino acids from *C*-vinyl glucosides and vinyl glycine.[14d] Either no reaction or low yields of cross-metathesis products were observed. One successful example of a cross-metathesis reaction using *C*-(1-propenyl) glycosides to prepare *C*-glycosyl amino acids was reported by McGarvey.[14c] However, the cross-metathesis partner used for this study was a *β*-substituted vinyl alanine derivative, in which the carbon-carbon double bond was far away from bulky protecting groups on the amino acid residues. The success of cross-metathesis was presumably due to the improved reactivity of the amino acid-containing olefins. The resultant metathesis product possessed the same side chain length as **97** as opposed to desired glycoconjugate **99**.

Since olefin cross-metathesis was proven not suitable for coupling *C*-1-propenyl-galactose derivative **89** with vinyl glycine derivative **95**, a different approach was needed to be employed to prepare the SPPS building block **62**.

3.2.3.3 Preparation of SPPS Building Blocks 63 and 64

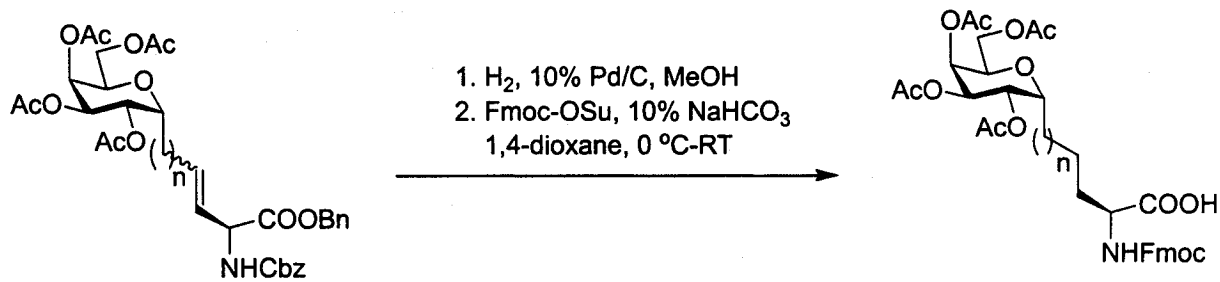

n=1, **97**
n=2, **98**

n=1, **63**, 55%
n=2, **64**, 87%

Scheme 3.16 Preparation of SPPS building blocks **63** and **64**.

The resulting carbon-carbon double bonds in cross-metathesis products **97** and **98** were reduced by hydrogenation with palladium on carbon (Scheme 3.16). Under the same reaction conditions, the amino protecting group Cbz and benzyl ester were cleaved simultaneously. The

amino group was then re-protected with Fmoc-succinimide (Fmoc-OSu) to afford *C*-galactosyl amino acids **63** and **64**, which could be used to assemble *C*-linked AFGP analogues **58** and **59** by employing Fmoc chemistry-based solid-phase peptide synthesis, respectively.

3.2.4 Preparation of *C*-Galactosyl L-Serine Derivative by Catalytic Asymmetric Hydrogenation

Since olefin cross-metathesis failed to furnish *C*-galactosyl L-serine derivative **99**, we decided to adopt a different strategy, namely catalytic asymmetric hydrogenation (CAH) of a *C*-galactosyl enamide ester, to furnish this building block for SPPS. Toone *et al.* successfully used this method to prepare both L- and D-type *C*-glycosyl amino acids with high efficiency and high diastereoselectivity.[11, 12] The diastereoselectivity of the asymmetric hydrogenation is dependent on the configuration of the chiral rhodium catalyst used. The retrosynthesis for *C*-galactosyl L-serine building block **62** using CAH is illustrated in Scheme 3.17. The *S*-configuration of the α carbon in the serine moiety can be introduced by using an *S*-alkyl substituted rhodium catalyst. The hydrogenation substrate, *C*-galactosyl enamide ester, can be prepared by Horner-Emmons olefination from a phosphonate glycine derivative and a *C*-galactosyl aldehyde.

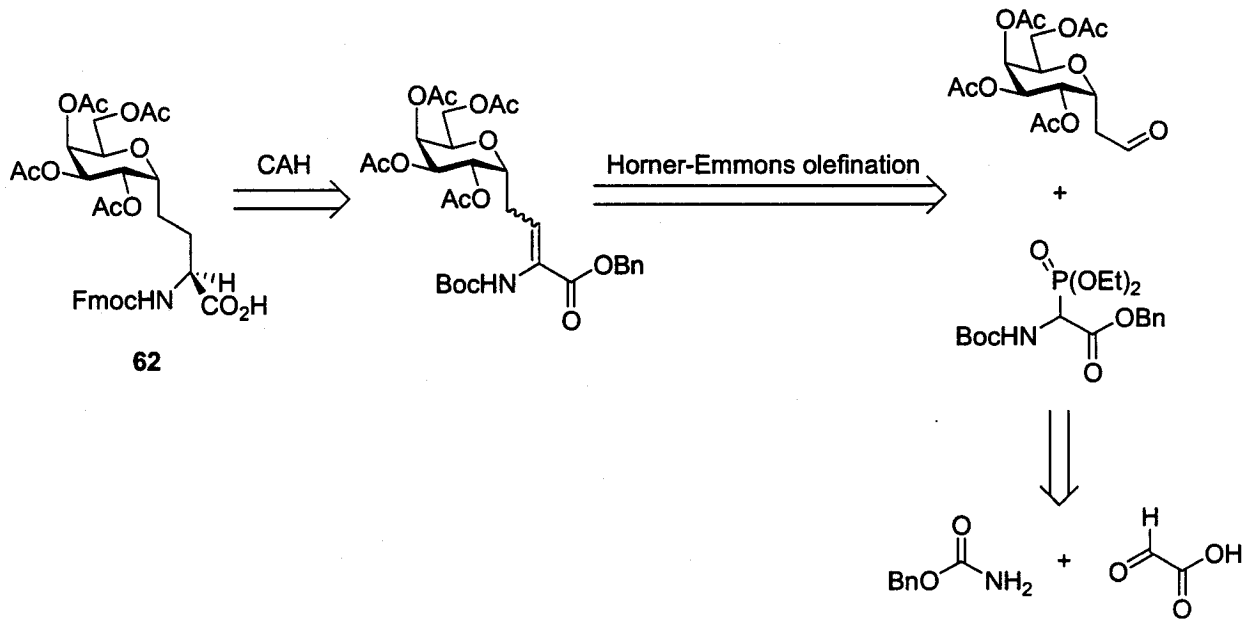

Scheme 3.17 Retrosynthesis of *C*-galactosyl L-serine building block **62**.

As illustrated in Scheme 3.18, *N*-Boc protected phosphonate glycine benzyl ester **107** was synthesized via six steps starting from benzyl carbamate **100** and glyoxylic acid **101**.[34] *N*-Cbz protected α-hydroxyl glycine **102** was readily prepared by stirring **100** and **101** in ether. After treatment with concentrated sulfuric acid, the carboxylic acid and the α-hydroxyl group in **102** were converted to their respective methyl ester and ether form to obtain **103**. The phosphonate functionality was introduced by heating **103** with phosphorus trichloride followed by triethyl phosphite. *N*-Cbz protected phosphonate glycine methyl ester **104** was prepared in 66% yield. Considering the sensitivity of the Cbz group to the reaction conditions employed in the following asymmetric hydrogenation step, we switched the *N*-Cbz protecting group to *N*-Boc to form **105** in order to avoid any potential cleavage reactions during hydrogenation. In addition, the methyl ester in **105** is not a compatible protecting group for SPPS. Removal of the methyl ester requires strongly basic conditions, which may cause epimerization of amino acids. Therefore, we converted the methyl ester **106** to the more amenable benzyl ester **107** before introducing the α-chirality in amino acid moieties.

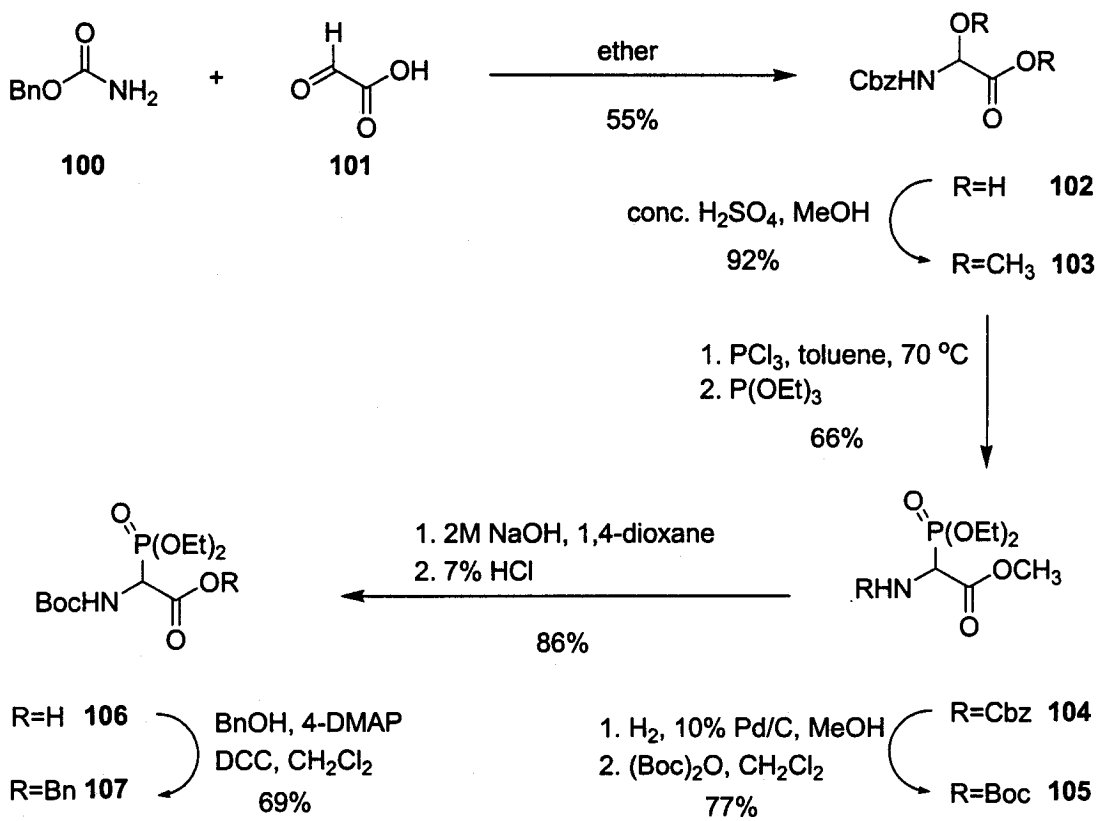

Scheme 3.18 Preparation of *N*-Boc protected phosphonate glycine benzyl ester **107**.[34]

C-Galactosyl aldehyde **108** was prepared via ozonolysis of *C*-allylated galactose **84** (Scheme 3.19). The Horner-Emmons olefination of phosphonate glycine **107** with aldehyde **108** was performed in THF at -78 °C following published procedures.[11, 35] Tetramethylguanidine (TMG) was used for condensation instead of strong alkali bases in order to be compatible with the acetate protecting groups on the carbohydrate moiety. The olefination proceeded smoothly and afforded *C*-galactosyl enamide ester **109** in 80% yield. The *E*/*Z* isomeric ratio of **109** was not determined. According to Burk's previous study on the DuPHOS-Rh^+ catalyst, [36] the diastereoselectivity of asymmetric hydrogenation is independent of substrate's relative configuration. Therefore, the separation of *E*/*Z* isomers is unnecessary. This conclusion was later verified by Toone's study on asymmetric hydrogenation of *C*-glycosyl enamides.[11,12]

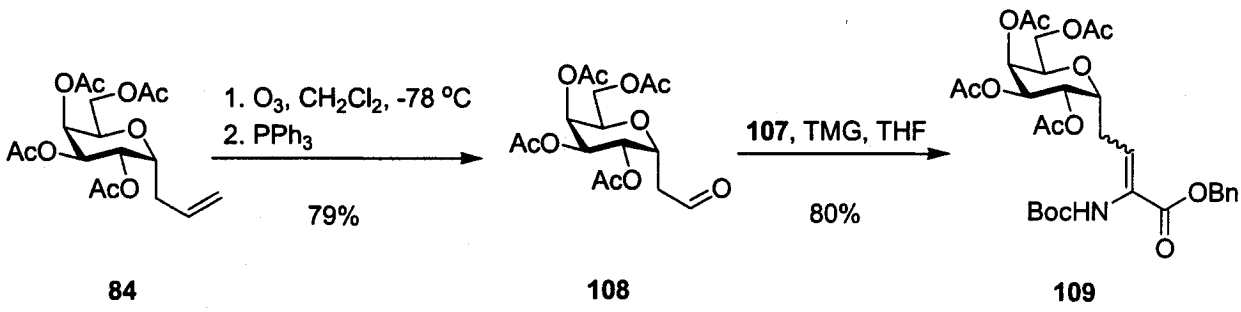

84 **108** **109**

Scheme 3.19 Preparation of *C*-glycosyl enamide ester **109**.[11,35]

According to Toone's study,[11] cationic rhodium-DuPHOS catalyst demonstrated excellent catalyst control for the diastereoselective hydrogenation of *C*-glycosyl enamides. The chirality formed at the α-amino acid center is solely dependent on the configuration of the alkyl substituents on the DuPHOS ligand of the catalyst used. *S*-alkyl groups are required to obtain L-amino acids. When selecting alkyl groups on the ligand, a compromise between reactivity and diastereoselectivity must take place. Bulky substituents will deactivate catalysts; on the other hand, substituents that are too small cannot offer high diastereoselectivity for hydrogenation. For these reasons, commercially available *S*-ethyl substituted rhodium-DuPHOS catalyst **110** (Scheme 3.20) was used to reduce the carbon-carbon double bond in enamide ester **109**. The reaction was performed using 2 mol % of catalyst **110** under 90-100 psi hydrogen for two days to afford near quantitative yield of *C*-galactosyl L-serine derivative **111**. Diastereomeric excess was

estimated to be 66% based on the integration of the Boc protons in the ^{1}H NMR (500 MHz) spectrum (Figure 3.3). In order to determine the diastereomeric excess, ^{1}H NMR was performed in DMSO-D_6 at 297 K, 317 K, 337 K, 357 K and 377 K to reduce the excessive line broadening. It was found that heating **111** at 377 K gave the best resolution (Figure 3.3). The assignment of the major diastereomer with *S* configuration was based on the previous work by Burk and Toone.[11,36] As Burk[36a] pointed out, the configuration of the newly produced chiral center was predicable and solely dependent on the configuration of the alkyl substituents on the DuPHOS ligand. *S*-ethyl substituted rhodium-DuPHOS catalyst gave the major product with *S* configuration at the α-amino acid center.

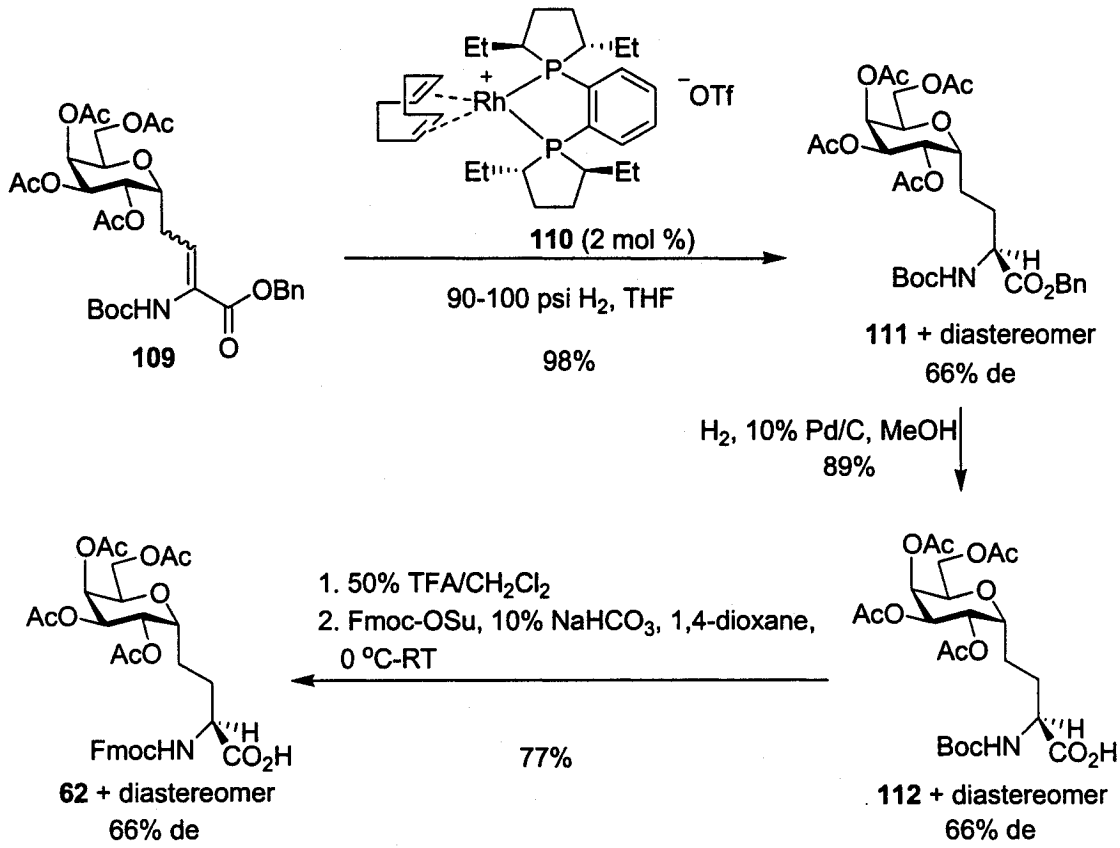

Scheme 3.20 Preparation of building block **62**.[11]

Comparing to Toone's results that high diastereoselectivity (> 95%) were observed in the asymmetric hydrogenation of *C*-glycosyl enamides, the relatively low diastereomeric excess of

the asymmetric hydrogenation of **109** was disappointing. The only structural difference between **109** and the hydrogenation substrates employed in Toone's study was that **109** possessed a benzyl ester instead of a methyl[11] or (trimethylsilyl)ethyl (TMSE)[12] ester as in Toone's study. However, based on the proposed mechanism of the asymmetric hydrogenation,[36a,37] the carboxyl protecting group preferred to lie in an unhindered quadrant in the square-planar catalyst-substrate complex and should not affect the diastereoselectivity of hydrogenation. One possible explanation for the low diastereomeric excess is that it might be due to the existence of acetate protecting groups on the galactose residue. Instead of chelating with the carbonyl group β to the prochiral olefin in the enamide residue, Rh (I) might form a complex with the carbonyl groups on the galactose residue.

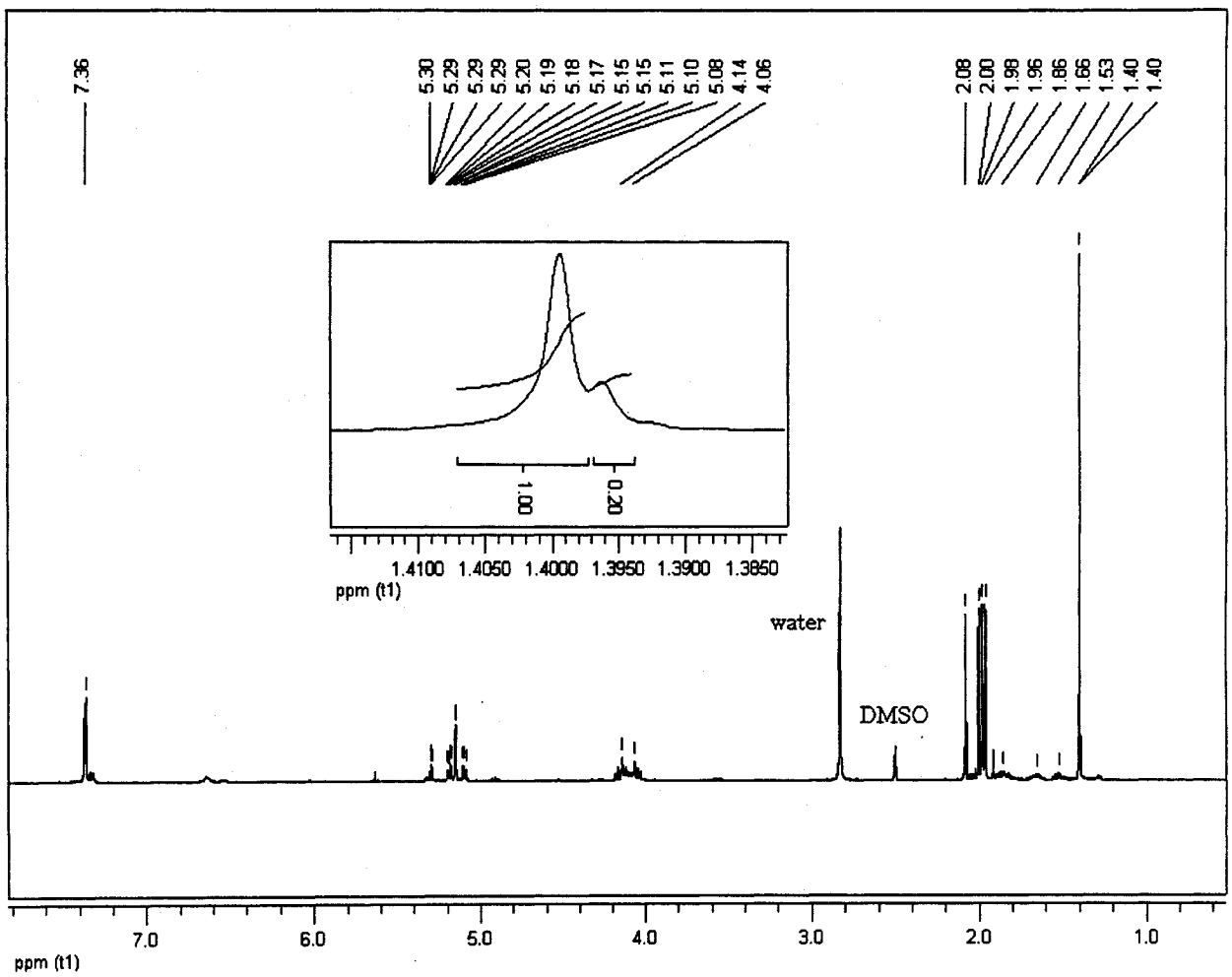

Figure 3.3 ^{1}H NMR (500 MHz, DMSO-D_6, 377 K) of compound **111**.

The purification of **111** was unsuccessful. The diastereomers could not be separated using flash chromatography. HPLC also failed to isolate the desired product with L-stereochemistry at the α-amino acid center due to excessive line broadening.[11]

Carboxylic acid **112** was obtained after removing the benzyl ester in **111** by hydrogenolysis with palladium over carbon. In order to be compatible with Fmoc-protocol SPPS, the *N*-Boc group was cleaved by treatment with TFA and the resulting free amine was re-protected with Fmoc-OSu to give the *N*-Fmoc protected *C*-galactosyl L-serine building block **62**. The purification of **62** was carefully performed on silica with a gradient of 0-10% MeOH in CH_2Cl_2. There was no evidence of the *R* diastereomer in the ^1H NMR spectrum, suggesting that **62** might be purified. While this could be verified by switching the protecting group from *N*-Fmoc to *N*-Boc, it was not performed because of shortage in material. On the other hand, as the chiral center is remote from the carbohydrate moiety, it is possible that both diastereomers exhibit the same ^1H and ^{13}C spectral data. Laursen and co-workers previously studied the effect of amino acids' relative configuration on antifreeze activity and found that polypeptides composed of pure L-, pure D- or a mixture of 1:1 L- and D-amino acids showed identical antifreeze activity.[38] Since certain ice surfaces were symmetrical, the authors proposed that the binding of these polypeptides to ice was analogous to the action of certain enzymes on achiral substrates. This study indicted that the relative configuration at the α-amino acid center might not be an important factor for antifreeze activity. Therefore, we decided to use building block **62** for the synthesis of *C*-linked AFGP analogue **57**.

3.2.5 SPPS of *C*-Linked Galactosyl AFGP Analogues

Using 9-fluorenylmethoxycarbonyl (Fmoc) as an α-amino protecting group for SPPS was first introduced by Carpino[39] and later developed into a powerful strategy to prepare biologically active polypeptides and proteins.[40] Scheme 3.21[41] describes the basic steps in solid-phase peptide synthesis using Fmoc-chemistry. A resin acts as the solid support for sequential coupling of *N*-protected amino acids. An acid-labile ester bond tethers the C-terminal amino acid to the resin. This linkage is stable to reaction conditions for unmasking α-amino protecting groups and amide bond condensation, but can be cleaved by trifluoroacetic acid (TFA) to free the synthesized polypeptides from solid resin. Amino acids to be assembled are protected temporarily by a basic

labile Fmoc group on the α-amino position, which is usually cleaved with 20-50% piperidine in *N*,*N*-dimethyl formamide (DMF) solution. After unmasking the α-amino group, the next amino acid is coupled to the resin-bound peptide. In order to improve the efficiency of coupling reactions and avoid racemization, α-carboxyl groups are activated to form *N*-hydroxybenzotriazole (HOBt) *in situ* with activators such as 2-(1H-Benzotriazole-1-yl)-1,1,3,3-tetramethyluronium hexafluorophosphate (HBTU). The α-carboxylic acid can also be activated by pre-forming activated esters, symmetrical anhydrides or acid halides. A new amide bond is formed between the activated amino acid and the resin-bound amino acid under basic conditions on solid resin. The Fmoc deprotection and amide bond condensation are repeated until the desired polypeptide is assembled. After coupling the *N*-terminal amino acid, the last Fmoc group is deprotected and the polypeptide is cleaved from the resin to afford the final product.

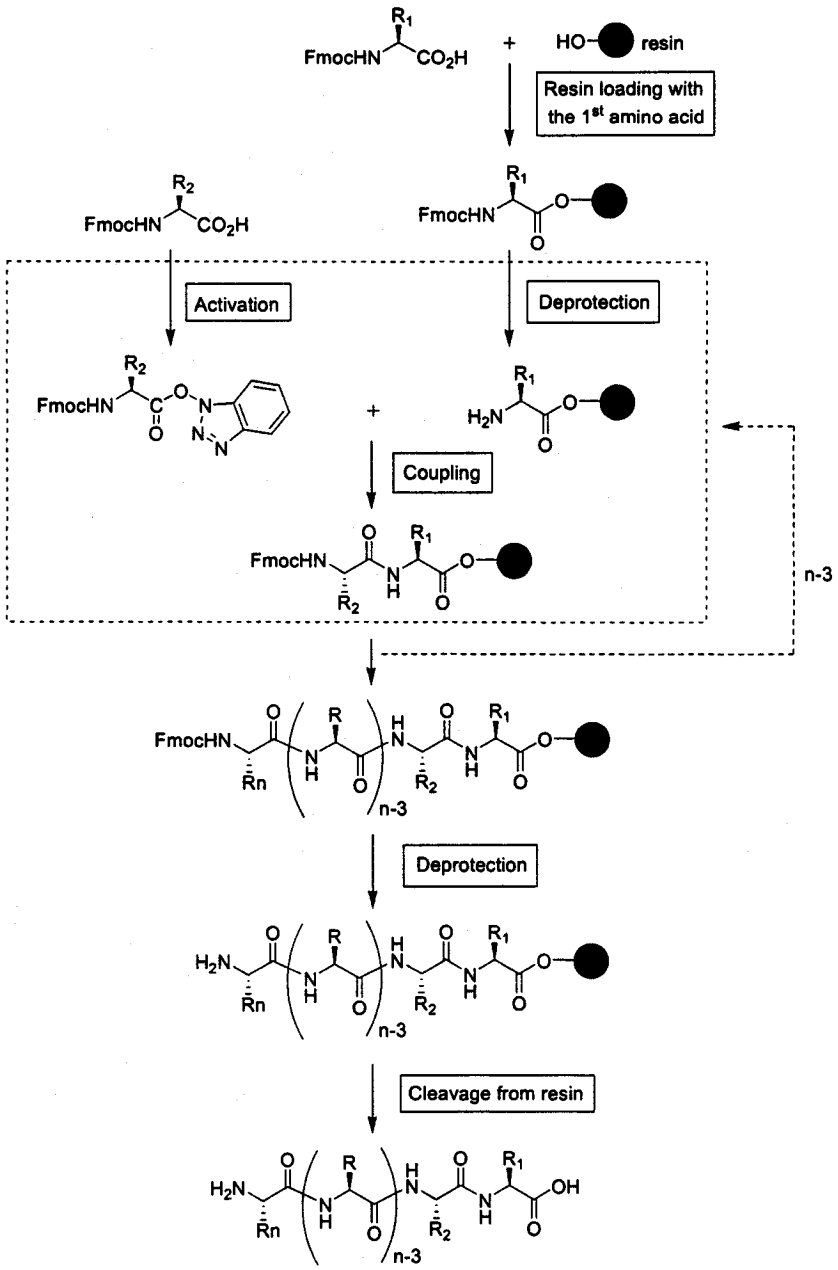

Scheme 3.21 Preparation of polypeptides using Fmoc strategy of SPPS.[41]

The selection of resin is important for the success of SPPS. A good solid resin should have enough active sites for polypeptide propagation, a functional linker compatible with coupling and cleavage conditions used in the Fmoc strategy and good swelling capability to make the functional sites in the polymer matrix accessible to reagents in solution phase. Based on this, we selected one glycine preloaded Wang resin, which has been widely used as a solid support for

Fmoc batch SPPS strategy.[42] Wang resins are made of cross-linked polystyrene (PS) beads, which are functionalized with an acid labile *p*-benzyloxyl benzylalcohol handle to load the first amino acid at the C-terminus through an ester bond. Cleavage of the ester bond by TFA is facilitated by the resonance stabilization of the resulting carbon cation by the *p*-benzyloxy phenyl group. The Wang resin used in this study has loading capacities of 0.6-0.65 mmol/g and a good swelling capacity of three folds in volume in DMF.

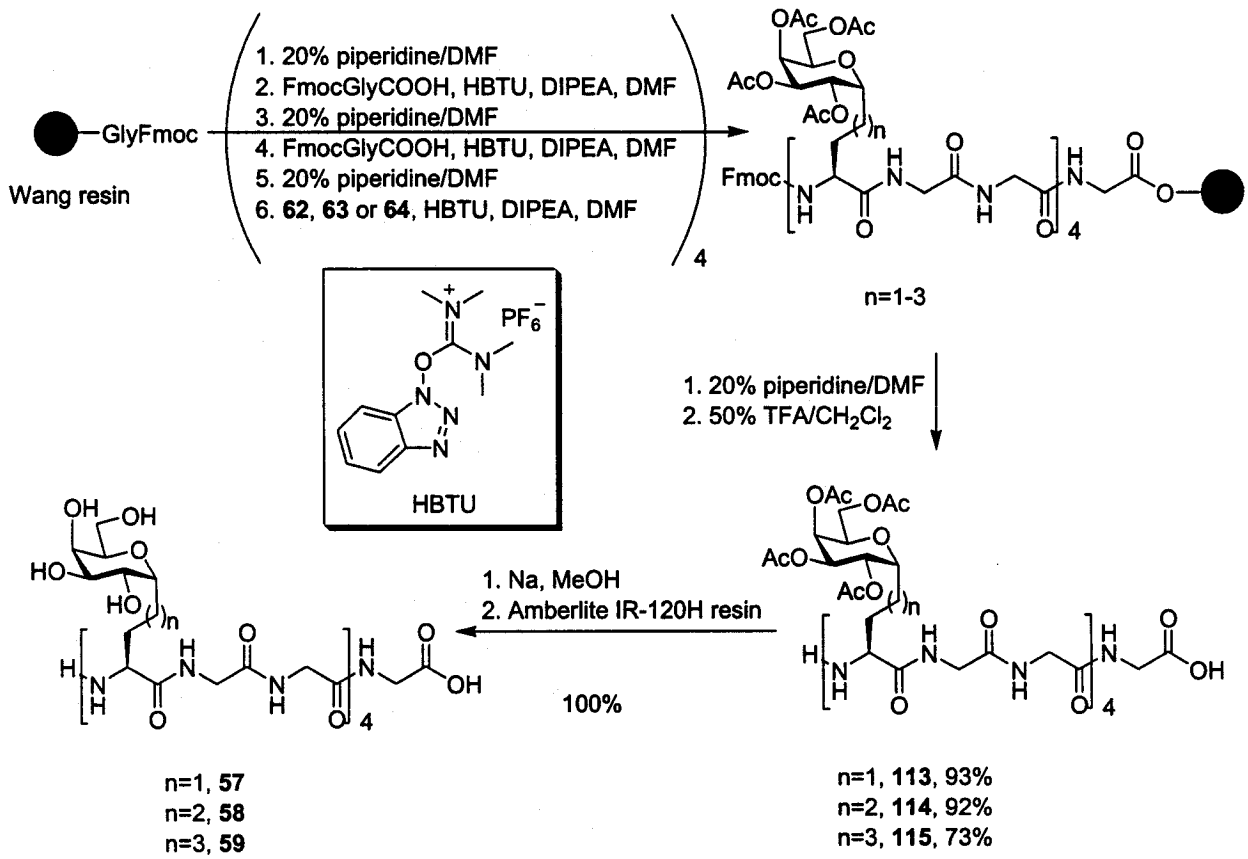

Scheme 3.22 Preparation of *C*-linked galactosyl AFGP analogues **57-59**.*

C-Linked AFGP analogues **57-59** were prepared by manual sequential assembly of building blocks **62**, **63**, and **64** with *N*-Fmoc glycine (Scheme 3.22). 20% piperidine in DMF solution was used to deprotect the Fmoc group at α-amino positions. HBTU was used as an *in situ* activating reagent for amide bond coupling in the presence of diisopropylethylamine (DIPEA). To ensure

* Analogue **57** may contain D-*C*-serine residues in the polypeptide backbone.

the completion of reactions, each Fmoc deprotection and amino acid coupling step was monitored by both Ninhydrin (Kaiser) and 2,4,6-trinitrobenzenesulfonic acid (TNBS) tests to detect the existence of free amino groups. The resin-bound polypeptides were prepared through twelve coupling reactions by assembling *N*-Fmoc glycine with building blocks **62**, **63**, or **64**. Each coupling step was run until negative Ninhydrin and TNBS test results (no free amino groups) were obtained. After the last building blocks were assembled, the *N*-Fmoc groups were removed and the polypeptides were cleaved from the resin with 50% TFA in dichloromethane solution to furnish acetate protected analogues **113-115**. To afford final *C*-linked AFGP analogues **57-59**, polypeptides **113-115** were treated with a basic solution (pH around 10) that was preformed by dissolving sodium in methanol, followed by neutralization with Amberlite® IR-120H ion-exchange resin. Polypeptides were then precipitated out from reaction mixtures with diethyl ether, re-dissolved in water and lyophilized. Purification of *C*-linked AFGP analogues was performed with reversed phase HPLC and the identity of the analogues were verified with mass spectrometry.

3.3 Preparation of *C*-Linked GalNAc L-Serine AFGP Analogue 60

C-linked GalNAc L-serine analogue **60** was also assembled using the Fmoc chemistry-based SPPS from the corresponding *N*-Fmoc *C*-GalNAc L-serine building block (**65**). Most strategies[43] for making *C*-glycosyl amino acids can be employed to prepare building block **65**. However, it has been shown that the 2-amino-2-deoxy functionality in amino sugars is not easy to work with. This is due to the fact that the nitrogen-based functional groups at the C2 position are not always compatible with the common strategies for preparing *C*-glycosides.[15] For example, Lewis acid-catalyzed glycosylation had limited success in preparing *C*-linked 2-amino-2-deoxy glycosides, which was due to the dysfunction of Lewis acids through binding to the nitrogen atom.[44]

Radical-mediated synthesis of *C*-glycosides has proven to be a good strategy for preparing *C*-linked 2-amino-2-deoxy glycosides.[45] Therefore, to prepare building block **65**, we decided to use a radical-mediated addition of α-phenyl selenoglycosides to a β, γ-dehydro alanine derivative to construct the *C*-linked amino-containing glycosyl amino acid derivative (Scheme 3.23).[46] This method has the advantages of a short synthetic route and high stereoselectivity. The phenyl

selenoglycoside can be obtained from galactal by a diastereoselective and regioselective addition of diphenyl diselenide.

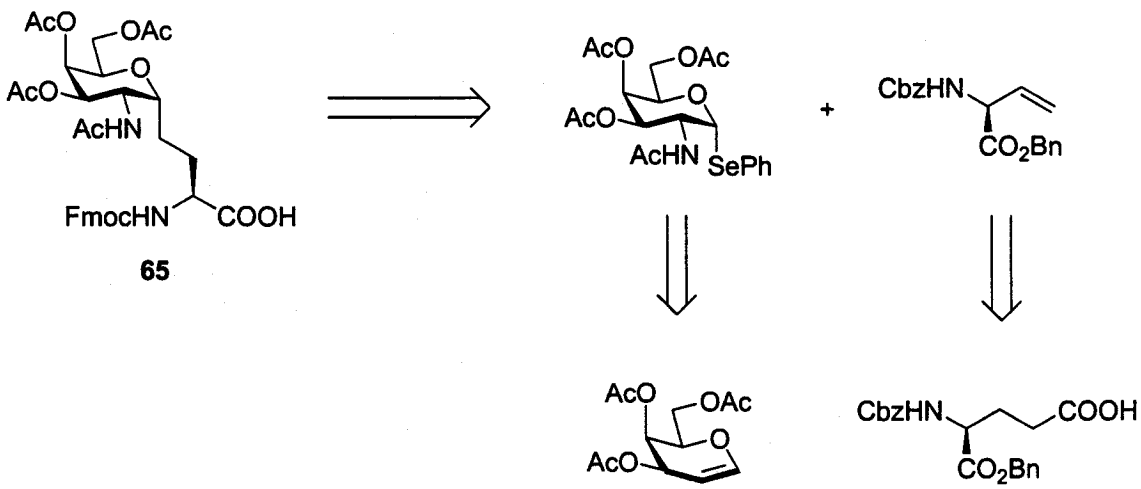

Scheme 3.23 Retrosynthesis of building block **65**.[46]

3.3.1 Preparation of *N*-Fmoc *C*-GalNAc L-Serine Building Block 65 Using Radical-Mediated Addition of Selenoglycoside 118 to Vinyl Glycine Derivative 95

The synthesis of selenogalactosamine **118** started from α-bromo galactose **85** (Scheme 3.24). Galactal **116** was first prepared via reductive elimination by treating **85** with activated zinc in acetic acid.[47, 48] 2-Azido-1-selenogalactoside **117** was obtained by an azidophenylselenylation of galactal **116** with sodium azide and diphenyl diselenide in the presence of oxidant iodobenzene diacetate.[46, 49] The addition of azido and phenylseleno radicals to the endocyclic double bond was both highly regioselective and diastereoselective. Only the α-1-phenylseleno anomer possessing a *syn* 2-azido group was detected. The acetamide functionality at C2 was introduced by reducing the azido group to a primary amine with 1,3-propanedithiol followed by amine protection with acetic anhydride to produce α-phenylseleno galactosamine **118**.

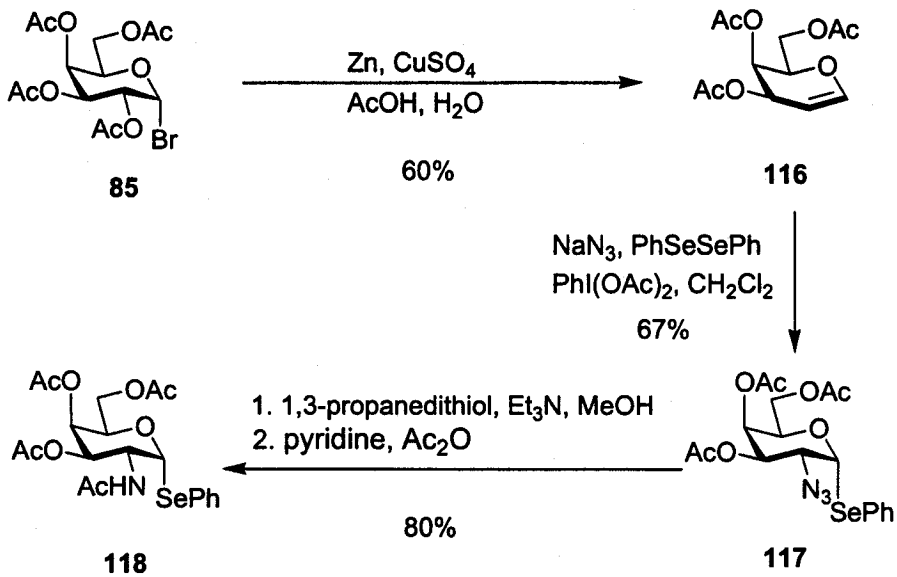

Scheme 3.24 Preparation of phenylselenogalactosamine **118**.[46-49]

Scheme 3.25 illustrates the reaction mechanism of the highly selective azidophenylselenylation.[49d] The reaction is initiated by oxidation of the azide anion to an azido radical by iodobenzene diacetate. The azido radical prefers to add to C2 rather than C1, because the C2 addition results in a more stable anomeric radical that can be stabilized by the electrons on the endocyclic oxygen through conjugation. Furthermore, the addition of the azido radical to C2 from the equatorial direction is preferred, presumably due to the quasi-axial acetate group on C4 which blocks the addition of the azido radical from the axial direction. The resulting anomeric radical is stabilized in the α-configuration by the anomeric effect, and reacts with diphenyl diselenide homolytically to afford α-phenylseleno galactoside **117**.

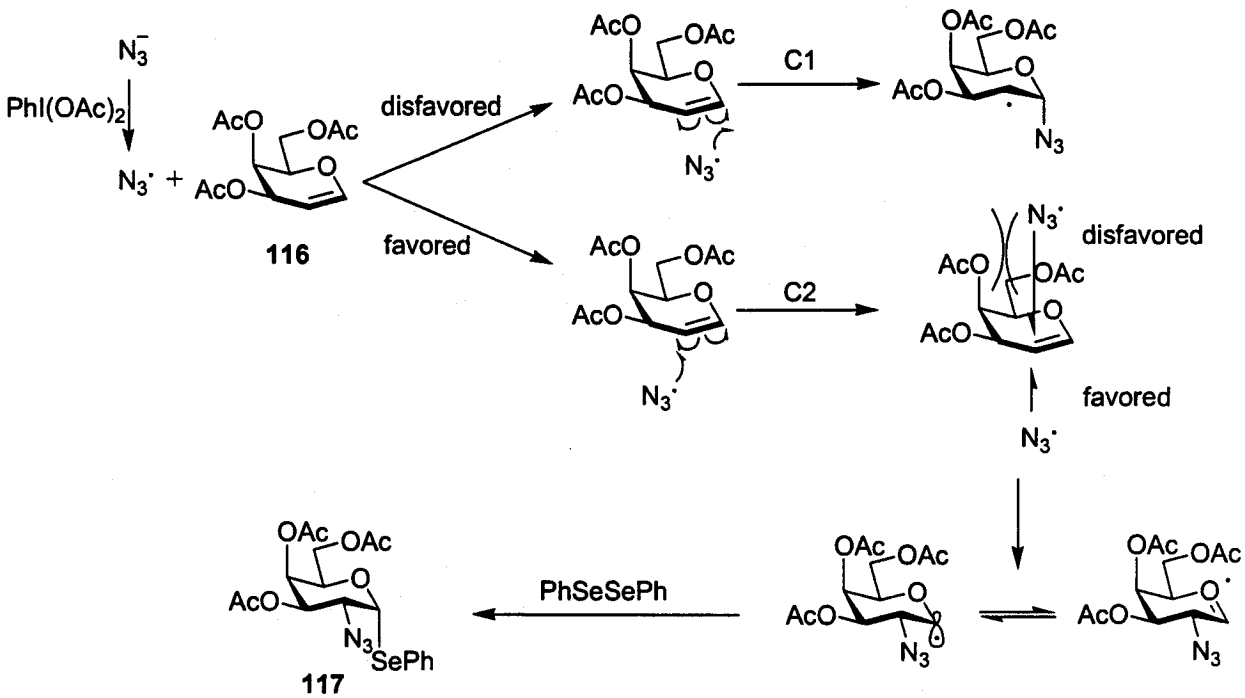

Scheme 3.25 Mechanism of azidophenylselenylation of galactal **116**.[49d]

The radical-mediated addition of **118** to vinyl glycine **95** (Scheme 3.26) was performed following Gallagher's procedure.[46] Tributyltin hydride was used as the hydrogen source to quench the radical intermediate. However, the addition of selenoglycoside **118** to vinyl glycine **95** failed to furnish any *C*-GalNAc L-serine **119**. The only isolated product was the anomeric reduced galactosamine **120** even with the use of five equivalents of vinyl glycine **95**.

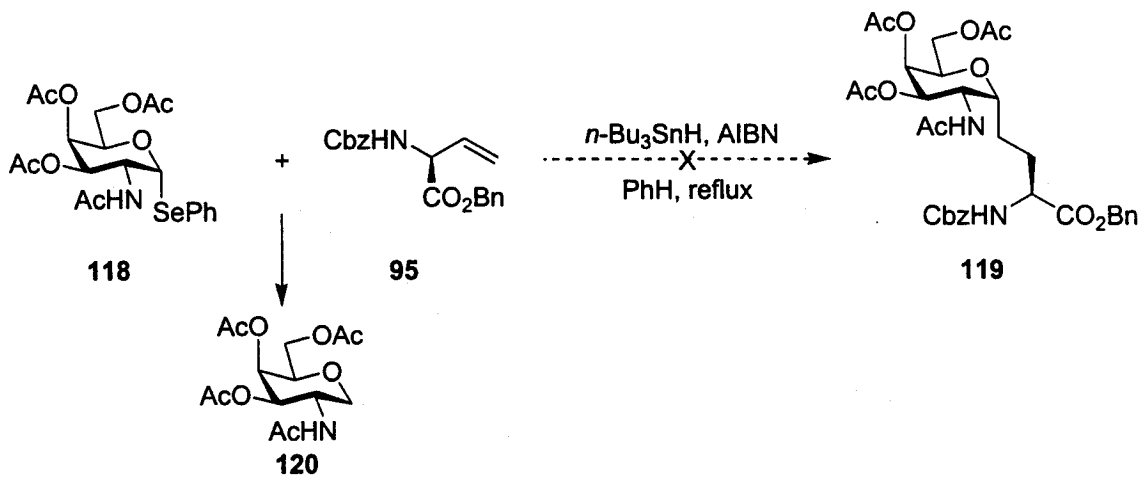

Scheme 3.26 Radical-mediated addition of **118** to vinyl glycine **95**.

This result is presumably due to the fact that vinyl glycine **95** is not an activated alkene. As illustrated in Scheme 3.27, the homolysis of the labile carbon-selenium bond in **118** would produce an anomeric radical, which could be trapped by the carbon-carbon double bonds in the alkenes. For activated alkenes such as styrene, the resulting α-radical could be stabilized by the vicinal functional groups.[46] However, the addition of the anomeric radical to vinyl glycine **95** resulted in an unstable β-radical. The reaction was more likely to go in the reverse direction to form the more stable anomeric radical, which could react with tributyltin hydride to give the anomeric reduced product **120**. To circumvent this problem, an α, β-dehydroalanine derivative could be used as the alkene substrate for the anomeric radical addition. However, the second radical addition with tin hydride was not expected to be diastereoselective.

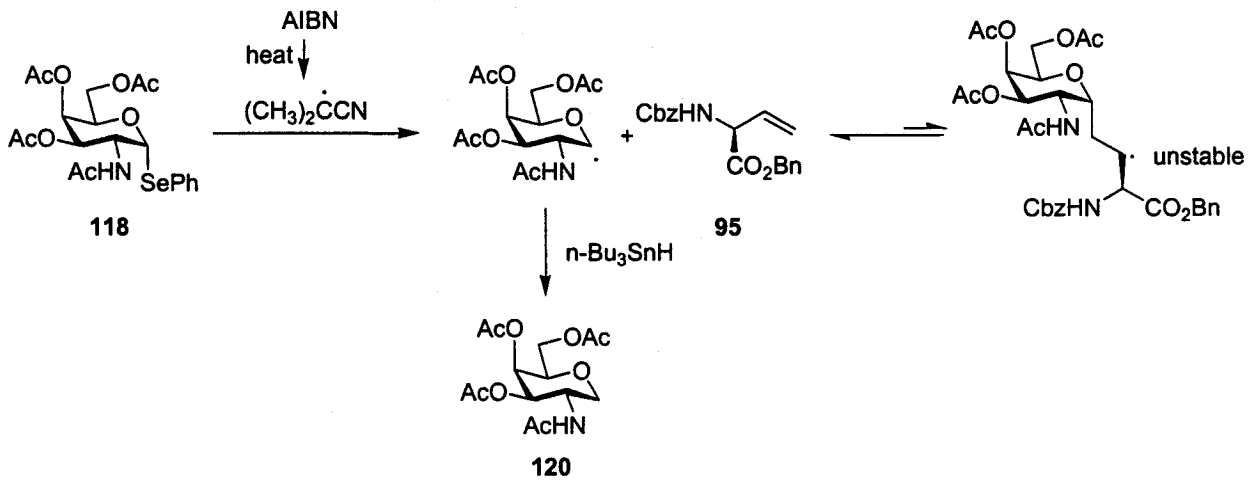

Scheme 3.27 Proposed mechanism of forming **120**.

3.3.2 Preparation of *N*-Fmoc *C*-GalNAc L-Serine Building Block 65 Using Catalytic Asymmetric Hydrogenation

An alternative method to prepare the *N*-Fmoc *C*-GalNAc L-serine building block is to perform an asymmetric hydrogenation of *C*-GalNAc enamide ester, which has been successfully employed in preparing *C*-linked galactosyl L-serine building block **62**. The major challenge is to prepare the α-*C*-allylated galactosamine, the important intermediate for preparing the *C*-GalNAc enamide ester.

Keck-type allylation has been widely used to prepare *C*-allylated glycosides.[17] Glycosyl halides are the most popular radical precursors that are employed in the Keck-type allylation.[43] Several successful examples have been reported for preparing *C*-2-aminoglycosides from glycosyl chlorides and bromides by Keck-type allylation.[15, 45] Since phenylselenogalactosamine **118** has already been prepared, we wanted to study whether this selenoglycoside can also serve as the radical precursor for the Keck-type allylation to prepare α-*C*-allylated galactosamine **121**. Refluxing **118** with allyltributyltin using AIBN as the radical initiator afforded the α-anomer of *C*-allylated galactosamine **121** in 50% yield (Scheme 3.28). Aldehyde **122** was prepared by ozonolysis of alkene **121**.

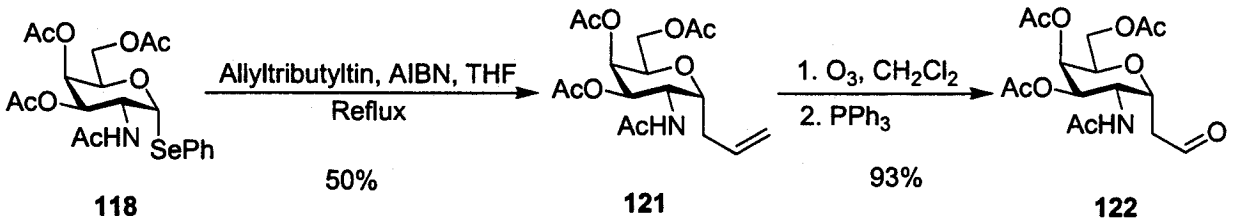

118 **121** **122**

Scheme 3.28 Preparation of aldehyde **122**.[45]

The procedures used to prepare the *N*-Fmoc *C*-GalNAc L-serine building block **65** (Scheme 3.29) were the same as those used to prepare building block **62**. Horner-Emmons olefination of aldehyde **122** with phosphonate glycine **107** gave enamide ester **123** in 80% yield. Similar to **109**, the *E*/*Z* isomeric ratio of **123** was not determined as previous studies demonstrated that the relative configurations of substrates do not affect the diastereoselectivity of asymmetric hydrogenation with the employment of the DuPHOS-Rh^+ catalyst.[11,12,36] An asymmetric hydrogenation[11] of **123** was performed using 2 mol % *S*-ethyl substituted rhodium-DuPHOS catalyst **110**, which afforded quantitative yield of *C*-GalNAc L-serine derivative **124**. The diastereomeric excess of **124** was estimated to be 71% based on the integration of the Boc protons in ^{1}H NMR (500 MHz) spectrum. The assignment of the major diastereomer with *S* configuration at the α-amino acid center was based on previous work by Burk and Toone.[11,36] *S*-ethyl substituted rhodium-DuPHOS catalyst **110** gave the major product with *S* configuration at the α-amino acid center.

Similar to *C*-galactosyl L-serine derivative **111**, the purification of **124** was unsuccessful and the diastereomeric mixture of **124** was used directly for the following steps. Hydrogenolysis of the benzyl ester gave acid **125**. Subsequent conversion of the Boc carbamate to an Fmoc carbamate furnished building block **65**. After being carefully purified with flash chromatography using a gradient of 0-9% MeOH in CH_2Cl_2, the major *S* diastereomer might have been separated as no signals of the *R* diastereomer could be observed in the ^1H NMR spectrum. On the other hand, as the chiral center is remote from the carbohydrate moiety, it is possible that both diastereomers exhibit the same ^1H and ^{13}C spectral data. Although this was not further verified due to the shortage in material, **65** was still used as the building block for the SPPS of analogue **60** as previous study by Laursen[38] indicated that the relative configuration at the α-amino acid center is not an important factor for antifreeze activity.

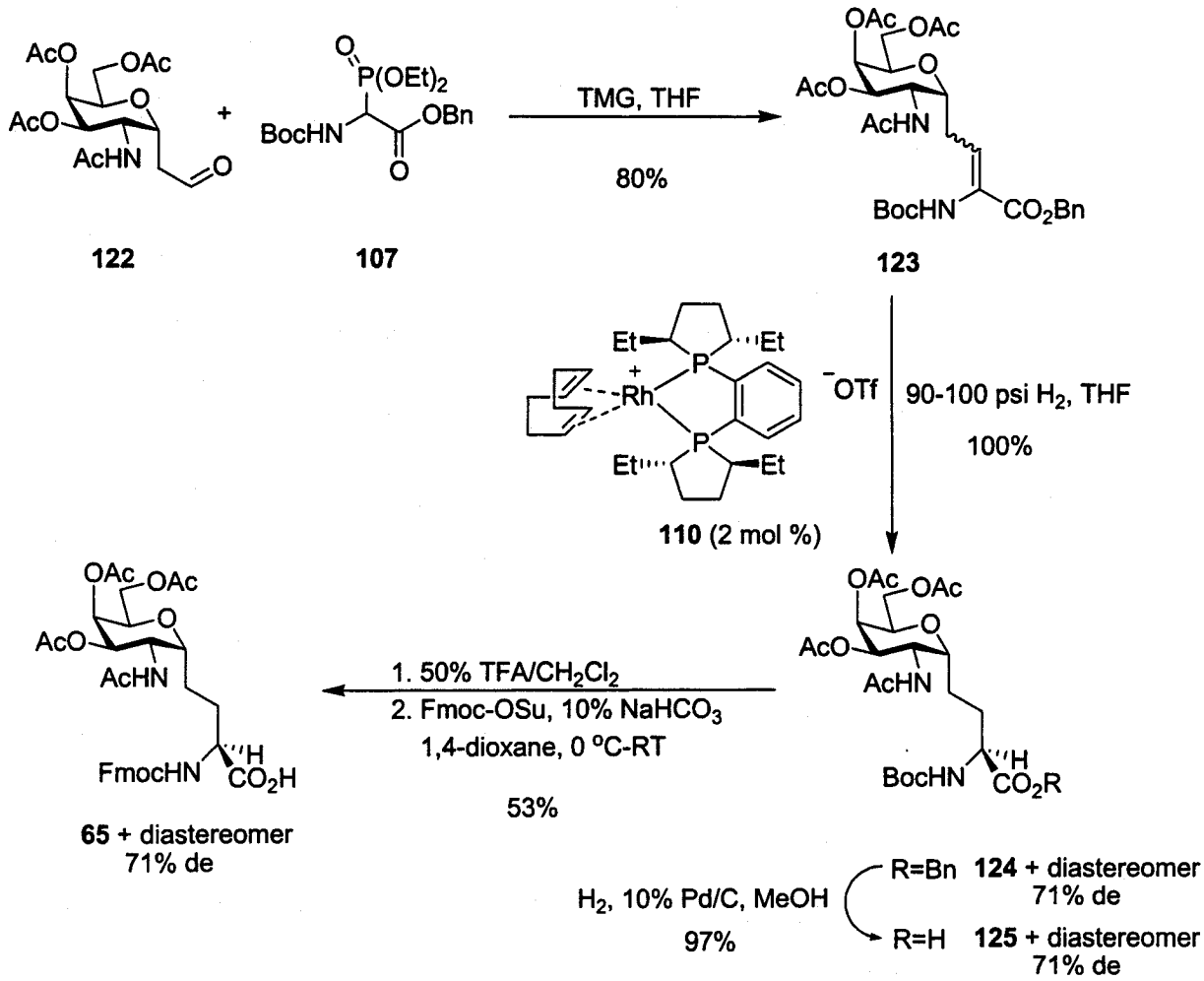

Scheme 3.29 Preparation of *N*-Fmoc *C*-GalNAc L-serine building block **65**.[11]

3.3.3 SPPS of *C*-Linked GalNAc L-Serine AFGP Analogue 60

As shown in Scheme 3.30, analogue **60** was prepared using Fmoc-chemistry SPPS. One L-glycine preloaded Wang resin with 0.65 mmol/g loading capacity was selected as the solid support. After manually assembling either *N*-Fmoc glycine or building block **65** with the desired sequence, the resulting polypeptide was cleaved from the resin to afford acetate-protected analogue **126** in 79% yield. The final analogue **60** was obtained in 85% yield after removing all acetate protecting groups from the carbohydrate residue.

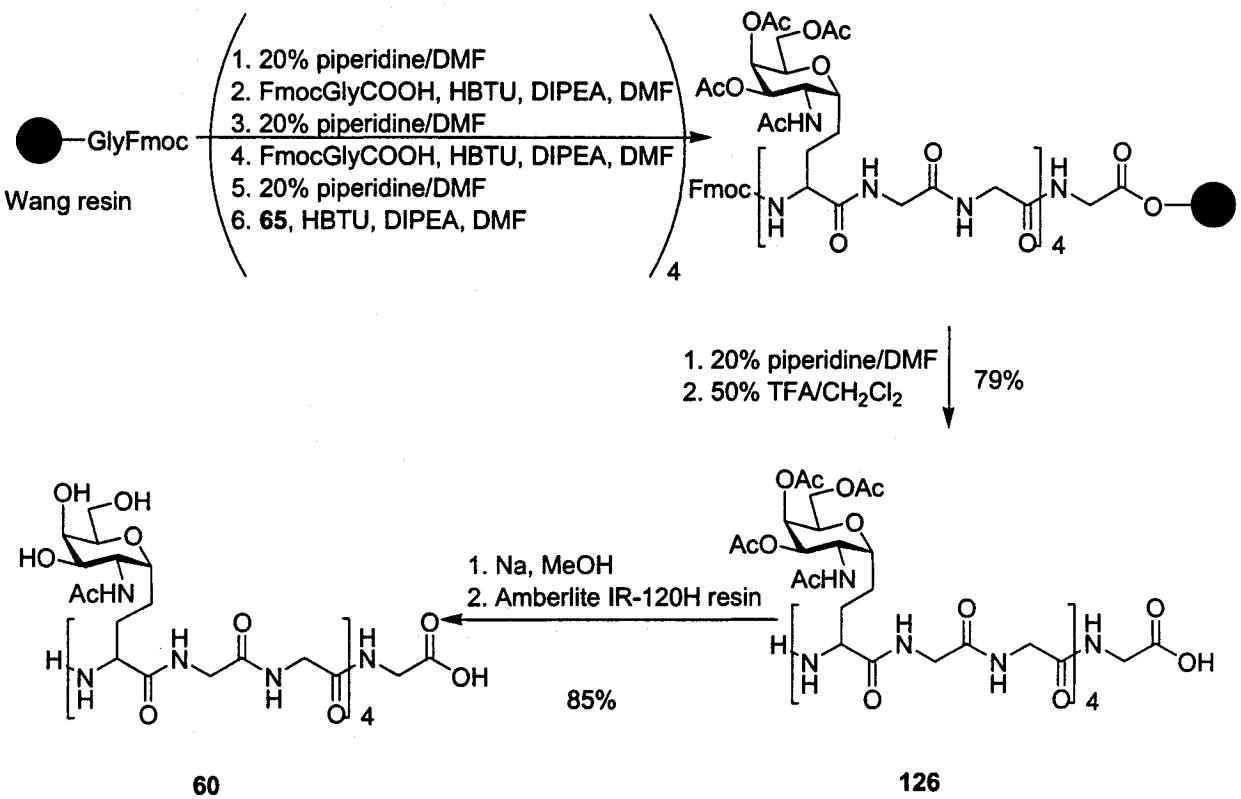

Scheme 3.30 SPPS of *C*-linked GalNAc L-serine AFGP analogue **60**.

3.4 Preparation of Neoglycopolymer 61

Radical polymerization was the preferred method to prepare glycopolymers until Grubbs[50] demonstrated the feasibility and advantages of the ring-opening metathesis polymerization

(ROMP) strategy. The driving force of ROMP is the release of the ring strain of the cyclic olefin in the norbornene residue. The high initiation rate of Grubbs' catalysts and the relatively stable ruthenium-carbene residues at the growing polymeric chain terminal formed during polymerization make ROMP a living polymerization process.[51] The resultant polymers usually show narrow polydispersities.[52] Therefore, neoglycopolymers with the desired molecular weight can be produced by controlling the monomer to catalyst ratio. A lactose-bearing neoglycopolymer that is structurally similar to **61** has been prepared by Kiessling from a glycosyl norbornene derivative using ROMP.[53] Neoglycopolymer **61** can be prepared using the same strategy from the corresponding *C*-glycosylated norbornene imide (Scheme 3.31). This monomer for polymerization can be easily prepared by coupling an *α*-*C*-galactosyl alcohol with a norbornene imide in a type of Mitsunobu reaction.

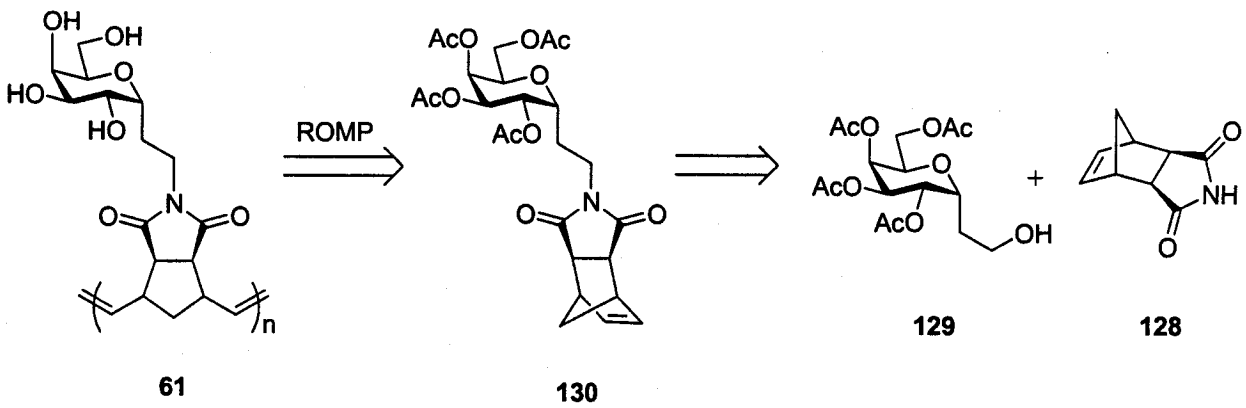

Scheme 3.31 Retrosynthesis of neoglycopolymer **61**.

The norbornene imide **128** was prepared starting from *endo*-norbornene anhydride. In order to simulate the relative configuration of the side chain in native AFGPs, the *exo*-form of norbornene anhydride **127** is required. Furthermore, the *exo*-form of glycosylated norbornene is a better monomer for ROMP than its *endo*-form, in which the bulky glycosyl side chain can block the interaction of the olefin with the catalyst. *Exo*-norbornene anhydride is thermodynamically more stable and can be prepared by heating its *endo*-form isomer.[54] Heating *endo*-norbornene anhydride at 190 °C resulted in a mixture of a 1:1 ratio of *endo*- and *exo*-anhydrides (Scheme 3.32). The pure *exo*-form anhydride **127** was purified by fractional recrystallization from benzene. The unconverted *endo*-norbornene anhydride was recycled and the heating-

recrystallization process was repeated three times to afford **127** in 85% cumulative yield. The norbornene imide **128** was prepared by heating the mixtures of **127** with urea at 150 °C.[55]

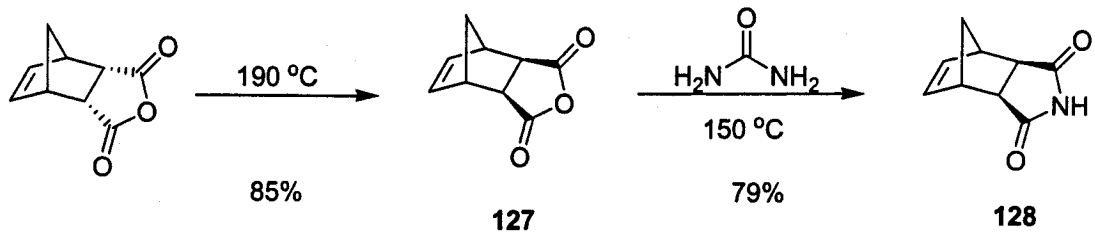

Scheme 3.32 Preparation of *exo*-norbornene imide **128**.[54,55]

C-Galactosyl alcohol **129** was prepared by ozonolysis of *C*-allylated galactose **84** and subsequent reduction with sodium borohydride (Scheme 3.33). The Mitsunobu coupling[53] of **129** with imide **128** using coupling reagent diethylazodicarboxylate (DEAD) afforded acetate-protected monomer **130** in 68% yield.

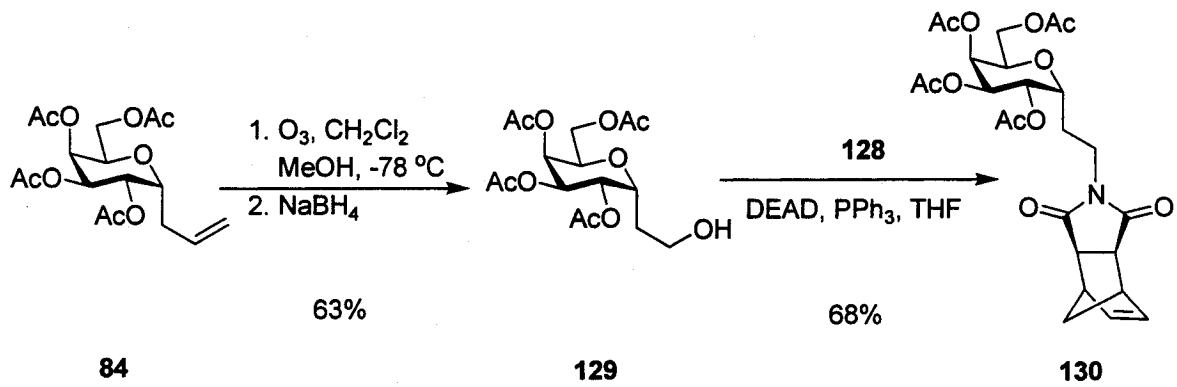

Scheme 3.33 Preparation of acetate protected monomer **130**.[53]

Grubbs' catalysts are well known for their stability to oxygen and humidity, and their tolerance to many polar functional groups, which makes it possible to carry out ROMP on in aqueous solution for unprotected carbohydrate-bearing monomers.[50,52,53] For this reason, monomer **130** was first deprotected by removing all acetate groups from the galactose moiety

under mild basic conditions before polymerization (Scheme 3.34). ROMP of monomer **131** was performed following Kiessling's procedure[53] using a first generation Grubbs' catalyst. A mixture of methanol, water and 1,2-dichloroethane was used as the solvent for polymerization. The heterogeneous two-phase reaction system was selected in order to dissolve both the hydrophilic monomer **131** and the hydrophobic Grubbs' catalyst. The living polymerization was quenched by ethyl vinyl ether and the resulting neoglycopolymer **61** had a maximum of fifteen monomers in length as analyzed by mass spectroscopy.

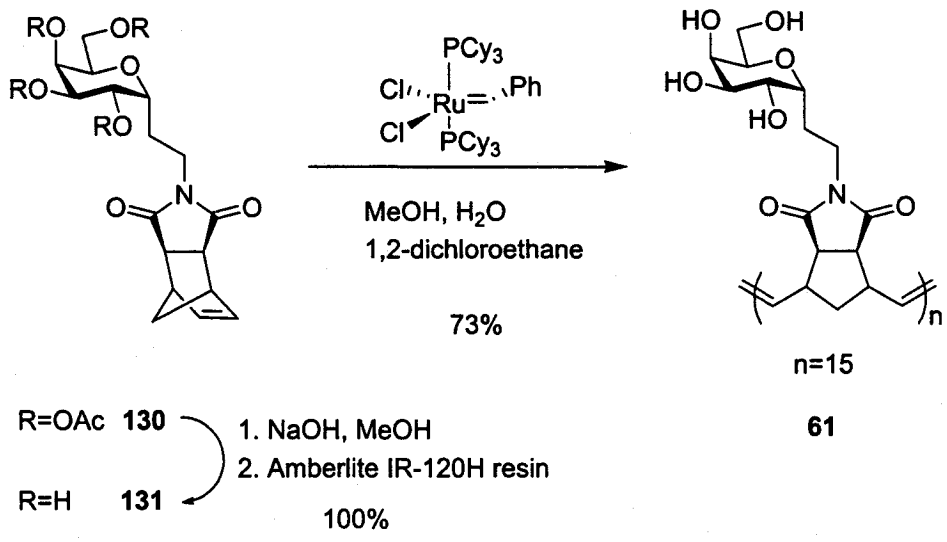

Scheme 3.34 Preparation of neoglycopolymer **61** using ROMP.[53]

In summary, *C*-linked AFGP analogues **57-60** were prepared using the Fmoc chemistry-based SPPS and a neoglycopolymer **61** was prepared using ROMP from a galactosyl norbornene monomer. The SPPS building blocks for analogues **57** and **60** were prepared using an olefin cross-metathesis strategy. However, the same method was proven not suitable for preparing the SPPS building blocks with only two methylene groups in the side chain. Instead, a catalytic asymmetric hydrogenation strategy was employed to prepare the SPPS building blocks for analogues **58** and **59**.

References

1. (a) Bielfeldt, T., Peters, S., Meldal, M., Bock, K., Paulsen, H. *Angew. Chem. Int. Ed.* **1992**, *31*, 857-859.
   (b) Filira, F., Biondi, L., Scolaro, B., Foffani, M. T., Mammi, S., Peggion, E., Rocchi, R. *Int. J. Biol. Macromol.* **1990**, *12*, 41-49.
   (c) Ben, R. N., Eniade, A. A., Hauer, L. *Org. Lett.* **1999**, *1*, 1759-1762.
2. (a) Dondoni, A., Marra, A. *Chem. Rev.* **2000**, *100*, 4395-4421.
   (b) Von Moos, E., Ben, R. N. *Curr. Top. Med. Chem.* **2005**, *5*, 1351-1361.
3. Bertozzi, C. R., Hoeprich, P. D. Jr., Bednarski, M. D. *J. Org. Chem.* **1992**, *57*, 6092-6094.
4. Dondoni, A., Marra, A., Massi, A. *Tetrahedron* **1998**, *54*, 2827-2832.
5. (a) Campbell, A. D., Paterson, D. E., Raynham, T. M., Taylor, R. J. K. *Chem. Commun.* **1999**, 1599-1600.
   (b) Paterson, D. E., Griffin, F. K., Alcaraz, M.-L., Taylor, R. J. K. *Eur. J. Org. Chem.* **2002**, *67*, 1323-1336.
6. Nolen, E. G., Watts, M. M., Fowler, D. J. *Org. Lett.* **2002**, *4*, 3963-3965.
7. Dorgan, B. J., Jackson, R. F. W. *Synlett* **1996**, 859-861.
8. Urban, D.; Skrydstrup, T.; Beau, J. *Chem. Commun.* **1998**, 955-956.
9. (a) Dondoni, A., Marra, A., Massi, A. *Chem. Commun.* **1998**, 1741-1742.
   (b) Dondoni, A., Marra, A., Massi, A. *J. Org. Chem.* **1999**, *64*, 933-944.
10. (a) Ben, R. N., Orellana, A., Arya, P. *J. Org. Chem.* **1998**, *63*, 4817-4820.
    (b) Dondoni, A., Mariotti, G., Marra, A. *Tetrahedron Lett.* **2000**, *41*, 3483-3486.
    (c) Dondoni, A., Mariotti, G., Marra, A. *J. Org. Chem.* **2002**, *67*, 4475-4486.
    (d) Vincent, S. P.; Schleyer, A.; Wong, C.-H. *J. Org. Chem.* **2000**, *65*, 4440-4443.
11. Debenham, S. D., Debenham, J. S., Burk, M. J., Toone, E. J. *J. Am. Chem. Soc.* **1997**, *119*, 9897-9898.
12. Debenham, S. D., Cossrow, J., Toone, E. J. *J. Org. Chem.* **1999**, *64*, 9153-9163.
13. (a) Roy, R., Das, S. K. *Chem. Commun.* **2000**, 519-529.
    (b) Jørgensen, M., Hadwiger, P., Madsen, R., Stütz, A. E., Wrodnigg, T. M. *Curr. Org. Chem.* **2000**, *4*, 565-588.
14. (a) Dominique, R., Liu, B. C., Das, S. K., Roy, R. *Synthesis* **2000**, 862-868.

(b) Dondoni, A.; Giovannini, P. P.; Marra, A. *J. Chem. Soc., Perkin Trans.* **2001**, *1*, 2380-2388.

(c) McGarvey, G. J.; Benedum, T. E.; Schmidtmann, F. W. *Org. Lett.* **2002**, *4*, 3591-3594.

(d) Nolen, E. G.; Kurish, A. J.; Wong, K. A.; Orlando, M. D. *Tetrahedron Lett.* **2003**, *44*, 2449-2453.

(e) Nolen, E. J., Kurish, A. J., Potter, J. M., Donahue, L. A., Orlando, M. D. *Org. Lett.* **2005**, *7*, 3383-3386.

15. Roe, B. A., Boojamra, C. G., Griggs, J. L., Bertozzi, C. R. *J. Org. Chem.* **1996**, *61*, 6442-6445.

16. (a) Lewis, M. D., Cha, J. K., Kishi, Y. *J. Am. Chem. Soc.* **1982**, *104*, 4976-4978.

(b) Kozikowski, A. P., Sorgi, K. L., Wang, B. C., Xu, Z.-B. *Tetrahedron Lett.* **1983**, *24*, 1563-1566.

(c) Hosomi, A., Sakata, Y., Sakurai, H. *Tetrahedron Lett.* **1984**, *25*, 2383-2386.

(d) Giannis, A., Sandhoff, K. *Tetrahedron Lett. 1985*, **26**, 1479-1482.

(e) Horton, D. Miyake, T. *Carbohydr. Res.* **1988**, *184*, 221-229.

(f) Panek, J. S., Sparks, M. A. *J. Org. Chem.* **1989**, *54*, 2034-2038.

(g) Bertozzi, C. R., Cook, D. G., Kobert, W. R., Gonzalez-Scarano, F., Bednarski, M. D. *J. Am. Chem. Soc.* **1992**, *114*, 10639-10641.

17. (a) Keck, G. E., Enholm, E. J. *Tetrahedron* **1985**, *41*, 4079-4094.

(b) Giese, B., Linker, T., Muhn, R. *Tetrahedron* **1989**, *45*, 935-940.

18. Bertozzi, C. R., Bednarski, M. D. *Tetrahedron Lett.* **1992**, *33*, 3109-3112.

19. Boons, G. J., Hale, K. J. *Organic Synthesis with Carbohydrates*, Blackwell Science: Malden, MA. **2000**.

20. Pontén, F., Magnusson, G. *J. Org. Chem.* **1996**, *61*, 7463-7466.

21. Keck, G. E., Yates, J. B. *J. Am. Chem. Soc.* **1982**, *104*, 5829-5831.

22. Keck, G. E., Byers, J. H. *J. Org. Chem.* **1985**, *50*, 5444-5446.

23. (a) Corey, E. J., Suggs, J. W. *Tetrahedron Lett.* **1975**, *31*, 2647-2650.

(b) Perkins, M. V.; Sampson, R. A. *Org. Lett.* **2001**, *3*, 123-126.

24. Abad, A.; Agulló, C.; Cuñat, A. C.; García, A. B.; Giménez-Saiz, C. *Tetrahedron* **2003**, *59*, 9523-9536.

25. Wong, C.-H., Moris-Varas, F., Hung, S.-C., Marron, T. G., Lin, C.-C., Gong, K. W., Weitz-Schmidt, G. *J. Am. Chem. Soc.* **1997**, *119*, 8152-8158.

26. Afzali-Ardakani, A. Rapoport, H. *J. Org. Chem.* **1980**, *45*, 4817-4820.

27. Tashiro, T., Fushiya, S., Nozoe, S. *Chem. Pharm. Bull.* **1988**, *36*, 893-901.

28. (a) Bacha, J. D., Kochi, J. K. *Tetrahedron* **1968**, *24*, 2215-2226.
(b) Hanessian, S., Sahoo, S. P. *Tetrahedron Lett.* **1984**, *25*, 1425-1428.

29. Schuster, M., Blechert, S. *Angew. Chem. Int. Ed. Engl.* **1997**, *36*, 2036-2056.

30. (a) Grubbs, R. H. *Tetrahedron* **2004**, *60*, 7117-7140.
(b) Huang, J. K., Stevens, E. D., Nolan, S. P., Petersen, J. L. *J. Am. Chem. Soc.* **1999**, *121*, 2674-2678.
(c) Trnka, T. M., Grubbs, R. H. *Acc. Chem. Res.* **2001**, *34*, 18-29.

31. (a) Weskamp, T., Kohl, F. J., Herrmann, W. A. *J. Organomet. Chem.* **1999**, *582*, 362-365.
(b) Weskamp, T., Kohl, F. J., Hieringer, W., Gleich, D., Herrmann, W. A. *Angew. Chem. Int. Ed.* **1999**, *38*, 2416-2419.
(c) Ackermann, L., Ftirstner, A., Weskamp, T., Kohl, F. J., Herrmann, W. A. *Tetrahedron Lett.* **1999**, *40*, 4787-4790.

32. (a) Arduengo, A. J. III, Krafczyk, R., Schmutzler, R., Craig, H. A., Goerlich, J. R., Marshall, W. J., Unverzagt, M. *Tetrahedron* **1999**, *55*, 14523-14534.
(b) Huang, J. K., Schanz, H.-J., Stevens, E. D., Nolan, S. P. *Organometallics* **1999**, *18*, 5375-5380.
(c) Scholl, M., Trnka, T. M., Morgan, J. P., Grubbs, R. H. *Tetrahedron Lett.* **1999**, *40*, 2247-2250.
(d) Trnka, T. M., Morgan, J. P., Sanford, M. S., Wilhelm, T. E., Scholl, M., Choi, T.-L., Ding, S., Day, M. W., Grubbs, R. H. *J. Am. Chem. Soc.* **2003**, *125*, 2546-2558.

33. Chatterjee, A. K., Choi, T.-L. Sanders, D. P., Grubbs, R. H. *J. Am. Chem. Soc.* **2003**, *125*, 11360-11370.

34. (a) Schmidt, U., Lieberknecht, A., Wild, J. *Synthesis* **1984**, 53-60.
(b) Shankar, R., Scott, A. I. *Tetrahedron Lett.* **1993**, *34*, 231-234.

35. (a) Schmidt, U.; Lieberknecht, A.; Schanbacher, U.; Benttler, T.; Wild, J. *Angew. Chem., Int. Ed. Engl.* **1982**, *21*, 776-777.

(b) Schmidt, U.; Griesser, H.; Leitenberger, V.; Lieberknecht, A.; Mangold, R.; Meyer, R.; Riedl, B. *Synthesis* **1992**, 487-490.

36. (a) Burk, M. J., Feaster, J. E., Nugent, W. A., Harlow, R. L. *J. Am. Chem. Soc.* **1993**, *115*, 10125-10138.

(b) Burk, M. J., Harper, T. G. P., Kalberg, C. S. *J. Am. Chem. Soc.* **1995**, *117*, 4423-4424.

(c) Burk, M. J., Gross, M. F., Martinez, J. P., *J. Am. Chem. Soc.* **1995**, *117*, 9375-9376.

(d) Burk, M. J., Wang, Y. M., Lee, J. R. *J. Am. Chem. Soc.* **1996**, *118*, 5142-5143.

37. Knowles, W. S. *Acc. Chem. Res.* **1983**, *16*, 106-112.

38. Wen, D. Y., Laursen, R. A. *FEBS Lett.* **1993**, *317*, 31-34.

39. Carpino, L. A., Han, G. Y. *J. Org. Chem.* **1972**, *37*, 3404-3409.

40. Fields, G. B., Noble, R. L. *Int. J. Pept. Protein Res.* **1990**, *35*, 161-214.

41. The scheme is modified from Aldrich's online note: http://www.sigmaaldrich.com/img/assets/19200/solid_phase_synthesis.pdf.

42. (a) Wang, S.-S. *J. Org. Chem.* **1976**, *41*, 3258-3261.

(b) Lu, G.-S., Mojsov, S., Tam, J. P., Merrifield, R. B. *J. Org. Chem.* **1981**, *46*, 3433-3436.

43. Xie, J. *Recent Res. Devel. Organic Chem.* **1999**, *3*, 505-523.

44. Garcia Martin, M. G., Horton, D. *Carbohydr. Res.* **1989**, *191*, 223-228.

45. Cui, J. R., Horton, D. *Carbohydr. Res.* **1998**, *309*, 319-330.

46. (a) SanMartin, R., Tavassoli, B., Walsh, K. E., Walter, D. S., Gallagher, T. *Org. Lett.* **2000**, *2*, 4051-4054.

(b) Grant, L., Liu, Y., Walsh, K. E., Walter, D. S., Gallagher, T. *Org. Lett.* **2002**, *4*, 4623-4625.

47. Roth, W., Pigman, W. *Methods Carbohydr. Chem.* **1963**, *2*, 405-408.

48. Mitchell, S. A., Pratt, M. R., Hruby, V. J., Polt, R. *J. Org. Chem.* **2001**, *66*, 2327-2342.

49. (a) Tingoli, M., Tiecco, M., Chianelli, D., Balducci, R., Temperini, A. *J. Org. Chem.* **1991**, *56*, 6809-6813.

(b) Santoyo-González, F., Calvo-Flores, F. G., García-Mendoza, P., Hernández-Mateo, F., Isac-García, J., Robles-Díaz, R. *J. Org. Chem.* **1993**, *58*, 6122-6125.

(c) Czernecki, S., Randriamandimby, D. *Tetrahedron Lett.* **1993**, *34*, 7915-7916.

(d) Czernecki, S., Ayadi, E., Randriamandimby, D. *J. Org. Chem.* **1994**, *59*, 8256-8260.

(e) Rubinstenn, G., Esnault, J., Mallet, J.-M., Sinaÿ, P. *Tetrahedron-Asymmetry* **1997**, *8*, 1327-1336.

50. Fraser, C., Grubbs, R. H. *Macromolecules* **1995**, *28*, 7248-7255.
51. Schrock, R. R. *Pure Appl. Chem.* **1994**, *66*, 1447-1454.
52. Lynn, D. M., Kanaoka, S., Grubbs, R. H. *J. Am. Chem. Soc.* **1996**, *118*, 784-790.
53. Pohl, N. L., Kiessling, L. L. *Synthesis* **1999**, *SI*, 1515-1519.
54. (a) Craig, D. *J. Am. Chem. Soc.* **1951**, *73*, 4889-4892.
    (b) Canonne, P., Bélanger, D., Lemay, G. *J. Org. Chem.* **1982**, *47*, 3953-3959.
55. Crockett, G. C., Swanson, B. J., Anderson, D. R., Koch, T. H. *Synthetic Commun.* **1981**, *11*, 447-454.

Chapter 4 Assessing Antifreeze Activity and Solution Conformation of *C*-Linked AFGP Analogues

Thermal hysteresis (TH) and recrystallization inhibition (RI) are the two distinct properties that differentiate biological antifreezes from colligatively acting cryoprotectants. TH is a non-colligative phenomenon that results in a freezing point depression below that of the equilibrium melting point. Alternatively, RI actually shows protecting effects to cells by prohibiting small ice crystals from growing into harmful large ice grains.

Both TH and RI activities are believed to be caused by the direct binding of antifreeze molecules to ice crystals.[1] Conformational studies of biological antifreezes are important for us to understand whether antifreeze molecules need to adopt certain conformations to meet the crystallographic requirement and form effective interactions with ice lattices. Circular dichroism (CD) has been widely used to measure the conformation of biological macromolecules. Therefore, in this study, CD spectroscopy was used to characterize the conformations of *C*-linked AFGP analogues.

4.1 Assessing Thermal Hysteresis (TH) and Dynamic Ice-Shaping (DIS) Activities of *C*-Linked AFGP Analogues

Nanoliter osmometry has been widely used to assess thermal hysteresis.[2] In this technique, a drop (sub-microliter) of solution in distilled water is introduced into an oil-filled cylindrical well. Then, the solution is flash frozen at -40 °C and slowly warmed up to acquire a stable single ice crystal. The equilibrium melting point and the non-equilibrium freezing point are determined when the ice crystal starts shrinking during warming or starts growing during cooling respectively. Both the warming and the cooling processes are controlled at a constant rate of 10 mOsmol (0.0186 °C) per 15 seconds.

In addition to the TH activity, the quantitative indicator for the effectiveness of freezing point depression,[3] antifreezes can also modify the morphology of ice crystals and change the dynamics of the ice growing process.[4] A single ice crystal is used as the seed ice in the nanoliter

osmometry assay. This is important for studying the morphological and dynamic changes of the seed ice at temperatures around the TH gap. During the cooling process of a colligative solution, solutes are excluded from the ice crystal and remain in the solution phase.[5] Therefore, the ice crystal grows independently without interaction with the colligative solutes and forms a circular disk (Figure 4.1 A). Dynamically, the growth of the ice crystal initiates from the beginning of the cooling process and proceeds gradually until the entire solution is frozen.

In contrast, biological antifreezes can selectively bind to specific prism or secondary prism faces of the ice crystal and force ice to grow only on the basal planes, which results in formation of the characteristic bipyramidal structures (Figure 4.1 B). This unique ability is known as dynamic ice-shaping (DIS).[6] Dynamically, the ice crystal in an antifreeze solution does not grow within the TH gap. However, once the temperature is lowered beyond the TH gap, the seed ice crystal can "sprout" with dramatically accelerated growth rate and form a needle-shaped ice fiber (Figure 4.1 C), which followed by the immediate frozen of the entire solution. The temperature at which the seed ice crystal starts to grow into a needle-shaped structure is defined as the non-equilibrium freezing point of the antifreeze solution.

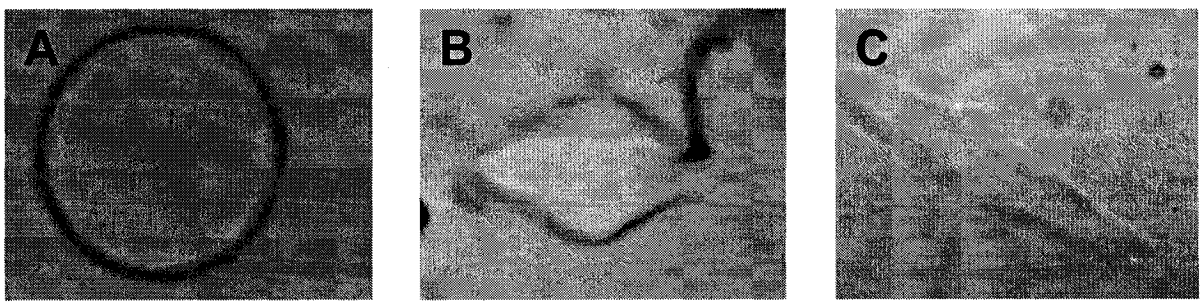

Figure 4.1 Nanoliter osmometry images of ice crystals.

A: In water; **B**: In AFGP8 solution at temperatures within the TH gap; **C**: In AFGP8 solution at temperatures below the TH gap.

In our studies, TH and dynamic ice-shaping activities of *C*-linked AFGP analogues **57-61** were studied using a Clifton nanoliter osmometer and the results are shown in Table 4.1. Analogues **57-59** are *C*-Linked galactosyl AFGP analogues with different side chain lengths (three single carbon-carbon bonds for **57**, four for **58** and five for **59**). Analogue **60** is composed

of four *C*-L-serine-(D-GalNAc)-glycine-glycine tripeptide repeating units. *C*-Galactosyl norbornene neoglycopolymer **61** has a maximum of fifteen monomers in length. Similar to most of previously prepared analogues, the solutions of analogues **57-61** in water displayed no difference between melting and freezing points, which indicated that none of the new generation of *C*-linked AFGP analogues has thermal hysteresis activity. In the solutions of analogues **57-59** and **61**, ice crystals grew as circular disks, indicating that these analogues have no dynamic ice-shaping ability, either. However, the ice crystal demonstrated a weak hexagonal structure in the solution of analogue **60**, which possesses an acetamide functionality in the carbohydrate moiety. This result indicated that analogue **60** has the dynamic ice-shaping activity and can interact with ice lattices.

Table 4.1 Nanoliter osmometry assay results of *C*-linked AFGP analogues **57-61**.*

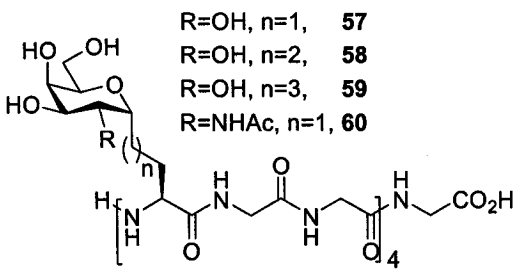

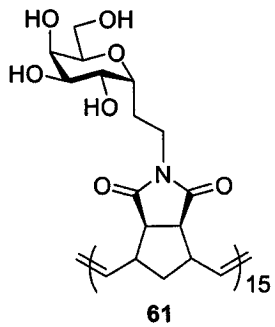

61

Analogues	TH	Dynamic ice-shaping
57	0 °C	none
58	0 °C	none
59	0 °C	none
60	0 °C	 hexagonal
61	0 °C	none

Given that many structural moieties, such as the L-alanine unit in the polypeptide backbone and the β-methyl group on the L-threonine residue, were modified in our new *C*-linked AFGP

* Analogues **57** and **60** may contain D-*C*-serine residues in the polypeptide backbones.

analogues, the fact that none of them demonstrated TH activity is not surprising. One of the purposes in preparing analogues **57-59** was to study the function of the relatively rigid amide bond in the side chain linker of previously prepared *C*-linked AFGP analogues. The only analogues which demonstrated TH are analogues **54** and **55** having six and nine L-lysine-(D-galactose)-glycine-glycine tripeptide repeating units, respectively. In our new analogues **57-59**, the rigid amide bonds in analogues **54** and **55** were substituted by more flexible carbon-carbon bonds and the analogues demonstrated no TH and DIS activities. This result is consistent with previously prepared non-effective divalent analogue **56**, in which the amide bonds in analogues **54** and **55** were replaced by carbon-nitrogen bonds and no TH and DIS activities were exhibited. Therefore, it seems reasonable that a relatively rigid side chain is necessary for *C*-linked AFGP analogues to show effective TH and DIS activities. It is also possible that the rigid side chain can directly affect the orientation of the carbohydrate moiety, which may be important for forming effective interactions with ice lattices. However, the absence of the amide bond in the side chain may not be the only reason for the fact that analogues **57-59** did not demonstrate TH and DIS activities. The length of the polypeptide backbones in analogues **54** (six tripeptide repeating units) and **55** (nine tripeptide repeating units) are longer than that in analogues **57-59** (four tripeptide repeating units). Therefore, the polypeptide length may also be an important factor for TH and DIS activities in these *C*-linked AFGP analogues.

C-Linked GalNAc Serine AFGP analogue **60** did not show detectable TH activity. However, instead of a circular disk, a hexagonal ice crystal was observed in the solution of **60** (Table 4.1), indicating that analogue **60** has interactions with the ice lattice. The major structural difference between analogues **60** and **57** is that analogue **60** possesses a C2 acetamide group on the pyranose ring, while analogue **57** possesses a hydroxyl group at the same position. Therefore, this result suggested that the acetamide group is an important structural motif for the *C*-linked AFGP analogue to form interactions with ice lattices. However, although analogue **60** modified the structure of the ice crystal from circular disk to hexagon, it could not cause the formation of a bipyramidal ice crystal as temperature decreased and did not show any TH activity. This result implied that the interaction between analogue **60** and ice lattices is not strong enough to prohibit ice from growing on the non-basal planes of ice crystals.

Our reason for using a non-polypeptide chain as the backbone for AFGP analogues was to study the importance of the polypeptide scaffold for antifreeze-specific activities. In

neoglycopolymer **61**, the polypeptide backbone in native AFGPs was replaced by the polymeric chain of alternating ethylene groups and cyclopentane rings, which resulted in a complete loss of TH and DIS activities, although neoglycopolymer **61** contains D-galactose, the most effective monosaccharide for antifreeze activities. This result indicated that a polypeptide backbone with specific amino acid composition is required for maintaining TH and DIS activities. It is known that amino acid variations on polypeptide backbones exist in native AFGPs.[1] For example, in AFGP6-8, the first L-alanine following the glycosylated L-threonine is occasionally replaced by an L-proline. However, this amino acid variation is usually found in only one tripeptide unit. Therefore, the loss of TH and DIS activities in neoglycopolymer **61** is probably due to the complete removal of the polypeptide backbone. Thus, it seems that the polypeptide backbone is necessary for antifreeze-specific activities.

In summary, the TH and DIS activity study on analogues **57-61** with nanoliter osmometry indicates that a rigid side chain, the orientation of the carbohydrate moiety, an acetamide functionality on the carbohydrate moiety (at the C2 position of the galactosamine residue) and a polypeptide backbone with specific amino acid composition are all important structural motifs for *C*-linked AFGP analogues to form effective interactions with ice lattices and show TH activity.

4.2 Assessing Recrystallization Inhibition (RI) Activity of *C*-Linked AFGP Analogues

Recrystallization inhibition (RI) is another property of biological antifreezes. RI protects organisms in partially frozen environments with a different mechanism from TH. Ice recrystallization transforms small ice grains to larger grains that can physically deform or rupture cell membranes, causing mechanical injury to cells and tissues.[7] As described previously in section 1.2.3, recrystallization is the result of the boundary migration of ice grains with different crystallographic orientations. The driving force of this spontaneous process is to lower the overall interfacial energy of the system by decreasing the overall number of ice grains. The mechanism by which biological antifreezes inhibit ice recrystallization has been thoroughly studied by Knight.[8] Biological antifreezes can effectively bind to the ice surface at the ice-

solution interfaces between the neighboring grain boundaries and immobilize the migration of ice grains, thus preventing them from merging with each other to form large ice crystals.

The RI activities of *C*-linked AFGP analogues were measured using a recrystallization inhibition assay developed by Myers and Horwath.[9] A "splat cooling" method was used to produce fine-grained ice samples for the RI activity study.[8, 9] In this assay, a 10 μL analogue solution in PBS was dropped from three meters high through a shielding tube to a polished aluminum block, which was pre-cooled to -80 °C on dry ice. With this method, analogue solutions formed a thin ice wafer composed of extremely tiny ice grains. The wafer was then moved onto a microscope cover glass and quickly transferred into a cold chamber, which was dried with continuous air flow to avoid moisture condensing on the ice wafer. The sample was annealed at -6 °C for 30 minutes before the size of the ice grains was photographed through a microscope. Ice recrystallization happens during this annealing process. The size of the ice grains is dependent on the sample's recrystallization inhibition ability.

For each sample, six photographs were taken from different areas of the ice wafer. Ice grains were regarded as two dimensionals[8a] and the size of ice grains was calculated by taking the average surface area of the ten largest ice grains in each photograph. The surface of each ice grain was approximated as an elliptical area (Figure 4.2). The major and minor elliptical axes were defined by the two largest dimensions orthogonally across the ice grain surface. The surface area of each ice grain was calculated based on the formula: $A = \pi ab$, in which A represented area; a and b represented the radii of the major and minor elliptical axes, respectively.

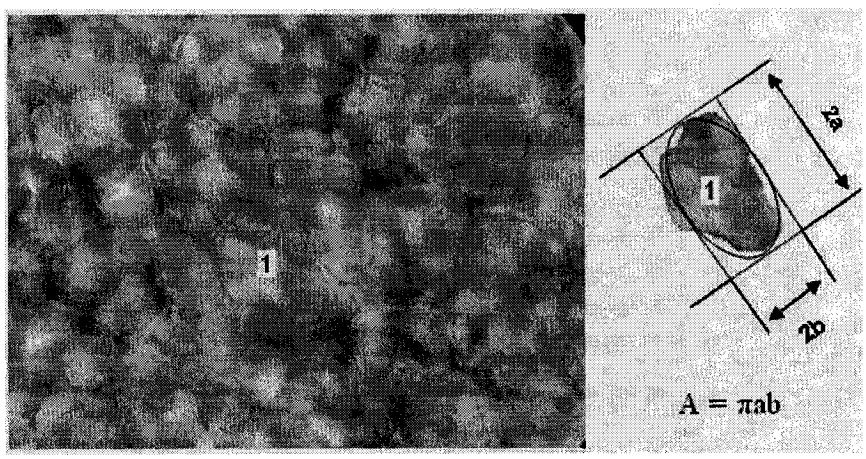

Figure 4.2 Illustration of calculating surface areas of ice grains.

Although biological antifreezes depress freezing points in a non-colligative manner, it is known that the RI effects of biological antifreezes are still somewhat concentration-dependent.[9a] Figure 4.3 shows the RI assay result of native AFGP8 with different concentrations in PBS. Given this, the RI activity of AFGP8 dramatically increases as a function of concentrations. Compared to PBS, AFGP8 demonstrated obvious RI activity at concentrations as low as 10^{-8} M. When the concentration of AFGP8 was increased to be greater than 10^{-5} M, the ice grains became smaller than the thickness of the ice wafer (about 20 μm)[8a] even after 30 minutes annealing, which caused ice grains to be very difficult to be resolved on photographs. For these reasons, three concentrations, $5.5X10^{-6}$ M, $5.5X10^{-8}$ M and $5.5X10^{-11}$ M, were selected for measuring the RI activity of each *C*-linked AFGP analogue and compared to that of native AFGP8.

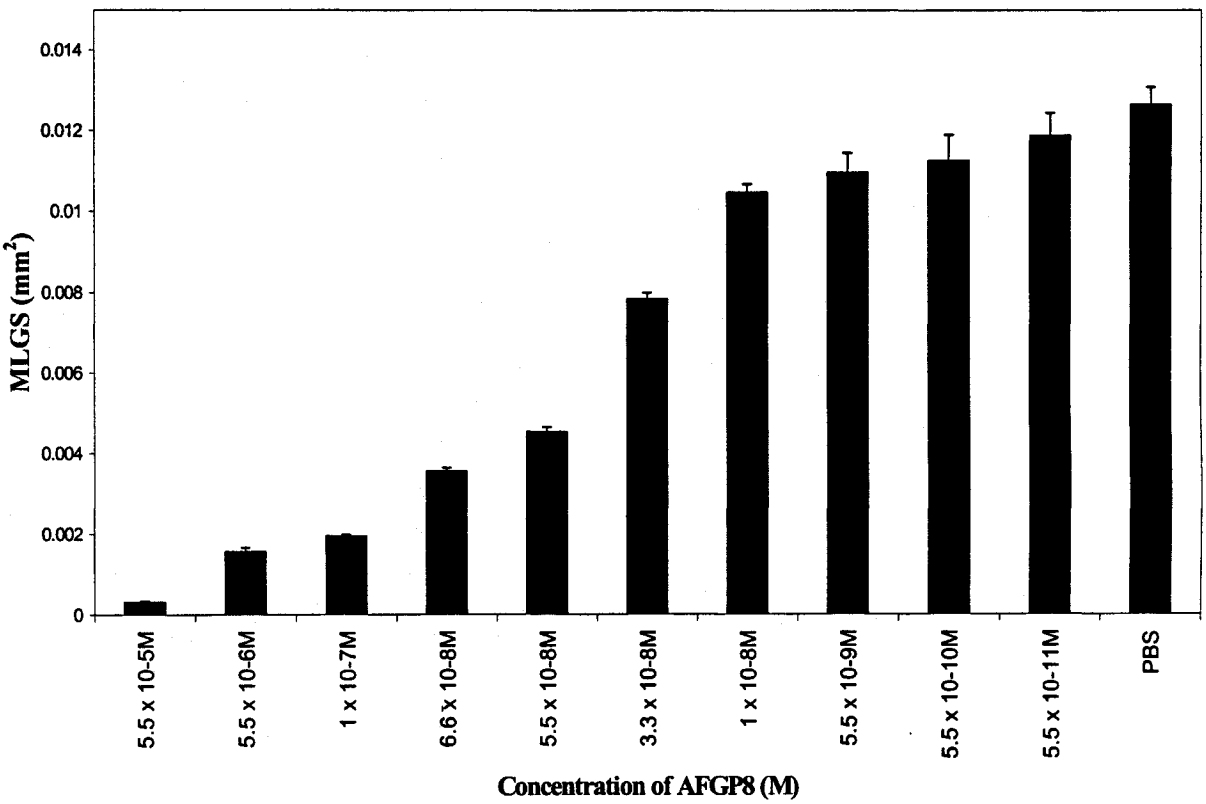

Figure 4.3 Recrystallization inhibition assay of AFGP8.

Another important reason for using three different concentrations to measure the RI activity is to rule out the non-specific RI effect of regular proteins.[8a, 9a] These TH-inactive proteins can display weak RI activity by simply inhibiting the mobility of the solid/liquid boundary. However, this non-specific RI activity is a linear response and does not increase dramatically as the concentration increases. Therefore, we can differentiate these regular proteins from RI-active proteins by using three different concentrations to assess the RI activity. For the same reason, the RI activity of *C*-linked AFGP analogues was tested in PBS solution instead of water because the presence of inorganic salts can also help to remove the non-specific RI effect.[8a]

It is worth to point out that the effective concentrations for showing RI activity (10^{-8} M, or $2.6X10^{-5}$ mg/mL for AFGP8) is much lower than that required for showing TH activity (usually 10 mg/mL). This is probably due to the "splat cooling" method used for preparing the ice wafer in the RI assay.[3b] With this technique, the sample solution is rapidly frozen and solutes are excluded from tiny ice grains and congregated on grain boundaries, thus causing a localized concentration increase in these areas.[3b] Therefore, a relatively low concentration of antifreeze solution can still inhibit the grain boundary migration and ice recrystallization.

The RI assay results of *C*-linked galactosyl AFGP analogues **57-59** are shown in Figure 4.4 and Table 4.2. Although no TH and DIS activities were detected, all analogues demonstrated RI activity compared to PBS solution. *C*-Linked galactosyl serine analogue **57** is the most effective analogue. At a concentration of $5.5X10^{-6}$ M, analogue **57** demonstrated the average ice grain size about 0.0025 mm^2, which is about 80% smaller than the grain size in PBS ice wafer. More importantly, analogue **57** demonstrated very comparable RI activity to native AFGP8. At molar concentration of $5.5X10^{-6}$ M, the RI activity of analogue **57** is about 92% as effective as native AFGP8. Analogue **57** is also a more effective recrystallization inhibitor than the type III AFP isolated from the ocean pout (*Macrozoarces americanus*), which has an effective concentration for RI activity at $7.1X10^{-7}$ M compared with $5.5X10^{-8}$ M in analogue **57**.[10] Interestingly, the RI activities of analogues **58** and **59** are very limited compared to analogue **57**. The size of ice grains is about 92% as large as that in PBS wafer. No significant difference in ice grain size exists between these two analogues in three different concentrations tested for each analogue. This result is consistent with the non-specific RI effect,[8a, 9a] which suggests that analogues **58** and **59** do not possess effective RI activity.

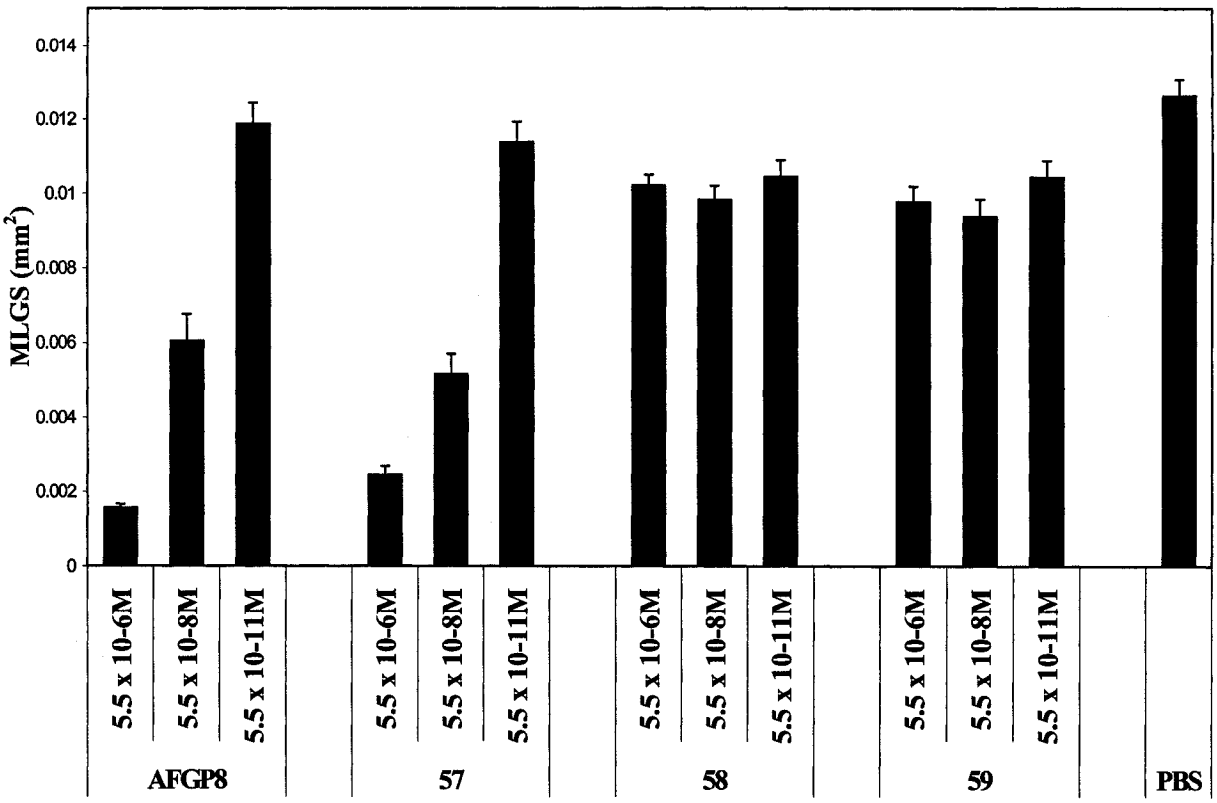

Figure 4.4 RI assay results of AFGP8 and *C*-linked AFGP analogue **57-59**.

Table 4.2 MLGS of AFGP8, **57-59** and PBS (surface area ± SEM[11], unit: mm^2).

	AFGP8	**57**	**58**	**59**	**PBS**
$5.5x10^{-6}$ M	0.0016±0.0001	0.0025±0.0002	0.0102±0.0003	0.0098±0.0004	0.0126±0.0004
$5.5x10^{-8}$ M	0.0061±0.0007	0.0052±0.0005	0.0098±0.0004	0.0094±0.0005	
$5.5x10^{-11}$ M	0.0119±0.0006	0.0114±0.0005	0.0104±0.0004	0.0104±0.0005	

Since no TH and DIS activities were detected, the potent RI activity demonstrated by analogue **57** was not expected. Compared to native AFGP8, drastic modifications were made in analogue **57**, such as using D-galactose to replace the disaccharide unit, using *C*-linked L-serine to replace the *O*-linked L-threonine and using glycine to replace L-alanine. These structural changes

resulted in the complete loss of TH and DIS activities in analogue **57**. However, based on its potent RI activity, it seems that analogue **57** does have interactions with ice surfaces and inhibits grain boundary migration. Since DIS is the standard for assessing sample-ice interactions, these results seem controversial. We hypothesize that the requirements of interactions between analogue **57** and ice lattices are different for demonstrating RI and DIS activities. These results also verify that TH, DIS and RI activities are not necessarily coupled effects for AFGP analogues.[12]

Although it may contain some D-*C*-serine residues in the polypeptide backbone, analogue **57** still showed much more potent RI activity than analogues **58** and **59**. This result is in agreement with Laursen's study that antifreeze activity is not affected by the relative configuration at the α-amino acid center.[13]

The difference in RI activity between analogue **57** and analogues **58** and **59** was surprising as these *C*-linked AFGP analogues share similar structural features. Except for analogue **57** which may contain some D-*C*-serine residues, the major difference among these analogues is the length of the side chain between the carbohydrate and polypeptide moieties. Analogue **57** possesses an almost identical side chain length as native AFGPs and demonstrated similar RI activity. However, an increase of the length of side chain by one (analogue **58**) or two (analogue **59**) additional carbon-carbon bonds caused the complete loss of RI activity in both resulting analogues. The correlation between the increased side chain length and decreased RI activity suggested that an optimal distance between the carbohydrate and polypeptide moieties exists and plays a key role in RI activity of our *C*-linked analogues.

Based on the above discussion, it seems that a shorter side chain length, which is similar to that in native AFGP8, is important for *C*-linked AFGP analogues to show potent RI activity. However, the side chain length is not the only factor that can affect RI activity. Previously prepared analogue **42** contains a side chain that is much longer even than that in analogue **59**, but still demonstrated similar activity to analogue **57** (Figure 4.5). Compared to the flexible side chains in analogues **57-59**, a relatively rigid amide bond with partial double bond character exists in the side chain of analogue **42**. The rigidity of the side chain in AFGP analogues can directly affect the orientation of the carbohydrate moieties, and previous studies have indicated that the RI activity of *C*-linked AFGP analogues is proportional to the carbohydrate concentration.[14]

Therefore, the potent RI activity of analogue **42** is presumably due to the fact that the rigid side chain can limit the extent of free rotations of the carbohydrate moiety and stabilize it in a certain orientation, so as to increase vicinal carbohydrate concentrations. On the other hand, in analogues **58** and **59**, the side chains are too flexible to keep the carbohydrate moiety in a certain orientation, thus causing these two analogues to show very limited RI activities.

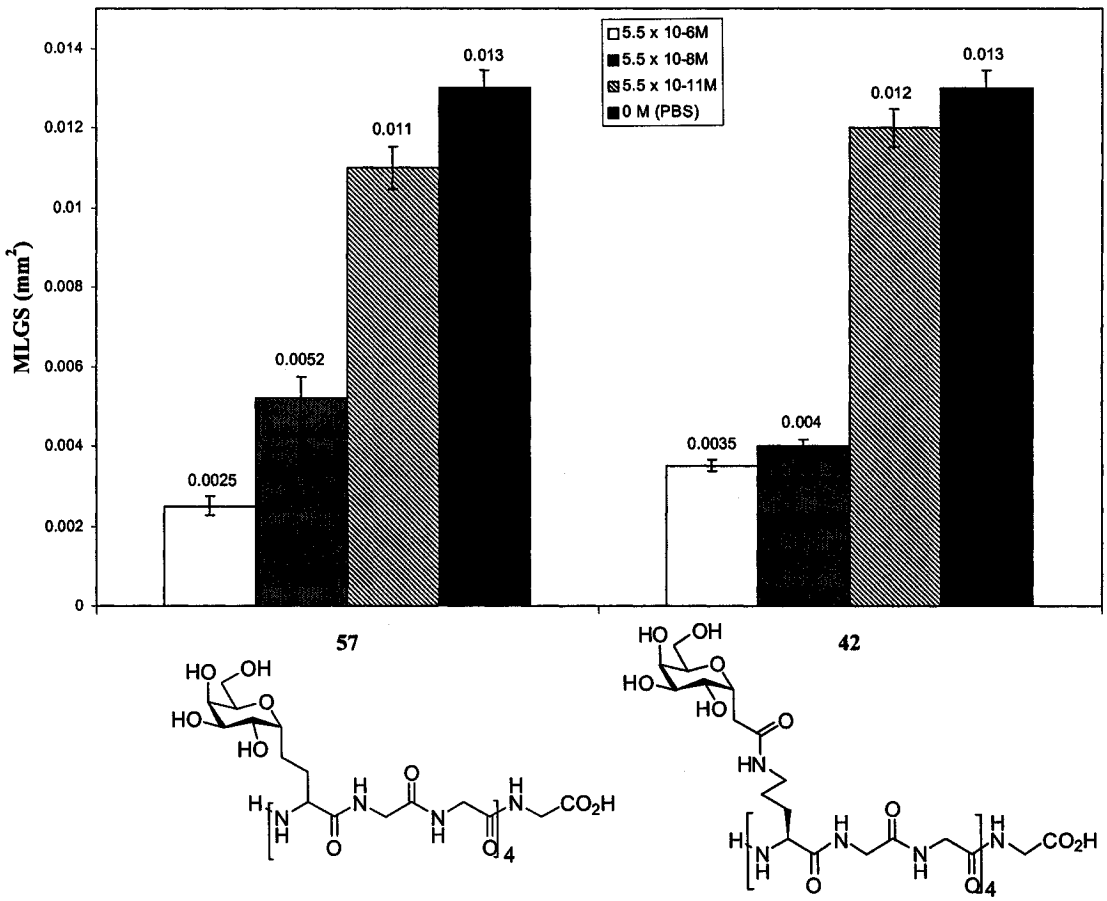

Figure 4.5 Comparison of RI activities between analogue **57** and analogue **42**.

The RI activity of *C*-linked GalNAc serine analogue **60** is shown and compared to analogue **57** in Figure 4.6. At a concentration of $5.5X10^{-6}$ M, the RI activity of analogue **60** is only about 31% of analogue **57**. This result was confusing, since analogue **60** is the only analogue that demonstrated dynamic ice-shaping ability, which indicated that there is interaction between analogue **60** and ice lattices. Furthermore, the length of the side chain in analogue **60** is exactly

the same as that in analogue **57**. Therefore, we expected analogue **60** to have at least the same RI activity as analogue **57**.

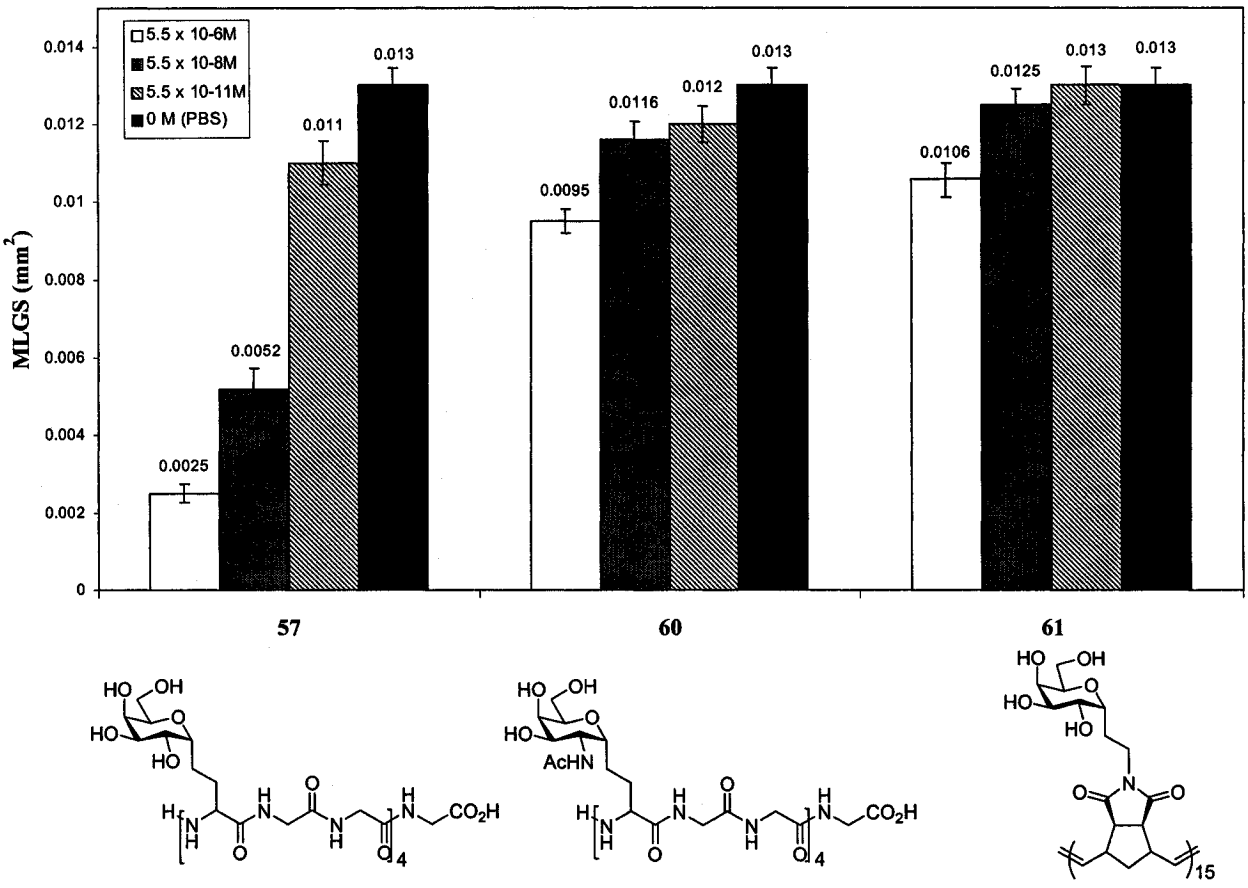

Figure 4.6 Comparison of RI activities between analogue **57** and analogue **60**.

The major structural difference in analogue **60** from analogue **57** is the acetamide group at the C2 position on the carbohydrate moiety. The nanoliter osmometry assay indicated that the C2 acetamide group is an important structural motif for showing DIS in *C*-linked AFGP analogues. Nishimura also indicated that the acetamide group is essential for TH and DIS activities in *O*-linked AFGP analogues.[15] However, the induction of the acetamide functionality into analogue **57** proved to be detrimental for RI activity, as the resulting analogue **60** demonstrated very limited ability to inhibit recrystallization. Therefore, it seems that the interaction between analogue **60** and ice lattices which can cause DIS activity is not necessarily effective enough for RI activity. A previous NMR study indicated that the secondary amine proton in the acetamide

group is capable of forming hydrogen bonds with the carbonyl oxygen in the L-threonine residue in native AFGPs.[3b, 16] If this were the case for analogue **60**, it might change the local conformation of small segments on the polypeptide backbone to be different from analogue **57**, and cause analogue **60** to lose the ability to form an effective interaction with ice lattices that is required for RI activity. Therefore, although the acetamide group has been identified as an important structural motif for TH and DIS activities in native AFGPs,[3b, 16] our study indicated that the acetamide group is not a favorable functionality for RI activity in the *C*-linked AFGP analogues. This result also suggested that efficient antifreeze-specific activities can not be achieved by the simple addition of individual favorable structural motifs that have been identified in native AFGPs.

Neoglycopolymer **61** also did not show effective RI activity (Figure 4.6). At molar concentrations of $5.5X10^{-8}$ M and $5.5X10^{-11}$ M, the size of the ice grains is almost identical to that in the PBS wafer. The weak RI activity displayed by **61** at molar concentration of $5.5X10^{-6}$ M is presumably caused by the non-specific RI effect.[8a, 9a] This result indicates that the polypeptide scaffold with a specific amino acid composition in AFGPs is important for showing effective RI activity, and the loss of RI activity in **61** is presumably due to the complete removal of the polypeptide backbone.

In conclusion, none of the *C*-linked AFGP analogues displayed thermal hysteresis activity. However, some analogues demonstrated RI activity, especially for analogue **57**. This study suggests that small structural modifications can cause dramatic change of activities in the *C*-linked AFGP analogues. Different structural motifs may have different effects on TH, DIS and RI activities. Furthermore, the three antifreeze-specific activities are associated, but are not necessarily shown in a specific analogue simultaneously. This result suggests that rational design of AFGP analogues with desired antifreeze-specific activity is feasible. However, our current limited knowledge is not enough to prepare AFGP analogues with tailored antifreeze-specific activity. In order to realize this goal, additional structure-activity studies need to be performed.

Based on this study, *C*-linked AFGP analogues **57-61** may not have the ability to be used in hypothermic (non-frozen) preservation for tissues and organs since they do not possess TH activity. However, at cryogenic (frozen) temperatures, the major protective effect of biological antifreezes comes from the inhibition of ice recrystallization, and TH becomes a detrimental

effect which can cause tissue damage due to the formation of needle-shaped ice crystals. Therefore, at cryogenic temperatures, *C*-linked AFGP analogue **57** possesses good potential as cryoprotectants for preservations in the food and biomedical industries.

4.3 Assessing Solution Conformation of *C*-Linked AFGP Analogues Using Circular Dichroism (CD)

In order to understand whether the different antifreeze activities demonstrated in *C*-linked AFGP analogues **57-60** are related to their solution conformations, we performed a CD spectroscopy study with these analogues. CD is a technique that can determine the conformation of optically active molecules by measuring the differential absorption of left- and right-handed polarized light.[17] The secondary structural elements of proteins and polypeptides, such as α-helix, β-sheet, β-turn and random coil can give characteristic absorption bands at the far-UV region (190-250 nm). Therefore, CD spectroscopy has been used as a valuable tool to characterize the secondary structures of folded proteins and polypeptides.[18]

Although AFGPs were first discovered more than 30 years ago,[19] their conformations have not been unanimously defined.[3b, 20] Feeney and co-workers' early CD studies of AFGPs' conformation in solution phase suggested that neither α-helix nor β-structures dominated and the conformation of AFGPs was more likely made up of random coil and unfolded structure.[21] However, although the overall molecule was flexible, later evidence indicated AFGPs were not random coil, but local small segments with well-ordered structure existed.[3a] A separate study by Franks using CD and ^{1}H NMR indicated that AFGPs had a specific conformation which was similar to β-sheet except having a reverse sign.[18] Later, a three-fold left-handed helix conformation, which resembled the symmetry of polyproline type II (PPII), was proposed and supported by different experimental evidence including CD and NMR.[15, 22] However, some new conformational studies pointed out that the proportion of three-fold helical structure in AFGPs was very small.[23] Drewes and Rowlen studied the vibrational spectroscopy (Raman and IR) of amide bonds in AFGPs and believed that there were substantial γ-turn motifs instead of α-helix or PPII.[24] More recently, new studies using high field NMR (500 MHz), molecular dynamics calculation and CD spectroscopy indicated that AFGPs had no long range order in solutions and

appeared to be flexible random coil.[25] Overall, the exact solution conformation of AFGPs is still in debate. However, based on the above data, it is safe to say that AFGPs are composed of locally ordered small segments that have enough mobility to prevent the formation of long-range ordered conformation.[3a] An overall flexible coil conformation is preferred.

The CD spectra (Figure 4.7) of *C*-linked AFGP analogues **57-60** and AFGP8 were measured in water at 25 °C. In order to understand whether the conformations of AFGPs and analogues are related to antifreeze-specific activities, it is ideal to perform the CD spectroscopy study at temperatures below 0 °C and with ice existing in the system. However, previously quasi-elastic light scattering and CD studies proved that no obvious conformational changes were observed for AFGPs at different temperatures.[21b, 22c, 25c]

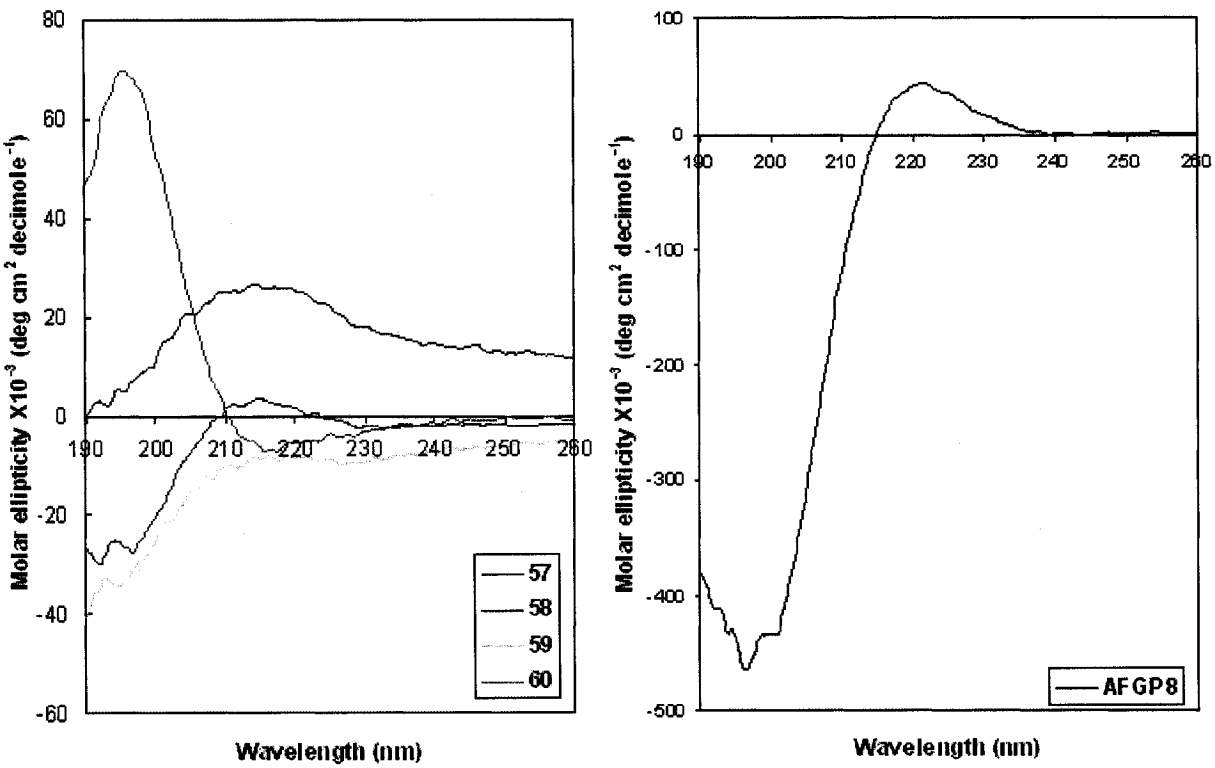

Figure 4.7 CD spectra of *C*-linked AFGP analogues **57-60** and AFGP8.

The CD spectra of *C*-linked AFGP analogues **57-60** and AFGP8 were analyzed by deconvolution using the SELCON3 program[26] of a CDPro software package.[27] In this program, the fractions of secondary structures, including α-helix, β-sheet, β-turn, polyproline type II helix

and random coil, are calculated by comparing the CD data to a set of different reference proteins with known conformations. Therefore, the deconvolution algorithm can mathematically extract the secondary structure contents from the CD data of *C*-linked AFGP analogues.

In this study, SP37A (IBasis 5), which contains 37 soluble proteins, was selected as the reference set because it gave consistent results for the deconvolution calculation of AFGP8.[25c] The 37 reference proteins are not all glycoproteins. Admittedly, it is ideal to calculate the fractions of secondary structures in AFGPs and analogues based on a reference set that is composed of only glycoproteins with similar structural composition. Unfortunately, such a reference set currently has not been developed. Obviously, it is not practical to understand the exact conformation of AFGP8 and *C*-linked AFGP analogues **57-60** based on the CD deconvolution study alone. However, if all the deconvolution calculations are performed on the same set of reference proteins, useful information still can be gained on the conformational differences among the *C*-linked AFGP analogues. This method has previously been employed to study the solution conformation of AFGP8 and its analogues to understand the effect of structural modification on the conformation.[14,25c] The deconvolution analysis results for *C*-linked AFGP analogues **57-60** and AFGP8 are listed in Table 4.3.[28]

Table 4.3 CD deconvolution data of *C*-linked AFGP analogues **57-60** and AFGP8.

Compound	α-helix	β-sheet	β-turn	PPII	Random coil	Sum
57	0.101	0.212	0.136	0.108	0.434	0.99
58	-0.016	0.325	0.093	0.119	0.438	0.959
59	0.163	0.246	0.122	0.081	0.393	1.006
60	0.712	0.04	0.063	0.026	0.17	1.011
AFGP8	0.129	0.159	0.156	0.136	0.445	1.025

As shown in Figure 4.7, the CD curves of analogues **57-59** do not resemble the typical α-helix, β-sheet, PPII or random coil pattern. Furthermore, they do not fit the CD spectrum of native AFGP8, which represents a main random coil conformation, in either shape or magnitude. Most obviously, the characteristic negative band in AFGP8 between 190 – 200 nm is not present in all

C-linked AFGP analogues. This result indicates that *C*-linked AFGP analogues **57-59** may not possess any current known, well-defined conformations, which is verified by the deconvolution results (Table 4.3). The highest fractions of secondary structures in analogues **57-59** are all random coil (ranging from 39-44%). Weak positive bands at wavelengths between 210-220 nm are shown in galactosyl analogues **57-59**, which resemble the same trend in AFGP8 except the peak location is around 220 nm for AFGP8. The overall CD spectra of analogue **57** and analogue **59** share very similar shape, which is also verified by the similar deconvolution data. These results, taken together with the fact that although analogue **57** is a very effective ice recrystallization inhibitor, limited RI activity is shown by analogue **59**, indicate that conformation may not be the only determining factor for RI activity.

The CD pattern demonstrated by analogue **60** resembles the α-helix structure, which is very different from the CD patterns demonstrated by analogues **57-59**. As shown in the deconvolution results, about 71% of secondary structures in analogue **60** are α-helix, and random coil structure only accounts for 17%. It is worth to point out that the acetamide group is the major structural moiety that causes the conformational difference between analogue **60** and analogue **57**. Therefore, this result suggests that the acetamide functionality in the galactosamine residue of analogue **60** has a drastic effect on the solution conformations of these *C*-linked AFGP analogues. Furthermore, this conformational difference may be one of the reasons causing the dramatic difference of RI activities between analogue **60** and analogue **57**.

In summary, analogues **57** and **59** demonstrate similar conformations to AFGP8 with the major fraction of random coil structures. Analogue **58** contains high fractions of both random coil and β-sheet structures. The main secondary structure portion in analogue **60** is α-helix. However, all these *C*-linked AFGP analogues do not possess well-defined secondary structures. This preliminary CD spectroscopic study indicates that the conformation of *C*-linked AFGP analogues is an important, though not the only factor for antifreeze-specific activities. In order to further understand the effects of conformation on antifreeze-specific activities, more studies, especially X-ray investigations, are required. The application of this technique is currently hindered by the difficulty to obtain a good sample for X-ray crystallography due to the high density of carbohydrate moieties in AFGPs.[15]

References

1. Harding, M. M., Anderberg, P. I., Haymet, A. D. J. *Eur. J. Biochem.* **2003**, *270*, 1381-1392.
2. (a) Houston, M. E., Chao, H., Hodges, R. S., Sykes, B. D., Kay, C. M., Sonnichsen, F. D., Loewen, M. C., Davies, P. L. *J. Biol. Chem.* **1998**, *273*, 11714-11718.
   (b) Fletcher, G. L, Hew, C. L., Davies, P. L. *Annu. Rev. Physiol.* **2001**, *63*, 359-390.
3. (a) Feeney, R. E., Burcham, T. S., Yeh, Y. *Annu. Rev. Biophys. Biophys. Chem.* **1986**, *15*, 59-78.
   (b) Yeh, Y., Feeney, R. E. *Chem. Rev.* **1996**, *96*, 601-618.
4. Scholander, P. F., Maggert, J. E. *Cryobiology* **1971**, *8*, 371-374.
5. (a) Knight, C. A., DeVries, A. L., Oolman, L. D. *Nature* **1984**, *308*, 295-296.
   (b) Raymond, J. A., DeVries, A. L. *Proc. Natl. Acad. Sci. U.S.A.* **1977**, *74*, 2589-2593.
6. Davies, P. L., Hew, C. L. *FASEB J.* **1990**, *4*, 2460-2468.
7. Meryman, H. T. *Annu. Rev. Biophys. Bioeng.* **1974**, *3*, 341-363.
8. (a) Knight, C. L., Wen, D. Y., Laursen, R. A. *Cryobiology* **1995**, *32*, 23-34.
   (b) Knight, C. L. *Nature* **2000**, *406*, 249-251.
   (c) Knight, C. A., Hallett, J., DeVries, A. L. *Cryobiology* **1988**, *25*, 55-60.
9. (a) Myers, K. L. "Quantification of recrystallization inhibition: an assay for antifreeze protein activity" M.A. Thesis, Binghamton University (S. U. N. Y.) 1999.
   (b) Horwath, K. L., Easton, C. M., Poggioli Jr., G. J., Myers, K., Schnorr, L. *Eur. J. Entomol.* **1996**, *93*, 419-433.
10. Tomczak, M. M.; Marshall, C. B.; Gilbert, J. A.; Davies, P. L. *Biocem. Biophys. Res. Commun.* **2003**, *311*, 1041-1046.
11. Standard error of the mean was used to express the error propagation and data distribution.
12. Sidebottom, C., Buckley, S., Pudney, S. P., Twigg, S., Jarman, C., Holt, C., Telford, J., McArthur, A., Warrall, D., Hubbard, R., Lillford, P. *Nature* **2000**, *406*, 256.
13. Wen, D. Y., Laursen, R. A. *FEBS Lett.* **1993**, *317*, 31-34.
14. Murphy, A. V. "Preparation of structurally diverse *C*-linked antifreeze antifreeze glycoprotein analogues and assessment for antifreeze protein-specific activity" PhD Thesis, Binghamton University (S. U. N. Y.), 2004.

15. Tachibana, Y., Fletcher, G. L., Fujitani, N., Tsuda, S., Monde, K., Nishimura, S. *Angew. Chem. Int. Ed.* **2004**, *43*, 856 –862.
16. Mimura, Y., Yamamoto, Y., Inoue, Y., Chujo, R. *Int. J. Bio. Macromol.* **1992**, *14*, 242-248.
17. Sreerama, N., Woody, R. W. *Method Enzymol.* **2004**, *383*, 318-351.
18. Franks, F., Morris, E. R. *Biochim. Biophys. Acta* **1978**, *540*, 346-356.
19. DeVries, A. L., Wohlschlag, D. E. *Science* **1969**, *163*, 1073-1075.
20. Avanov, A. Y. *Mol. Biol.* **1990**, *24*, 473-487.
21. (a) DeVries, A. L., Komatsu, S. K., Feeney, R. E. *J. Biol. Chem.* **1970**, *245*, 2901–2908.
(b) Ahmed, A. I., Feeney, R. E., Osuga, D. T., Yeh, Y. *J. Biol. Chem.* **1975**, *250*, 3344-3347.
(c) Tomimatsu, Y., Scherer, J., Yeh, Y., Feeney, R. E. *J. Biol. Chem.* **1976**, *251*, 2290-2298.
(d) Berman, E., Allerhand, A., DeVries, A. L. *J. Biol. Chem.* **1980**, *255*, 4407-4410.
22. (a) Bush, C. A., Ralapati, S., Matson, G. M., Yamasaki, R. B., Osuga, D. T., Yeh, Y., Feeney, R. E. *Arch. Biochem. Biophys.* **1984**, *232*, 624-631.
(b) Bush, C. A., Feeney, R. E. *Int. J. Pept. Protein Res.* **1986**, *28*, 386-397.
(c) Bush, C. A., Feeney, R. E., Osuga, D. T., Ralapati, S., Yeh, Y. *Int. J. Pept. Protein Res.* **1981**, *17*, 125-129.
23. Filira, R., Biondi, L., Scolaro, B., Foffani, M. T., Mammi, S., Peggion, E., Rocchi, R. *Int. J. Biol. Macromol.* **1990**, *12*, 41-49.
24. Drewes, J. A., Rowlen, K. L. *Biophys. J.* **1993**, *65*, 985-991.
25. (a) Lane, A. N., Hays, L. M., Tsvetkova, N., Feeney, R. E., Crowe, L. M., Crowe, J. H. *Biophys. J.* **2000**, *78*, 3195-3207.
(b)Tsvetkova, N. M., Phillips, B. L., Krishnan, V. V., Feeney, R. E., Fink, W. H., Crowe, J. H., Risbud, S. H., Tablin, F., Yeh, Y. *Biophys. J.* **2002**, *82*, 464-473.
(c) Bouvet, V. R., Lorello, G. R., Ben, R. N. *Biomacromol.* **2006**, *7*, 565-571.
26. The CDPro software consists of three programs, SELCON3, CDSSTR and CONTIN. In this study, SELCON3 (self-consistent method) was used to deconvolute the CD spectra of *C*-linked AFGP analogues.
27. The CDPro software were downloaded from: http://lamar.colostate.edu/~sreeram/CDPro/

28. The deconvolution data of AFGP8 was taken from reference 13.

Chapter 5 Assessing *In Vitro* Cytotoxicity and Interactions of AFGP8 and *C*-Linked AFGP Analogues

AFGPs' unique antifreeze-specific activities make them attractive candidates for a variety of applications in agriculture, food and biomedical industries (Section 1.5). To date, most of our studies on AFGPs have been performed to better understand the mechanism of action so that we can design analogues with more potent activities and improved stability for their applications. However, in order to realize their various applications, it is essential to learn whether natural AFGPs and their analogues have any toxic effects on the applied organisms in both their physiological conditions and low temperature preservation conditions. Given the long-term mammalian applications, assessing the potential *in vitro* cytotoxicity of AFGP8 and *C*-linked AFGP analogues is a worthwhile objective that may have a significant impact on biomedical applications.

Despite the potential commercial, industrial and medical applications, there have been very few studies performed to examine the potential toxicity of biological antifreezes in mammalian systems. Crevel and co-workers examined the effects of human exposure to biological antifreezes (including both AFPs and AFGPs) by statistically estimating the consumption of fish containing biological antifreezes.[1] According to this study, the average amounts of biological antifreezes in the diet were around 1-10 mg/day in the USA and 50-500 mg/day in Iceland. The history of antifreeze consumption suggested that antifreezes had no evidence of adverse health effects, either in the short- or long-term. However, as the author pointed out, the evidence of food consumption containing AFPs or AFGPs was circumstantial in this statistic study.[1]

Recently, Hall-Manning's study on a type III AFP also indicated that there was no evidence of genotoxic potential or notable subchronic toxicity following oral administration of this AFP for up to three months in rats at 580 mg/kg/day.[2] Rubinsky and co-workers studied the chemical toxicity of 10 mg/mL type I AFP in different cancer cells at both 37 °C and room temperature using a Trypan Blue dye exclusion test and did not detect any toxic effect after 20 minutes incubation.[3] All these results demonstrated that AFPs had no significant toxic effect on biological organisms. In contrast, some studies indicated that both AFPs and AFGPs could cause

damage to cells following low temperature incubation,[4] which indicated that the potential toxicity of antifreezes existed at low temperatures. Overall, detailed toxicity studies with AFGPs in human cells at physiological and cryogenic temperatures have not been reported. Since the ultimate goal of our research is to develop stable AFGP analogues as potent cryoprotectants, it is important to perform *in vitro* cytotoxicity and cryotoxicity studies of AFGPs and their analogues with selected human cell lines.

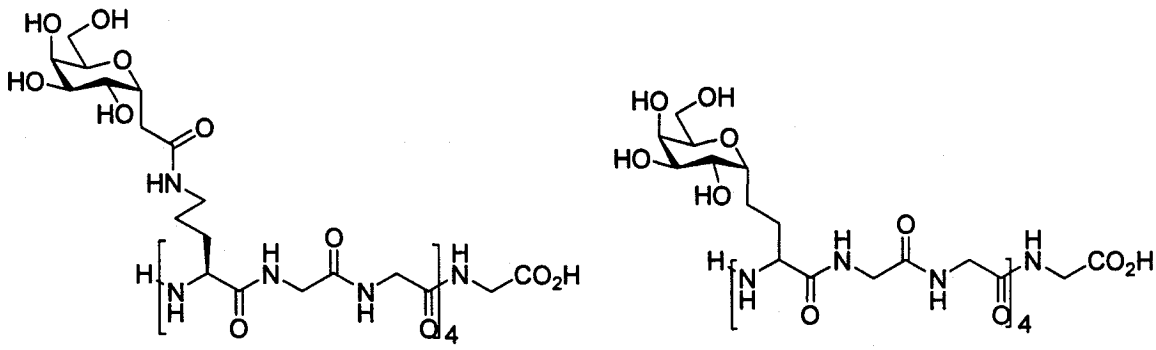

42 **57**

Figure 5.1 Structures of *C*-linked AFGP analogues **42** and **57**.

Both *C*-linked AFGP analogue **57** and previously prepared analogue **42** (Figure 5.1) possess potent recrystallization inhibition ability, which is comparable to native AFGP8. On the other hand, neither of these two analogues demonstrated thermal hysteresis and dynamic ice-shaping activities. It has been shown that recrystallization results in significant cellular damage during the freezing-thawing cycle[5] and dynamic ice-shaping can cause detrimental physical damage to cell membranes at temperatures below the TH gap during freezing.[6] Therefore, the unique features of analogues **42** and **57**, together with their improved stability over native *O*-linked AFGPs against chemical and enzymatic hydrolysis, make them ideal candidates as protecting agents to be employed for cell cryopreservation. However, the toxic effects of these analogues need to be first evaluated before the applications can be realized.

In this study, the *in vitro* cytotoxicity of native AFGP8 and *C*-linked AFGP analogues **42** and **57** was evaluated with three different cell lines. Fish gill epithelial (RTgill-W1, ATCC) cells from *Oncorhynchus mykiss* (Rainbow Trout) were used as the representative fish cell line. To

study the cytotoxicity effect on human tissues, human embryonic liver (WRL 68, ATCC) and human embryonic kidney (HEK 293, ATCC) cell lines were selected as representative human cell lines. We selected these two cell lines because humans are most commonly exposed to AFGPs through food, and the liver is the main metabolization and detoxication factory in the human body. Liver and kidney are also among the most commonly transplanted organs that would require cryopreservation.

In the process of cryopreservation, samples are exposed to cryoprotecting agents before freezing and after thawing. Therefore, it is important to understand the potential cytotoxic effects of AFGP8 and *C*-linked AFGP analogues at the physiological conditions of each cell line. In addition, since most applications of antifreezes occur at low temperatures, the cytotoxic effects to human liver cells were also studied at cryogenic temperatures (cryotoxicity).

5.1 Assessing *In Vitro* Cytotoxicity of AFGP8 and *C*-Linked AFGP Analogues 42 and 57

One method used to study cytotoxicity is based on the permeability of the plasma membrane.[7] Once the integrity of the plasma membrane is lost, both release of intracellular components and uptake of normally excluded compounds will occur. Most cytotoxicity studies based on this principle are performed by observing the cellular uptake of fluorescent labeled dyes.

An alternate way to study cytotoxicity focuses on the metabolic activity.[7] Unlike living cells, dead cells lose the ability to produce energy for normal metabolic activities, most obviously, in the form of losing mitochondrial activities. Therefore, viable cells and dead cells can be differentiated by the indirect measure of cell viability. Compared to the permeability assay, cytotoxicity can be readily quantified in a microplate using the metabolic activity assay. For this reason, the cytotoxicity study of AFGP8 and analogues **42** and **57** was performed using a MTT (methylthiazolydiphenyl-tetrazolium bromide) assay. This is a colorimetric assay that can quantitatively determine cell proliferation, viability and cytotoxicity by measuring the mitochondrial dehydrogenase activity.[8] MTT dissolves in water or cell culture medium to give a yellow solution. In liver cells, the mitochondrial enzyme succinate-dehydrogenase cleaves the tetrazolium ring in MTT to produce formazan (Scheme 5.1),[9] which can be dissolved in acidified

isopropanol to show a purple color. The solubilized formazan product can be photometrically quantified by optical adsorptions at the wavelength of 570 nm. Since only metabolically active cells (living cells) can perform this reaction, the optical density (OD) displayed at 570 nm is proportional to the amount of viable cells. The existence of any toxic effects will cause a decrease of total metabolic activity, the formation of a weaker purple color and a lower optical density reading. In contrast, higher OD reading will correlate to no or minimal cytotoxic effects.

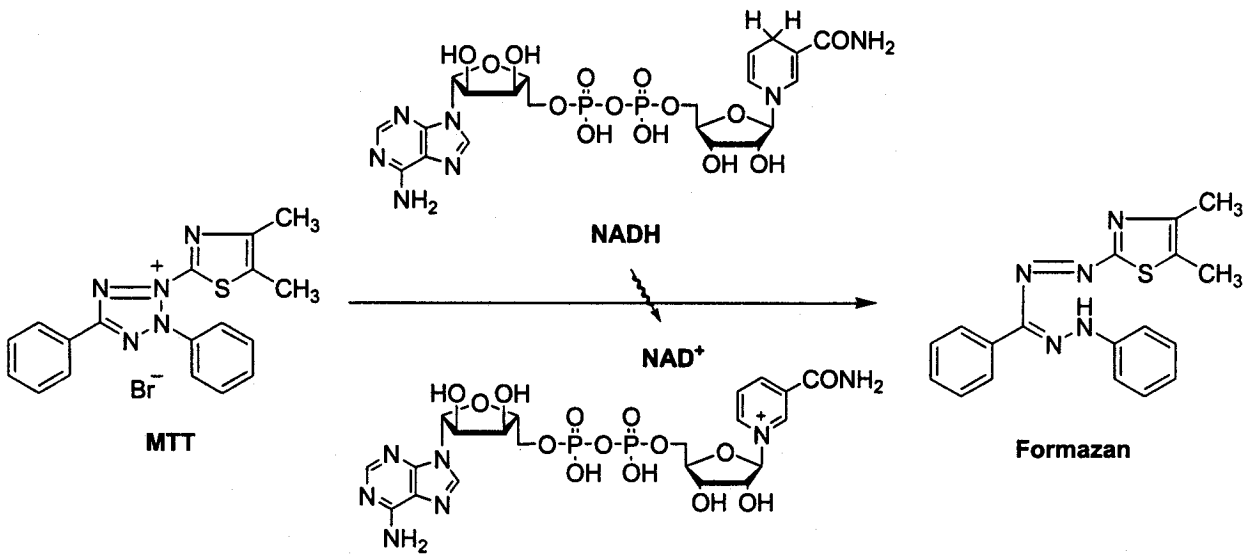

Scheme 5.1 The principle of MTT assay.[9]

All three cell lines were cultured in their respectively optimal growing conditions (37 °C, 5% CO_2 for WRL 68 and HEK 293; 19 °C for RTgill-W1) to reach 100% confluence in 96-well microplates before the MTT assay. Cells were treated with different concentrations of AFGP8 or *C*-linked AFGP analogues and incubated under the same conditions overnight (18-24 hours). Then, the MTT reagent was added into each well and the plate was further incubated for 2-5 hours before being read with a plate spectrophotometer.

5.1.1 Assessing the Cytotoxicity of AFGP8 and *C*-Linked AFGP Analogues 42 and 57 at Physiological Temperatures

5.1.1.1 Assessing the Cytotoxicity of AFGP8 at Physiological Temperatures

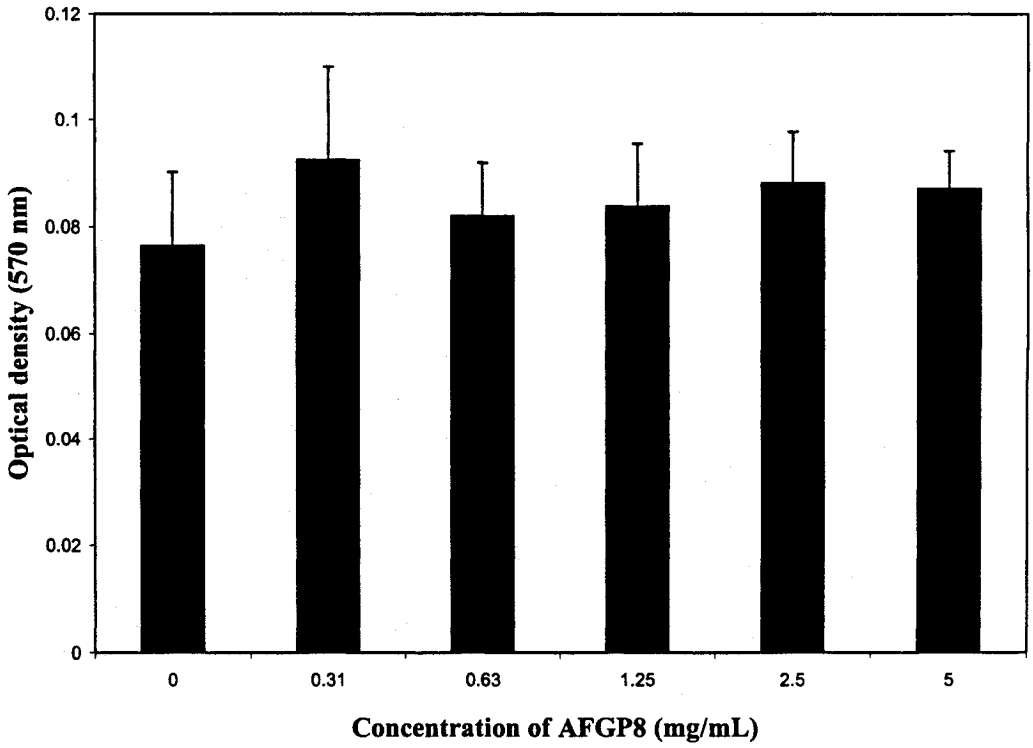

Figure 5.2 Cytotoxicity of AFGP8 to fish gill epithelial cells (RTgill-W1) at 19 °C. Rtgill-W1 cells were incubated with various concentrations of AFGP8 in MEM at 19 °C for 20 hours. Data are mean ± standard deviation.

The concentration of AFGP8 introduced into cells ranged from 0 (control) to 5 mg/mL. Figure 5.2[10] shows the MTT assay results. As expected, incubating fish cells with AFGP8 did not cause any detectable cytotoxic effects. In contrast, the optical densities of fish cells treated with varying concentrations of AFGP8 are slightly higher than that of cells growing at normal conditions (0 mg/mL of AFGP8), especially for the 0.31 mg/mL AFGP8 control. Since AFGPs

are isolated from fish, this result is easy to rationalize and can be regarded as a negative control to be compared with *C*-linked AFGP analogues or assays conducted in different cell lines.

The same assay was performed in human embryonic liver (WRL 68) and kidney (HEK 293) cells. In contrast to the non-toxic effect shown in fish cells, high concentrations of AFGP8 were found to be cytotoxic to the two human cell lines (Figure 5.3 & 5.4). Reduced cell viability was observed as the introduced concentration of AFGP8 increased. For liver cells, the mitochondrial dehydrogenase activity in cells treated with 4 mg/mL AFGP8 was only about 85% of that of cells growing at normal conditions (Figure 5.3). The same trend is more obvious in kidney cells. Significantly decreased metabolic activity was observed in cells treated with the highest concentration of AFGP8 (5 mg/mL). The viability was only 77% of cells growing at normal conditions (Figure 5.4).

All data was analyzed by the "Student's t-test" to statistically evaluate whether a significant difference exists between cell treatments with and without AFGP8.[11] Student's t-test is one of the most commonly used techniques for comparing the difference between two means in relation to the variance. The standards used for student's t-test are two-tailed test and two-sample assuming equal variances. Significant difference is believed to exist between two groups of data when the calculated P value is smaller than 0.05.

Compared to no AFGP8 treatment, the OD difference is significant for liver cells treated with high concentrations (>2 mg/mL) of AFGP8 ($P<0.05$ for 2 mg/mL and 4 mg/mL). However, liver cells with low concentrations of AFGP8 treatment displayed no significant difference ($P>0.05$ for 0.25, 0.5 and 1 mg/mL). Similar results were obtained from the MTT assay data of kidney cells. However, the lowest concentration of AFGP8 that can cause significant cytotoxicity is only 0.63 mg/mL ($p<0.05$) in kidney cells, which is lower than that displayed in liver cells (1 mg/mL). Cells treated with higher concentrations of AFGP8 all showed significant difference ($p<0.05$ for all 1.25, 2.5 and 5 mg/mL) in OD compared to cells with no AFGP8 treatment. 0.31 mg/mL AFGP8 was the only treatment that showed no cytotoxic effect ($P>0.05$).

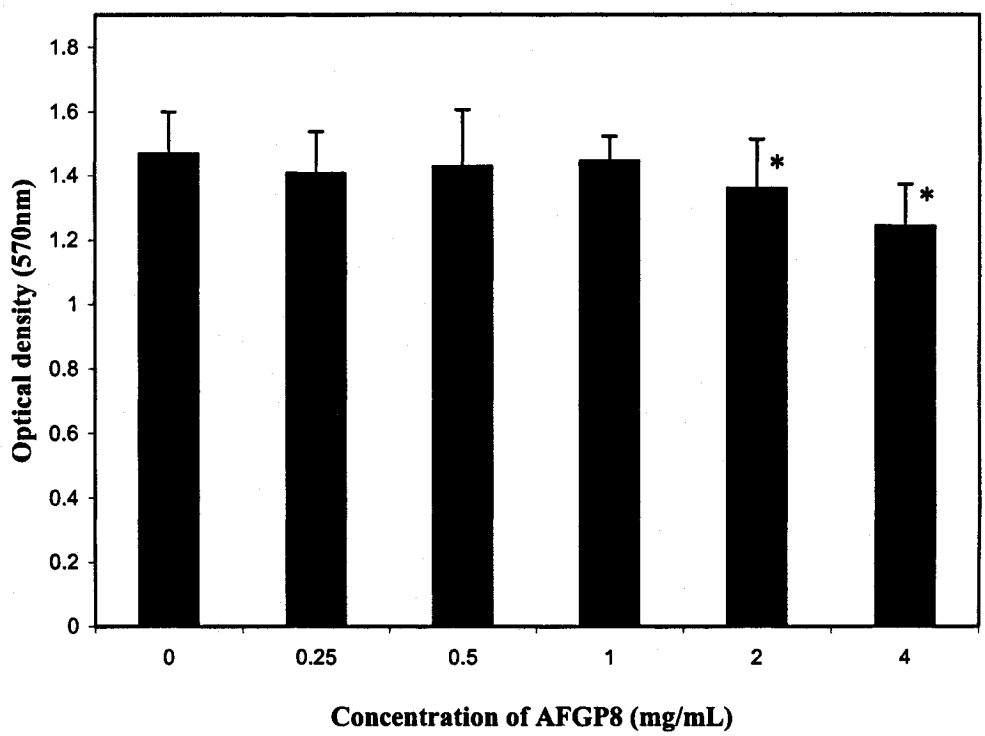

Figure 5.3 Cytotoxicity of AFGP8 to human embryonic liver cells (WRL 68) at 37 °C. WRL 68 cells were incubated with various concentrations of AFGP8 in MEM at 37 °C for 20 hours. Data are mean ± standard deviation. Data was analyzed using the "Student's t-test". Asterisks indicate significant difference ($P<0.05$) from cells without AFGP8 treatment.

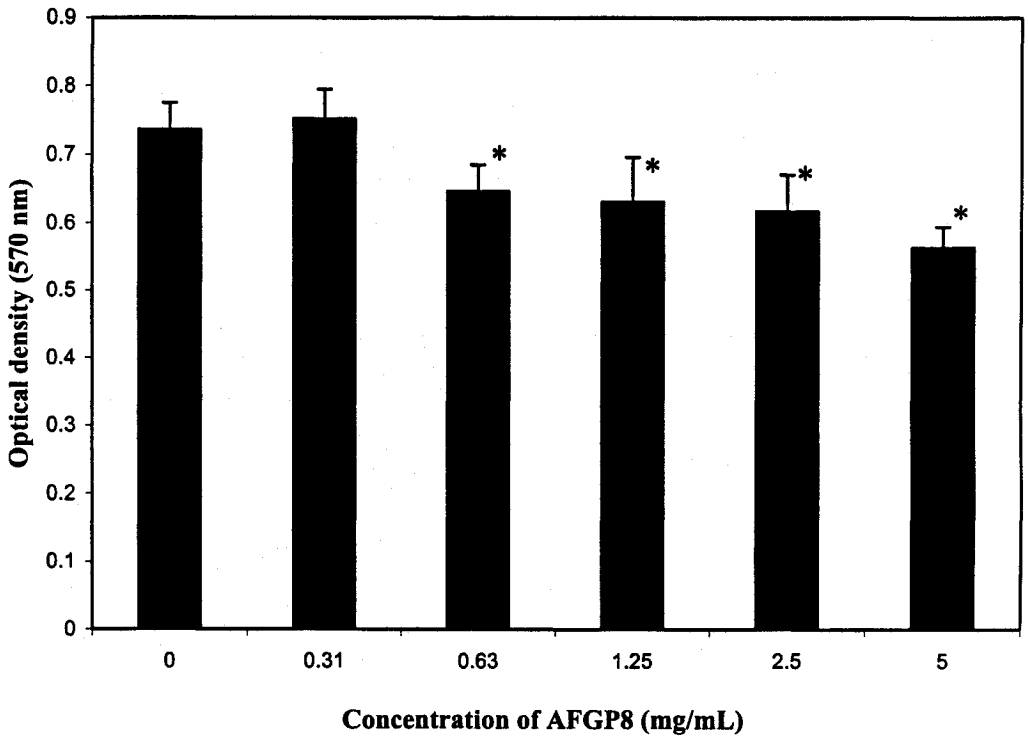

Figure 5.4 Cytotoxicity of AFGP8 to human embryonic kidney cells (HEK 293) at 37 °C. HEK 293 cells were incubated with various concentrations of AFGP8 in MEM at 37 °C for 20 hours. Data are mean ± standard deviation. Data was analyzed using the "Student's t-test". Asterisks indicate significant difference ($P<0.05$) from cells without AFGP8 treatment.

In summary, the cytotoxicity caused by AFGP8 is dependent on concentration and cell type. High concentrations of AFGP8 can cause significant cytotoxic effects in human liver and kidney cells at 37 °C, which may limit its application as a cryoprotecting agent in human tissues. Low concentrations of AFGP8 (10^{-4} M) did not show significant cytotoxicity in both human cell lines. Since the effective concentrations of AFGP8 (10^{-5} to 10^{-8} M, Figure 4.3) to inhibit ice recrystallization can be much lower than the lowest cytotoxic concentrations, AFGP8 still has the potential to be used for cell cryopreservation provided concentrations are low. Rubinsky also noticed a similar trend when assessing the cryotoxicity of type I AFP for cryosurgical applications.[3] The lowest cytotoxic concentration of AFGP8 can be different for cells from

different tissues. It seems that liver cells have a higher threshold for AFGP8's drug toxic effects than kidney cells. Therefore, cytotoxicity study is crucial when using AFGP8 as protecting agent in a specific tissue.

The cytotoxicity of AFGP8 at high concentrations represents a serious limitation for its use in the cryopreservation of cells, tissues and organs. This may also explain the controversial effects of AFGPs on cell viability reported in literature.[12] The detrimental effect of AFGPs has been attributed to the shearing effect caused by the formation of spicular ice[4e] and the lethal intracellular freezing[4d, 13] promoted by AFGPs at temperatures beyond the thermal hysteresis gap. However, cytotoxicity of AFGPs introduced into cells at physiological conditions (before cooling or after thawing) may also play an important role in the cell destruction. DeVries and co-workers[14] have shown that after freezing, there was no increase in the viability of mouse oocytes from AFGPs introduced at physiological temperatures. This is probably due to the compromise of AFGPs' protective and destructive dual actions. In contrast, adding AFGPs after cells were pre-cooled greatly increased the viability after freezing. This might be because the cytotoxicity that was observed at physiological conditions did not occur in cells at low temperatures.

5.1.1.2 Assessing the Cytotoxicity of *C*-Linked AFGP Analogues 42 and 57 at Physiological Temperatures

The potential cytotoxic effects of *C*-linked AFGP analogues **42** and **57** were also evaluated using a MTT assay in human liver cells. Surprisingly, both analogues did not show any detectable cytotoxicity, even for cells treated with analogues at the highest concentration (5 mg/mL). For analogue **42** (Figure 5.5), treatments with AFGP8 (0.63-5 mg/mL) resulted in no significant difference in mitochondrial dehydrogenase activity ($P>0.05$ for all treatments). For analogue **57** (Figure 5.6), cells treated with AFGP8 (0.31-5 mg/mL) even displayed slightly better viability than cells without AFGP8 treatment.

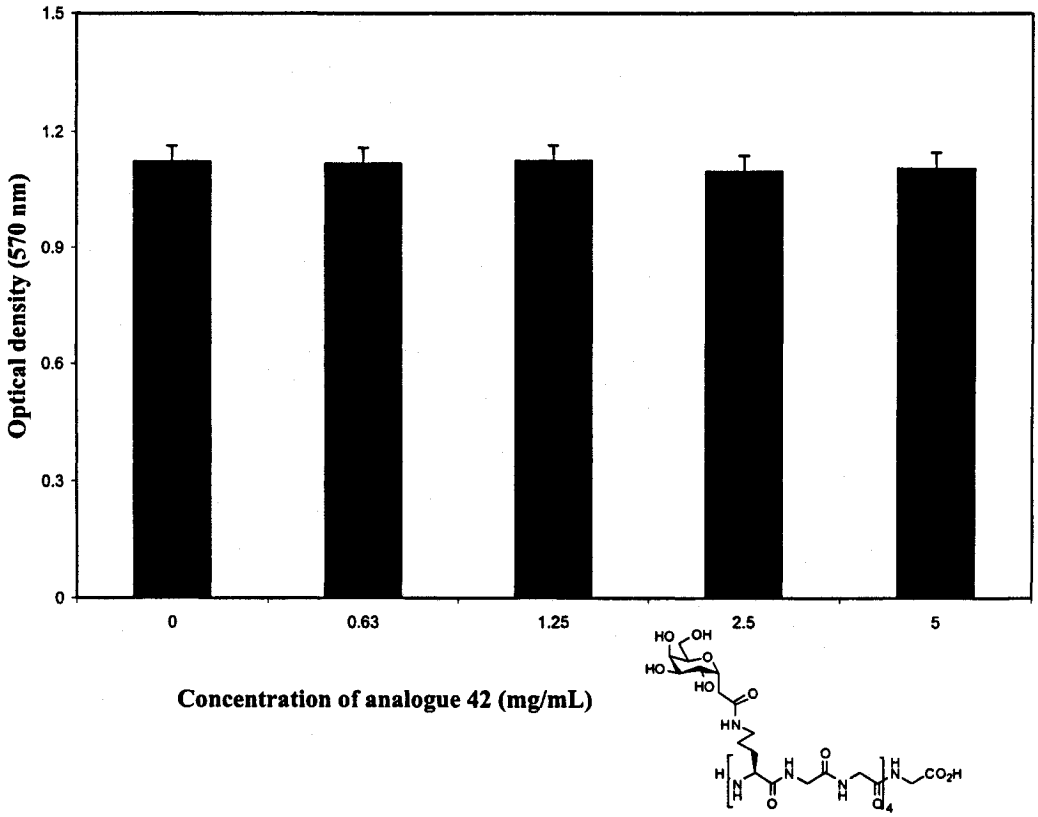

Figure 5.5 Cytotoxicity of analogue **42** to human embryonic liver cells (WRL 68) at 37 °C. WRL 68 cells were incubated with various concentrations of analogue **42** in MEM at 37 °C for 20 hours. Data are mean ± standard deviation.

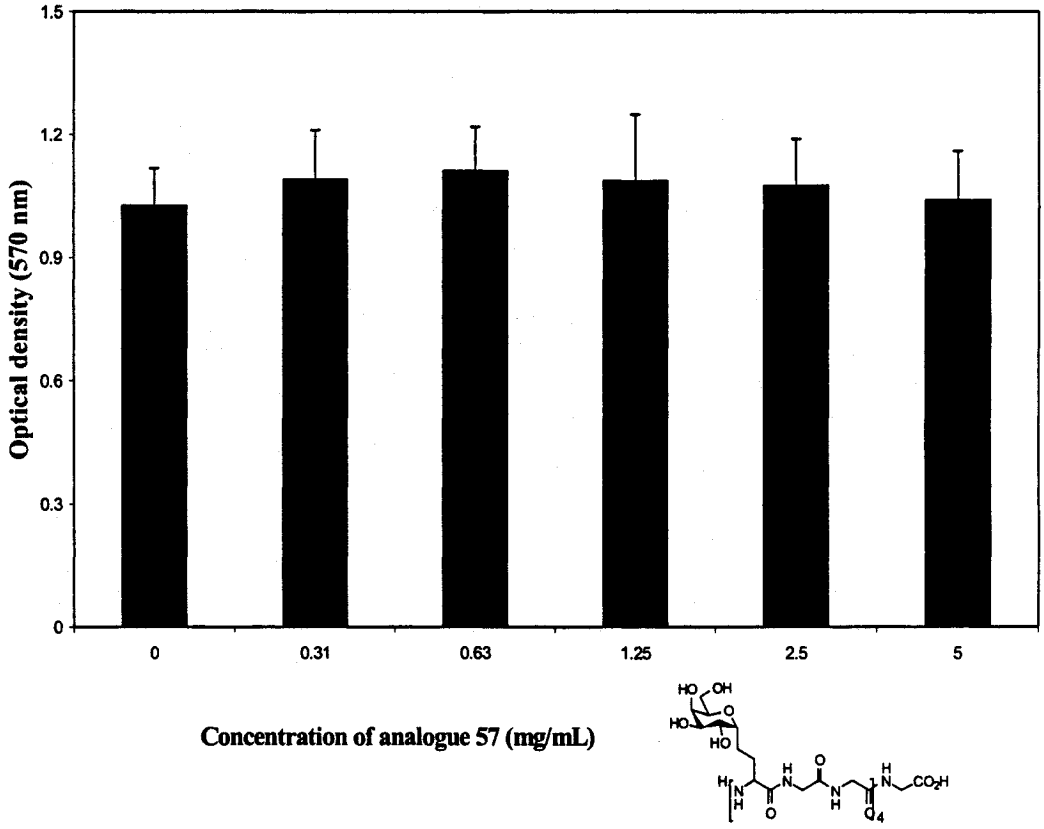

Figure 5.6 Cytotoxicity of analogue **57** to human embryonic liver cells (WRL 68) at 37 °C. WRL 68 cells were incubated with various concentrations of analogue **57** in MEM at 37 °C for 20 hours. Data are mean ± standard deviation.

The cytotoxicity difference observed between AFGP8 and analogues **42** and **57** in human liver cells may be attributed to their structural differences. Native AFGP8 is an *O*-linked glycopeptide and the carbon-oxygen glycosidic linkage can be easily hydrolyzed under chemical and enzymatic conditions.[15] In *C*-linked analogues **42** and **57**, the unstable carbon-oxygen glycosidic linkage is replaced by a stable carbon-carbon bond, which may be the reason for their nontoxic effects in human liver cells. However, in order to verify this hypothesis and clearly understand the cytotoxicity difference, further investigations of *in vitro* interactions of AFGP8 and *C*-linked AFGP analogues **42** and **57** need to be performed.

Nevertheless, it has been demonstrated that *C*-linked AFGP analogues **42** and **57** possess potent recrystallization inhibition activity and no detrimental dynamic ice-shaping ability. This

property, together with the fact that they are not toxic to human cells, make them ideal candidates to be used for the cryopreservation of cells and tissues.

5.1.2 Assessing the Cytotoxicity of AFGP8 and *C*-Linked AFGP Analogue 57 at Cryogenic Temperatures

Given that the ambient temperature of organisms utilizing AFGPs is lower than 37 °C, and that the temperatures for current cryopreservation protocols are well below 0 °C, we assessed the toxicity of AFGP8 and *C*-linked AFGP analogue **57** in human liver cells (WRL 68) at sub-zero temperatures. The University of Wisconsin (UW) solution has been considered the standard preservation solution for livers, kidneys and other organs and tissues at low temperatures with excellent clinical and experimental preservation effects.[16] For this reason, UW solution was used as the cell preservation medium in these experiments. Homogeneous low temperatures were acquired using a cryobath by submerging samples in absolute ethanol. To prevent contamination, 96-well plates containing samples were sealed before being placed into the cryobath.

In order to optimize the experimental conditions, a control MTT assay was performed to evaluate the effect of AFGP8 incubation time on the viability of human liver cells at -20 °C. Similar cell viability was observed with AFGP8 incubation for both 18 hours and 72 hours (Figure 5.7), which indicated that the detrimental effects caused by AFGP8 mainly occurred during the freezing and thawing processes rather than in relation to the incubation time at cryogenic temperatures. Data was analyzed by the "Student's t-test".[11] The inclusion of AFGP8 can cause significant cryotoxicity ($P<0.05$) to human liver cells at cryogenic temperatures. At 37 °C, AFGP8 displayed no significant cytotoxicity to liver cells at concentrations lower than 1 mg/mL (Figure 5.3). In contrast, at -20 °C, significant amounts of cell death were observed in all treatments with variant AFGP8 concentrations ($P<0.05$ for all 0.01-5 mg/mL treatments).

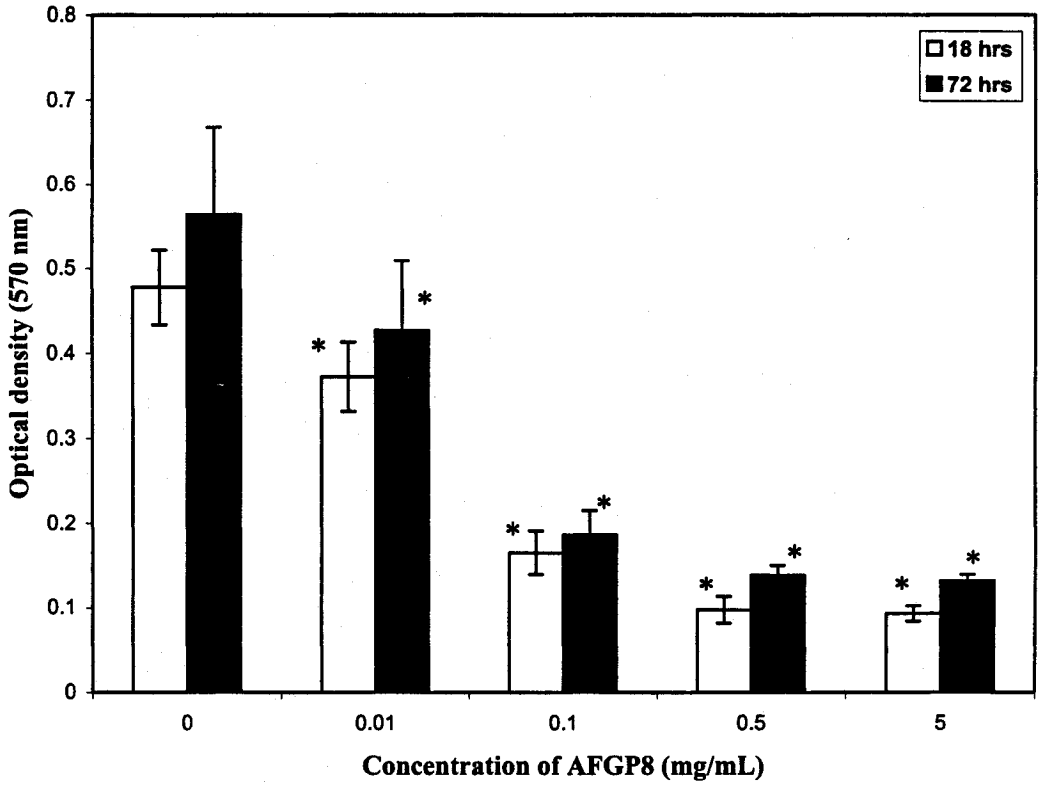

Figure 5.7 Cytotoxicity of AFGP8 to human embryonic liver cells (WRL 68) at -20 °C in cryobath. WRL 68 cells were incubated with various concentrations of AFGP8 in UW solution at -20 °C for either18 or 72 hours. Data are mean ± standard deviation. Data was analyzed using the "Student's t-test". Asterisks indicate significant difference ($P<0.05$) from cells without AFGP8 treatment (with the same incubation time).

For MTT assays performed in the cryobath, cells were sealed and submerged in absolute ethanol. It was hypothesized that these experimental conditions might cause oxygen depletion (hypoxia), which could be a plausible explanation for the observed cell death.[7] Therefore, we performed a control MTT assay in both the cryobath and the freezer to evaluate the effect of oxygen on cell viability at low temperatures (Figure 5.8). The cryobath causes hypoxic conditions while the freezer is non-hypoxic. Both assays were performed at around the same temperature (-25 °C for cryobath and about -27 °C for freezer) for 18 hours. Data was analyzed by the "Student's t-test".[11] No significant difference ($P>0.05$ for all treatments with the same

AFGP8 concentrations, 0-5 mg/mL) in cell viability was observed for experiments conducted in hypoxic and non-hypoxic conditions (Figure 5.8), which suggested that the cryotoxicity observed from the MTT assay performed in the cryobath was not caused by hypoxia.

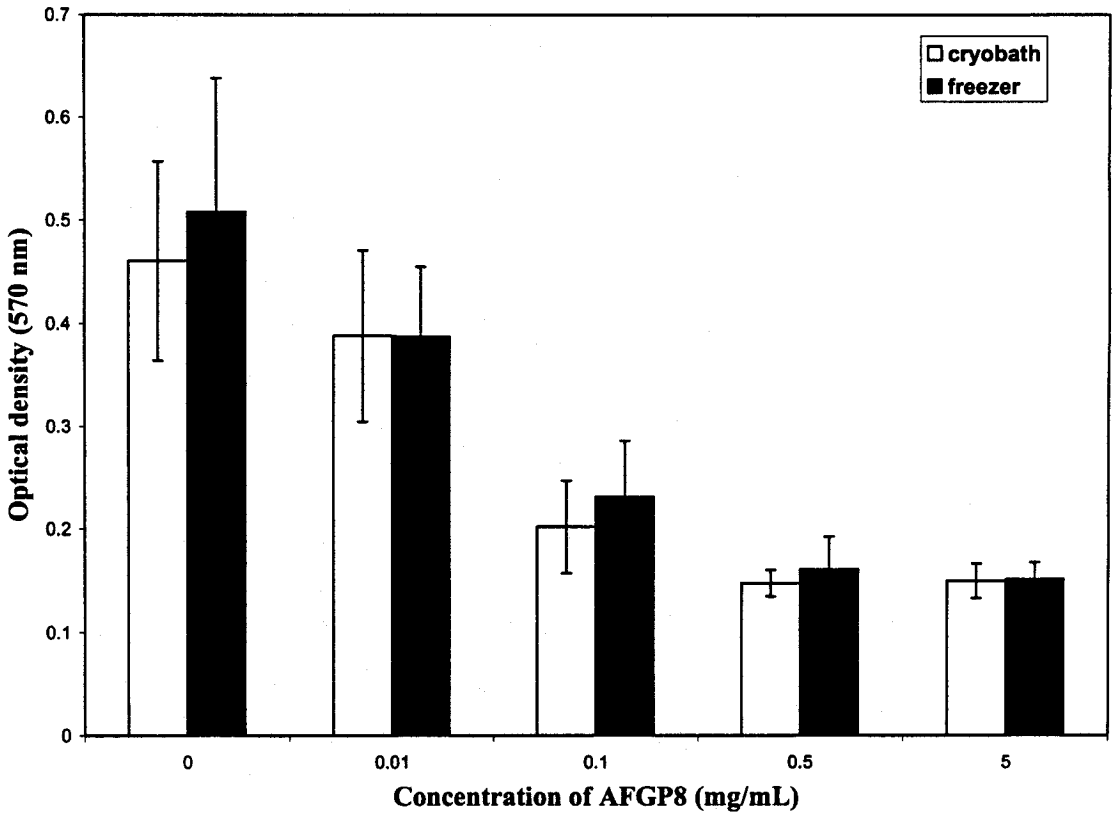

Figure 5.8 Comparison of cytotoxicity of AFGP8 to human embryonic liver cells (WRL 68) in cryobath and freezer. WRL 68 cells were incubated with various concentrations of AFGP8 in UW solution at either -25 °C (cryobath) or -27 °C (freezer) for 18 hours. Data are mean ± standard deviation. Cells incubated with the same AFGP8 concentration were analyzed using the "Student's t-test". No significant difference exists between treatments with the same AFGP8 concentration ($P>0.05$ for all 0-5 mg/mL treatments).

Analogue **57** is the most efficient recrystallization inhibitor of all *C*-linked AFGP analogues that have been prepared. Potential toxic effects of this analogue to human liver cells (WRL 68) at cryogenic conditions (incubation at -25 °C in cryobath for 18 hours) were also studied using the

MTT assay (Figure 5.9). Interestingly, compared to control cells, the addition of analogue **57** did not cause further decrease in cell viability at concentrations of 0.3-4.3 mg/mL. In contrast, cell viability was improved as the concentration of analogue **57** was increased. This trend became saturated when the concentration reached 1 mg/mL. At this point, about 60% more cells can survive freezing compared to cells that were not treated with analogue **57**.

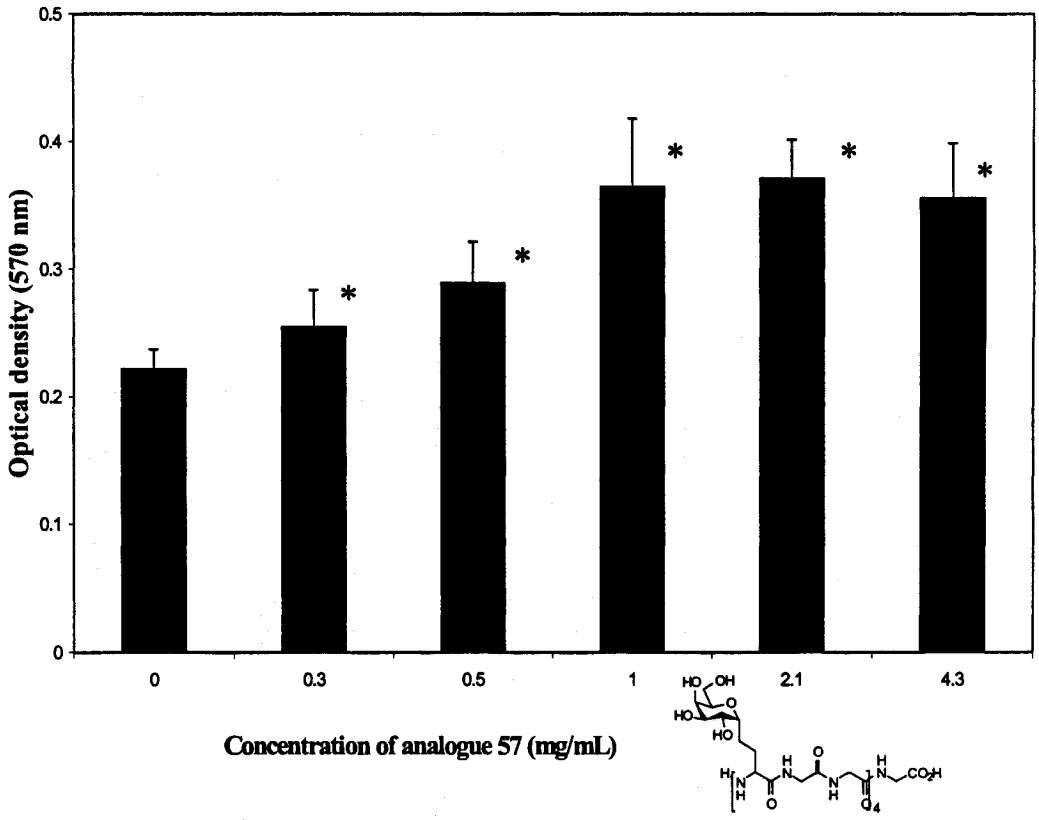

Figure 5.9 Cytotoxicity of analogue **57** to human embryonic liver cells (WRL 68) at -25 °C. WRL 68 cells were incubated with various concentrations of analogue **57** in UW solution at -25 °C for 18 hours. Data are mean ± standard deviation. Data was analyzed using the "Student's t-test". Asterisks indicate significant difference ($P<0.05$) from cells without AFGP8 treatment.

At cryogenic conditions, it is not surprising that AFGP8 causes dramatic cryotoxicity to human liver cells. Although there is evidence that AFGPs can protect the integrity of certain mammalian cell membranes at cryogenic temperatures,[17] it seems that the destructive effect caused by AFGP8-promoted spicular ice formation and intracellular freezing plays a more

important role in affecting the viability of human liver cells. In contrast, *C*-linked AFGP analogue **57** does not possess detrimental DIS activity. The only effect of analogue **57** on human liver cells is the beneficial recrystallization inhibition activity, which can protect cells by preventing the formation of harmful large ice crystals. Therefore, analogue **57** demonstrated an overall protective effect on human liver cells.

In summary, the cytotoxicity study indicated that high concentration AFGP8 had significant toxic effects on human liver and kidney cells at both physiological and cryogenic temperatures. In contrast, *C*-linked AFGP analogues **42** and **57** did not show any toxicity to human embryonic liver cells at the physiological temperature. In addition, analogue **57** did not cause a decrease in cell viability at cryogenic temperatures. These results suggest that these *C*-linked AFGP analogues have more potential to be used as cryoprotectants than native AFGP8.

5.2 Investigating the Mechanism of Cell Death Caused by AFGP8

In order to understand the mechanism of cell death caused by AFGP8 in human cell lines, we studied the *in vitro* interactions of AFGP8 and *C*-linked AFGP analogues **42** and **57** in human embryonic liver cells. This study is important to explain the different cytotoxic effects observed between native AFGP8 and *C*-linked AFGP analogues. Furthermore, it can also help us to design future analogues that retain desirable properties for cell cryopreservation.

Cell death generally occurs through two distinct mechanisms: necrosis and apoptosis.[18] Necrosis is a pathological process caused by physical disruption or chemical poisoning of cells, such as through injury and toxins. Therefore, necrosis is also referred to as "accidental cell death", and it is always accompanied by surrounding tissue damage. In contrast, apoptosis is a well-regulated or "programmed" way of cell death. It is a physiological process that is employed by organisms to dispose of useless cells during normal biological processes and usually involves no harmful effects.

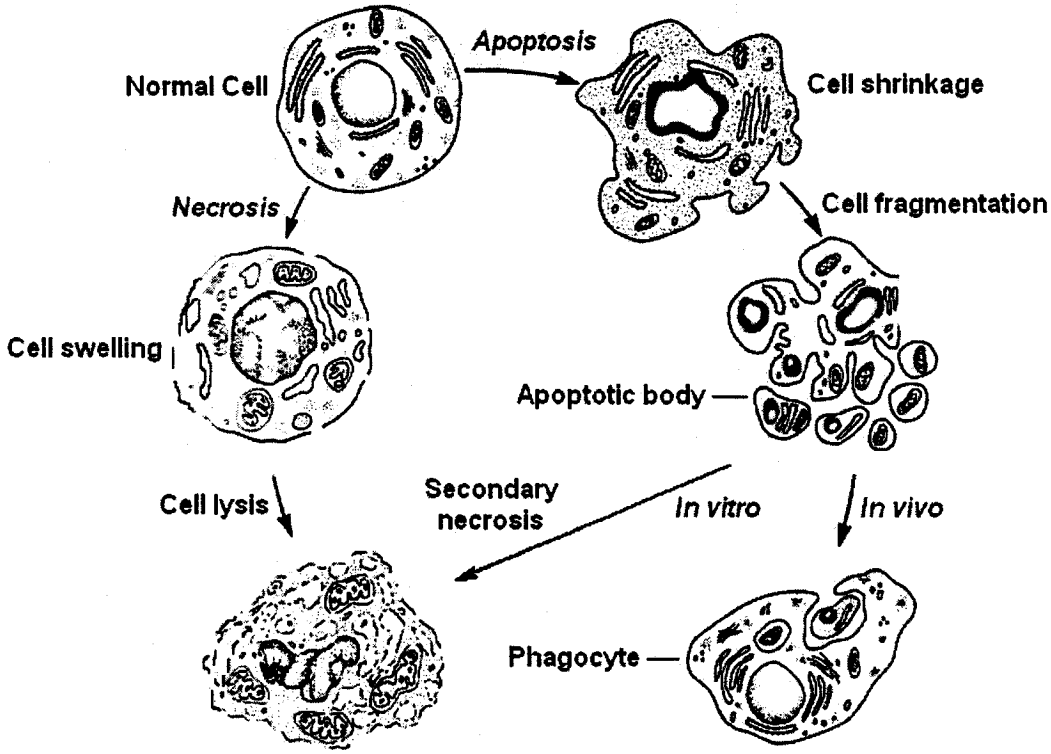

Figure 5.10 Illustration of morphological changes during necrosis and apoptosis.[19]

Necrosis and apoptosis can be differentiated by their characteristic morphological changes (Figure 5.10[19]). Necrotic cells are accompanied by cell and intracellular organelles swelling, resulting from uncontrolled water influx through the disintegrated and permeabilized plasma membrane. The irreversible swelling eventually causes cells to burst and the cytotoxic intracellular components (such as the lysosome) to leak out, which can cause tissue damage and inflammation. Instead of swelling, initial apoptosis causes cell shrinkage, nuclear condensation and blebbing. The integrity of the plasma membrane and intracellular organelles is kept intact. Later, cells are fragmented into small membrane-bound apoptotic bodies and can be recognized and phagocytized by cells from the immune systems *in vivo*.[20] Therefore, no harmful effect is produced. *In vitro*, apoptotic bodies undergo a secondary necrosis to cause cell lysis.[18, 21]

During the live cell imaging using confocal microscopy, we noticed morphological changes in the AFGP8-treated human liver cells that were consistent with morphological changes that cells exhibit during apoptosis (such as the nuclear blebbing and the punctate cytoplasm, Figure 2.11)

To better understand the mechanism of cell death, an apoptosis study was performed in AFGP8-treated human liver cells.

Besides the morphological changes, many characteristic biochemical features are also present during the process of apoptosis and can be used to differentiate apoptotic cells from necrotic cells. One of the most important features is the involvement of a family of cysteine-type aspartic acid-specific proteases, which are known as caspases.[22] Caspases act as the central mediator in the apoptosis pathway (Figure 5.11[23]). Under normal conditions, caspases exist as inactive zymogens (enzyme precursors) in cells. Upon stimulation of various death signals, initiator caspases (such as caspases 8 and 9) are first converted into active heterodimers. Caspases can be activated by either intrinsic or extrinsic signals. The intrinsic pathway is initiated by different stimuli such as DNA damage or the presence of intracellular toxic compounds, which can cause the release of cytochrome c from the mitochondria to the cytosol. Then, procaspase 9 is activated by forming an active complex with cytochrome c and the apoptotic-protease activating factor 1 (Apaf-1).[24] The extrinsic pathway is initiated through cell surface death receptors. The intracellular domains of these death receptors can promote the formation of the death-inducing signaling complex (DISC) by assembling the Fas-associated death domain (FADD) and procaspase 8. Thus, initiator caspase 8 is activated. Initiator caspases possess only weak proteolytic activity, but they can trigger a cascade of caspase activation and specifically activate effector caspases (such as caspase 3 and 7),[25] which can cleave a wide range of proteins (such as structural proteins and cell signaling proteins)[20] that are critical for cell function and eventually lead to apoptotic cell death. Since the activation of caspases is a distinctive biochemical feature involved in the apoptotic process, it has been employed to study the mechanism of apoptosis and to differentiate the cytotoxicity resulting from apoptosis and necrosis.[26]

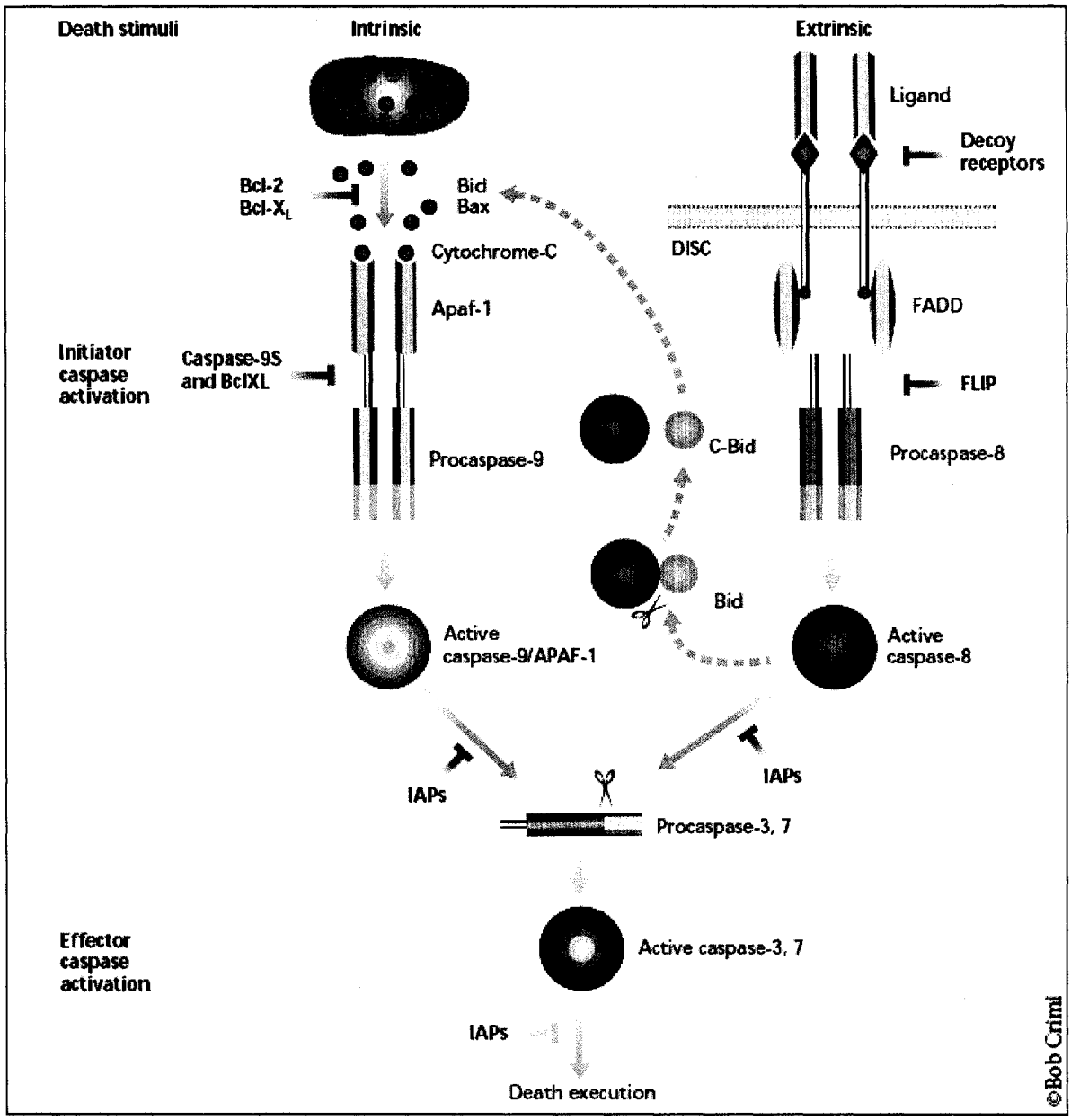

Figure 5.11 Caspase activation pathways. The intrinsic pathway involves the formation of an active complex with cytochrome c and Apaf-1, while the extrinsic pathway involves the formation of DISC with FADD. Both intrinsic and extrinsic activation pathways lead to the activation of effector caspases 3 and 7. (IAPs, Inhibitors of apoptosis proteins; FLIP, FLICE-like inhibitory protein; Bcl-2 and Bcl-X_L are anti-apoptotic proteins; Bid and Bax are pro-apoptotic proteins.)[23]

5.2.1 Caspase-3/7 Assay

A caspase-3/7 assay (Promega) was employed to determine whether these effector caspases were activated in human liver cells upon exposure to AFGP8 and *C*-linked AFGP analogues. In this assay, a profluorescent caspase-3/7 substrate, rhodamine 110, bis-(*N*-Cbz-L-aspartyl-L-glutamyl-L-valyl-L-aspartic acid amide) (Z-DEVD-R110) was used to detect activated caspase 3 and 7 activity in cells. These caspases have the specificity to cleave at the C-terminus of the aspartate residue in the tetrapeptide sequence and give rhodamine 110 as a leaving group, which is intensely fluorescent upon excitation.[27] Therefore, the cleavage activity of the activated caspase 3 and 7 in cells can be measured by the produced fluorescent units.

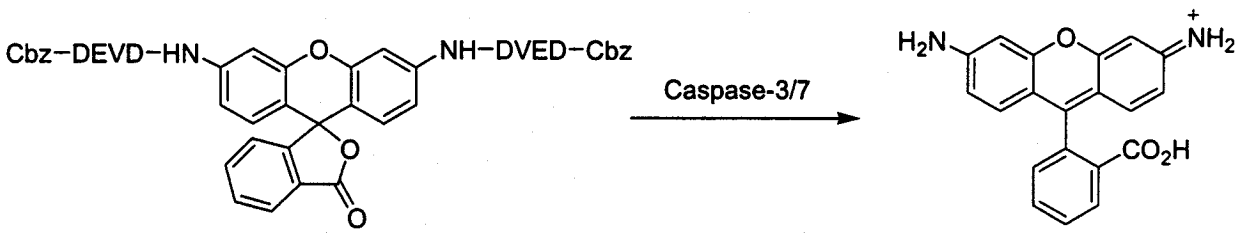

Z-DEVD-R110 (profluorescent) **Rhodamine 110** (fluorescent)

Scheme 5.2 Mechanism of caspase-3/7 assay. Z represents Cbz, DEVD represents L-aspartyl-L-glutamyl-L-valyl-L-aspartyl and R110 represents rhodamine 110.[27]

In this study, staurosporine, a known inducer of apoptosis in mammalian cells, was used as a positive control.[26, 28] Since staurosporine is not soluble in aqueous solution, 2% DMSO (Sigma) was used to improve its solubility in the culture medium and added in all treatments. In order to quantify the caspase-3/7 activity in the normal cell culture, cells growing under normal conditions without drug treatment act as a negative control. Cells were cultured in a 96-well plate to reach 100% confluence before being treated with AFGP8 or staurosporine for 18 hours. To find the optimal incubation time of the caspase-3/7 substrate in this particular human liver cell line, the fluorescence level was measured as a function of time. Staurosporine seemed to be a feasible positive control for human liver cells, because as shown in Figure 5.12, strong caspase-3/7 activation was observed in cells treated with 20 μM staurosporine. Some background of

fluorescence was observed in the negative control, which is presumably due to the regular cell death that occurs during cell culture. Incubating cells with 5 mg/mL of AFGP8 caused significantly increased caspase-3/7 activity. Data was analyzed by the "Student's t-test".[11] The difference in the fluorescence produced in AFGP8-treated cells and cells with no treatment (negative control) was significant even after only 4 hours incubation with the caspase-3/7 substrate ($P<0.05$), and this trend became more obvious as the incubation time was increased. After 48 hours incubation, AFGP8-treated cells displayed over 60% more caspase-3/7 activation than negative control cells. This result confirmed that the cell death caused by AFGP8 is via apoptosis.

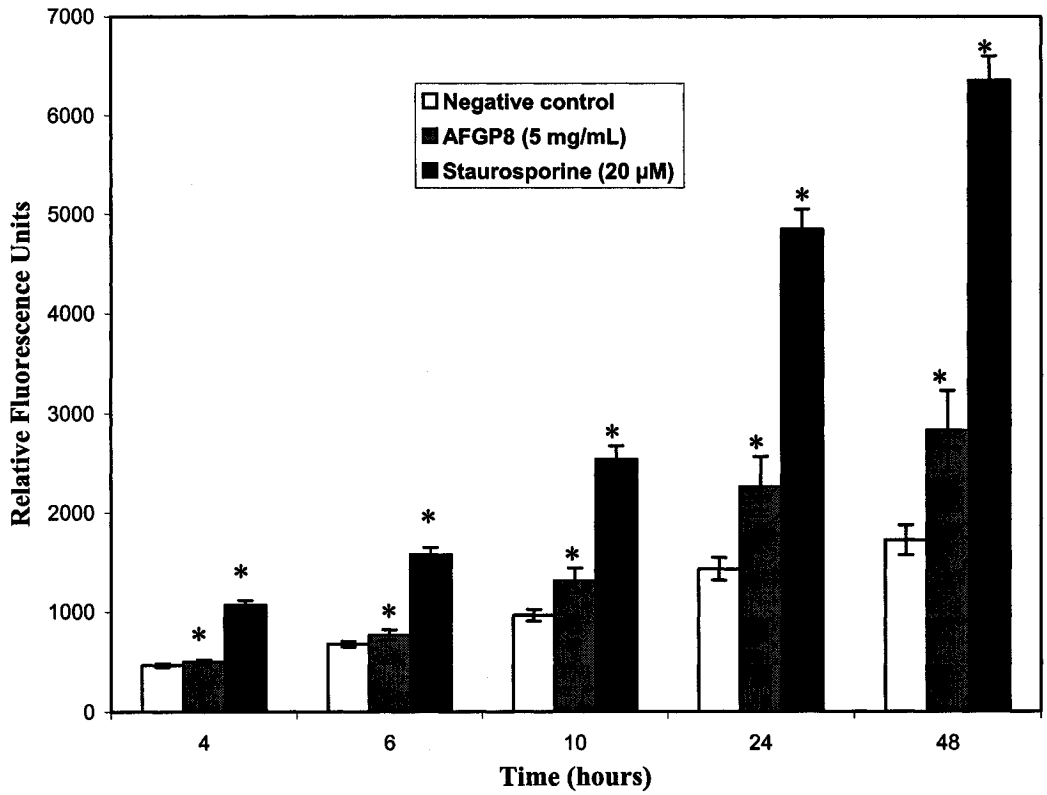

Figure 5.12 Caspase-3/7 assay of AFGP8 with human embryonic liver cells (WRL 68). WRL 68 cells incubated with vehicle treatment (2% DMSO in MEM) act as negative control. Experimental treatment shows WRL 68 cells incubated with 5 mg/mL AFGP8 solution at 37 °C for 18 hours. The positive Control shows WRL 68 cells incubated with 20 µM staurosporine solution at 37 °C for 18 hours. Relative fluorescence units were measured with excitation at 499

nm and emission at 521 nm. Data are mean ± standard deviation. Data was analyzed using the "Student's t-test". Asterisks indicate significant difference ($P<0.05$) from the negative control.

In order to verify whether apoptosis is the reason for the cytotoxicity difference of AFGP8 and *C*-linked analogues in human liver cells, the caspase-3/7 assay was performed with *C*-linked AFGP analogues following the same conditions as for AFGP8. Some cells were pre-incubated with either a *C*-linked AFGP analogue or staurosporine for 18 hours before the addition of caspase-3/7 substrate. Since both analogues displayed no cytotoxic effects to human liver cells, it was expected that the level of activated caspase-3/7 in cells treated with *C*-linked analogues to be about the same as that in negative controls. Surprisingly, the inclusion of analogue **42** can inhibit the activation of caspase-3/7 in human liver cells. As shown in Figure 5.13, cells treated with 5 mg/mL of analogue **42** produced much lower levels of fluorescence than cells without analogue treatment. Furthermore, the level of activated caspase-3/7 in cells treated with analogue **42** did not change as the incubation time with the casapse-3/7 substrate was increased. Data was analyzed by the "Student's t-test".[11] With the exception of 4 hours incubation, analogue **42** significantly inhibited the activation of caspase-3/7 in human liver cells compared to the negative control ($P>0.05$ for 4 hours incubation; $P<0.05$ for 6, 10, 24 and 48 hours incubation).

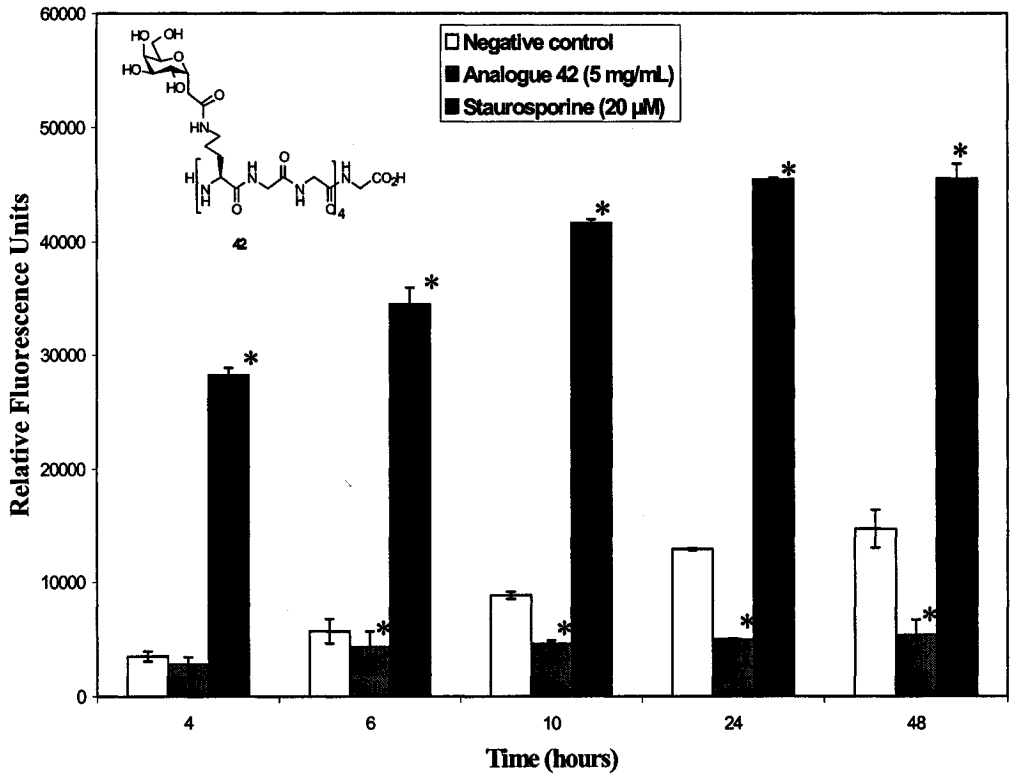

Figure 5.13 Caspase-3/7 assay of analogue **42** with human embryonic liver cells (WRL 68). Experimental conditions were the same as described in Figure 5.12, except that experimental treatment shows WRL 68 cells incubated with 5 mg/mL analogue **42** solution at 37 °C for 18 hours. Data are mean ± standard deviation. Data was analyzed using the "Student's t-test". Asterisks indicate significant difference ($P<0.05$) from the negative control.

Analogue **57** is also a potent caspase-3/7 inhibitor. As shown in Figure 5.14, the presence of 5 mg/mL analogue **57** caused a significant decrease in the fluorescence produced in human liver cells ($P<0.05$ for all 4, 6, 10, 24, 48 hours incubations compared to negative control). Unlike for analogue **42**, although the activation of caspase-3/7 was inhibited by analogue **57** compared to the negative control, the overall caspase-3/7 activity still increased as the incubation time with the caspase-3/7 substrate was increased.

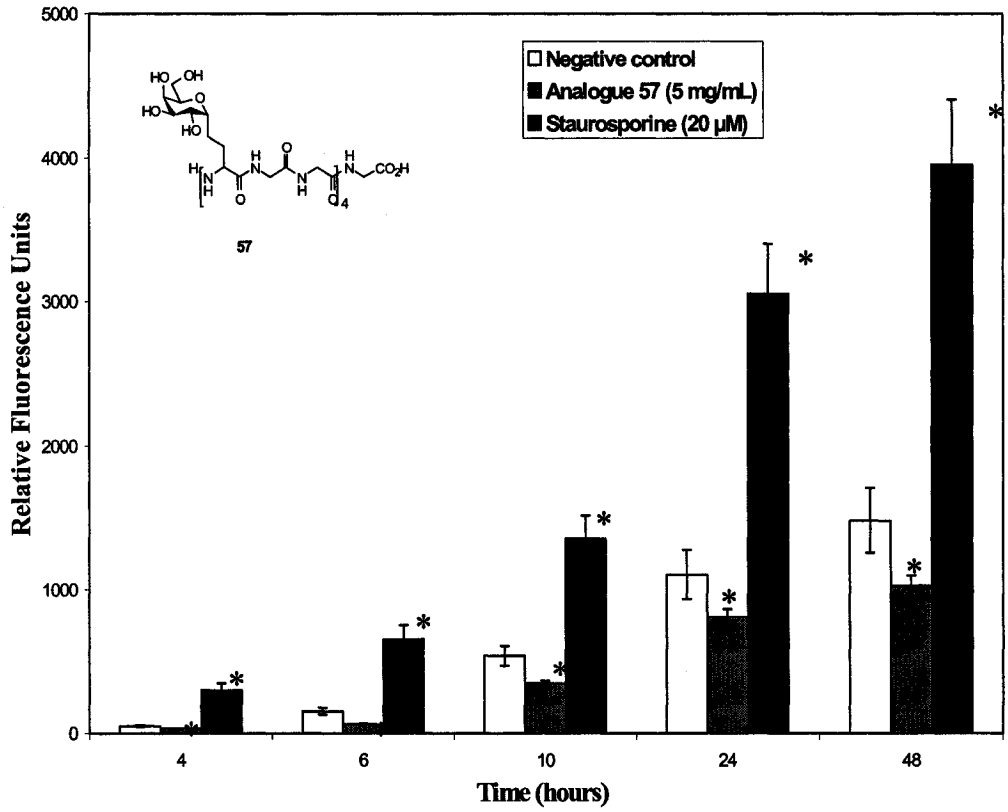

Figure 5.14 Caspase-3/7 assay of analogue **57** with human embryonic liver cells (WRL 68). Experimental conditions were the same as described in Figure 5.12, except that experimental treatment shows WRL 68 cells incubated with 5 mg/mL analogue **57** solution at 37 °C for 18 hours. Data are mean ± standard deviation. Data was analyzed using the "Student's t-test". Asterisks indicate significant difference ($P<0.05$) from the negative control.

The caspase-3/7 assay results are in agreement with the MTT assay results and suggest that the cytotoxicity difference between AFGP8 and *C*-linked AFGP analogues is due to their different ability to induce apoptosis in human liver cells. AFGP8 can activate the caspase-3/7 activity while analogues **42** and **57** are caspase inhibitors, which gives these analogues more potential for their use as cryoprotecting agents since it has been shown that cold-induced apoptosis is also a reason that causes the low recovery rate after cell cryopreservation.[29]

The decrease of cell viability after cryopreservation has been considered to be caused by the ice- and osmotic stress-related physical cell rupture and cold stress-caused pathological cell

death.[30] Recently, it has been found that the complete damage to cells after cryopreservation was not observed until an extended post-thaw period was performed.[31] Cells which survive freezing can still lose viability when they are cultured for a prolonged period of time. Later, Baust found that cryopreservation-induced delayed-onset cell death (CIDOCD) is an important factor that accounts for the low cell recovery rate after freezing.[32] Cryopreservation-induced apoptosis has been identified as the major mechanism that causes delayed cell death.[29] For example, Glander found that caspases 1, 8 and 9 in spermatozoa became more activated than donor's fresh sperm after cryopreservation.[33] To solve this problem, caspase inhibitors have been added into cell solutions before or after cryopreservation.[32, 34] Baust and co-workers demonstrated that the post-thaw viability of a renal cell line was improved by supplementing the traditional freezing medium with an apoptotic inhibitor (caspase I inhibitor V).[34c] They proposed that the regulation of apoptosis is essential for improving cryopreservation. More recently, Schulze-Osthoff and Los discovered that the recovery of cryopreserved hematopoietic and other cells was significantly improved by the inclusion of an irreversible caspase inhibitor zVAD-fmk, either in the freezing solution before cryopreservation or in the culture medium after thawing.[34b] The caspase inhibitor not only prevented caspase 3 activation, but also displayed no obvious affects on cell physiology.

The caspase-3/7 assay results clearly demonstrated that *C*-linked AFGP analogues **42** and **57** can inhibit the activation of caspase 3 and 7 in human liver cells. Therefore, they may also be effective in preventing or reducing cryopreservation-induced apoptosis. This property, together with their potent ice recrystallization inhibition ability and absence of cytotoxicity to cells at physiological conditions, makes these analogues very promising protecting agents for cell cryopreservation. Admittedly, it is impossible to determine from the caspase-3/7 assay the exact acting point of AFGP8 and *C*-linked AFGP analogues **42** and **57** in the caspase cascades. Continued investigation into the detailed mechanism of these glycopeptides in the apoptosis process is necessary for understanding their different cytotoxic effects in cells.

5.2.2 Independent Confirmation of AFGP8-Induced Apoptosis Using a Fluorescence Apoptosis Assay

In order to verify that the cytotoxicity in human cell lines caused by AFGP8 inclusion is mainly an apoptotic process, we performed a fluorescence apoptosis assay, which differentiates

viable cells, apoptotic cells and necrotic cells based on the permeability of the plasma membrane. During apoptosis, the compaction and fragmentation of nuclear chromatins is a characteristic feature within cells. These morphological changes are coordinately employed with membrane permeability to identify apoptosis using fluorescent nuclear acid stain solutions. Cells with a damaged plasma membrane can be stained by fluorescent dyes, while cells with intact plasma membrane are not permeable, and therefore are not stained.

A Vybrant® apoptosis assay (Molecular Probes) was used in this fluorescence apoptosis study. Three nuclear acid stains with differing cell membrane permeability were simultaneously incubated with human liver cells. The YO-PRO-1 iodide stain can selectively pass through the disturbed plasma membrane of apoptotic cells and label the nucleus with moderate green fluorescence, but is impermeant to the intact membrane of viable cells.[35] Hoechst 33342 is a blue fluorescent dye and can stain the normal chromatin of viable cells and the condensed chromatin of apoptotic cells.[36] Red-fluorescent propidium iodide (PI) is membrane impermeable and can only be taken up by necrotic cells through the compromised membrane and late-stage apoptotic cells which have a membrane with increased permeability. Therefore, by simultaneously incubating cells with these fluorescent nucleic acid stain solutions, apoptotic cells can be differentiated from viable cells and necrotic cells (Table 5.1).

Table 5.1 Three fluorescent nuclear acid stains used for fluorescence apoptosis assay.

Nuclear acid stain	Living cells	Apoptotic cells	Necrotic and late-apoptosis cells
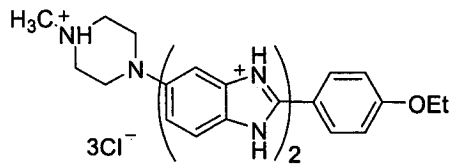 **Hoechst 33342**	Blue	Blue	Blue
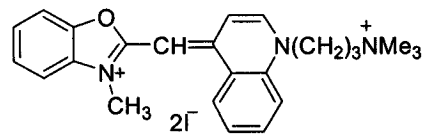 **YO-PRO-1 iodide**	No stain	Green	Green
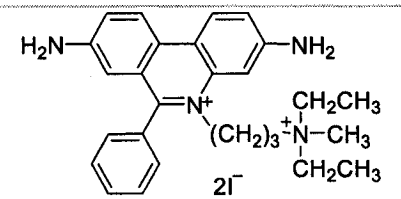 **Propidium iodide**	No stain	No stain	Red

In order to clearly visualize the morphology of individual cells, human liver cells were incubated in a petridish until they reached about 50% confluence, followed by treatment with 5 mg/mL AFGP8 for 4 hours. In this assay, parallel negative and positive controls were also performed. Cells growing under normal conditions without drug treatment acted as the negative control. 20 μM staurosporine was used to incubate cells for 4 hours to act as the positive control.

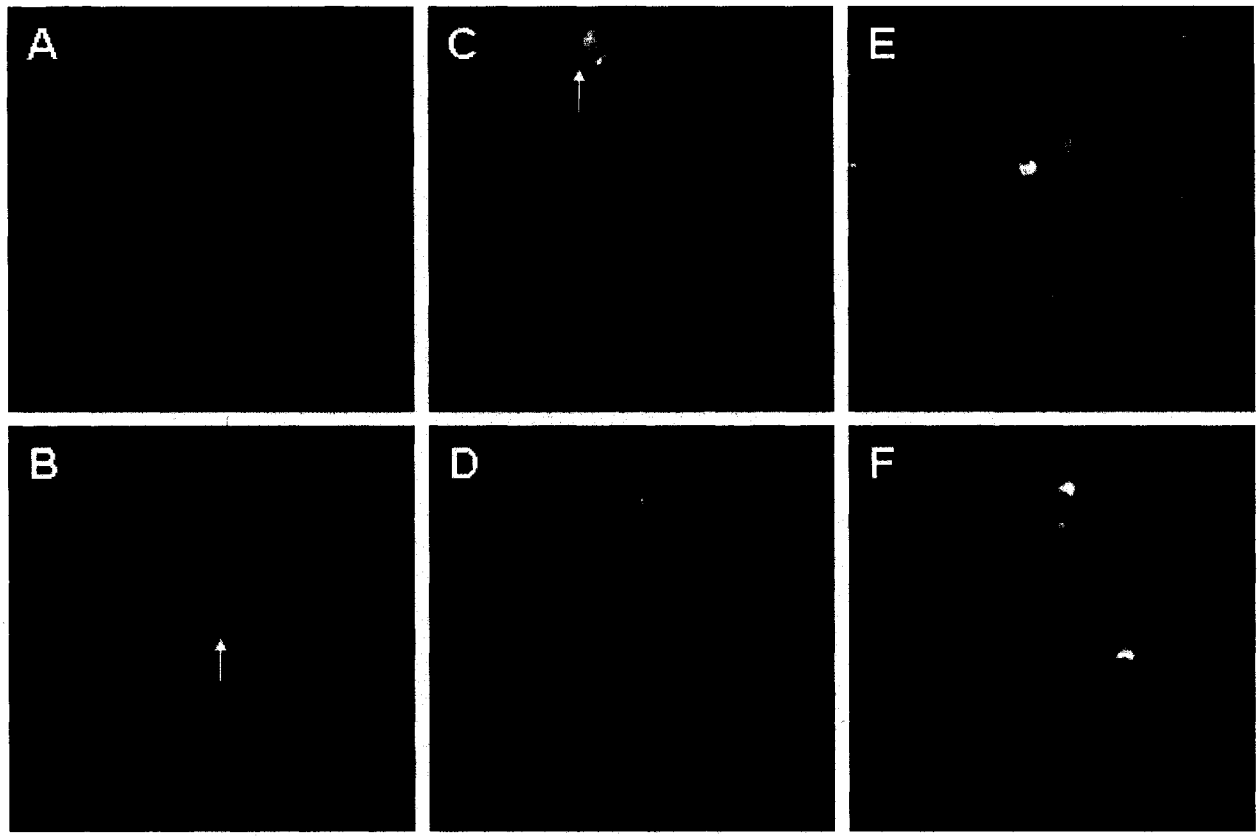

Figure 5.15 Fluorescence apoptosis assay of AFGP8-treated human embryonic liver cells (WRL 68). Cells were incubated with a solution of 8.1 μM hoechst 33342 (stains the nuclei of all cells blue), 0.1 μM YO-PRO-1 (stains the nuclei of early apoptotic cells green) and 1.5 μM propidium iodide (stains the nuclei of dead cells and late apoptotic cells red) in MEM at 0 °C for 30 minutes. **A, B:** negative control; **C, D:** WRL 68 cells were pre-incubated with 5 mg/mL AFGP8 in MEM at 37 °C for 4 hours; **E, F**: WRL 68 cells were pre-incubated with 20 μM staurosporine in MEM at 37 °C for 4 hours.

As shown in Figure 5.15, cells without drug treatment (panel A & B) were stained only by blue-fluorescent Hoechst 33342 solution, which indicated that these cells were living cells. A few cells could lose viability during regular cell culture and accounted for the green stain by YO-PRO-1 in panel B (arrowhead). Most of AFGP8-treated cells (panel C & D) were intensely stained by both Hoechst 33342 and YO-PRO-1 solutions. However, almost no cells were stained by red-fluorescent PI dye. This result verified that the cell death caused by AFGP8 was mainly via an apoptotic process instead of necrosis, which was in agreement with the conclusion drawn

from the caspase-3/7 assay. There were very few cells stained by both YO-PRO-1 and PI (panel C, arrowhead). However, this cell might be in the late-stage apoptosis or secondary necrosis, because it is known that the secondary necrosis can be derived from the apoptotic bodies *in vitro*.[18, 21] As for staurosporine-treated cells (panel E & F), both high levels of YO-PRO-1 stained cells and moderate amounts of PI stained cells were observed. Yellow-stained cells were the results of co-localization of green YO-PRO-1 and red PI nuclear acid. This result indicated that staurosporine was a very potent apoptosis-inducer, as many cells in the late-stage apoptosis and necrosis were observed in staurosporine-treated human liver cells.

This fluorescence microscopy study provided the qualitative evidence of AFGP8-induced apoptosis in human embryonic liver cells. However, in order to quantify the population of living cells, early apoptotic cells, late apoptotic and necrotic cells, further studies including the use of flow cytometry are needed.

In summary, the result of the fluorescence apoptosis assay was consistent with the caspase-3/7 assay, and verified that the cell death caused by AFGP8 in human embryonic liver cells is via an apoptotic pathway.

5.3 Internalization of Glycopeptides by Human Embryonic Liver Cells (WRL 68)

Both caspase-3/7 and fluorescence apoptosis assays indicated that AFGP8 can induce apoptosis in human liver cells, whereas *C*-linked AFGP analogues **42** and **57** may actually prevent cell death by inhibiting the activation of apoptotic process. One unanswered question is whether the cytotoxic effects of these glycopeptides are intracellular or extracellular events. One obvious hypothesis that may explain the cytotoxicity difference between AFGP8 and *C*-linked AFGP analogues is that AFGP8 was selectively taken up by human embryonic liver cells, but *C*-linked AFGP analogues **42** and **57** were excluded. In addition, the different cellular uptake modes may also account for the cytotoxicity difference of AFGP8 observed between fish and human cell lines. Therefore, an internalization study of AFGP8 and *C*-linked AFGP analogues **42** and **57** was performed to examine this hypothesis.

5.3.1 Fluorescence Labeling of Glycopeptides with Oregon Green® 488

Before the internalization assay, AFGP8 and *C*-linked AFGP analogues **42** and **57** were first labeled with a green-fluorescent dye, Oregon Green® 488 (Molecular Probes) on the N-terminus of the polypeptides (Scheme 5.3). The labeling reaction proceeds between the primary amine on the glycopeptide and the succinimidyl ester on Oregon Green® 488 to afford a stable dye-peptide conjugate.[37] Fluorescence-labeled glycopeptides were then purified using a polyacrylamide desalting column (Pierce) before being incubated with cells.

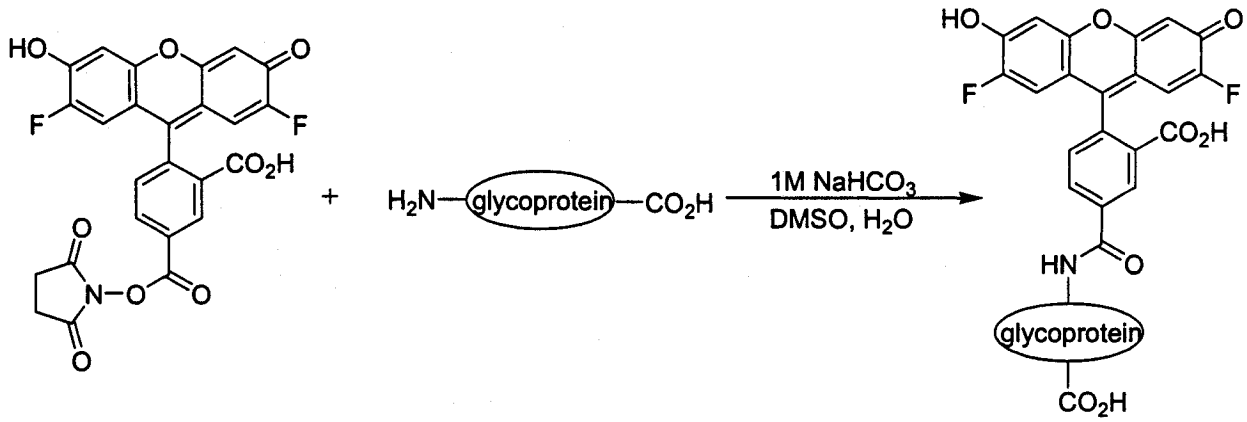

Scheme 5.3 Glycopeptides labeling with fluorescent agent Oregon Green® 488.[37]

5.3.2 Internalization Assay of AFGP8, *C*-Linked AFGP Analogues 42 and 57

Fish gill epithelial cells (Rtgill-W1) were studied to determine whether they are permeable to AFGP8 and *C*-linked AFGP analogues. A red-fluorescent membrane and lipid probe, (*N*-4-sulfobutyl)-4-(6-(4-(dibutylamino)phenyl)hexatrienyl)pyridium inner salt (RH 237) was used as the counter stain and reference for determining the relative location of glycopeptides. As shown in Figure 5.16, after incubating fish cells simultaneously with each glycopeptide and RH 237 at 19 °C for 10 minutes, both AFGP8 (panel A) and *C*-linked AFGP analogue **42** (panel B) were internalized into fish cells.

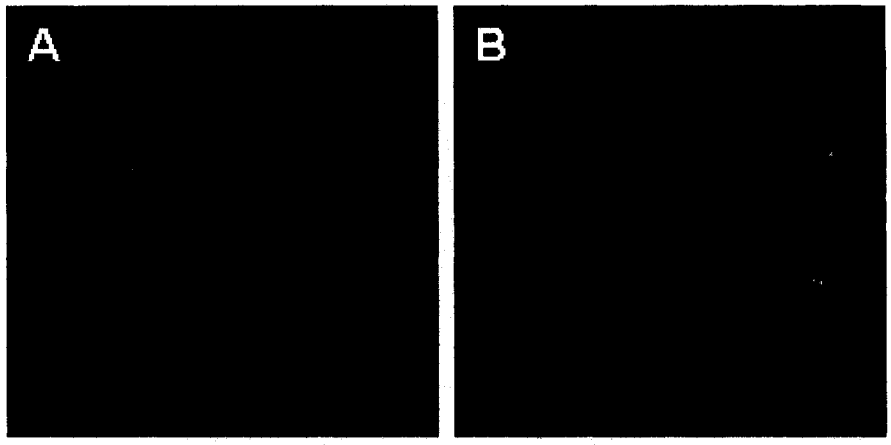

Figure 5.16 Internalization study in fish gill epithelial cells (Rtgill-W1) at 19 °C. **A**: Cells were incubated with fluorescence-labeled AFGP8 (1.5 mg/mL, green) and RH-237 (10 μM, red) for 10 minutes; **B**: Cells were incubated with fluorescence-labeled analogue **42** (1.5 mg/mL, green) and RH-237 (10 μM, red) for 10 minutes.

The same experiment was performed on human liver cells (WRL 68). After incubating cells with different glycopeptides at 37 °C, all AFGP8 (panel A, 20 minutes incubation) and *C*-linked AFGP analogues **42** (panel B, 10 minutes incubation) and **57** (panel C, 10 minutes incubation) were taken up into human liver cells.

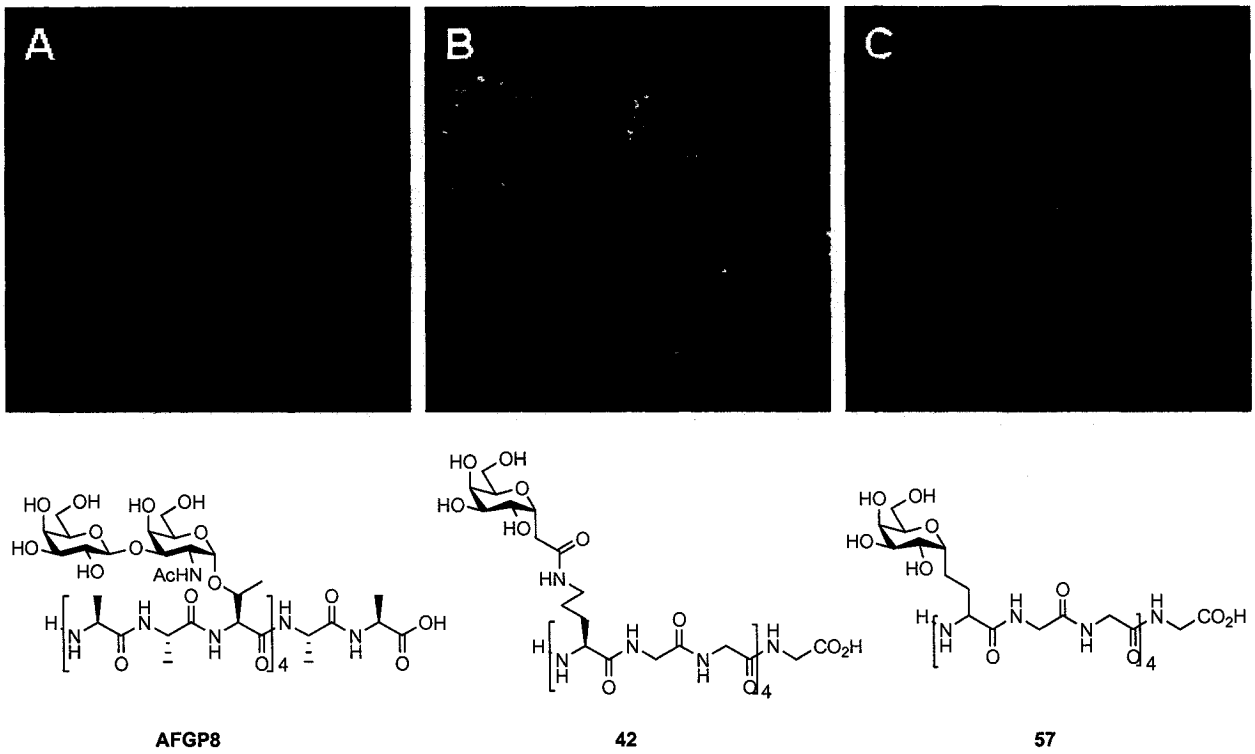

Figure 5.17 Internalization study in human embryonic liver cells (WRL 68) at 37 °C. **A**: Cells were incubated with fluorescence-labeled AFGP8 (1.5 mg/mL, green) and RH-237 (10 μM, red) for 20 minutes; **B**: Cells were incubated with fluorescence-labeled analogue **42** (1.5 mg/mL) and RH-237 (10 μM) for 10 minutes (green channel); **C**: cells were incubated with fluorescence-labeled analogue **57** (1.5 mg/mL, green) and RH-237 (10 μM, red) for 10 minutes.

The internalization study demonstrated that AFGP8 could readily internalize into both fish and human liver cells, as could *C*-linked AFGP analogues **42** and **57**. These results suggest that the difference of the cytotoxic effects observed between AFGP8-treated fish and human liver cells, and the difference observed between AFGP8- and *C*-linked AFGP analogue-treated human liver cells are not due to the difference in cellular uptakes. Instead, it is possible that the cytotoxicity occurs after internalization and the different intracellular events of internalized glycopeptides account for the cytotoxicity difference.

The time-dependency of the internalization process was also studied with AFGP8 in human liver cells. The use of the confocal microscope makes it possible to observe the events occurring at different intracellular positions. As shown in Figure 5.18, panel A1 to A5 are different planes

scanned on the same cell along the Z-axis starting from the cell surface to the middle plane. In panel B1 to B5, the same series of images is shown for a different cell. In this study, it is found that AFGP8 congregated on the plasma membrane after 20 minutes incubation, as a green fluorescent ring was observed in panel A5, which displayed the cell's middle plane. There was no significant amount of fluorescent stain observed inside the cytoplasm. However, after 50 minutes incubation, the fluorescent ring disappeared and the whole cell was stained by AFGP8 (panel B5). This result suggests that the internalization is a time-dependent process.

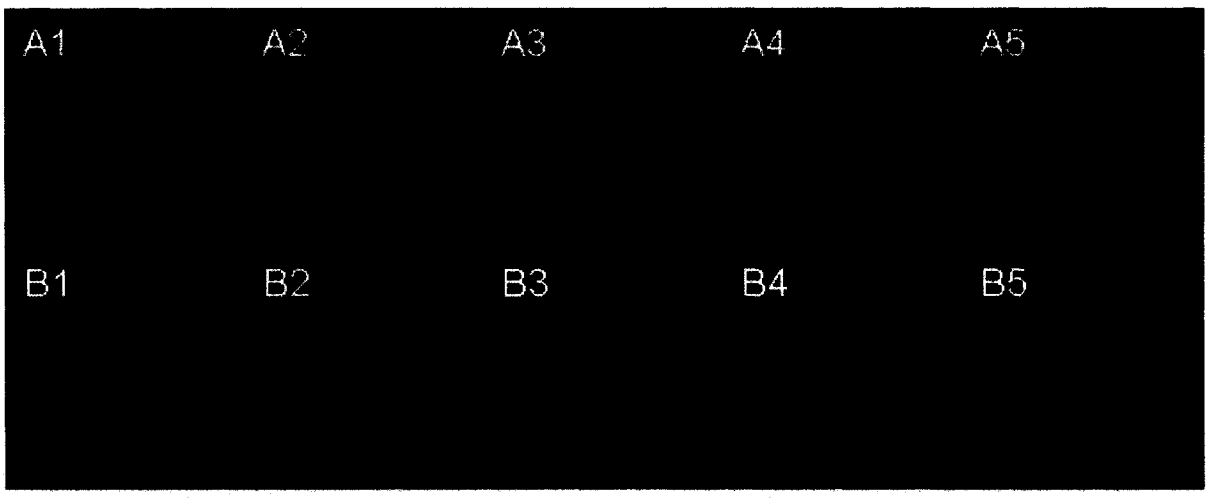

Figure 5.18 Internalization of AFGP8 by human embryonic liver cells (WRL 68). Panel A1 to A5 represent the same cell scanned at different planes along the Z-axis from top to middle. Panel B1 to B5 show the same series of images for a different cell. Cells were incubated with fluorescence-labeled AFGP8 (1.5 mg/mL) at 37 °C for 20 minutes (A1-A5) or 50 minutes (B1-B5).

Extracellular material can gain entry into cells by either direct diffusion through the cell plasma membrane or ATP-dependent endocytosis,[38] although it is unlikely that the relative large AFGP8 and *C*-linked AFGP analogues could fit through the pores between the plasma membrane proteins. In order to understand how AFGP8 internalized into cells, we incubated AFGP8 with human liver cells at 0 °C. As shown in Figure 5.19, neither AFGP8 nor *C*-linked AFGP analogues **42** and **57** could stain human liver cells, which were only labeled by red-fluorescent membrane probe RH 237. Therefore, the internalization of glycopeptides by cells at

their physiological temperatures (19 °C for fish cells and 37 °C for human cells) is probably through an endocytic process instead of direct diffusion. The function of endocytosis requires the cleavage of ATP in the budding step, which is temperature-dependent and stops at 0 °C,[38b] whereas diffusion will not be affected. In addition, the physical state of membranes may become highly ordered and lose their fluidity at low temperatures, which can affect the endocytic process.[39]

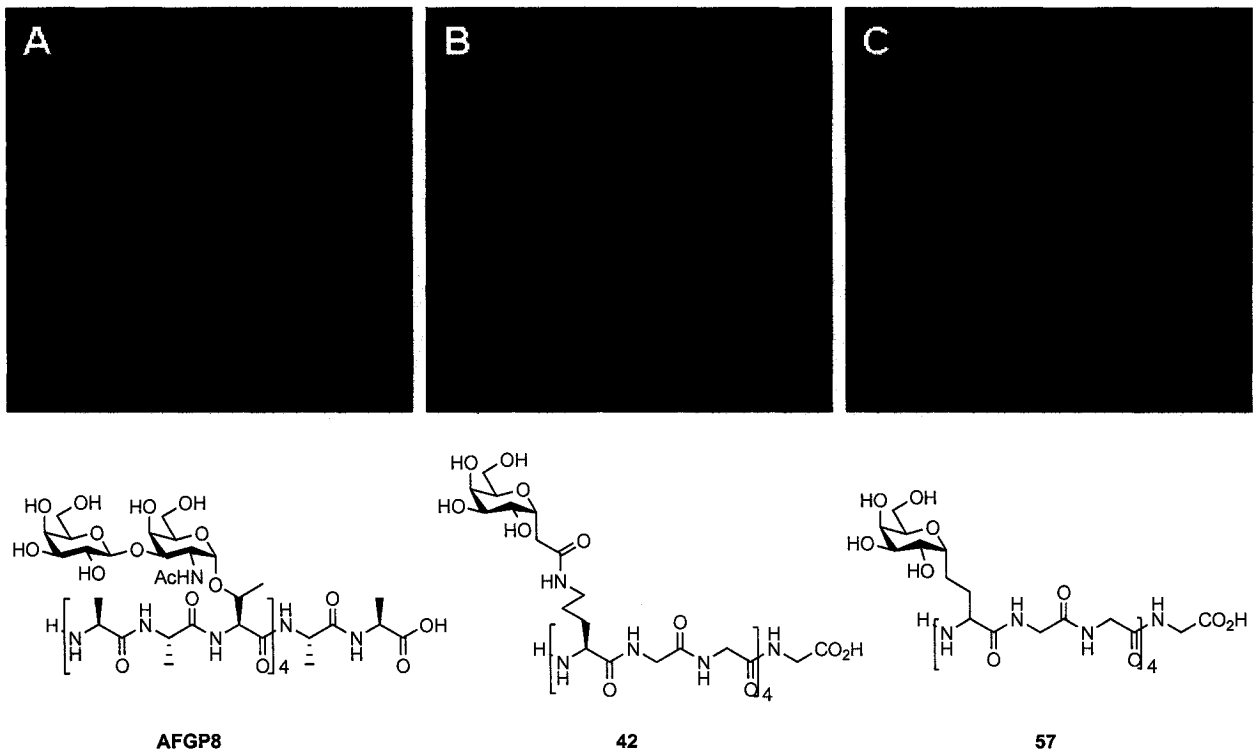

Figure 5.19 Internalization study in human embryonic liver cells (WRL 68) at 0 °C. **A**: Cells were incubated with fluorescence-labeled AFGP8 (1.5 mg/mL) and RH-237 (10 μM) for 50 minutes; **B**: Cells were incubated with fluorescence-labeled analogue **42** (1.5 mg/mL) and RH-237 (10 μM) for 50 minutes; **C**: Cells were incubated with fluorescence-labeled analogue **57** (1.5 mg/mL) and RH-237 (10 μM) for 30 minutes.

Endocytosis is further classified into three types: pinocytosis ("cellular drinking", uptake of particles larger than 250 nm), phagocytosis (cell "eating", uptake of fluid and solutes smaller than 200 nm) and receptor mediated endocytosis.[38] Except for pinocytosis, the other two

pathways are related to the receptors on cell plasma membrane. Galactose-recognizing receptors on the plasma membrane of liver cells have been reported to mediate the binding and uptake of glycoproteins by exposing terminal galactose residues.[40] Therefore, the internalization of AFGP8 and *C*-linked AFGP analogues by human liver cells might also be mediated by the galactose-recognizing receptor.

To clarify which type of endocytosis is employed by glycopeptides, an internalization assay was performed using proteinase K to remove cell plasma membrane receptors. Cells were treated with proteinase K for 1 hour before being exposed to AFGP8 at 37 °C. Same cellular uptake was observed, as in cells without proteinase K-treatment. AFGP8 readily internalized into human liver cells (Figure 5.20). Since proteinase K can effectively remove the receptors on the cell plasma membrane and leave intracellular receptors unaffected,[41] it is possible that the endocytic mechanism of AFGP8 being taken up by human liver cells is likely via pinocytosis. However, we can not exclude the possibility of the receptor-mediated internalization considering that proteinase K may not exclusively remove all the receptors on the cell plasma membrane.

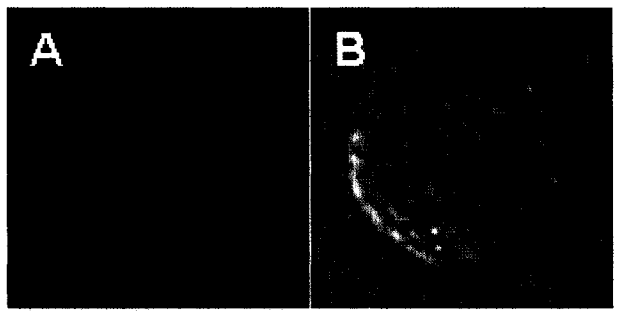

Figure 5.20 Internalization of AFGP8 by human embryonic liver cells (WRL 68) after being treated with proteinase K. Cells were pre-incubated with proteinase K (0.5mg/ml) at 37 °C for 1 hour, then incubated by fluorescence-labeled AFGP8 (1.5 mg/mL) at 37 °C for 20 minutes. **A**: Green channel; **B**: Phase contrast. Both images displayed the same plane of the same cell.

In summary, both AFGP8 and *C*-linked AFGP analogues **42** and **57** can readily internalize into both fish and human liver cells at their physiological temperatures. The internalization process might be an ATP-dependent endocytosis. However, at sub-zero temperatures, most AFGPs are distributed in fish blood[42] and might not internalize into cells. This is in agreement to

the cryoprotective function of AFGPs as most ice nucleation and growth are extracellular.[43] Since internalization of AFGP8 and *C*-linked AFGP analogues **42** and **57** occurs at higher temperatures, it seems that the internalized glycopeptides do not function to prevent the ice formation. However, caspases-3/7 study indicated that *C*-linked AFGP analogues **42** and **57** could improve cell viability by reducing the cryopreservation-induced apoptosis.

5.3.3 Intracellular Pathway of AFGP8, *C*-Linked AFGP Analogues 42 and 57

The common consequence of endocytic materials is the formation of membrane-bound intracellular vesicles, or endosomes, which are later translocated and fused with lysosomes. The internalized materials then can be degraded by the digestive enzymes inside of lysosomes. To investigate the intracellular events of internalized glycopeptides, a co-localization study was performed by incubating human liver cells with a combination of the green fluorescence-labeled glycopeptide and a red-fluorescent lysosome dye, LysoTracker® Red DND-99 (Molecular Probe). This probe consists of a fluorophore-linked base, which can selectively accumulate in organelles with low internal pH. Therefore, it has been used to label and track acidic lysosomes.[44]

The main reason for performing the co-localization study is to clarify whether the internalized glycopeptides have different intracellular pathways that may cause them to have different cytotoxicity in human embryonic liver cells. Therefore, the intracellular pathways of AFGP8 and *C*-linked AFGP analogues **42** and **57** were only studied in human embryonic liver cells. For AFGP8 and *C*-linked AFGP analogues **42** and **57**, both green-fluorescent glycopeptide and red-fluorescent LysoTracker Red were observed after short-term incubation (Figure 5.21, panel A for AFGP8, panel B for analogue **42**, panel C for analogue **57**). As the incubation time was increased, intense yellow-fluorescent spots were observed in cells for all three glycopeptides (Figure 5.21, panel D for AFGP8, panel E for analogue **42**, panel F for analogue **57**). The formation of the yellow fluorescence was due to the combination of green and red fluorescence, which indicated the localization of internalized glycopeptides in lysosomes. Therefore, AFGP8 and *C*-linked AFGP analogues **42** and **57** followed a similar intracellular pathway and were transferred into lysosomes. Taking into account the structural differences, AFGP8 and *C*-linked

AFGP analogues may undergo different enzymatic degradations in lysosomes. It is possible that the metabolites of the unstable *O*-linked AFGP8 caused the cytotoxicity in human liver cells.

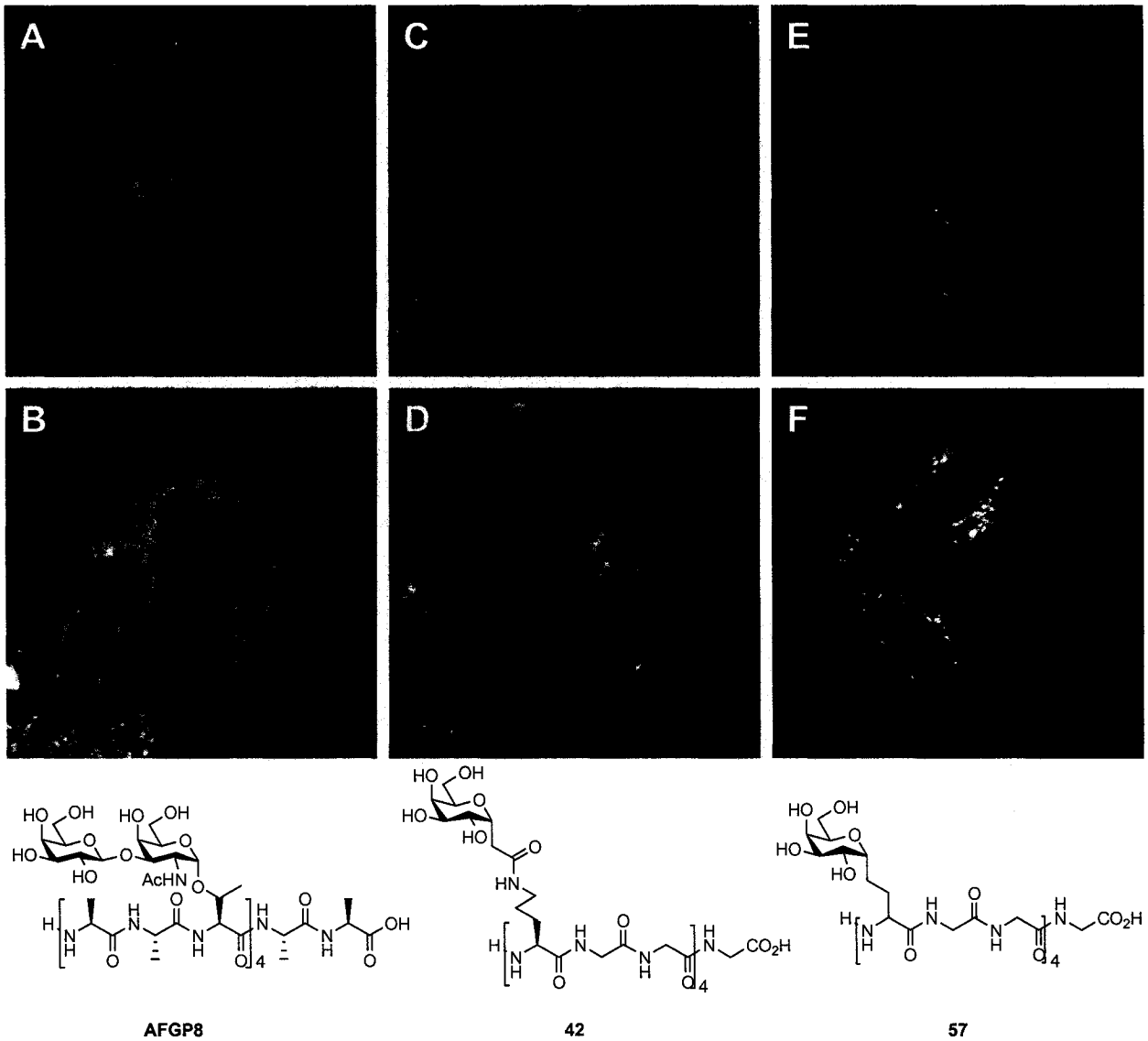

Figure 5.21 Co-localization of glycopeptides with LysoTracker red in human embryonic liver cells (WRL 68). Cells were incubated with a combination of each fluorescence-labeled glycopeptide (1.5 mg/mL for all glycopeptides) and LysoTracker Red DND-99 (75 nM) at 37 °C. Yellow fluorescence indicates co-localization of the fluorescence-labeled glycopeptide and LysoTracker red. **A**: AFGP8, 25 minutes; **B**: AFGP8, 80 minutes; **C**: Analogue **42**, 10 minutes; **D**: Analogue **42**, 20 minutes; **E**: Analogue **57**, 10 minutes; **F**: Analogue **57**, 50 minutes.

The results of *in vitro* cytotoxicity and interactions of AFGP8 and *C*-linked AFGP analogues **42** and **57** are summarized in Table 5.2. It is found the cytotoxicity of AFGP8 is concentration-dependent and tissue-specific. High concentrations of AFGP8 are toxic to human embryonic liver and kidney cells, whereas they are not toxic to fish gill epithelial cells at the respective physiological temperatures. All *C*-linked AFGP analogues **42** and **57** demonstrated no cytotoxicity to human cell lines. At cryogenic temperatures, AFGP8 demonstrated significant toxicity. In contrast, *C*-linked AFGP analogue **57** displayed protective effects on liver cells.

Table 5.2 Summary of *in vitro* cytotoxicity and interactions of AFGP8 and *C*-linked AFGP analogues **42** and **57** in human embryonic liver cells

Glycopeptides	Cytotoxicity	Apoptotic assay	Internalization assay	Co-localization assay
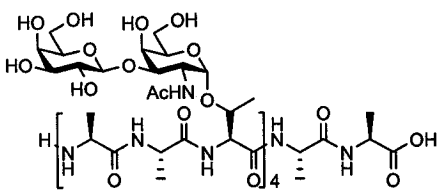 **AFGP8**	Cytotoxic	Activating caspases 3 and 7	Internalized at 37 °C, but excluded at 0 °C	Co-localized into lysosomes
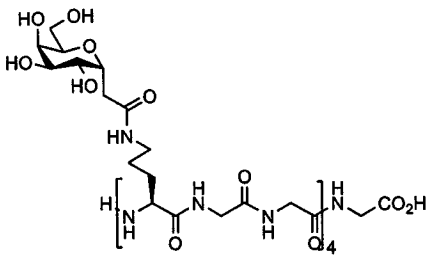 **Analogue 42**	Not cytotoxic	Inhibiting caspases 3 and 7		
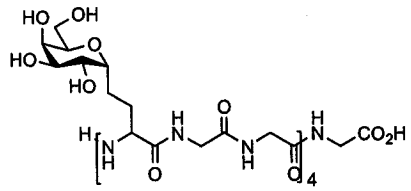 **Analogue 57**	Not cytotoxic	Inhibiting caspases 3 and 7		

The cytotoxicity caused by AFGP8 is due to the induction of apoptosis in human embryonic liver cells. On the other hand, the inclusion of *C*-linked AFGP analogues **42** and **57** can inhibit the activation of caspases 3 and 7. All three glycopeptides displayed no difference in cellular uptake modes, which is possibly via an ATP-dependent endocytosis and all internalized glycopeptides are sequestered into lysosomes. The cytotoxicity difference displayed between AFGP8 and *C*-linked AFGP analogues **42** and **57** may be due to their structural difference (*O*-glycosidic linkage in AFGP8, *C*-glycosidic linkage in analogues **42** and **57**), which can produce different metabolites in lysosomes. Therefore, the cytotoxicity of AFGP8 observed in this study may be derived from its intrinsic, unstable structure.

One major conclusion from this study is that *C*-linked AFGP analogues **42** and **57** have advantages to be used as cryoprotective agents over native AFGPs. These analogues are potent ice recrystallization inhibitors, but have no detrimental dynamic ice-shaping properties. In addition, they have no cytotoxic effects on human cells. In contrast, they can improve cell viability after cryopreservation by suppressing the cold-induced apoptosis. Therefore, the rational design of *C*-linked AFGP analogues as cryoprotecting agents is a feasible endeavor. These analogues may be used in the future for medical, commercial and industrial applications.

References

1. Crevel, R. W., Fedyk, J. K. & Spurgeon, M. J. *Food Chem. Toxicol.* **2002**, *40*, 899-903.
2. Hall-Manning, T., Spurgeon, M., Wolfreys, A. M. & Baldrick, A. P. *Food Chem. Toxicol.* **2004**, *42*, 321-333.
3. Pham, L., Dahiya, R. & Rubinsky, B. *Cryobiology* **1999**, *38*, 169-175.
4. (a) Hincha, D. K., DeVries, A. L., Schmitt, J. M. *Biochim. Biophys. Acta* **1993**, *1146*, 258-264.

   (b) Wang, T., Zhu, Q., Yang, X., Layne, J. R., DeVries, A. L. *Cryobiology* **1994**, *31*, 185-192.

   (c) Zhu, Q., Yang, X., Layne, J. R., Jr., DeVries, A. L., Wang, T. *Cryobiology* **1992**, *29*, 783-784.

   (d) Mugnano, J. A., Wang, T., Layne, J. R., Jr., DeVries, A. L., Lee, R. E., Jr. *Am. J. Physiol.-Reg. I.* **1995**, 269, R474-R479.

   (e) Rubinsky, B., DeVries, A. L. *Cryobiology* **1989**, *26*, 580.

   (f) Pegg, D. E. *Cryobiology* **1992**, *29*, 774.

   (g) Hansen, T. N., Smith, K. M., Brockbank, K. G. M. *Cryobiology* **1993**, *30*, 646.

   (h) Koushafar, H., Pham, L., Lee, C., Rubinsky, B. *Cryobiology* **1997**, *35*, 324.
5. Raymond, J. A., Fritsen, C. H. *Cryobiology* **2001**, *43*, 63-70.
6. Davies, P. L., Hew, C. L. *FASEB. J.* **1990**, *4*, 2460-2468.
7. *Apoptosis, cell death and cell proliferation, 3rd edition.* Roche Diagnostics GmbH, Roche Applied Science, Mannheim, Germany, pp. 2-70. Available online: http://www.roche-applied-science.com/sis/apoptosis/docs/manual_apoptosis.pdf.
8. (a) Mosmann, T. *J. Immunol. Methods* **1983**, *65*, 55-63.

   (b) Denizot, F., Lang, R. *J. Immunol. Methods* **1986**, *89*, 271-277.
9. Slater, T. F., Sawyer, B., Sträuli, U. *Biochim. Biophys. Acta* **1963**, *77*, 383-393.
10. For all MTT assay data, standard deviation from the mean is presented as error.
11. Horgan, G. W. *J. Stat. Edu.* **1999**, *7*, n.1. Available online: http://www.amstat.org/publications/jse/secure/v7n1/horgan.cfm.
12. Wang, J.-H. *Cryobiology* **2000**, *41*, 1-9.

13. Larese, A., Acker, J., Muldrew, K., Yang, H. Y. McGann, L. *Cryo-Letters* **1996**, *17*, 175-182.

14. O'Neil, L., Paynter, S. J., Fuller, B. J., Shaw, R. W., DeVries, A. L. *Cryobiology* **1998**, *37*, 59-66.

15. Boons, G. J., Hale, K. J. *Organic Synthesis with Carbohydrates*, Blackwell Science: Malden, MA. **2000**, pp. 156-160.

16. (a) Southard, J. H. Belzer, F. O. *Annu. Rev. Med.* **1995**, *46*, 235-247.
(b) Mühlbacher, F., Langer, F., Mittermayer, C. *Transplant. Proc.* **1999**, *31*, 2069-2070.

17. Rubinsky, B., Arav, A., Fletcher, G. L. *Biochem. Biophys. Res. Commun.* **1991**, *180*, 566-571.

18. Schwartzman, R. A., Cidlowski, J. A. *Endocr. Rev.* **1993**, *14*, 133-151.

19. Picture is taken and regenerated from Dr. Julie Gough's online lecture note (http://personalpages.umist.ac.uk/staff/j.gough/).

20. Earnshaw, W. C., Martins, L. M., Kaufmann, S. H. *Annu. Rev. Biochem.* **1999**, *68*, 383-424.

21. (a) Searle, J., Lawson, T. A., Abbott, P. J., Harmon, B., Kerr, J. F. R. *J. Pathol.* **1975**, *116*, 129-138.
(b) Don, M. M., Ablett, G., Bishop, C. J., Bundesen, P. G., Donald, K. J., Searle, J., Kerr, J. F. R. *Aust. J. Exp. Biol. Med. Sci.* **1977**, *55*, 407-417.

22. Denault, J.-B., Salvesen, G. S. *Chem. Rev.* **2002**, *102*, 4489-4499.

23. Zheng, T. S., Flavell, R. A. *Nat. Biotechnol.* **2000** *18*, 717-718.

24. (a) Zou, H., Li, Y. C., Liu, X. S., Wang, X. D. *J. Biol. Chem.* **1999**, *274*, 11549-11556.
(b) Rodriguez, J., Lazebnik, Y. *Gene Dev.* **1999**, *13*, 3179-3184.
(c) Costantini, P., Bruey, J.-M., Castedo, M., Métivier, D., Loeffler, M., Susin, S. A., Ravagnan, L., Zamzami, N., Garrido, C., Kroemer, G. *Cell Death Differ.* **2002**, *9*, 82-88.

25. Porter, A. G., Jänicke, R. U. *Cell Death Differ.* **1999**, *6*, 99-104.

26. (a) Humpal-Winter, J. Niles, A., Bjerke, M. *Promega Notes* **2001**, *79*, 33-35.
(b) Hoffman, R. *Cell Notes (Promega)* **2002**, *4*, 2-5.

27. Technical bulletin No. 295 for APO-ONE^{TM} homogeneous Caspase-3/7 assay kit, Progema (G7790). Available online: http://www.promega.com/tbs/tb295/tb295.pdf.

28. Tafani, M., Minchenko, D. A., Serroni, A., Farber, J. L. *Cancer Res.* **2001**, *61*, 2459-2466.

29. (a) Jurisicova, A., Varmuza, S., Casper, R. F. *Hum. Reprod. Update* **1995**, *1*, 558-566.

(b) Borderie, V. M., Lopez, M., Lombet, A., Carvajal-Gonzalez, S., Cywiner, C., Laroche, L. *Invest Ophthalmol. Vis. Sci.* **1998**, *39*, 1511-1519.

(c) Hilbert, S. L., Luna, R. E., Zhang, J., Wang, Y. N., Hopkins, R. A., Yu, Z.-X., Ferrans, V. J. *J. Thorac. Cardiovasc. Surg.* **1999**, *117*, 454-462.

(d) Fowke, K. R., Behnke, J., Hanson, C., Shea, K., Cosentino, M. *J. Immunol. Methods* **2000**, *244*, 139-144.

(e) Schmidt-Mende, J., Hellström-Lindberg, E., Joseph, B., Zhivotovsky, B. *J. Immunol. Methods* **2000**, *245*, 91-94.

(f) Vogel, M. J., Baust, J. M., Van Buskirk, R., Baust, J. G. *Cryobiology* **2000**, *41*, 390-391.

(g) Baust, J. M., Van Buskirk, R., Baust, J. G. *Cryobiology* **2000**, *41*, 338-339.

30. (a) Meryman, H. T. *Annu. Rev. Biophys. Bioeng.* **1974**, *3*, 341-363.

(b) Baust, J. M. *Cell Preserv. Technol.* **2002**, *1*, 17-31.

31. Frim, J., Snyder, R. A., McGann, L. E., Kruuv, J. *Cryobiology* **1978**, *15*, 502-516.

32. Baust, J. M., Vogel, M. J., Van Buskirk, R., Baust, J. G. *Cell Transplant.* **2001**, *10*, 561-571.

33. Grunewald, S., Paasch, U., Wuendrich, K., Glander, H.-J., *Arch. of Androl.* **2005**, *51*, 449-460.

34. (a) Baust, J. M., Baust, J. G., Hollister, W., Van Buskirk, R., *Cryobiology* **1998**, *37*, 410-411.

(b) Stroh, C., Cassens, U., Samraj, A. K., Sibrowski, W., Schulze-Osthoff, K., Los, M. *FASEB. J.* **2002**, *16*, 1651-1653.

(c) Baust, J. M., Van Buskirk, R., Baust, J. G. *In Vitro Cell Dev. Biol. Anim.* **2000**, *36*, 262-270.

(d) Yagi, T., Hardin, J. A., Valenzuela, Y. M., Miyoshi, H., Gores, G. J., Nyberg, S. L. *Hepatology* **2001**, *33*, 1432-1440.

35. (a) Idziorek, T., Estaquier, J., De Bels, F., Ameisen J.-C. *J. Immunol. Methods* **1995**, *185*, 249-258.

(b) Estaquier, J., Idziorek, T., Zou, W. P., Emilie, D., Farber, C.-M., Bourez, J.-M., Ameisen, J. C. *J. Exp. Med.* **1995**, *182*, 1759-1767.

36. Product information of Vybrant apoptosis assay kit #7, Molecular Probes (MP 23201). Available online: http://probes.invitrogen.com/media/pis/mp23201.pdf.
37. Product information of FluoReporter® Oregon Green® 488 protein labeling kit, Molecular Probes (F-6153). Available online: http://probes.invitrogen.com/media/pis/mp06153.pdf.
38. (a) Mukherjee, S., Ghosh, R. N., Maxfield, F. R. *Physiol. Rev.* **1997**, *77*, 759-803.
    (b) Gruenberg, J., Howell, J. G. Annu. Rev. Cell. Biol. 1989, 5, 453-481
39. (a) Mamdouh, Z., Giocondi, M. C., Laprade, R., Le Grimellec, C. *Biochim. Biophys. Acta-Biomembranes* **1996**, *1282*, 171-173.
    (b) Avery, S. V., Lloyd, D., Harwood, J. L. *Biochem. J.*, **1995**, *312*, 811-816.
40. (a) Kouyoumdjian, M., Borges, D. R., Prado, E. S., Prado, J. L. *Biochim. Biophys. Acta-Biomembranes* **1989**, *980*, 299-304.
    (b) Biessen, E. A. L., Vietsch, H., Van Berkel, T. J. C. *Circulation* **1995**, *91*, 1847-1854.
41. (a) Stoorvogel, W., Oorschot, V., Neve, B. *J. Cell Sci.* **1993**, *106*, 1201-1209.
    (b) Stoorvogel, W., Geuze, H. J., Griffith, J. M., Schwartz, A. L., Strous, G. J. *J. Cell Biol.* **1989**, *108*, 2137-2148.
42. Fletcher, G. L, Hew, C. L., Davies, P. L. *Annu. Rev. Physiol.* **2001**, *63*, 359-390.
43. Meryman, H. T. *Annu. Rev. Biophys. Bioeng.* **1974**, *3*, 341-363.
44. (a) Product information of LysoTracker® and LysoSensor® probes, Molecular Probes (L-7528). Available online: http://probes.invitrogen.com/media/pis/mp07525.pdf.
    (b) Griffiths, G., Hoflack, B., Simons, K., Mellman, I., Kornfeld, S. *Cell* **1988**, *52*, 329-341.

Chapter 6 Experimental Section

6.1 Preparation of *C*-Linked AFGP Analogues

General experimental

All anhydrous reactions were performed in flame-dried or oven-dried glassware under a positive pressure of dry argon or nitrogen. Air or moisture-sensitive reagents and anhydrous solvents were transferred with oven-dried syringes or cannulae. All flash chromatography was performed with E. Merck silica gel 60 (230-400 mesh). Analytical thin layer chromatography (TLC) was performed with 0.2 mm pre-coated silica gel plates 60 F_{254} (E. Merck). Components were visualized by illumination with a short-wavelength ultra-violet light and/or staining (ceric ammonium molybdate stain solution).

All solvents used for reactions were distilled unless aqueous systems. Tetrahydrofuran (THF) and diethyl ether were distilled from sodium/benzophenone under nitrogen. Dichloromethane, triethylamine, benzene and diisopropylethylamine (DIPEA) were distilled from calcium hydride. Methanol was distilled from calcium sulfate. *N*,*N*-dimethylformamide (DMF) was stored over activated molecular sieves under argon.

Solid-phase peptide synthesis (SPPS) was performed using Fmoc-Gly-Wang resin (Novabiochem). SPPS reactions were monitored using both Ninhydrin (Kaiser) and 2,4,6-trinitrobenzenesulfonic acid (TNBS) tests to detect the existence of free amino groups. Ninhydrin test was performed by adding two drops of a mixture solution (5g of ninhydrin in 100 ml ethanol, 80g liquefied phenol in 20 ml ethanol, and 2ml of 0.001M aqueous potassium cyanide to 98 ml of pyridine) to a sampling of resin and heating to 120 °C. A dark blue solution indicated the existence of free amino groups. TNBS test was performed by adding one drop of a mixture solution (10% diisopropylethyl amine in DMF and 1% 2,4,6-trinitrobenzenesulfonic acid in DMF) to a sampling of resin. A resulting red resin indicated the existence of free amino groups.

^{1}H (300, 360 or 500 MHz) and ^{13}C NMR (75, 90 or 125 MHz) spectra were obtained at ambient temperature on a Bruker Avance 300, Bruker AC 300, Bruker AM 360, Bruker Avance 500 or Varian Inova 500 spectrometer. Deuterated chloroform ($CDCl_3$) was used for NMR

experiments, unless otherwise stated. Chemical shifts are reported in ppm downfield from TMS and corrected using the chloroform trace as a reference. Splitting patterns are designated as follows: s, singlet; d, doublet; t, triplet; q, quartet; m, multiplet and br, broad. Low resolution mass spectroscopy (MS) was performed on a Micromass Quatro-LC Electrospray spectrometer with a pump rate of 20 μL/min using electrospray ionization (ESI) or a Micromass MALDI LR system using matrix-assisted laser desorption ionization – time of flight (MALDI-TOF). Infrared absorption spectra (IR) were recorded on a Shimadzu FTIR-8400S spectrometer as a neat film from 4000 cm^{-1} to 650 cm^{-1}. Analytical and preparatory scale RP-HPLC were carried out with C-18 columns on a Varian ProStar/Dynomax HPLC system equipped with a variable wavelength detector (ProStar 330 PDA) or a Waters Delta 600E HPLC system equipped with a variable wavelength detector.

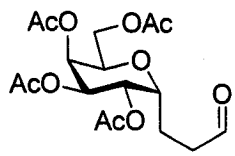

87

Preparation of 3-(2,3,4,6-tetra-*O*-acetyl-*α*-D-galactopyranosyl)-propaldehyde (87)

This compound was prepared according to the previously published procedure.[1] 490 mg of (1.32 mmol) compound **84** was dissolved in 10 mL dry THF and the solution was cooled to 0 °C. 4.1 mL of a 1M solution of BH_3·THF was added and the reaction was stirred for 2 hrs at 0 °C and 0.5 hr at room temperature under N_2 atmosphere. Following this, the reaction was quenched with 0.23 mL water. The reaction mixture was concentrated under reduced pressure. The residue was re-dissolved in 40 mL dry CH_2Cl_2. To this solution was added 3.1 g (14.9 mmol) PCC and the solution was stirred at room temperature overnight. The reaction mixture was filtered through celite and concentrated. The crude product was purified using flash chromatography (silica, 1:1 Hexane:EtOAc) to afford 259 mg (51%) of a white foam.

IR (neat) 3024, 2962, 2930, 1736, 1431, 1369, 1213 cm^{-1}.

^{1}H NMR (300 MHz, $CDCl_3$) δ 9.77 (s, 1H), 5.37 (t, J = 2.2 Hz, 1H), 5.19 (ddd, J = 18 Hz, 9 Hz, 3 Hz, 2H), 4.28-4.14 (m, 2H), 4.08-3.96 (br, 2H), 2.60-2.50 (m, 2H), 2.10 (s, 3H), 2.08 (s, 3H), 2.05 (s, 3H), 2.01 (s, 3H), 1.97-1.90 (br, 1H), 1.84-1.70 (br, m, 1H).

^{13}C NMR (75 MHz, $CDCl_3$) δ 201.2, 170.8, 170.2, 170.1, 71.5, 68.7, 68.5, 68.0, 67.6, 61.4, 40.0, 21.0, 20.9.

MS (ESI): Calcd for $C_{17}H_{25}O_{10}$ $(M+H)^+$ 389.1, found 389.2.

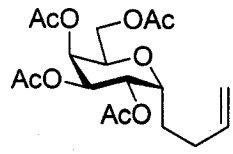

88

Preparation of 2,3,4,6-tetra-*O*-acetyl-1-(3-butenyl)-*α*-D-galactopyranoside (88)

This compound was prepared according to the previously published procedure.[2] To a suspension of 1.139 g (3.2 mmol) methyltriphenylphosphonium bromide in 30 mL dry Et_2O was added 339.9 mg (3 mmol) ^{t}BuOK at 0 °C under argon. The mixture was stirred for 1.5 hrs at 0 °C. A second solution of 618.7 mg (1.5 mmol) of compound **87** in 15 mL dry Et_2O was added to the suspension under argon and the resulting solution was stirred at room temperature under argon for 30 mins. Water was added to obtain a clear solution. The organic layer was separated and concentrated. The crude product was purified with flash chromatography (silica, 5:2 Hexane:EtOAc) to afford 432 mg (70%) of a white foam.

IR (neat) 1740, 1713, 1641, 1437, 1367, 1213 cm^{-1}.

^{1}H NMR (300 MHz, $CDCl_3$) δ 5.86-5.73 (m, 1H), 5.40 (t, J = 3 Hz, 1H), 5.26 (dd, J = 12 Hz, 6 Hz, 1H), 5.17 (dd, J = 9 Hz, 3 Hz, 1H), 5.10-4.95 (m, 2H), 4.22 (dd, J = 9 Hz, 6 Hz, 2H), 4.11-3.99 (m, 2H), 2.11 (s, 3H), 2.06 (s, 3H), 2.05 (s, 3H), 2.03-2.02 (m, 1H), 2.01 (s, 3H), 1.88-1.70 (br, m, 1H), 1.68-1.44 (br, m, 2H).

^{13}C NMR (75 MHz, $CDCl_3$) δ 170.8, 170.4, 170.2, 170.1, 137.5, 115.8, 76.8, 71.7, 68.6, 68.3, 67.9, 61.8, 29.5, 25.2, 21.0, 20.9.

MS (ESI): Calcd for $C_{18}H_{27}O_9$ $(M+H)^+$ 387.2, found 387.3.

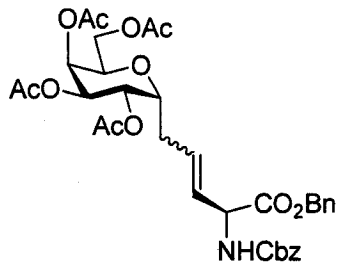

97

Preparation of benzyl (2*S*)-5-(2,3,4,6-tetra-*O*-acetyl-*α*-D-galactopyranosyl)-3-ene-2-(*N*-benzyloxycarbonyl)pentenoate (97)

This compound was prepared according to the previously published procedure.[3] To a solution of 100 mg (0.27 mmol) 2,3,4,6-tetra-*O*-acetyl-1-allyl-*α*-D-galactopyranoside **84** in 5 mL degassed CH_2Cl_2, 186.1 mg (0.572 mmol) (*S*)-benzyl 2-(benzyloxycarbonyl)but-3-enoate **95** and 23 mg (0.027 mmol) (10mol%) second generation Grubbs' catalyst were added successively under argon atmosphere. The mixture was then stirred while refluxing. After 24 hrs, another 23 mg (0.027 mmol) second generation Grubbs' catalyst was added and the reaction was allowed to stir with refluxing for another 24 hrs. Then the reaction was concentrated under reduced pressure and the residue was purified with flash chromatography (silica, 6:1 to 3:2 Hexane:EtOAc) to afford 177 mg (98%) of a white foam. The *E*/*Z* isomeric ratio was not determined as the carbon carbon double bond was hydrogenated in the following step.

^{1}H NMR (300 MHz, $CDCl_3$) δ 7.36-7.28 (br, 10H), 5.78-5.52 (br, m, 3H), 5.37 (s, 1H), 5.22-5.12 (br, 4H), 5.09 (s, 2H), 4.90 (t, J = 6 Hz, 1H), 4.32-4.14 (br, m, 2H), 4.04-3.90 (m, 2H), 2.48-2.32 (br, m, 1H), 2.26-2.15 (br, m, 1H), 2.09 (s, 3H), 2.04 (s, 3H), 2.01 (s, 3H), 1.98 (s, 3H).

^{13}C NMR (75 MHz, $CDCl_3$) δ 171.1, 170.8, 170.2, 170.1, 170.0, 155.8, 136.4, 135.3, 129.7, 128.8, 128.7, 128.5, 128.4, 128.3, 127.2, 127.1, 70.9, 69.0, 68.5, 68.0, 67.7, 67.4, 67.3, 61.10, 55.7, 30.0, 21.0, 20.9.

MS (ESI): Calcd for $C_{34}H_{40}NO_{13}$ $(M+H)^+$ 670.2, found 670.3.

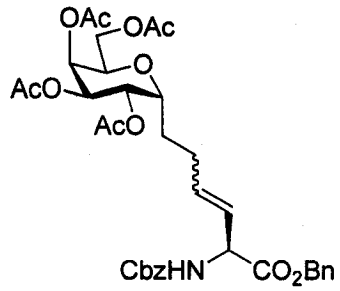

98

Preparation of benzyl (2*S*)-6-(2,3,4,6-tetra-*O*-acetyl-*α*-D-galactopyranosyl)-3-ene-2-(*N*-benzyloxycarbonyl)hexenoate (98)

This compound was prepared according to the previously published procedure.[3] To a solution of 100 mg (0.26 mmol) compound **88** in 5 mL degassed CH_2Cl_2, 168.5 mg (0.518 mmol) (*S*)-benzyl 2-(benzyloxycarbonyl)but-3-enoate **95** and 23 mg (0.027 mmol) (10 mol%) second generation Grubbs' catalyst were added successively under argon atmosphere. The mixture was then stirred while refluxing. After 24 hrs, another 23 mg (0.027 mmol) second generation Grubbs' catalyst was added and the reaction was allowed to stir with refluxing for another 24 hrs. Then the reaction was concentrated under reduced pressure and the residue was purified with flash chromatography (silica, 6:1 to 3:2 Hexane:EtOAc) to afford 177 mg (100%) white foam. The *E*/*Z* isomeric ratio was not determined as the carbon carbon double bond was hydrogenated in the following step.

^{1}H NMR (300 MHz, $CDCl_3$) δ 7.38-7.26 (br, 10H), 5.82-5.65 (m, 1H), 5.58-5.45 (m, 2H), 5.37 (t, J = 2.6 Hz, 1H), 5.26-5.11 (m, 4H), 5.09 (s, 2H), 4.89 (t, J = 6 Hz, 1H), 4.25-4.11 (m, 2H), 4.06-3.93 (m, 2H), 2.34-2.12 (br, m, 2H), 2.10 (s, 3H), 2.04 (s, 3H), 2.02 (s, 3H), 2.00 (s, 3H), 1.79-1.62 (br, m, 1H), 1.52-1.39 (br, m, 1H).

^{13}C NMR (75 MHz, $CDCl_3$) δ 170.8, 170.7, 170.3, 170.1, 170.0, 155.6, 136.3, 135.3, 133.5, 128.8, 128.7, 128.4, 128.3, 125.3, 71.4, 68.4, 68.3, 68.1, 67.7, 67.5, 67.2, 61.6, 55.8, 28.0, 25.1, 21.2, 21.0, 20.9, 20.8.

MS (ESI): Calcd for $C_{35}H_{42}NO_{13}$ $(M+H)^+$ 684.3, found 684.2.

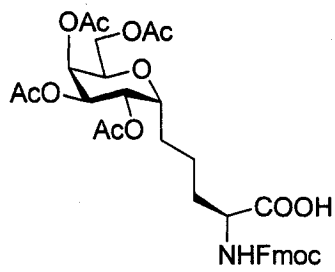

63

Preparation of (2*S*)-5-(2,3,4,6-tetra-*O*-acetyl-*α*-D-galactopyranosyl)-2-(*N*-9-fluorenylmethyloxycarbonyl)pentanoic acid (63)

80 mg (0.12 mmol) of compound **97** was dissolved in 10 mL distilled MeOH. To this solution, 63 mg of 10% Pd/C was added. The reaction flask was filled with H_2 after three vacuum/H_2 cycles. After stirring at room temperature for 5 hrs, the catalyst was filtered through celite. The filtrate was concentrated and the resulting oil-like residue was dissolved in 6 mL 10% $NaHCO_3$ and 2.3 mL 1,4-dioxane. This solution was then cooled to 0 °C, followed by the addition of a second solution of 45 mg (0.13 mmol) *N*-(9-fluorenylmethoxycarbonyloxy)-succinimide in 1.5 mL 1,4-dioxane under argon. The reaction was stirred at 0 °C for 1 hr and stirred at room temperature overnight. The next morning, water was added, and the mixture was washed with Et_2O. The aqueous solution was acidified with 2N HCl and extracted with EtOAc three times. All EtOAc solutions were combined, dried over $MgSO_4$ and concentrated. Purification of the crude product by flash chromatography (silica, 0-5% MeOH in CH_2Cl_2) yielded 44 mg (55%) of a white foam.

IR (neat) 3350, 3067, 1740, 1717, 1516, 1452, 1371, 1225 cm^{-1}.

^{1}H NMR (300 MHz, $CDCl_3$) δ 7.74 (d, J = 7.2 Hz, 2H), 7.57 (s, 2H), 7.33 (td, J = 27.9 Hz, 7.1 Hz, 4H), 5.70-5.50 (br, 1H), 5.38 (s, 1H), 5.26-5.12 (br, m, 2H), 4.50-4.30 (br, 3H), 4.22-4.10 (br, 3H), 4.03-3.90 (br, 2H), 2.11 (s, 3H), 2.06 (s, 3H), 2.02 (s, 6H), 1.80-1.59 (br, 2H), 1.56-1.32 (br, 3H), 1.28-1.20 (br, 1H).

^{13}C NMR (75 MHz, $CDCl_3$) δ 171.3, 170.4, 170.3, 156.3, 144.0, 143.8, 141.5, 127.9, 127.3, 125.2, 125.0, 120.2, 72.0, 68.8, 68.6, 68.2, 68.1, 67.7, 67.3, 61.7, 61.5, 63.6, 47.3, 32.0, 25.3, 21.2, 21.0, 20.9.

MS (ESI): Calcd for $C_{34}H_{40}NO_{13}$ $(M+H)^+$ 670.2, found 670.3.

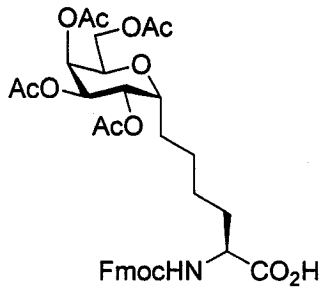

64

Preparation of (2*S*)-6-(2,3,4,6-tetra-*O*-acetyl-*α*-D-galactopyranosyl)-2-(*N*-9-fluorenylmethyloxycarbonyl)hexanoic acid (64)

627.6 mg (0.92 mmol) of compound **98** was dissolved in 77 mL distilled MeOH. To this solution, 490 mg of 10% Pd/C was added. The reaction flask was filled with H_2 after three vacuum/H_2 cycles. After stirring at room temperature for 5 hrs, the catalyst was filtered through celite. The filtrate was concentrated and the resulting oil-like residue was dissolved in 46 mL 10% $NaHCO_3$ and 18 mL 1,4-dioxane. This solution was cooled to 0 °C and to it was added a second solution of 403 mg (1.19 mmol) *N*-(9-fluorenylmethoxycarbonyloxy)-succinimide in 12 mL 1,4-dioxane under argon. The reaction was stirred at 0 °C for 1 hr and then stirred at room temperature overnight. The next morning, water was added, and the mixture was washed with Et_2O. The aqueous solution was acidified with 2N HCl and extracted with EtOAc three times. All EtOAc solutions were combined, dried over $MgSO_4$ and concentrated. Purification of the crude product by flash chromatography (silica, 0-5% MeOH in CH_2Cl_2) yielded 544.1 mg (87%) of a white foam.

^{1}H NMR (300 MHz, $CDCl_3$) δ 7.75 (d, J = 7.5 Hz, 2H), 7.59 (d, J = 7.5 Hz, 2H), 7.39 (t, J = 7.5 Hz, 2H), 7.30 (dt, J = 7.5 Hz, 1 Hz, 2H), 5.44-5.35 (m, 2H), 5.20 (ddd, J = 18.9 Hz, 9.2 Hz, 3.0 Hz, 2H), 4.55-4.32 (br, m, 3H), 4.30-4.12 (m, 3H), 4.08-3.96 (m, 2H), 2.11 (s, 3H), 2.06 (s, 3H), 2.02 (s, 3H), 2.01 (s, 3H), 1.95-1.82 (br, 1H), 1.80-1.58 (br, 2H), 1.55-1.20 (br, 5H).

^{13}C NMR (75 MHz, $CDCl_3$) δ 176.2, 171.2, 170.4, 170.3, 170.2, 156.3, 144.0, 143.9, 141.5, 128.0, 127.3, 125.3, 120.2, 77.4, 72.0, 68.7, 68.3, 68.2, 67.7, 67.3, 61.6, 53.7, 47.3, 32.3, 25.7, 25.0, 21.1, 21.0, 20.9.

MS (MALDI): Calcd for $C_{35}H_{42}NO_{13}$ $(M+H)^+$ 684.3, found 684.3.

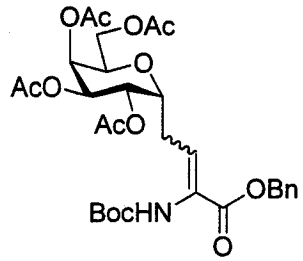

109

Preparation of benzyl 4-(2,3,4,6-tetra-*O*-acetyl-*α*-D-galactopyranosyl)-2-ene-2-(*N*-*t*-benzyloxycarbonyl)butenoate (109)

This compound was prepared according to the previously published procedure.[4] To a solution of 320 mg (0.8 mmol) benzyl 2-(*tert*-butoxycarbonyl)-2-(diethoxyphosphoryl)acetate **107** in 3 mL dry THF at -78 °C, was added 0.1 mL (0.8 mmol) TMG. The solution was stirred for 10 min at –78 °C. Following this a solution of 285 mg (0.76 mmol) of compound **108** in 1 mL dry THF was added. The reaction was stirred at room temperature for 1 hr. 100mL EtOAc was added to the reaction followed by washing with 1 M HCl and saturated $NaHCO_3$, successively. The organic layer was dried with $MgSO_4$. After filtration, solvent was removed under reduced pressure. The crude product was purified by flash chromatography (silica, 5:1 to 3:1 Hexane:EtOAc) to isolate 380 mg of foam (80%).

IR (neat) 3348, 3020, 2980, 1744, 1713, 1659, 1489, 1456, 1367, 1217 cm^{-1}.

^{1}H NMR (300 MHz, $CDCl_3$) δ 7.30 (m, 5H), 6.53 (t, J = 6 Hz, 1H), 6.30 (s, 1H), 5.36 (t, J = 2.8 Hz, 1H), 5.23-5.10 (m, 4H), 4.29 (td, J = 10.3 Hz, 4.1 Hz, 1H), 4.27-4.19 (m, 1H), 4.10-4.01 (m, 1H), 3.97 (dd, J = 11.6 Hz, 4.7 Hz, 1H), 2.59 (ddd, J = 16.4 Hz, 10.2 Hz, 2.3 Hz, 1H), 2.36 (ddd, J = 16.3 Hz, 6.9 Hz, 4.6 Hz, 1H), 2.05 (s, 3H), 1.99 (s, 3H), 1.97 (s, 3H), 1.86 (s, 3H), 1.40 (s, 9H).

^{13}C NMR (75 MHz, $CDCl_3$) δ 170.8, 170.7, 170.4, 170.2, 170.0, 169.9, 164.5, 153.4, 135.5, 130.9, 128.8, 128.7, 128.6, 128.5, 81.0, 74.3, 72.1, 70.8, 69.2, 69.0, 68.5, 68.0, 67.8, 67.5, 67.4, 61.4, 28.3, 26.4, 20.9, 20.8, 20.7.

MS (ESI): Calcd for $C_{30}H_{40}NO_{13}$ $(M+H)^+$ 622.2, found 622.3. Calcd for $C_{30}H_{39}NO_{13}Na$ $(M+Na)^+$ 644.2, found 644.3.

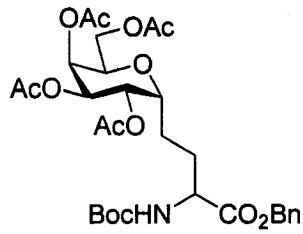

111

Preparation of benzyl (2*S*)-4-(2,3,4,6-tetra-*O*-acetyl-*α*-D-galactopyranosyl)-2-(*N*-*t*-benzyloxycarbonyl)butanoate (111)

This compound was prepared according to the previously published procedure.[4a] In a glove box, 246 mg (0.40 mmol) *E*/*Z* mixtures of **109** and 5 mg (7.6 μmol) [(COD)Rh-((*S*, *S*)-Et-DuPHOS)]$^+$OTf **110** were dissolved in 15 mL degassed dry THF (freeze-dry-thaw for three cycles). After the reaction mixture was purged with H_2 (about 500 psi) for five cycles, the reaction was pressured with 100 psi of H_2. After stirring at room temperature for 2 days, the pressure was released. The reaction was filtered through a plug of silica gel and concentrated under reduced pressure to afford 241 mg of foam (98% yield, 66% de) Diastereomeric excess was estimated based on the integration of Boc protons in ^{1}H NMR.

IR (neat) 3375, 3020, 2978, 1740, 1709, 1501, 1456, 1367, 1217 cm^{-1}.

^{1}H NMR (500 MHz, DMSO-D_6) δ 7.36 (m, 5H), 5.30 (dd, J = 3.3 Hz, 2.6 Hz, 1H), 5.19 (dd, J = 9 Hz, 3.5 Hz, 1H), 5.15 (d, J = 1.1 Hz, 2H), 5.10 (dd, J = 9 Hz, 5 Hz, 1H), 4.18-4.12 (m, 3H), 4.11-4.03 (m, 3H), 2.08 (s, 3H), 2.00 (s, 3H), 1.98 (s, 3H), 1.96 (s, 3H), 1.90-1.77 (m, 2H), 1.70-1.61 (m, 1H), 1.56-1.46 (m, 1H), 1.40 (s, 9H, 5:1 *S*-diastereomer:*R*-diastereomer).

^{13}C NMR (75 MHz, $CDCl_3$) δ 172.4, 170.7, 170.3, 170.1, 170.0, 155.5, 135.5, 128.9, 128.8, 128.7, 128.4, 80.3, 77.4, 72.1, 68.3, 68.0, 67.7, 67.4, 67.3, 61.7, 53.5, 29.9, 29.2, 28.5, 21.0, 20.9.

MS (ESI): Calcd for $C_{30}H_{42}NO_{13}$ $(M+H)^+$ 624.3, found 624.2.

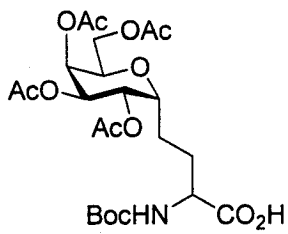

112

Preparation of (2*S*)-4-(2,3,4,6-tetra-*O*-acetyl-*α*-D-galactopyranosyl)-2-(*N*-*t*-benzyloxycarbonyl) butanoic acid (112)

To a solution of 240 mg (0.38 mmol) of compound **111** in 15 mL MeOH was added 200 mg of 10% Pd/C. The reaction flask was filled with H_2 after three vacuum/H_2 cycles. After stirring at room temperature overnight, the catalyst was filtered through a plug of silica gel. The filtrate was concentrated under reduced pressure to afford 178.7 mg (89%) of a white solid.

IR (neat) 3381, 3022, 2974, 1740, 1705, 1506, 1367, 1215 cm^{-1}.

^{1}H NMR (300 MHz, $CDCl_3$) δ 5.39 (t, J = 2 Hz, 1H), 5.28-5.12 (m, 2H), 4.33-4.22 (br, m, 1H), 4.21-4.13 (br, m, 2H), 4.11-3.99 (m, 2H), 3.45 (d, J = 13.8 Hz, 1H), 2.11 (s, 3H), 2.06 (s, 3H), 2.05 (s, 3H), 2.01 (s, 3H), 1.92-1.75 (br, m, 2H), 1.73-1.62 (br, m, 1H), 1.61-1.50 (br, m, 1H), 1.43 (s, 9H).

^{13}C NMR (75 MHz, $CDCl_3$) δ 175.9, 171.1, 170.4, 170.3, 170.2, 155.9, 80.6, 77.4, 74.4, 72.1, 69.1, 68.4, 68.2, 67.8, 61.8, 53.5, 30.5, 28.8, 28.5, 22.2, 21.0, 20.9.

MS (ESI): Calcd for $C_{23}H_{35}NO_{13}Na$ $(M+Na)^+$ 556.2, found 556.3.

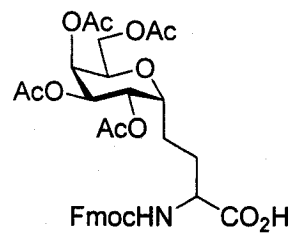

62

Preparation of (2*S*)-4-(2,3,4,6-tetra-*O*-acetyl-*α*-D-galactopyranosyl)-2-(*N*-9-fluorenylmethyloxycarbonyl)butanoic acid (62)

To an-ice cooled solution of 100 mg (0.187 mmol) of compound **112** in 8 mL dry CH_2Cl_2 was added 4 mL TFA dropwise. The reaction was stirred at 0 °C for 1 hr. Solvent was removed under reduced pressure to give a viscous oil. 8 mL 10% $NaHCO_3$ followed by 3 mL 1,4-dioxane were added to dissolve the oil and the resulting solution was cooled to 0 °C. To this solution, a second solution of 65 mg (0.193 mmol) *N*-(9-fluorenylmethoxycarbonyloxy)-succinimide in 2 mL 1,4-dioxane was added slowly through a cannula under argon atmosphere. The reaction was allowed to stir at 0 °C for 1 hr, then at room temperature overnight. Water was added to dilute the

reaction, followed by washing with Et_2O. After being acidified to pH 2 with 2N HCl, the aqueous layer was extracted with EtOAc three times. The combined EtOAc layers were dried with $MgSO_4$. After filtration, solvent was removed under reduced pressure. The crude product was purified by flash chromatography (silica, 0-10% MeOH in CH_2Cl_2) to isolate 95 mg (77%) of white foam.

IR (neat) 3344, 3067, 3020, 2957, 1740, 1713, 1522, 1452, 1371, 1217 cm^{-1}.

^{1}H NMR (300 MHz, $CDCl_3$) δ 7.76 (d, J = 7.6 Hz, 2H), 7.59 (t, J = 6 Hz, 2H), 7.35 (dt, J = 27.5 Hz, 7.9 Hz, 4H), 5.59 (d, J = 8.2 Hz, 1H), 5.38 (t, J = 2.5 Hz, 1H), 5.21 (ddd, J = 21.9 Hz, 9.2 Hz, 4.7 Hz, 2H), 4.52-4.30 (m, 3H), 4.22 (t, J = 6.2 Hz, 3H), 4.05-3.92 (m, 3H), 2.11 (s, 3H), 2.10-2.06 (m, 1H), 2.05 (s, 3H), 2.02 (s, 3H), 1.99 (s, 3H), 1.84-1.70 (br, m, 2H), 1.63-1.45 (br, m, 1H).

^{13}C NMR (75 MHz, $CDCl_3$) δ 171.4, 170.5, 170.4, 170.3, 156.6, 144.0, 143.9, 141.5, 128.0, 127.3, 125.3, 125.2, 120.2, 77.4, 72.2, 68.4, 68.1, 67.8, 67.3, 61.9, 51.1, 47.2, 29.9, 28.6, 21.9, 21.0, 20.9.

MS (ESI): Calcd for $C_{33}H_{38}NO_{13}$ $(M+H)^+$ 656.2, found 656.2

General procedure A for solid-phase peptide synthesis of compounds 57-60

All polypeptides are prepared by linear solid-phase synthesis starting from Fmoc-Gly-Wang resin with loading capacities of 0.6-0.65 mmol/g. The resin was first swollen with DMF for 1 hr. A solution of 20% piperidine in DMF was added and the reaction was stirred for 30 mins. The resin was washed with DMF. Kaiser and TNBS tests were positive. For the coupling reaction performed with Fmoc-Gly-OH, a premixed solution of 3 equivalents of Fmoc-Gly-OH, 3 equivalents of HBTU and 3 equivalents of DIPEA was added to the solid-phase synthesizer. The coupling reaction was run for about 6 hrs until negative results were acquired by Kaiser and TNBS tests. For the coupling reactions performed with building blocks **62-65**, a premixed solution of 1.3 equivalents of appropriate building block, 1.3 equivalents of HBTU and 1.3 equivalents of DIPEA in DMF was added to the solid-phase synthesizer. The reaction mixture was allowed to stir overnight until negative Kaiser and TNBS test results were obtained. Each individual coupling reaction with either Fmoc-Gly-OH or building blocks **62-65** was performed for one cycle. The coupling reactions with either Fmoc-Gly-OH or building blocks **62-65** were

repeated for 12 times until the targeted polypeptide was obtained. As the polypeptide elongated on the solid resin, it took longer for the coupling reactions to finish to give negative Kaiser and TNBS test results (the coupling reaction with building blocks **62-65** could take up to two days to finish). Following the last coupling reaction, the Fmoc protecting group was removed with a solution of 20% piperidine in DMF. The resin was washed successively with DMF, 4% acetic acid, CH_2Cl_2, and methanol, and dried over KOH under vacuum for 6 hrs. The resin was treated with 50% TFA in a solution of CH_2Cl_2 for 2 hrs. The solution was filtered and the resin was washed with TFA. All filtrate was collected and concentrated under reduced pressure. Et_2O was added to afford a white precipitate. This product was then dissolved in premixed solution of sodium in MeOH (pH = 10) and stirred overnight. Amberlite® IR-120H ion-exchange resin was added to neutralize the reaction mixture. The resin was filtered through a plug of cotton and the solvent was removed under reduced pressure. The product was dissolved in water and lyophilized to afford a white powder. The crude product was further purified by RP-HPLC with a gradient of 0-60% CH_3CN in H_2O (0.1% TFA) over 50 mins to furnish the final polypeptide. The chemical yield calculation of final products was based on the loading capacity of the Fmoc-Gly-Wang resin.

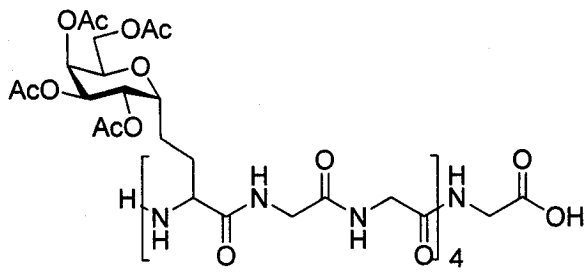

113

Compound 113

Prepared using procedure A. 58.5 mg (38.2 μmol) Fmoc-Gly-Wang resin (loading capacities: 0.65 mmol/g) was used to assemble **113**. For the coupling reaction performed with Fmoc-Gly-OH, a premixed solution of 34.0 mg (114 μmol) Fmoc-Gly-OH, 43.4 mg (114 μmol) HBTU and 0.02 mL (114 μmol) DIPEA was added to the solid-phase synthesizer. For the coupling reaction performed with building blocks **62**, a premixed solution of 30 mg (45.8 μmol) **62**, 17.4 mg (45.8 μmol) HBTU and 8 μL (45.8 μmol) DIPEA in DMF was added to the solid-phase synthesizer.

The whole SPPS process took about 10 days and 77.5 mg (93%) polypeptide **113** was precipitated from Et_2O and collected as a white solid.

^{1}H NMR (500 MHz, CD_3OD) δ 5.38 (s, 1H), 5.34-5.23 (br, 1H), 5.22-5.12 (br, 1H), 4.31-3.87 (br, m, 11H), 2.10 (s, 3H), 2.06 (s, 3H), 2.01 (s, 3H), 1.98 (s, 3H), 1.92-1.62 (br, 4H).

^{13}C NMR (75 MHz, CD_3OD) δ 174.9, 172.4, 172.0, 171.6, 73.6, 69.7, 69.6, 69.44, 69.35, 69.2, 69.1, 62.8, 55.1, 54.4, 43.7, 43.3, 41.8, 28.8, 22.5, 20.9, 20.8, 20.7, 20.6.

MS (ESI): Calcd for $C_{90}H_{129}N_{13}O_{50}$ M^+ 2191.8, found 2192.2; Calcd for $C_{90}H_{130}N_{13}O_{50}$ $(M+H)^+$ 2192.8, found 2193.1.

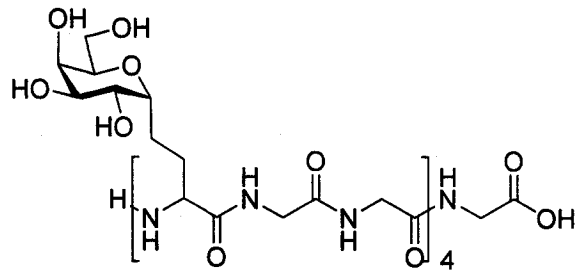

57

Compound 57

20 mg (9.1 μmol) glycopeptide **113** was dissolved in a premixed solution of sodium in MeOH (pH = 10) and stirred overnight. Amberlite® IR-120H ion-exchange resin was added to neutralize the reaction mixture. The resin was filtered through a plug of cotton and the solvent was removed under reduced pressure. The product was dissolved in water and lyophilized to afford 13.9 mg (100%) white powder. Analytically pure polypeptide was further purified by RP-HPLC with a gradient of 0-60% CH_3CN in H_2O (0.1% TFA) over 50 mins.

^{1}H NMR (300 MHz, D_2O) δ 4.38-4.30 (br, 1H), 4.03-3.85 (br, m, 9H), 3.78-3.60 (br, m, 5H), 2.10-1.82 (br, m, 2H), 1.80-1.56 (br, m, 2H).

^{13}C NMR (75 MHz, D_2O) δ 181.8, 172.2, 172.0, 75.7, 75.6, 72.2, 72.07, 72.05, 72.04, 69.9, 69.4, 68.5, 61.6, 54.5, 43.5, 42.9, 42.8, 23.6.

MS (ESI): Calcd for $C_{58}H_{98}N_{13}O_{34}$ $(M+H)^+$ 1520.6, found 1520.3.

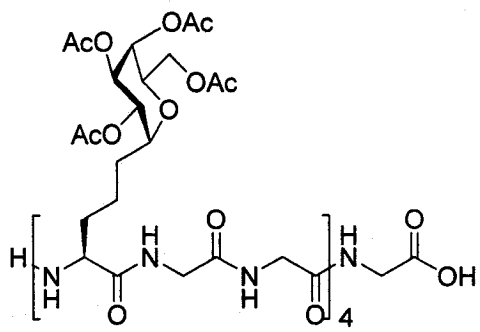

114

Compound 114

Prepared using procedure A. 57.5 mg (37.5 μmol) Fmoc-Gly-Wang resin (loading capacities: 0.65 mmol/g) was used to assemble **114**. For the coupling reaction performed with Fmoc-Gly-OH, a premixed solution of 33.3 mg (112 μmol) Fmoc-Gly-OH, 42.7 mg (112 μmol) HBTU and 19.5 μL (112 μmol) DIPEA was added to the solid-phase synthesizer. For the coupling reaction performed with building blocks **63**, a premixed solution of 30 mg (44.8 μmol) **63**, 17.0 mg (44.8 μmol) HBTU and 7.8 μL (44.8 μmol) DIPEA in DMF was added to the solid-phase synthesizer. The whole SPPS process took about 10 days and 78 mg (92%) polypeptide **114** was precipitated from Et_2O and collected as a white solid.

^{1}H NMR (300 MHz, CD_3OD) δ 5.39 (s, 1H), 5.30-5.15 (br, m, 2H), 4.50-3.72 (br, m, 11H), 2.11 (s, 3H), 2.06 (s, 3H), 2.03 (s, 3H), 1.99 (s, 3H), 1.95-1.68 (br, m, 3H), 1.63-1.30 (br, m, 3H).
^{13}C NMR (75 MHz, CD_3OD) δ 172.3, 172.1, 171.9, 171.7, 171.6, 73.7, 69.8, 69.3, 66.9, 62.5, 55.3, 54.7, 54.5, 43.7, 41.9, 32.2, 30.7, 26.0, 24.3, 22.9, 20.9, 20.8, 20.7, 20.6.
MS (MALDI): Calcd for $C_{94}H_{137}N_{13}O_{50}M^+$ 2247.9, found 2247.8.

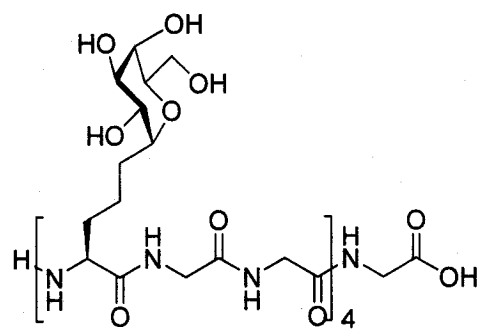

58

Compound 58

22.6 mg (10.1 μmol) glycopeptide **114** was dissolved in a premixed solution of sodium in MeOH (pH = 10) and stirred overnight. Amberlite® IR-120H ion-exchange resin was added to neutralize the reaction mixture. The resin was filtered through a plug of cotton and the solvent was removed under reduced pressure. The product was dissolved in water and lyophilized to afford 15.8 mg (100%) white powder. Analytically pure polypeptide was further purified by RP-HPLC with a gradient of 0-60% CH_3CN in H_2O (0.1% TFA) over 50 mins.

^{1}H NMR (500 MHz, D_2O) δ 4.38-4.28 (br, m, 1H), 4.07-3.92 (br, m, 11H), 3.76-3.68 (br, m, 5H), 1.89 (s, 1H), 1.77-1.70 (br, m, 2H), 1.62-1.50 (br, m, 2H), 1.41-1.29 (br, m, 1H).
^{13}C NMR (75 MHz, D_2O) δ 175.3, 172.3, 172.0, 75.5, 71.9, 70.0, 69.4, 68.6, 61.6, 54.3, 42.9, 42.6, 30.7, 23.3, 21.6.
MS (MALDI): Calcd for $C_{62}H_{105}N_{13}O_{34}$ M^+ 1575.7, found 1575.2.

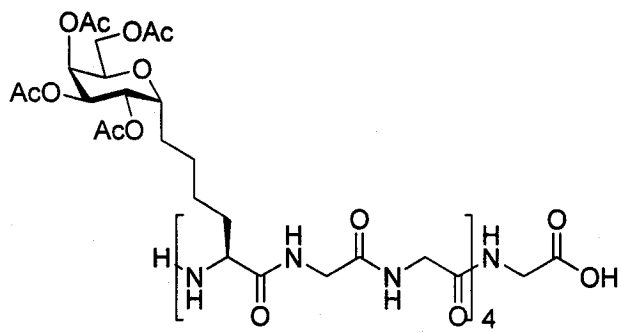

115

Compound 115

Prepared using procedure A. 63.5 mg (38.1 μmol) Fmoc-Gly-Wang resin (loading capacities: 0.6 mmol/g) was used to assemble **115**. For the coupling reaction performed with Fmoc-Gly-OH, a premixed solution of 34.0 mg (114 μmol) Fmoc-Gly-OH, 43.4 mg (114 μmol) HBTU and 20 μL (114 μmol) DIPEA was added to the solid-phase synthesizer. For the coupling reaction performed with building blocks **64**, a premixed solution of 33.9 mg (49.6 μmol) **64**, 18.8 mg (49.6 μmol) HBTU and 8.7 μL (49.6 μmol) DIPEA in DMF was added to the solid-phase

synthesizer. The whole SPPS process took about 10 days and 63.8 mg (73%) polypeptide **115** was precipitated from Et_2O and collected as a white solid.

^{1}H NMR (300 MHz, CD_3OD) δ 5.41-5.37 (br, 1H), 5.30-5.15 (br, m, 2H), 4.35-3.75 (br, m, 11H), 2.11 (s, 3H), 2.06 (s, 3H), 2.03 (s, 3H), 1.99 (s, 3H), 1.90-1.62 (br, 3H), 1.58-1.30 (br, 5H).

^{13}C NMR (75 MHz, CD_3OD) δ 172.3, 171.9, 171.6, 69.8, 69.43, 69.38, 69.2, 69.1, 62.81, 62.78, 43.4, 32.3, 26.28, 26.25, 26.1, 20.9, 20.8, 20.7, 20.6.

MS (MALDI): Calcd for $C_{98}H_{145}N_{13}O_{50}$ M^+ 2303.92, found 2303.92.

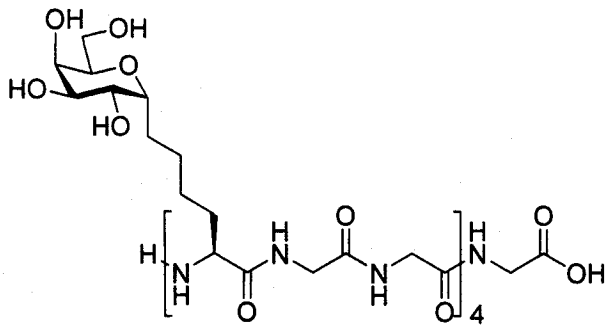

59

Compound 59

18.7 mg (8.1 μmol) glycopeptide **115** was dissolved in a premixed solution of sodium in MeOH (pH = 10) and stirred overnight. Amberlite® IR-120H ion-exchange resin was added to neutralize the reaction mixture. The resin was filtered through a plug of cotton and the solvent was removed under reduced pressure. The product was dissolved in water and lyophilized to afford 13.2 mg (100%) white powder. Analytically pure polypeptide was further purified by RP-HPLC with a gradient of 0-60% CH_3CN in H_2O (0.1% TFA) over 50 mins.

^{1}H NMR (500 MHz, D_2O) δ 4.37-4.25 (br, m, 1H), 4.10-3.85 (br, m, 8H), 3.78-3.65 (br, m, 4H), 1.95-1.65 (br, m, 3H), 1.56-1.25 (br, m, 5H).

^{13}C NMR (75 MHz, D_2O) δ 175.4, 172.3, 172.1, 75.6, 71.8, 70.0, 69.4, 68.7, 61.5, 54.4, 53.5, 42.9, 42.6, 41.5, 31.0, 30.5, 25.0, 24.5, 23.5.

MS (MALDI): Calcd for $C_{66}H_{113}N_{13}O_{34}$ M^+ 1631.75, found 1631.23.

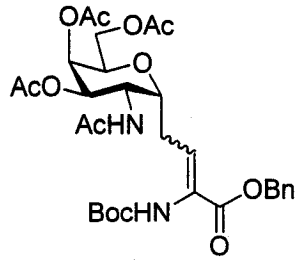

123

Preparation of benzyl 4-(2-(*N*-acetylamino)-3,4,6-Tri-*O*-acetyl-2-deoxy-*α*-D-galactopyranosyl)-2-ene-2-(*N*-*t*-butyloxycarbonyl)butenoate (123)

This compound was prepared according to the previously published procedure.[4a] To a solution of 330 mg (0.82 mmol) benzyl 2-(*tert*-butoxycarbonyl)-2-(diethoxyphosphoryl)acetate **107** in 3 ml dry THF at -78 °C, was added 0.1 ml (0.8 mmol) TMG. The solution was stirred for 10 mins at –78 °C, at which point a solution of 288 mg (0.77 mmol) 2-(2-(*N*-acetylamino)-3,4,6-tri-*O*-acetyl-2-deoxy-*α*-D-galactopyranosyl)-acetaldehyde **122** in 3 ml dry CH_2Cl_2 was added. The reaction was stirred at room temperature for 1 hr. EtOAc was added to the reaction followed by washing with 1M HCl and saturated $NaHCO_3$ successively. The organic layer was dried with $MgSO_4$ and after filtration the solvent was removed under reduced pressure. The crude product was purified by flash chromatography (silica, 2:1 to 1:3 Hexane:EtOAc) to isolate 383 mg of foam (80%).

IR (neat) 3294, 2978, 1740, 1713, 1659, 1533, 1497, 1367, 1225 cm^{-1}.

^{1}H NMR (300 MHz, $CDCl_3$) δ 7.37-7.31 (br, 5H), 6.80-6.68 (br, 1H), 6.63 (dd, J = 9 Hz, 5.2 Hz, 1H), 6.17 (s, 1H), 5.35 (t, J = 3 Hz, 1H), 5.20 (d, J = 1.5 Hz, 2H), 5.14 (dd, J = 10.5 Hz, 3.4 Hz, 1H), 4.66-4.53 (br, m, 1H), 4.42 (dd, J = 13.7 Hz, 6 Hz, 1H), 4.20-4.08 (br, 1H), 4.03 (dd, J = 15.9 Hz, 5.1 Hz, 2H), 2.92-2.72 (br, 1H), 2.41 (td, J = 15.2 Hz, 5 Hz, 1H), 2.11 (s, 3H), 2.00 (s, 3H), 1.97 (s, 3H), 1.80 (s, 3H), 1.46 (s, 9H).

^{13}C NMR (75 MHz, $CDCl_3$) δ 170.7, 170.6, 170.4, 164.4, 154.3, 135.3, 128.8, 128.7, 128.6, 128.4, 81.5, 69.0, 68.1, 68.0, 67.4, 66.9, 61.9, 47.8, 28.2, 25.6, 22.9, 20.8, 20.7.

MS (ESI): Calcd for $C_{30}H_{40}N_2O_{12}$ $(M+H)^+$ 621.3, found 621.1.

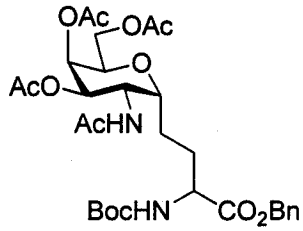

124

Preparation of benzyl (2*S*)-4-(2-(*N*-acetylamino)-3,4,6-Tri-*O*-acetyl-2-deoxy-*α*-D-galactopyranosyl)-2-(*N*-*t*-butyloxycarbonyl)butanoate (124)

In a glove box, 340 mg (0.55 mmol) benzyl 4-(2-(*N*-acetylamino)-3,4,6-Tri-*O*-acetyl-2-deoxy-*α*-D-galactopyranosyl)-2-ene-2-(*N*-*t*-butyloxycarbonyl)butenoate **123** and 8 mg (0.012 mmol) [(COD)Rh-((*S*, *S*)-Et-DuPHOS)]$^+$OTf$^-$ **110** were dissolved in 15 ml degassed dry THF (freeze-dry-thaw for three cycles). After the reaction mixture was purged with H_2 (about 500 psi) for five cycles, the reaction was pressurized with 100 psi H_2. After stirring at room temperature for two days, the pressure was released. The reaction was filtered through a plug of silica gel and concentrated under reduced pressure to afford 341 mg of foam (100% yield, 71% de). Diastereomeric excess was estimated based on the integration of Boc protons in ^{1}H NMR.

^{1}H NMR (500 MHz, DMSO-D_6) δ 8.08 (d, J = 8Hz, 1H), 7.38-7.31 (m, 5H), 5.25 (dd, J = 3.1 Hz, 1.8 Hz, 1H), 5.11 (dd, J = 34.7 Hz, 12.6 Hz, 2H), 4.99 (dd, J = 11.2 Hz, 3.3 Hz, 1H), 4.24 (ddd, J = 13.3 Hz, 8.1 Hz, 5.7 Hz, 1H), 4.09-4.01 (m, 2H), 3.99 (t, J = 5.3 Hz, 2H), 3.89 (ddd, J = 11.1 Hz, 5 Hz, 3 Hz, 1H), 2.07 (s, 3H), 1.921 (s, 3H), 1.918 (s, 3H), 1.88-1.80 (br, m, 1H), 1.79 (s, 3H), 1.76-1.72 (br, m, 1H), 1.53-1.40 (br, m, 2H), 1.38 (s, 7.6H, *S*-diastereomer), 1.26 (s, 1.3 H, *R*-diastereomer).

^{13}C NMR (75 MHz, $CDCl_3$) δ 172.4, 171.0, 170.8, 170.3, 155.6, 135.5, 128.9, 128.8, 128.7, 80.3, 76.8, 68.3, 67.4, 67.0, 61.6, 60.6, 53.6, 49.0, 29.4, 28.5, 23.4, 21.1, 20.9.

MS (ESI): Calcd for $C_{30}H_{42}N_2O_{12}$ $(M+H)^+$ 623.3, found 623.1.

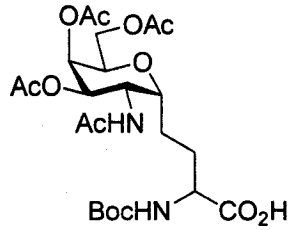

125

Preparation of (2*S*)-4-(2-(*N*-acetylamino)-3,4,6-Tri-*O*-acetyl-2-deoxy-*α*-D-galactopyranosyl)-2-(*N*-*t*-butyloxycarbonyl)butanoic acid (125)

To a solution of 732 mg (1.18 mmol) benzyl (2*S*)-4-(2-(*N*-acetylamino)-3,4,6-Tri-*O*-acetyl-2-deoxy-*α*-D-galactopyranosyl)-2-(*N*-*t*-butyloxycarbonyl)butanoate **124** in 50 mL MeOH was added 610 mg of 10% Pd/C. The reaction flask was filled with H_2 after three vacuum/H_2 cycles. After stirring at room temperature overnight, the catalyst was filtered through a plug of silica gel. The filtrate was concentrated under reduced pressure to afford 607.9 mg (97%) of white solid.

IR (neat) 3331, 3018, 2980, 2935, 1736, 1709, 1663, 1520, 1367, 1217 cm^{-1}.

^{1}H NMR (300 MHz, $CDCl_3$) δ 6.58 (t, J = 8.5 Hz, 1H), 6.31 (d, J = 8.3 Hz, 1H), 5.41 (d, J = 8.3 Hz, 1H), 5.32 (t, J = 2.8 Hz, 1H), 5.13 (dd, J = 9.6 Hz, 3.2 Hz, 1H), 4.56-4.41 (br, 1H), 4.33-3.99 (br, m, 5H), 2.11 (s, 3H), 2.05 (s, 6H), 1.99 (s, 3H), 1.90-1.60 (br, m, 3H), 1.60-1.50 (br, m, 1H), 1.43 (s, 9H).

^{13}C NMR (75 MHz, $CDCl_3$) δ 175.2, 171.4, 171.2, 170.6, 155.9, 80.4, 77.4, 68.4, 67.2, 62.0, 53.7, 53.5, 48.7, 29.1, 28.5, 28.4, 23.2, 21.2, 21.0, 20.9.

MS (ESI): Calcd for $C_{23}H_{36}N_2O_{12}$ $(M+H)^+$ 533.2, found 533.0; Calcd for $C_{23}H_{35}N_2O_{12}Na$ $(M+Na)^+$ 555.2, found 555.1.

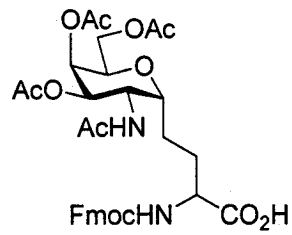

65

Preparation of (2*S*)-4-(2-(*N*-acetylamino)-3,4,6-Tri-*O*-acetyl-2-deoxy-α-D-galactopyranosyl)-2-(*N*-9-fluorenylmethyloxycarbonyl)butanoic acid (65)

To an ice-cooled solution of 100 mg (0.187 mmol) (2*S*)-4-(2-(*N*-acetylamino)-3,4,6-Tri-*O*-acetyl-2-deoxy-α-D-galactopyranosyl)-2-(*N*-*t*-butyloxycarbonyl)butanoic acid **125** in 8 mL dry CH_2Cl_2 was added dropwise 4 mL TFA. The reaction was stirred at 0 °C for 1.5 hrs. The solvent was removed under reduced pressure to give a viscous oil. 8 mL 10% $NaHCO_3$, and 3 mL 1,4-dioxane were added to dissolve the oil and the reaction was cooled to 0 °C. To the resulting solution, a second solution of 70 mg (0.21 mmol) *N*-(9-fluorenylmethoxycarbonyloxy)-succinimide in 3 mL 1,4-dioxane was added slowly through a cannula under argon atmosphere. The reaction was allowed to stir at 0 °C for 1 hr, then at room temperature overnight. Water was added to dilute the reaction, followed by washing with Et_2O. After being acidified to pH 2 with 2N HCl, the aqueous layer was extracted with EtOAc three times. The combined EtOAc layers were dried with $MgSO_4$. After filtration, the solvent was removed under reduced pressure. The crude product was purified by flash chromatography (silica, 0-9% MeOH in CH_2Cl_2) to isolate 66 mg (53%) of white foam.

IR (neat) 3356, 3018, 1740, 1709, 1647, 1533, 1450, 1369, 1215 cm^{-1}.

^{1}H NMR (300 MHz, DMSO-d6) δ 7.83 (dd, *J* = 15 Hz, 9 Hz, 4H), 7.37 (dt, *J* = 21 Hz, 6 Hz, 4H), 6.22 (s, 2H), 5.31 (s, 1H), 5.05 (d, *J* = 9 Hz, 1H), 4.38-4.22 (br, 2H), 4.20-3.90 (br, m, 5H), 2.06 (s, 3H), 2.01 (s, 3H), 1.96 (s, 3H), 1.85 (s, 3H).

^{13}C NMR (75 MHz, $CDCl_3$) δ 171.1, 170.5, 156.9, 143.9, 141.4, 127.9, 127.3, 125.2, 120.2, 77.4, 68.5, 67.3, 61.7, 55.3, 53.6, 50.8, 48.5, 47.1, 29.9, 23.0, 21.0, 20.8.

MS (ESI): Calcd for $C_{33}H_{38}N_2O_{12}$ $(M+H)^+$ 655.2, found 655.1. Calcd for $C_{33}H_{37}N_2O_{12}K$ $(M+K)^+$ 693.2, found 693.2.

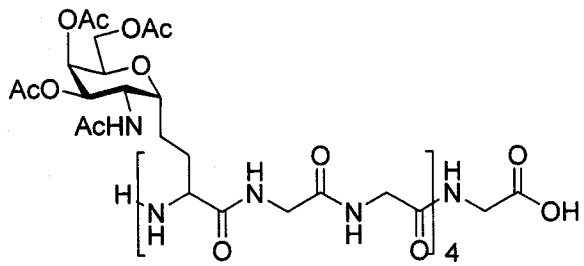

126

Compound 126

Prepared using procedure A. 58.5 mg (38.0 μmol) Fmoc-Gly-Wang resin (loading capacities: 0.65 mmol/g) was used to assemble **126**. For the coupling reaction performed with Fmoc-Gly-OH, a premixed solution of 34.0 mg (114 μmol) Fmoc-Gly-OH, 43.3 mg (114 μmol) HBTU and 0.02 mL (114 μmol) DIPEA was added to the solid-phase synthesizer. For the coupling reaction performed with building blocks **65**, a premixed solution of 32.5 mg (49.6 μmol) **65**, 18.8 mg (49.6 μmol) HBTU and 8.7 μL (49.6 μmol) DIPEA in DMF was added to the solid-phase synthesizer. The whole SPPS process took about 10 days and 66 mg (79%) polypeptide **126** was precipitated from Et_2O and collected as a white solid.

^{1}H NMR (300 MHz, CD_3OD) δ 5.41 (d, J = 5.1 Hz, 1H), 5.12 (td, J = 9.6 Hz, 2.7 Hz, 1H), 4.52-4.38 (br, m, 1H), 4.26-4.05 (br, m, 4H), 4.03-3.75 (br, m, 5H), 2.11 (s, 3H), 2.04 (s, 3H), 2.01-1.95 (m, 6H), 1.92-1.73 (br, m, 2H), 1.72-1.45 (br, m, 2H).

^{13}C NMR (75 MHz, CD_3OD) δ 175.4, 174.9, 173.7, 173.6, 172.9, 172.8, 172.5, 172.2, 172.1, 172.0, 171.9, 171.6, 171.0, 69.5, 69.0, 68.7, 68.3, 63.2, 62.6, 55.7, 55.3, 54.2, 44.2, 43.7, 43.3, 41.8, 29.0, 23.2, 22.8, 22.7, 20.9, 20.6.

MS (ESI): Calcd for $C_{90}H_{133}N_{17}O_{46}$ $(M+H)^+$ 2188.9, found 2189.3.

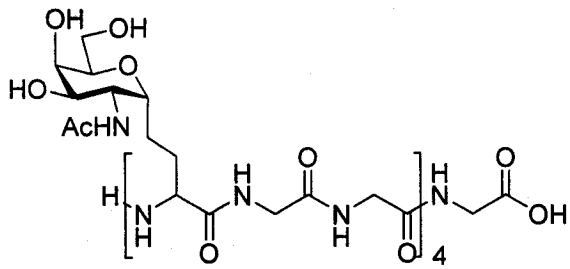

60

Compound 60

17.9 mg (8.2 μmol) glycopeptide **126** was dissolved in a premixed solution of sodium in MeOH (pH = 10) and stirred overnight. Amberlite® IR-120H ion-exchange resin was added to neutralize the reaction mixture. The resin was filtered through a plug of cotton and the solvent was removed under reduced pressure. The product was dissolved in water and lyophilized to

afford 11.7 mg (85%) white powder. Analytically pure polypeptide was further purified by RP-HPLC with a gradient of 0-60% CH_3CN in H_2O (0.1% TFA) over 50 mins.

^{1}H NMR (300 MHz, D_2O) δ 4.35-4.25 (br, 1H), 4.22-4.13 (br, m, 1H), 4.10-3.80 (br, m, 10H), 3.71-3.65 (br, 4H), 1.99 (s, 4H), 1.88-1.60 (br, m, 3H), 1.56-1.42 (br, m, 1H).

^{13}C NMR (75 MHz, D_2O) δ 181.8, 176.8, 174.8, 172.1, 172.0, 171.9, 171.7, 171.4, 171.1, 73.7, 72.1, 69.3, 68.8, 68.2, 67.5, 61.7, 54.3, 50.1, 43.5, 42.7, 27.6, 24.1, 23.7, 23.6, 23.4, 23.0, 22.9, 22.2, 21.7, 21.2.

MS (ESI): Calcd for $C_{66}H_{109}N_{17}O_{34}$ $(M+H)^+$ 1684.7, found 1685.1.

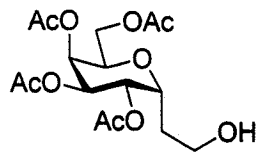

129

Preparation of 2,3,4,6-tetra-*O*-acetyl-1-2-hydroxyethyl-*α*-D-galactopyranoside (129)

A solution of 0.5 g (1.34 mmol) 2,3,4,6-tetra-*O*-acetyl-1-allyl-*α*-D-galactopyranoside **84** in 10 mL MeOH and 50 mL CH_2Cl_2 was treated with O_3 at -78 °C until the solution turned dark blue, and then N_2 was added to remove the excess O_3 from solution. 0.31 g (8.2 mmol) $NaBH_4$ was added and the reaction was stirred for 2 hrs. 2 M HCl was added to quench the reaction. The organic layer was separated and the aqueous layer was extracted with EtOAc. All organic layers were combined and washed with 2 M HCl and brine. The solvent was removed under reduced pressure to give a white solid. Further purification using flash chromatography (silica, 1:1 EtOAc:CH_2Cl_2) produced a light yellow viscous liquid (0.32 g, 63%).

IR (neat) 3522, 3022, 1740, 1369, 1213 cm^{-1}.

^{1}H NMR (300 MHz, $CDCl_3$) δ 5.38 (t, J = 3.0 Hz, 1H), 5.18 (t, J = 2.6 Hz, 2H), 4.37 (dd, J = 10.9 Hz, 8.6 Hz, 1H), 4.18-4.10 (m, 1H), 4.03 (dd, J = 11.4 Hz, 4.2 Hz, 1H), 3.68 (t, J = 5.1 Hz, 2H), 3.16 (br, s, 1H), 2.09 (s, 3H), 2.06 (s, 3H), 2.04 (s, 3H), 2.01 (s, 3H), 1.96-1.82 (br, m, 1H), 1.70-1.59 (br, m, 1H).

^{13}C NMR (75 MHz, $CDCl_3$) δ 170.7, 170.0, 169.8, 69.3, 68.6, 68.3, 67.8, 67.5, 61.4, 58.7, 28.7, 20.5, 20.4.

MS (ESI): Calcd for $C_{16}H_{24}O_{10}Na$ $(M+Na)^+$ 399.1, found 399.6; Calcd for $C_{16}H_{24}O_{10}$ M^+ 376.1, found 376.5.

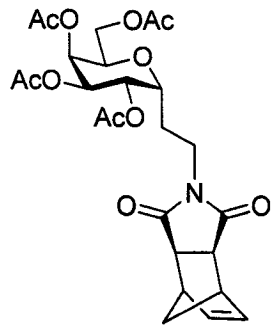

130

Preparation of 4-[2,3,4,6-tetra-*O*-acetyl-1-ethyl-*α*-D-galactopyranoside]-*exo*-4-aza-tricyclo[5.2.1.0^{2,6}]dec-8-ene-3,5-dione (130)

This compound was prepared according to the previously published procedure.[5] 141.4 mg (377 μmol) 2,3,4,6-tetra-*O*-acetyl-1-2-hydroxyethyl-*α*-D-galactopyranoside **129**, 86.9 mg (532 μmol) *exo*-bicyclo[2.2.1]hept-5-ene-2,3-dicarboximide **128** and 116.5 mg (443.8 μmol) PPh_3 were dissolved in 2.4 mL THF. To this solution, 70.3 μL (444 μmol) diethyl azodicarboxylate was added dropwise under slow N_2 flow environment. After 6 hrs, the reaction mixture was put under N_2. A yellow viscous syrup remained after the solvent was removed. Further purification using flash chromatography (silica, 3:2 Hexane:EtOAc) yielded product **130** as a viscous liquid (134 mg, 68%).

IR (neat) 3065, 2984, 2957, 1744, 1693, 1439, 1400, 1369, 1327, 1213 cm^{-1}.

^{1}H NMR (300 MHz, $CDCl_3$) δ 6.24 (t, J = 1.6 Hz, 2H), 5.34 (dd, J = 2.9 Hz, 1.7 Hz, 1H), 5.23 (dd, J = 9.4 Hz, 5.2 Hz, 1H), 5.08 (dd, J = 9.4 Hz, 3.3 Hz, 1H), 4.20-4.01 (br, m, 4H), 3.59-3.38 (m, 2H), 3.23 (d, J = 1.3 Hz, 2H), 2.64 (d, J = 0.9 Hz, 2H), 2.06 (s, 3H), 2.01 (s, 3H), 2.00 (s, 3H), 1.96 (s, 3H), 1.90-1.78 (m, 1H), 1.73-1.62 (m, 1H), 1.49 (dt, J = 9.8 Hz, 1.3 Hz, 1H), 1.15 (d, J = 9.8 Hz, 1H).

^{13}C NMR (75 MHz, $CDCl_3$) δ 178.0, 177.9, 170.7, 170.1, 170.0, 169.9, 137.9, 70.1, 68.5, 67.9, 67.8, 67.6, 61.5, 47.9, 45.2, 43.0, 35.1, 24.0, 20.9, 20.8.

MS (ESI): Calcd for $C_{25}H_{31}NO_{11}Na$ $(M+Na)^+$ 544.2, found 544.1.

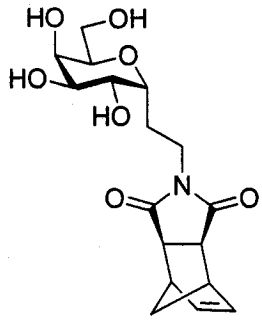

131

Preparation of 4-[1-ethyl-α-D-galactopyranoside]-*exo*-4-aza-tricyclo[5.2.1.0^{2,6}]dec-8-ene-3,5-dione (131)

A suspension of 67.5 mg (130 μmol) 4-[2,3,4,6-tetra-O-acetyl-1-ethyl-α-D-galactopyranoside]-*exo*-4-aza-tricyclo[5.2.1.0^{2,6}]dec-8-ene-3,5-dione **130** in 2.5 mL MeOH was treated with 0.325 mL of a 0.05 M NaOH in MeOH solution. The reaction mixture was stirred at room temperature for 3 hrs. Amberlite® IR-120H ion-exchange resin was added and the reaction was stirred until it was neutralized. The resin was filtered through glass wool and the filtrate was concentrated under reduced pressure. The crude product was purified with flash chromatography (silica, 5%-10% MeOH in $CHCl_3$) to produce a viscous gel (46 mg, 100%).

IR (neat) 3393, 3069, 2988, 2945, 1767, 1686, 1439, 1402, 1371, 1342, 1327, 1286, 1178 cm^{-1}.

^{1}H NMR (300 MHz, $CDCl_3$) δ 6.28 (s, 2H), 4.52-4.22 (br, 4H), 4.10-3.88 (br, 3H), 3.86-3.60 (br, 4H), 3.59-3.42 (br, 2H), 3.21 (s, 2H), 2.70 (s, 2H), 1.95-1.76 (br, 2H), 1.48 (d, J = 8.2 Hz, 1H), 1.19 (d, J = 8.2 Hz, 1H).

^{13}C NMR (75 MHz, CD_3OD) δ 179.0, 138.0, 77.4, 73.5, 71.8, 70.8, 69.4, 68.6, 61.8, 48.1, 45.3, 43.1, 36.0, 22.8.

MS (ESI): Calcd for $C_{17}H_{23}NO_7Na$ $(M+Na)^+$ 376.2, found 376.2.

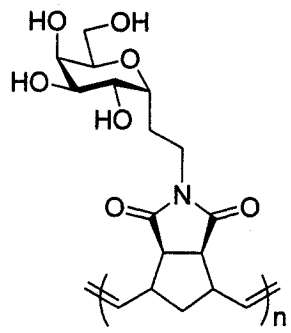

61

Preparation of neoglycopolymer 61

This compound was prepared according to the previously published procedure.[5] 93.2 mg (264 μmol) of 4-[1-ethyl-α-D-galactopyranoside]-*exo*-4-aza-tricyclo[5.2.1.$0^{2,6}$]dec-8-ene-3,5-dione **131** was dissolved in 308.2 μL MeOH and 80.6 μL H_2O. A second solution was prepared by dissolving 22 mg (29.4 μmol) first generation Grubbs' catalyst in 2 mL 1,2-dichloroethane. All the solutions were degassed using three freeze-pump-thaw cycles. The catalyst solution was then added to the monomer solution under argon atmosphere. An additional 1.65 mL MeOH and 550 μL H_2O were added. After the reaction was stirred for 2 hrs at room temperature, 3.66 mL ethyl vinyl ether was added and reaction was stirred at 45 °C for another 3 hrs. The solvent was removed under N_2. The crude product was washed with MeOH, dissolved in water, and filtered and the filtrate was dried with lyophilizer to afford a brown solid (68 mg, 73%). The longest polymer is composed of 15 monomers.

^{1}H NMR (360 MHz, D_2O) δ 7.46-7.20 (br, 1H), 5.90-5.32 (br, m, 2H), 4.12-3.98 (br, m, 1H), 3.98-3.85 (br, m, 2H), 3.82-3.61 (br, m, 4H), 3.59-3.33 (m, 3H), 3.23-2.95 (br, m, 2H), 2.78-2.20 (br, m, 2H), 2.01-1.72 (br, m, 2H), 1.52-1.02 (br, m, 2H).

^{13}C NMR (75 MHz, D_2O) δ 181.1, 132.7, 90.0, 73.7, 72.4, 70.1, 69.2, 68.2, 64.8, 61.5, 57.8, 55.6, 55.3, 55.2, 52.5, 51.4, 51.0, 49.2, 45.7, 36.3, 26.4, 23.4, 22.4, 19.4, 17.1, 14.6.

6.2 Methods for Assessing Antifreeze Activities and Solution Conformation of *C*-Linked AFGP Analogues

6.2.1 Assessing Thermal Hysteresis (TH) and Dynamic Ice-Shaping (DIS) Activities

TH and DIS activities of *C*-linked AFGP analogues **57-61** were studied using a Clifton nanoliter osmometer (Clifton Technical Physics). The analogue being tested was dissolved in distilled water to get a 10 mg/mL solution. Then, a drop (sub-microliter) of solution was introduced into an oil (microscope immersion oil)-filled cylindrical well on an aluminum plate. The solution was flash frozen at -40 °C and then nucleated by slow warming to acquire a stable single ice crystal. The melting and freezing points of the solution were determined by changing the temperature of the system at a constant rate of 10 mOsmol (0.0186 °C) per 15 seconds.

6.2.2 Assessing Recrystallization Inhibition (RI) Activity

The RI activities of *C*-linked AFGP analogues **57-61** were measured using a recrystallization inhibition assay developed by Myers and Horwath.[6] A 10 μL analogue solution in PBS was dropped from a height of three meters through a shielding tube to a polished aluminum block, which was pre-cooled to -80 °C on dry ice. The "splat cooling" of the analogue solution produced an ice wafer with about 1 cm in diameter and 20 μm in thickness. The wafer was then quickly moved onto a microscope cover glass and transferred into a cold chamber, which was dried with continuous air flow to avoid moisture condensing on the ice wafer. The sample was annealed at -6 °C for 30 minutes before the size of the ice grains was photographed using a microscope equipped with an LMPlanF1 20x/0.40 objective. The temperature of the cold chamber was controlled by a Series 800 temperature controller (Alpha Omega Instruments). For each sample, six photographs were taken from different areas of the ice wafer. The size of ice grains was calculated by taking the average surface area of the ten largest ice grains in each photograph (the method employed to calculate the surface area of each ice grain was discussed in detail in section 4.2).

6.2.3 Assessing Solution Conformation

The solution conformations of *C*-linked AFGP analogues **57-60** and AFGP8 were studied by Circular dichroism (CD) spectroscopy. The sample to be tested was prepared in distilled de-ionized water and held in a quartz cuvette (1 cm path length). The CD spectra were recorded from 260 nm to 190 nm on a Jasco J-810 spectropolarimeter at 25 °C. The CD spectrum of distilled de-ionized water was used as a blank and subtracted from each testing sample.

6.3 Methods and Materials for Assessing *In Vitro* Cytotoxicity and Interactions of AFGP8 and *C*-Linked AFGP Analogues

6.3.1 Cell Culture

WRL 68 human embryonic liver cells (ATCC, CL-48) and HEK 293 human embryonic kidney cells (ATCC, CRL-1573) were cultured in Eagle's Minimum Essential Media (MEM) (ATCC, 30-2003) supplemented with 10% fetal bovine serum (FBS) (ATCC, 30-2020) and 1% penicillin-streptomycin (GIBCO, 15140). Cells were incubated in a 37 °C incubator supplied with 5% CO_2. Passage 85 to 87 of WRL 68 cells and passage 34 of HEK 293 cells were used in our study.

Rainbow trout gill epithelial cells (Rtgill-W1) (ATCC, CRL-2523) were cultured in Leibovitz's L-15 Medium (LLM) (ATCC, 30-2008) supplemented with 10% FBS and 1% penicillin-streptomycin. Cells were incubated in a 19 °C incubator. All cells were trypsinized with trypsin-EDTA solution (0.25% trypsin, 1mM EDTA·4Na) (GIBCO, 25200) and incubated in half area 96 well plates with density of around $5X10^3$ cells/well until they reached 100 % confluence for experiments.

6.3.2 MTT Assay

The MTT assay kit was purchased from Sigma (TOX-1) and the *in vitro* toxicology assay was performed according to the product information sheet.[7] All experiments were repeated three

times and 12 parallel wells were used for each condition. For the MTT assay performed at physiological temperatures, cells were treated with different concentrations of AFGP8 (isolated from the Greenland cod, *Gagnus ogac*, A/F Protein Inc.) or *C*-linked AFGP analogues in culture media and incubated for 18-24 hours before MTT assays were performed. For the MTT assay performed at subzero temperatures, University of Wisconsin (UW) solution (ViaSpan, DuPont Pharmaceuticals) was used to replace culture media for cell incubations.

After incubating cells with AFGP8 or *C*-linked AFGP analogues, plates were centrifuged at 1500 rpm for three minutes before the culture medium or UW solution was replaced with 50 μL MTT (sigma, M5655) solution (5 mg/mL) in Hank's Balanced Salt Solution (HBSS, Invitrogen). Then, plates were incubated at 37 °C with 5% CO_2 for two to four hours. To each well was added with another 50 μL MTT solubilization solution (10% Triton X-100 plus 0.1 N HCl in isopropanol) and each well was aspirated until all the formazan precipitates were dissolved. The absorbance of each well was read at a wavelength of 570 nm with a multiwell plate reader (AD 340C Absorbance Detector, Beckman Coulter, Inc.).

6.3.3 Caspase-3/7 Assay

The Caspase-3/7 assay kit, APO-ONE^{TM} homogeneous Caspase-3/7 assay kit, was purchased from Promega (G7790) and the assay was performed according to the product protocol.[8] For assay performed with AFGP8, 5 parallel repeats were used for each condition. For assay performed with analogue **42**, 16 parallel repeats were used for each condition. For assay performed with analogue **57**, 16 parallel repeats were used for both negative and positive controls, and 6 parallel repeats were used for cells incubated with analogue **57**. The assay was performed in black 96-well plates (Nunclon Δ Surface, Nalge Nunc International) to reduce the loss of fluorescence. After cells grew to 100% confluence, the culture medium was replaced with new medium with different treatments. 2% DMSO (Sigma) was used to improve the solubility of staurosporine in the culture medium and added in all treatments. In the negative control, no additional compounds were added into the cell culture. The positive control consisted of 20 μM staurosporine (Sigma, from *Streptomyces sp.*, S4400). The experimental treatment consisted of 5 mg/mL AFGP8 or *C*-linked AFGP analogues **42** or **57**. After incubating cells at 37 °C with 5%

CO_2 for 20 hours, Caspase substrate was added into each well and the plate was incubated at room temperature on a plate shaker (200 rpm). The level of generated fluorescence was read at 4, 6, 10, 24 and 48 hours using a Spectra MAX GeminiXS fluorescence plate reader (Molecular Device) with excitation at 499 nm and emission at 521 nm.

6.3.4 Fluorescence (Vybrant®) Apoptosis Assay

This study was performed using the Vybrant® apoptosis assay kit # 7 (Molecular Probes, V-23201) and followed the product information.[9] WRL 68 cells were cultured in a 35 mm petridish (10 mm microwell, MatTek) at 37 °C with 5% CO_2. After cells grew to 50% confluence, the culture medium was replaced by new medium with different treatments. In the negative control, no additional compounds were added into the cell culture. The positive control consisted of 20 μM staurosporine (Sigma, from *Streptomyces sp.*, S4400). The experimental treatment consisted of 5 mg/mL AFGP8. After additional 4 hours incubation, all solutions were removed from the petridish and cells were washed with PBS three times. Then, a solution containing 8.1 μM Hoechst 33324, 0.1 μM YO-PRO-1 and 1.5 μM Propidium iodide in PBS was added into the petridish and cells were incubated at 0 °C for 30 minutes. The excess stain solution was removed from the petridish and cells were washed with PBS three times.

All studies involving confocal microscopy (including the fluorescence apoptosis study, internalization study and intercellular pathway study of glycopeptides) were performed with a Zeiss LSM 410 (Carl Zeiss, Thornwood, NY) inverted laser scanning microscope, equipped with a Krypton/Argon ion laser and Plan-Apochromat 63x, 1.4 NA objective. The pinhole was set to achieve a full width half-maximum z resolution of 1 μm. Images were 512 X 512 eight-bit gray scale pixels.

The Propidium iodide and YO-PRO-1 were excited using the 488 nm lines of a Krypton/Argon laser and the Hoechst dye was excited with the laser set at 760 nm using the Verdi 10W and Mira-900 combination (Coherent) for multiple photon absorption. Emission of Propidium iodide was detected at 590 nm using a Longpass filter. Emission of YO-PRO-1 was detected between 515-540 nm using a Bandpass filter. Emission of Hoechst was detected at 460 nm using a non-descanned detector and a Bandpass detector.

6.3.5 Fluorescence Labeling of Glycopeptides

AFGP 8 and *C*-linked AFGP analogues **42** and **57** were labeled with FluoReporter® Oregon Green® 488 protein labeling kit (Molecular Probes, F-6153). The labeling reaction was performed according to the product information.[10] In a reaction tube, 200 μL of 7.5 mg/mL glycopeptide solution in distilled water was mixed with 20 μL 1 M sodium bicarbonate solution (pH = 8.3). A second solution of 10 mg/mL reactive Oregon Green 488 dye (5 equivalents) in DMSO was added into the reaction tube. The reaction was protected from light and stirred at room temperature for 1 hour.

The labeled glycopeptide was purified using the D-Salt™ Polyacrylamide 1800 Desalting Column (Pierce, 43426) with sterile PBS as the mobile phase. Concentrations of the fractions containing fluorescence-labeled glycopeptide solution were measured using an Ultrospec 2100 pro UV/visible spectrophotometer (Biochrom).

6.3.6 Internalization Assay of Glycopeptides

WRL 68 cells (human liver) and Rtgill-W1 (fish gill epithelial) cells were all cultured in a 35 mm petridish (10 mm microwell, MatTek). For the internalization study performed at the cells' physiological temperatures, cultures were performed at 37 °C with 5% CO_2 for WRL68 cells and 19 °C without supplement of CO_2 for Rtgill-W1 cells. After cells grew to 50% confluence, the culture medium was replaced with a new medium solution containing 1.5 mg/mL Oregon Green 488-labelled glycopeptides and 10 μM membrane probe RH-237 (Molecular Probes, S-1109). Cells were further incubated for variant time ranging from 10 to 50 minutes at their physiological temperatures. Then, all solutions were removed from the petridish and cells were washed with HBSS or PBS three times to remove the excess dye solution. Cells were imaged using the 488 nm wavelength line attenuated by 97% with a neutral density filter. Oregon Green 488 was detected on a PMT using a Bandpass filter with wavelengths of 515-540 nm. RH-237 was detected on a second PMT using a Bandpass filter with wavelengths of 670-810 nm.

When studying the effect of cell membrane receptors on the glycopeptide internalization, cells were incubated with 0.5 mg/mL proteinase K (Roche) in PBS solution (pH 7.95) for 1 hour before being stained by fluorescence-labeled AFGP8.

The internalization study performed at 0 °C employed the same procedure as that at the physiological temperatures with the exception that all cells were incubated on ice.

6.3.7 Intracellular Pathway of Glycopeptides

WRL 68 cells were cultured in a 35 mm petridish (10 mm microwell, MatTek) at 37 °C with 5% CO_2. After cells grew to 50% confluence, the culture medium was replaced with a new medium solution containing 1.5 mg/mL Oregon Green 488-labeled glycopeptides and 75 nM LysoTracker Red DND-99 (Molecular Probes) and further incubated for variant time ranging from 10 to 80 minutes at 37 °C. Then, all solutions were removed from the petridish and cells were washed with HBSS or PBS three times to remove the excess dye solution. Oregon Green 488 was detected on a PMT using a Bandpass filter with wavelengths of 515-540 nm and LysoTracker Red DND-99 was detected at 590 nm.

6.3.8 Student's t-test

Both MTT assay and caspases-3/7 assay results were analyzed using the "Student's t-test" to statistically evaluate whether a significant difference exists.[11] The standards used for student's t-test are two-tailed test and two-sample assuming equal variances. Significant difference is believed to exist between two groups of data when the calculated t value exceeds the tabulated value for P = 0.05 or the calculated P value is smaller than 0.05.

To compare the means of two treatments (with the number of replicates of n_1 and n_2), the student's t-test was performed as follows:

1. Calculate the mean ($\bar{x}_1$, $\bar{x}_2$) and variance (σ_1^2, σ_2^2) of each treatment.
2. Calculate the square root of the variance of the difference between two means.

$$\sigma_d = \sqrt{\frac{\sigma_1^2}{n_1} + \frac{\sigma_2^2}{n_2}}$$

3. Calculate t value.

$$t = \frac{\bar{x}_1 - \bar{x}_2}{\sigma_d}$$

4. Look up the tabulated t value at the degree of freedom of $(n_1 + n_2 - 2)$ and $P = 0.05$.

5. Compare the calculated t value with the tabulated t value. If the calculated value exceeds the tabulated value, there is significant difference between the two treatments with 95% confidence.

References

1. (a) Corey, E. J., Suggs, J. W. *Tetrahedron Lett.* **1975**, *31*, 2647-2650.
   (b) Perkins, M. V.; Sampson, R. A. *Org. Lett.* **2001**, *3*, 123-126.
2. Abad, A.; Agulló, C.; Cuñat, A. C.; García, A. B.; Giménez-Saiz, C. *Tetrahedron* **2003**, *59*, 9523-9536.
3. McGarvey, G. J.; Benedum, T. E.; Schmidtmann, F. W. *Org. Lett.* **2002**, *4*, 3591-3594.
4. (a) Debenham, S. D., Debenham, J. S., Burk, M. J., Toone, E. J. *J. Am. Chem. Soc.* **1997**, *119*, 9897-9898.
   (b) Schmidt, U.; Lieberknecht, A.; Schanbacher, U.; Benttler, T.; Wild, J. *Angew. Chem., Int. Ed. Engl.* **1982**, *21*, 776-777.
   (c) Schmidt, U.; Griesser, H.; Leitenberger, V.; Lieberknecht, A.; Mangold, R.; Meyer, R.; Riedl, B. *Synthesis* **1992**, 487-490.
5. Pohl, N. L., Kiessling, L. L. *Synthesis* **1999**, *SI*, 1515-1519.
6. (a) Myers, K. L. "Quantification of recrystallization inhibition: an assay for antifreeze protein activity" M.A. Thesis, Binghamton University (S. U. N. Y.) 1999.
   (b) Horwath, K. L., Easton, C. M., Poggioli Jr., G. J., Myers, K., Schnorr, L. *Eur. J. Entomol.* **1996**, *93*, 419-433.
7. Product information of *in vitro* toxicology assay kit, MTT based, Sigma (TOX-1). Available online: http://www.sigmaaldrich.com/sigma/datasheet/tox1dat.pdf.
8. Technical bulletin No. 295 for APO-ONE™ homogeneous Caspase-3/7 assay kit, Progema (G7790). Available online: http://www.promega.com/tbs/tb295/tb295.pdf.
9. Product information of Vybrant® apoptosis assay kit # 7, Molecular Probes (V-23201). Available online: http://probes.invitrogen.com/media/pis/mp23201.pdf.
10. Product information of FluoReporter® Oregon Green® 488 protein labeling kit, Molecular Probes (F-6153). Available online: http://probes.invitrogen.com/media/pis/mp06153.pdf.
11. Horgan, G. W. *J. Stat. Edu.* **1999**, *7*, n.1. Available online: http://www.amstat.org/publications/jse/secure/v7n1/horgan.cfm.

Claims to Original Research

1. Synthesized a series of novel *C*-linked galactosyl and GalNAc AFGP analogues using the Fmoc protocol of solid-phase peptide synthesis (SPPS). The building blocks for SPPS were prepared using either olefin cross-metathesis or asymmetric catalytic hydrogenation.
2. Evaluated the thermal hysteresis (TH), dynamic ice-shaping (DIS) and recrystallization inhibition (RI) activities of new *C*-linked AFGP analogues. Although most analogues displayed no TH and DIS activities, *C*-linked galactosyl serine AFGP analogue **57** demonstrated potent RI activity.
3. Studied the solution conformation of new *C*-linked AFGP analogues. These analogues did not show well-defined secondary structures, which indicated that the conformation of these analogues might not be the determining factor for RI activity.
4. Assessed the *in vitro* cytotoxicity of native AFGP8 and *C*-linked AFGP analogues. The results indicated that high concentration AFGP8 had significant toxic effects on human cell lines. In contrast, *C*-linked AFGP analogues **42** and **57** with the same concentration did not show any cytotoxicity.
5. Studied the mechanism of cell death caused by AFGP8 using a caspase-3/7 assay and a fluorescence apoptosis assay. The results indicated that AFGP8 activated caspase 3 and 7 in human embryonic liver cells and the resulting cell death might be via an apoptotic process. In contrast, *C*-linked AFGP analogues **42** and **57** appeared to be caspase inhibitors.
6. Studied the *in vitro* interactions of AFGP8 and *C*-linked AFGP analogues **42** and **57**. The study showed that all three glycopeptides were taken up by human embryonic liver cells at the physiological temperature and sequestered into lysosomes.

Publications

1. **Liu, S.**, Ben, R. N. *C*-linked galactosyl serine AFGP analogues as potent recrystallization inhibitors. *Org. Lett.* **2005**, *7*, 2385-2388.
2. **Liu, S.**, Wang, W., VonMoos, E., Jackman, J., Mealing, G., Monette, R., Ben, R. N. *In Vitro* Studies of Antifreeze Glycoprotein (AFGP) and a *C*-Linked AFGP Analogue. *Submitted in Mar. 2006.*

Conference Presentations

1. **Liu, S.**, Ben, R. N. *C*-Linked AFGP analogues – rationally designed recrystallization inhibitors. *228th ACS National Meeting*, Philadelphia, PA, Aug. 2004 (Oral presentation and SciMix poster)
2. **Liu, S.**, Ben, R. N. Preparation of *C*-linked AFGP analogues and antifreeze specific property study. *15th Quebe-Ontario Mini-symposium in Synthetic and Bioorganic Chemistry*, Ottawa, ON, Nov.2004 (poster)
3. **Liu, S.**, Wang, W., Jackman, J., VonMoos, E., Ben, R. N. An i*n vitro* cytotoxicity study of native antifreeze glycoprotein 8 and *C*-linked antifreeze glycoprotein analogues. *229th ACS National Meeting*, San Diego, CA, Mar. 2005 (Oral presentation)

Appendix

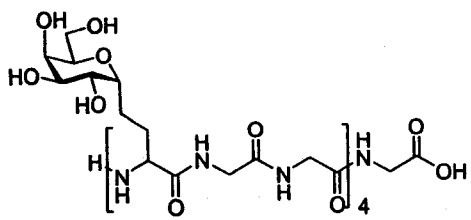

57

Current Data Parameters

NAME	rbs157
EXPNO	1
PROCNO	1

F2 - Acquisition Parameters

Date_	20060321
Time	10.44
INSTRUM	spect
PROBHD	5 mm QNP 1H/1
PULPROG	zg30
TD	30720
SOLVENT	CDCl3
NS	291
DS	0
SWH	5081.301 Hz
FIDRES	0.165407 Hz
AQ	3.0228980 sec
RG	512
DW	98.400 usec
DE	6.00 usec
TE	300.0 K
D1	1.00000000 sec

======== CHANNEL f1 ========

NUC1	1H
P1	10.00 usec
PL1	-3.00 dB
SFO1	300.1319477 MHz

F2 - Processing parameters

SI	65536
SF	300.1299688 MHz
WDW	EM
SSB	0
LB	0.10 Hz
GB	0
PC	1.00

1D NMR plot parameters

CX	20.00 cm
CY	1637.31 cm
F1P	10.000 ppm
F1	3001.30 Hz
F2P	-0.500 ppm
F2	-150.06 Hz
PPMCM	0.52500 ppm/cm
HZCM	157.56824 Hz/cm

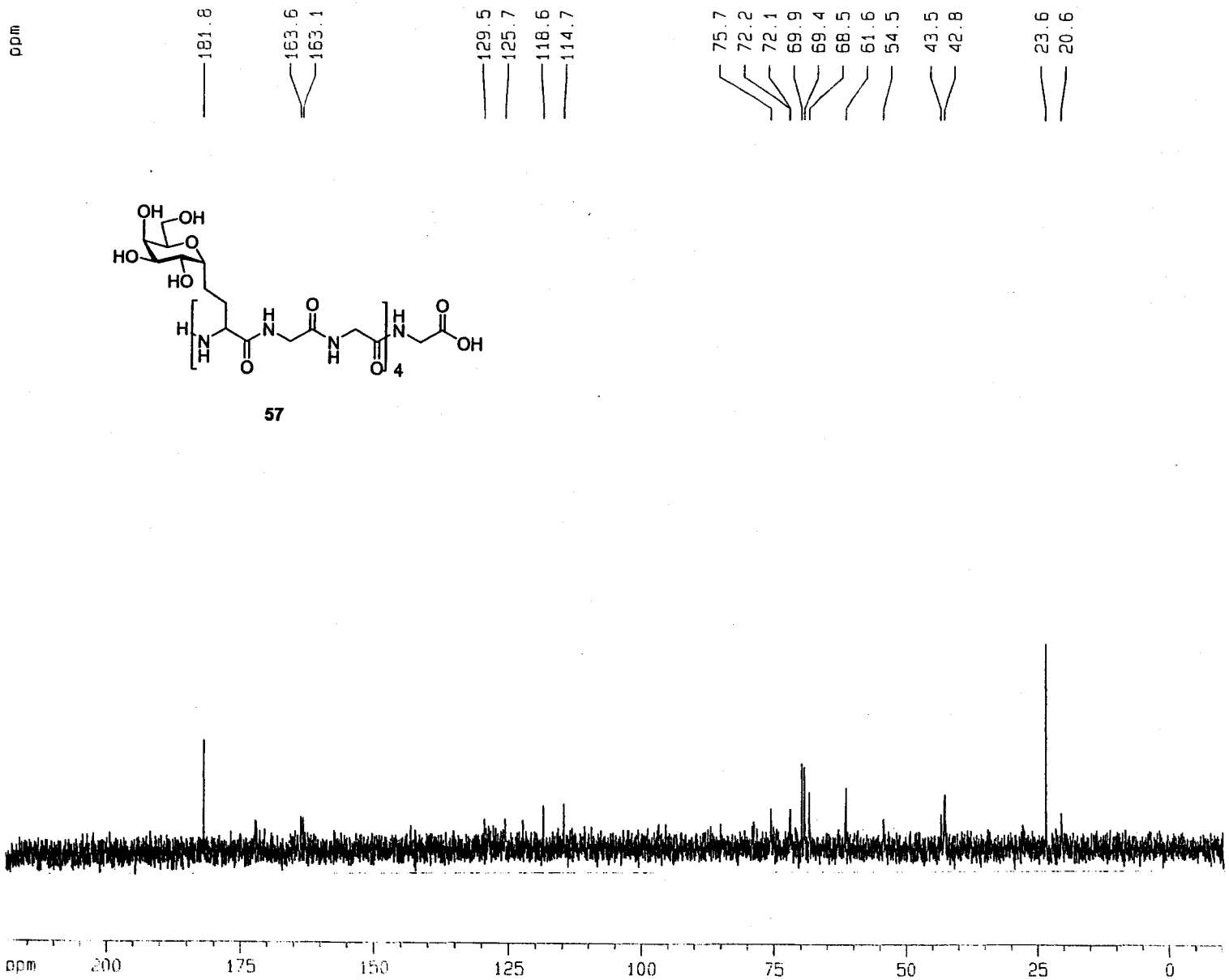

57

```
Current Data Parameters
NAME                  rbs11121041
EXPNO                           1
PROCNO                          1

F2 - Acquisition Parameters
Date_                    20041122
Time                         8.32
INSTRUM                     av300
PROBHD    5 mm QNP  1H/1
PULPROG                   zgpg30
TD                           32768
SOLVENT                     CDCl3
NS                           17731
DS                               0
SWH                    17985.611 Hz
FIDRES                  0.548877 Hz
AQ                      0.9110004 sec
RG                            3251
DW                          27.800 usec
DE                           6.00 usec
TE                          300.0 K
D1                      1.00000000 sec
D11                     0.03000000 sec
D12                     0.00002000 sec

============ CHANNEL f1 =============
NUC1                          13C
P1                           5.00 usec
PL1                         -6.00 dB
SFO1                   75.4752653 MHz

============ CHANNEL f2 =============
CPDPRG2                   waltz16
NUC2                          1H
PCPD2                       70.00 usec
PL2                         -3.00 dB
PL12                        13.48 dB
PL13                        15.63 dB
SFO2                  300.1314860 MHz

F2 - Processing parameters
SI                            65536
SF                     75.4677190 MHz
WDW                             EM
SSB                              0
LB                           1.00 Hz
GB                               0
PC                            1.40

1D NMR plot parameters
CX                           20.00 cm
CY                            7.98 cm
F1P                     220.000 ppm
F1                        16602.90 Hz
F2P                        -10.000 ppm
F2                         -754.68 Hz
PPMCM                   11.50000 ppm/cm
HZCM                   867.87878 Hz/cm
```

1H NMR

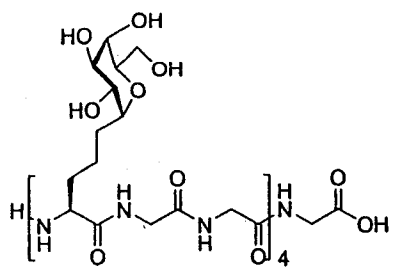

58

Current Data Parameters

NAME	rbs10106051
EXPNO	1
PROCNO	1

F2 - Acquisition Parameters

Date_	20050106
Time	13.56
INSTRUM	AV500WB
PROBHD	5 mm TBO BB/1H
PULPROG	zg30
TD	65536
SOLVENT	CDCl3
NS	870
DS	0
SWH	7440.476 Hz
FIDRES	0.113533 Hz
AQ	4.4040694 sec
RG	203.2
DW	67.200 usec
DE	6.00 usec
TE	300.0 K
D1	0.01000000 sec

======== CHANNEL f1 ========

NUC1	1H
P1	14.00 usec
PL1	0.00 dB
SFO1	500.1327766 MHz

F2 - Processing parameters

SI	65536
SF	500.1299512 MHz
WDW	EM
SSB	0
LB	0.00 Hz
GB	0
PC	1.00

1D NMR plot parameters

CX	20.00 cm
CY	707.42 cm
F1P	10.000 ppm
F1	5001.30 Hz
F2P	-0.500 ppm
F2	-250.06 Hz
PPMCM	0.52500 ppm/cm
HZCM	262.56821 Hz/cm

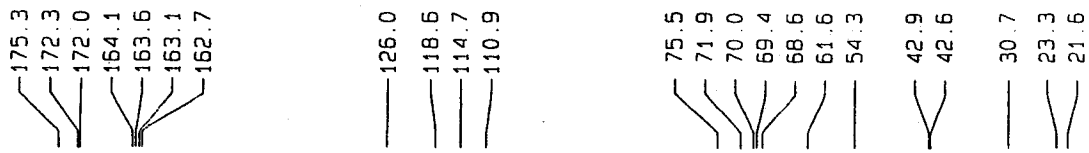

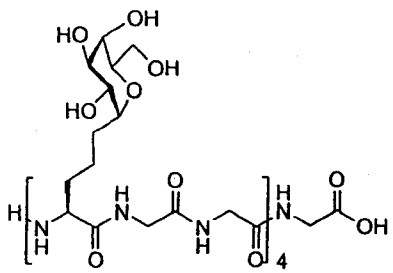

58

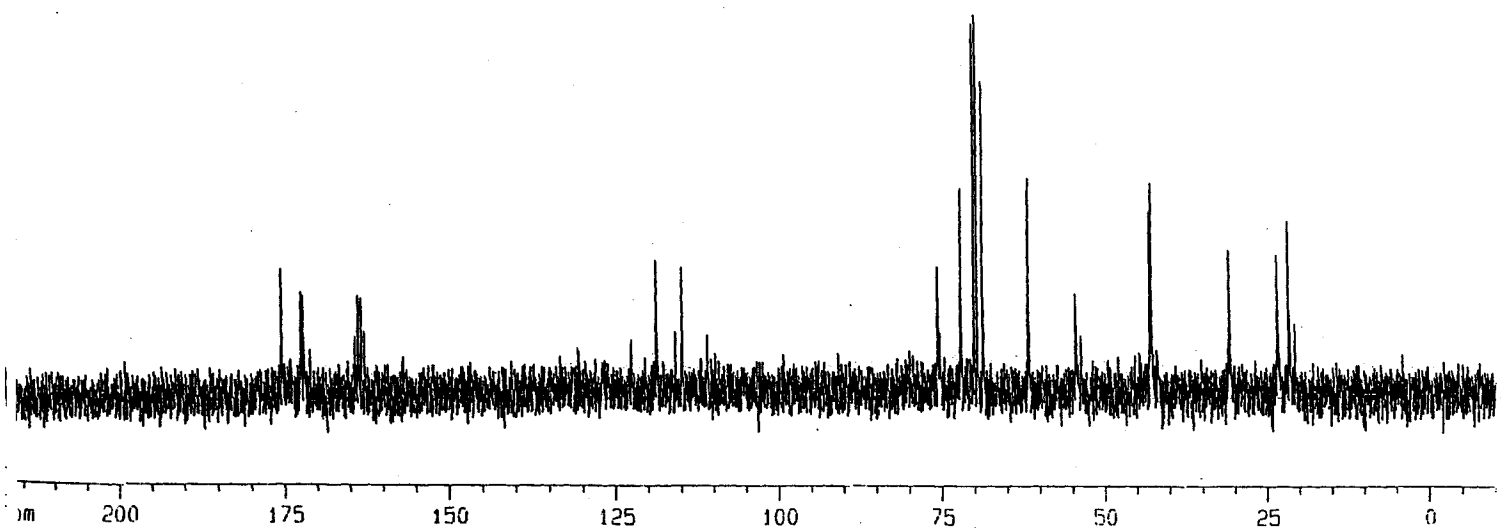


```
Current Data Parameters
NAME          rbs11220041
EXPNO                   1
PROCNO                  1

F2 - Acquisition Parameters
Date_           20041221
Time               9.06
INSTRUM           av300
PROBHD   5 mm QNP  1H/1
PULPROG         zgpg30
TD                32768
SOLVENT           CDCl3
NS                24158
DS                    0
SWH           17985.611 Hz
FIDRES        0.548877 Hz
AQ            0.9110004 sec
RG               3649.1
DW               27.800 usec
DE                6.00 usec
TE               300.0 K
D1            1.00000000 sec
d11           0.03000000 sec
d12           0.00002000 sec

============ CHANNEL f1 =============
NUC1                13C
P1                 5.00 usec
PL1               -6.00 dB
SFO1         75.4752653 MHz

============ CHANNEL f2 =============
CPDPRG2         waltz16
NUC2                1H
PCPD2             70.00 usec
PL2               -3.00 dB
PL12              13.48 dB
PL13              15.63 dB
SFO2        300.1314860 MHz

F2 - Processing parameters
SI                 65536
SF           75.4677190 MHz
WDW                  EM
SSB                   0
LB                 1.00 Hz
GB                    0
PC                 1.40

1D NMR plot parameters
CX                20.00 cm
CY                 5.15 cm
F1P              220.000 ppm
F1              16602.90 Hz
F2P              -10.000 ppm
F2              -754.68 Hz
PPMCM           11.50000 ppm/cm
```

1H NMR

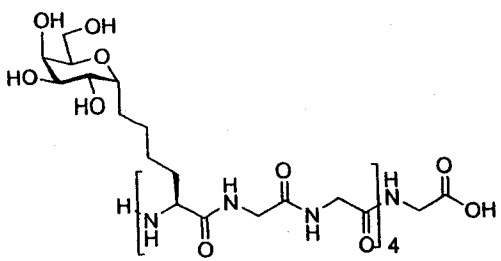

59

Current Data Parameters

NAME	ros10711043
EXPNO	1
PROCNO	1

F2 - Acquisition Parameters

Date_	20040711
Time	19.43
INSTRUM	AV500WB
PROBHD	5 mm TBO BB/1H
PULPROG	zg30
TD	65536
SOLVENT	C6D6
NS	10887
DS	0
SWH	7440.476 Hz
FIDRES	0.113533 Hz
AQ	4.4040694 sec
RG	128
DW	67.200 usec
DE	6.00 usec
TE	300.0 K
D1	0.01000000 sec

======== CHANNEL f1 ========

NUC1	1H
P1	14.00 usec
PL1	0.00 dB
SFO1	500.1327766 MHz

F2 - Processing parameters

SI	65536
SF	500.1299518 MHz
WDW	EM
SSB	0
LB	0.00 Hz
GB	0
PC	1.00

1D NMR plot parameters

CX	20.00 cm
CY	101.09 cm
F1P	10.000 ppm
F1	5001.30 Hz
F2P	-0.500 ppm
F2	-250.06 Hz
PPMCM	0.52500 ppm/cm
HZCM	262.56821 Hz/cm

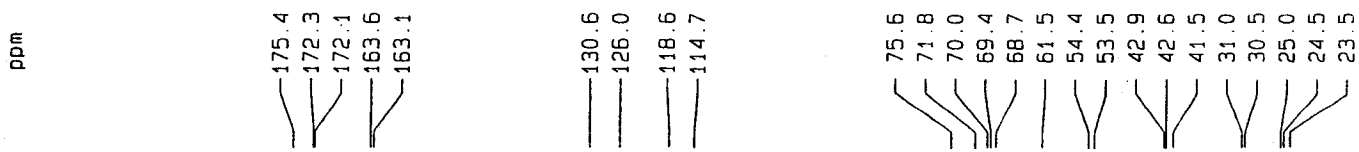

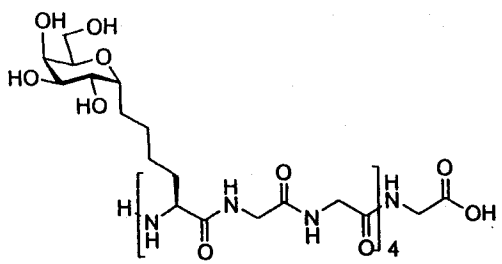

59

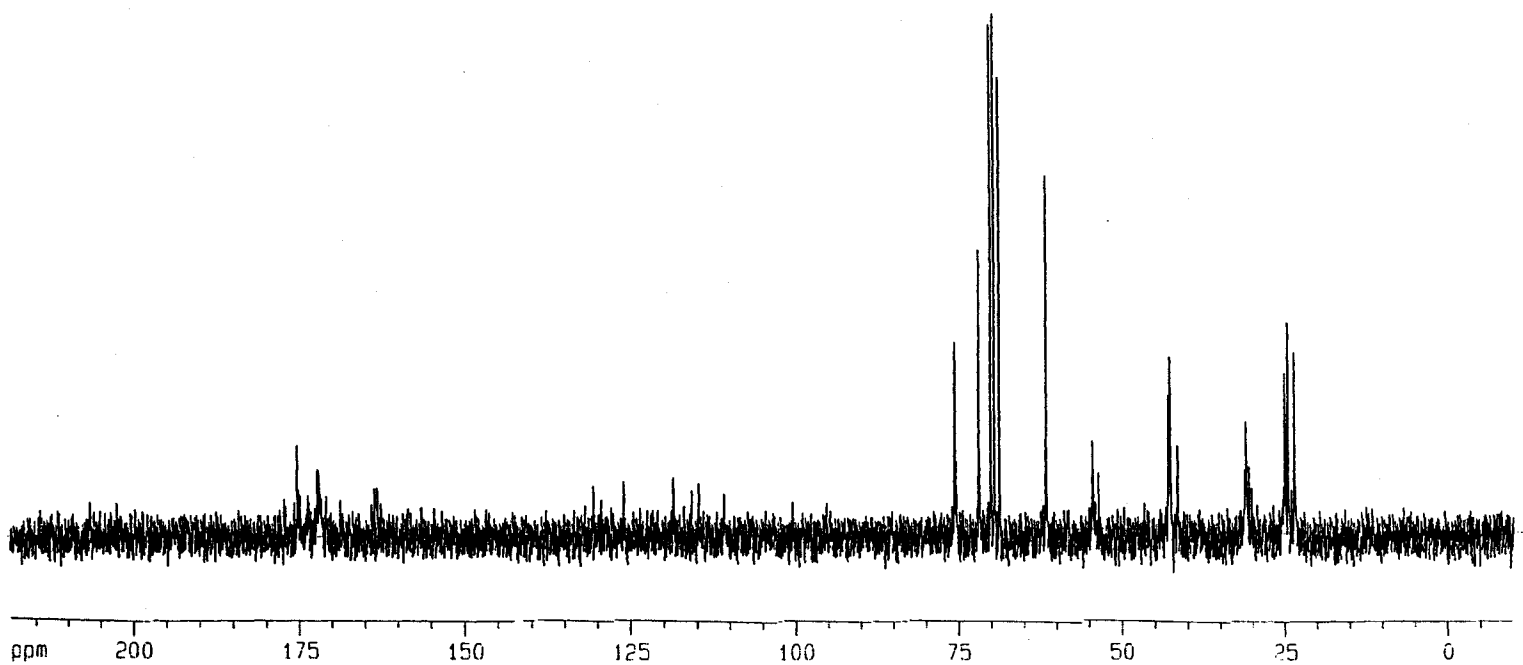

Current Data Parameters

NAME	rbs10713041
EXPNO	1
PROCNO	1

F2 - Acquisition Parameters

Date_	20040713
Time	20.12
INSTRUM	av300
PROBHD	5 mm QNP 1H/1
PULPROG	zgpg30
TD	32768
SOLVENT	CDCl3
NS	21811
DS	0
SWH	17985.611 Hz
FIDRES	0.548877 Hz
AQ	0.9110004 sec
RG	3649.1
DW	27.800 usec
DE	6.00 usec
TE	300.0 K
D1	1.00000000 sec
d11	0.03000000 sec
d12	0.00002000 sec

========== CHANNEL f1 ==========

NUC1	13C
P1	5.00 usec
PL1	-6.00 dB
SFO1	75.4752653 MHz

========== CHANNEL f2 ==========

CPDPRG2	waltz16
NUC2	1H
PCPD2	70.00 usec
PL2	-3.00 dB
PL12	13.48 dB
PL13	15.63 dB
SFO2	300.1314860 MHz

F2 - Processing parameters

SI	65536
SF	75.4677190 MHz
WDW	EM
SSB	0
LB	1.00 Hz
GB	0
PC	1.40

1D NMR plot parameters

CX	20.00 cm
CY	7.00 cm
F1P	220.000 ppm
F1	16602.90 Hz
F2P	-10.000 ppm
F2	-754.68 Hz
PPMCM	11.50000 ppm/cm
HZCM	867.87878 Hz/cm

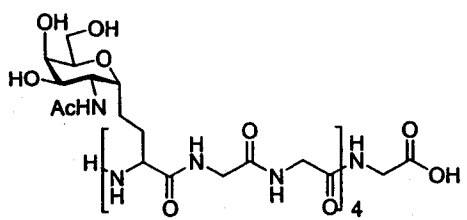

60

Current Data Parameters

NAME	rbs160
EXPNO	1
PROCNO	1

F2 - Acquisition Parameters

Date_	20060321
Time	14.44
INSTRUM	spect
PROBHD	5 mm QNP 1H/1
PULPROG	zg30
TD	30720
SOLVENT	D2O
NS	170
DS	0
SWH	5081.301 Hz
FIDRES	0.165407 Hz
AQ	3.0228980 sec
RG	406.4
DW	98.400 usec
DE	6.00 usec
TE	300.0 K
D1	1.00000000 sec

======== CHANNEL f1 ========

NUC1	1H
P1	10.00 usec
PL1	-3.00 dB
SFO1	300.1319477 MHz

F2 - Processing parameters

SI	65536
SF	300.1299689 MHz
WDW	EM
SSB	0
LB	0.10 Hz
GB	0
PC	1.00

1D NMR plot parameters

CX	20.00 cm
CY	235.15 cm
F1P	10.000 ppm
F1	3001.30 Hz
F2P	-0.500 ppm
F2	-150.06 Hz
PPMCM	0.52500 ppm/cm
HZCM	157.56824 Hz/cm

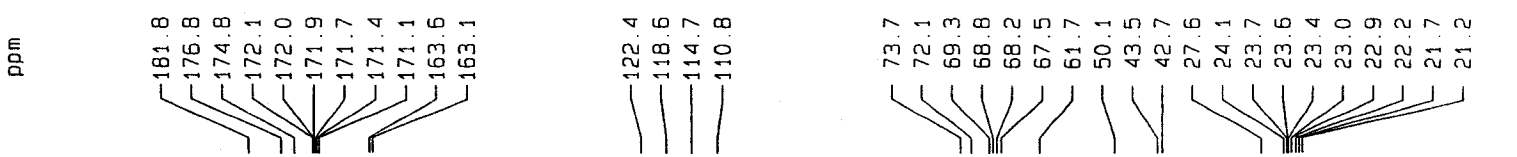

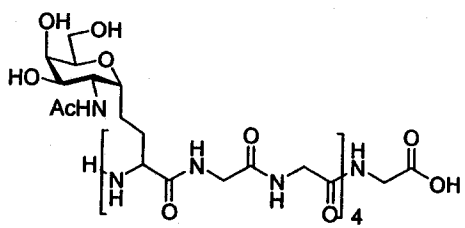

60

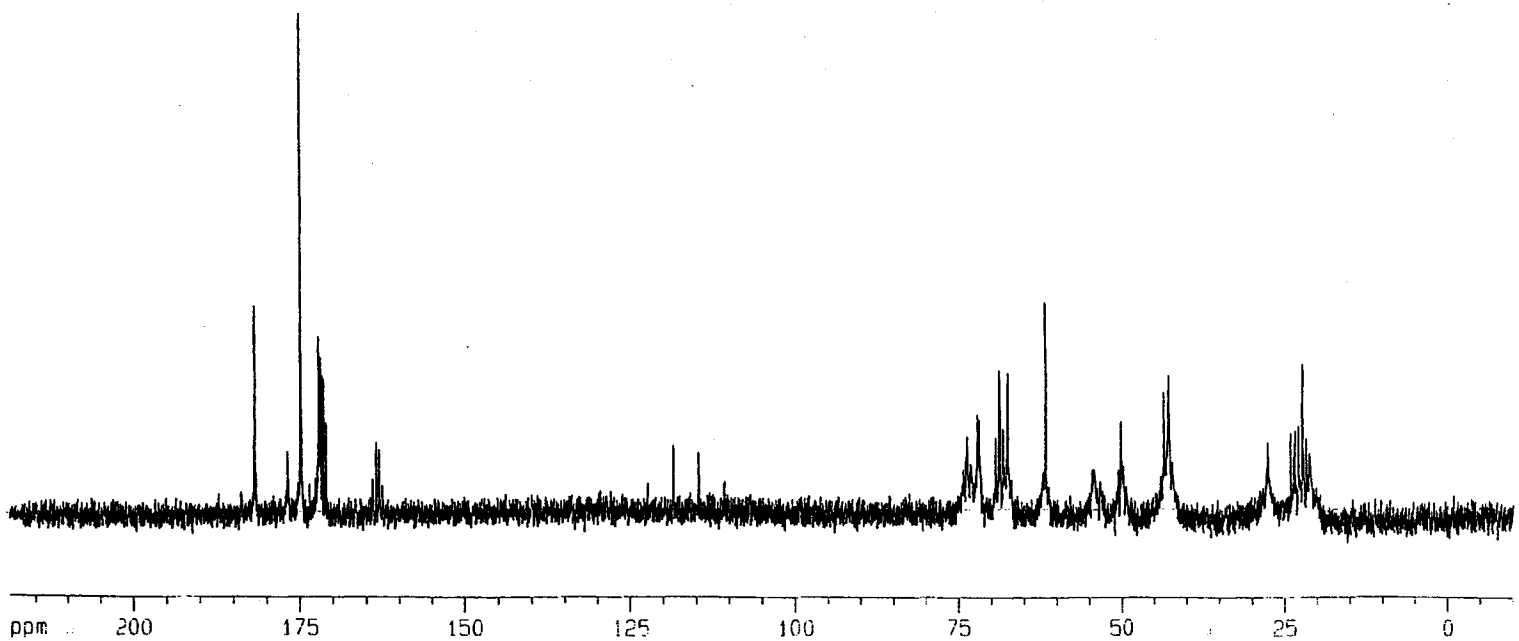

Current Data Parameters

NAME	ros10414051
EXPNO	2
PROCNO	1

F2 - Acquisition Parameters

Date_	20050415
Time	8.30
INSTRUM	av300
PROBHD	5 mm GNP 1H/1
PULPROG	zgpg30
TD	32768
SOLVENT	CDCl3
NS	21889
DS	0
SWH	17985.611 Hz
FIDRES	0.548877 Hz
AQ	0.9110004 sec
RG	3649.1
DW	27.800 usec
DE	6.00 usec
TE	300.0 K
D1	1.00000000 sec
d11	0.03000000 sec
d12	0.00002000 sec

========== CHANNEL f1 ==========

NUC1	13C
P1	5.00 usec
PL1	-6.00 dB
SFO1	75.4752653 MHz

========== CHANNEL f2 ==========

CPDPRG2	waltz16
NUC2	1H
PCPD2	70.00 usec
PL2	-3.00 dB
PL12	13.48 dB
PL13	15.63 dB
SFO2	300.1314860 MHz

F2 - Processing parameters

SI	65536
SF	75.4677190 MHz
WDW	EM
SSB	0
LB	1.00 Hz
GB	0
PC	1.40

1D NMR plot parameters

CX	20.00 cm
CY	6.70 cm
F1P	220.000 ppm
F1	16602.90 Hz
F2P	-10.000 ppm
F2	-754.68 Hz
PPMCM	11.50000 ppm/cm
HZCM	867.87878 Hz/cm

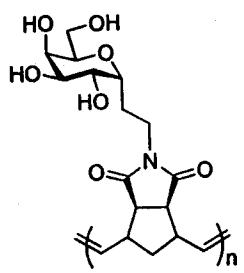
HO
OH
O
HO
HO
N
O
O
n

61

0.56
2.00
0.75
1.86
3.91
2.92
2.55
1.90
2.35
2.00
9.0
8.0
7.0
6.0
5.0
4.0
3.0
2.0
1.0
0.0
ppm (t1)

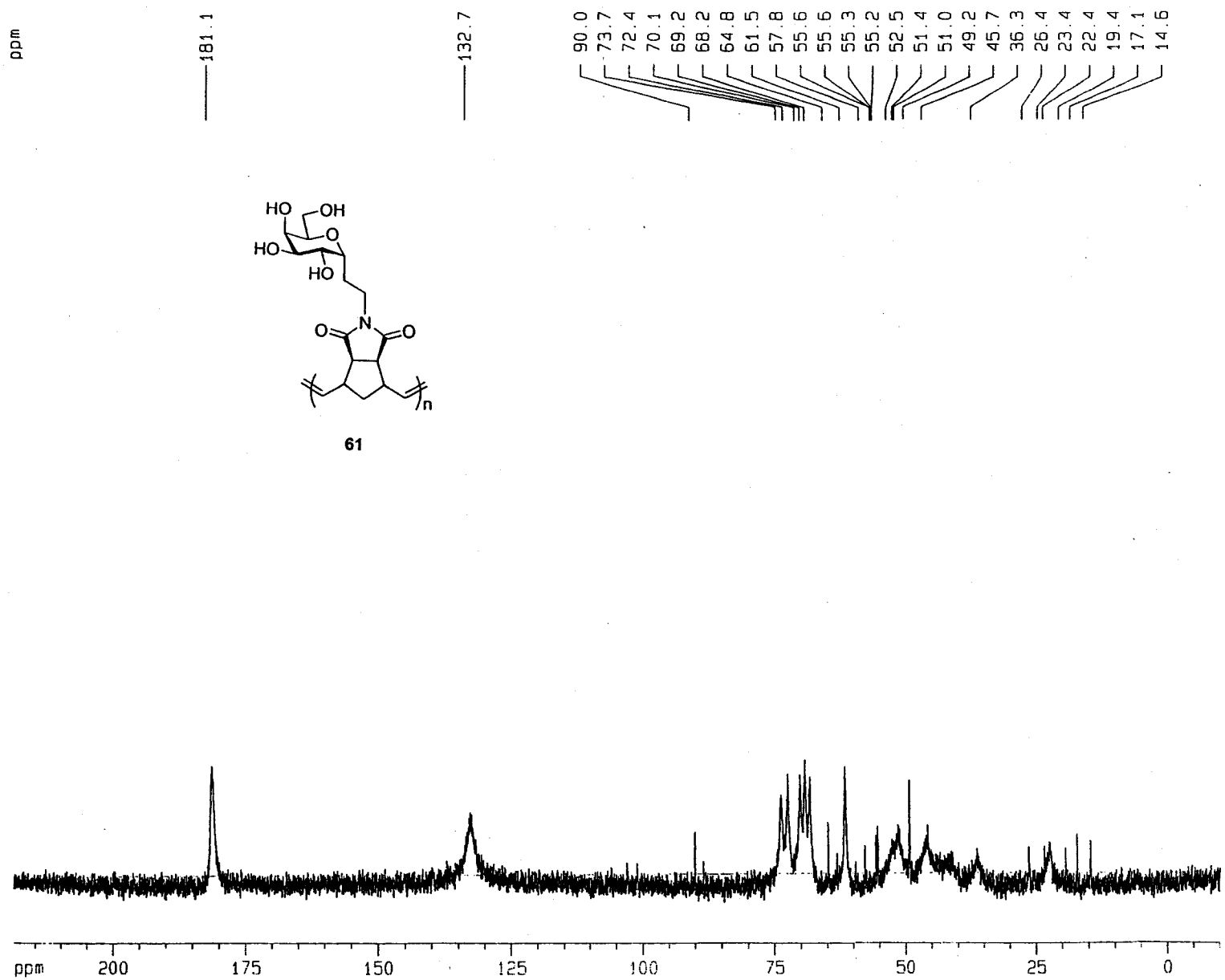

61

Current Data Parameters

NAME	rbslromp61
EXPNO	1
PROCNO	1

F2 - Acquisition Parameters

Date_	20060304
Time	23.37
INSTRUM	spect
PROBHD	5 mm QNP 1H/1
PULPROG	zgpg30
TD	32768
SOLVENT	D2O
NS	23028
DS	0
SWH	17985.611 Hz
FIDRES	0.548877 Hz
AQ	0.9110004 sec
RG	3649.1
DW	27.800 usec
DE	6.00 usec
TE	300.0 K
D1	1.00000000 sec
d11	0.03000000 sec
d12	0.00002000 sec

======== CHANNEL f1 ========

NUC1	13C
P1	5.10 usec
PL1	-6.00 dB
SFO1	75.4752653 MHz

======== CHANNEL f2 ========

CPDPRG2	waltz16
NUC2	1H
PCPD2	73.00 usec
PL2	-3.00 dB
PL12	15.00 dB
PL13	120.00 dB
SFO2	300.1314860 MHz

F2 - Processing parameters

SI	65536
SF	75.4677190 MHz
WDW	EM
SSB	0
LB	1.00 Hz
GB	0
PC	1.40

1D NMR plot parameters

CX	20.00 cm
CY	13.63 cm
F1P	220.000 ppm
F1	16602.90 Hz
F2P	-10.000 ppm
F2	-754.68 Hz
PPMCM	11.50000 ppm/cm
HZCM	867.87878 Hz/cm

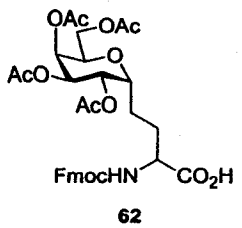

62

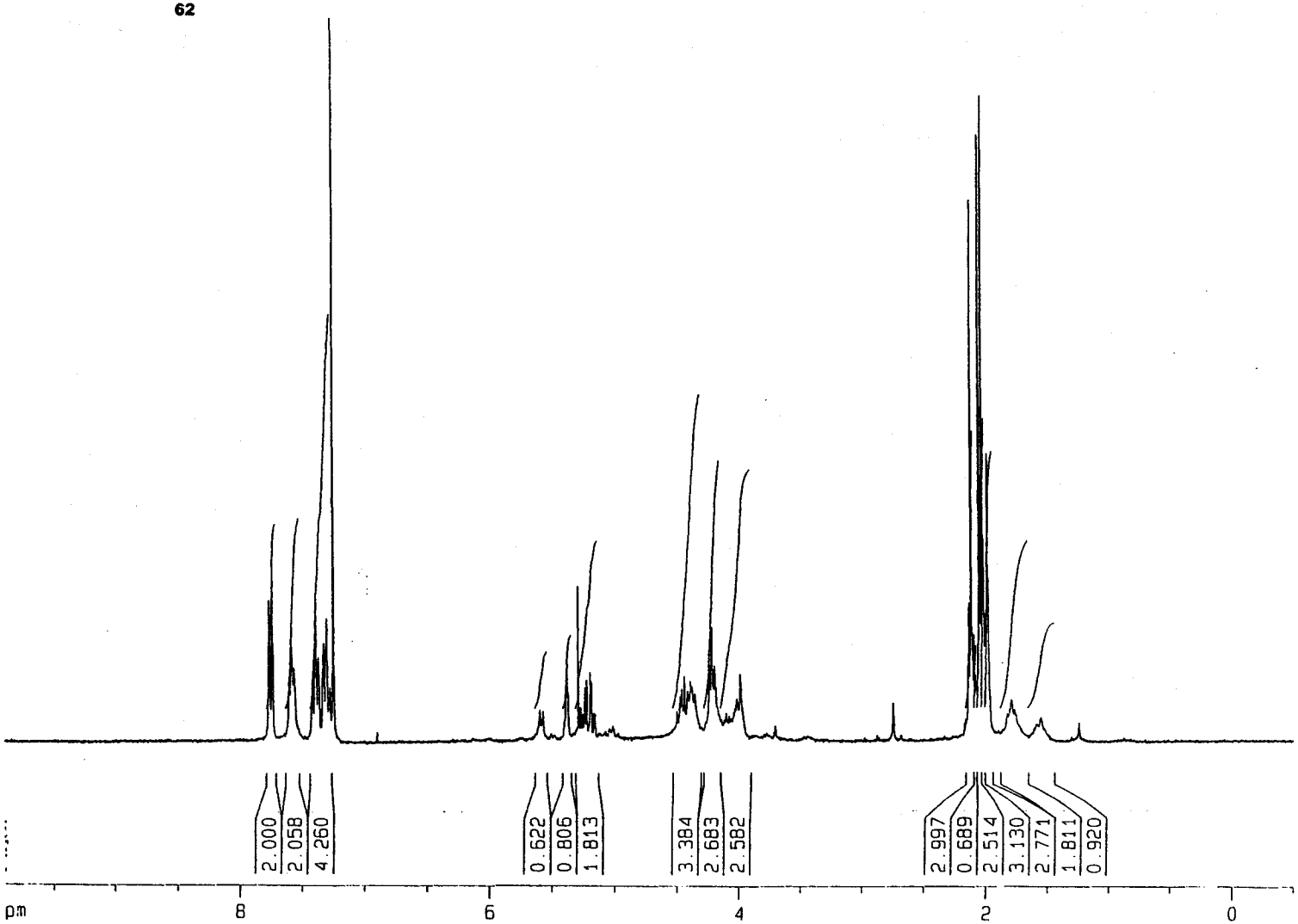

Current Data Parameters

NAME	rbs162
EXPNO	1
PROCNO	1

F2 - Acquisition Parameters

Date_	20060224
Time	14.59
INSTRUM	spect
PROBHD	5 mm QNP 1H/1
PULPROG	zg30
TD	30720
SOLVENT	CDCl3
NS	41
DS	0
SWH	5081.301 Hz
FIDRES	0.165407 Hz
AQ	3.0228980 sec
RG	812.7
DW	98.400 usec
DE	6.00 usec
TE	300.0 K
D1	1.00000000 sec

======== CHANNEL f1 ========

NUC1	1H
P1	10.00 usec
PL1	-3.00 dB
SFO1	300.1319477 MHz

F2 - Processing parameters

SI	65536
SF	300.1300093 MHz
WDW	EM
SSB	0
LB	0.10 Hz
GB	0
PC	1.00

1D NMR plot parameters

CX	20.00 cm
CY	26.43 cm
F1P	10.000 ppm
F1	3001.30 Hz
F2P	-0.500 ppm
F2	-150.06 Hz
PPMCM	0.52500 ppm/cm
HZCM	157.56825 Hz/cm

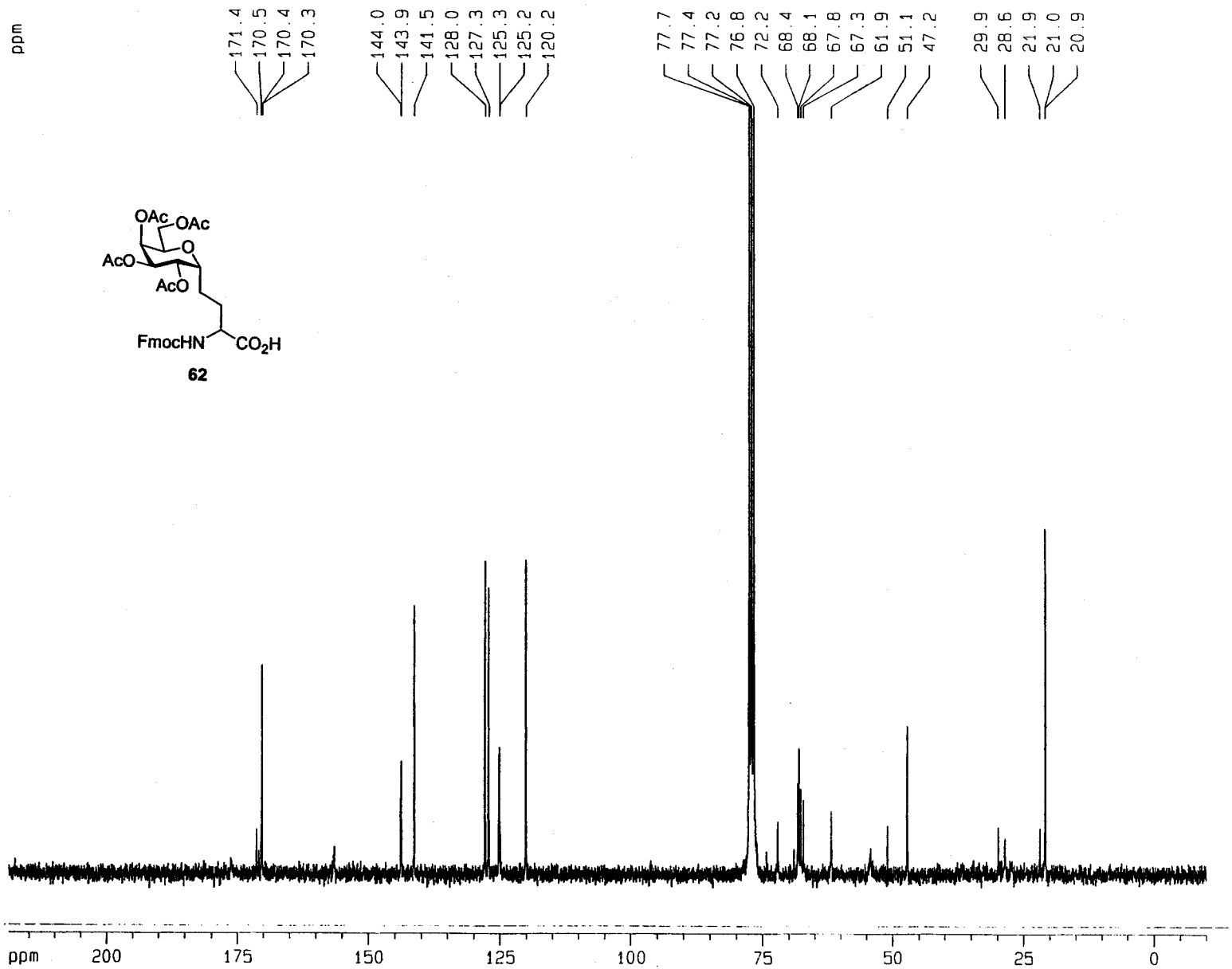

Current Data Parameters

NAME	rbs11017032
EXPNO	2
PROCNO	1

F2 - Acquisition Parameters

Date_	20031017
Time	23.20
INSTRUM	av300
PROBHD	5 mm QNP 1H/1
PULPROG	zgpg30
TD	32768
SOLVENT	CDCl3
NS	28170
DS	0
SWH	17985.611 Hz
FIDRES	0.548877 Hz
AQ	0.9110004 sec
RG	5792.6
DW	27.800 usec
DE	6.00 usec
TE	300.0 K
D1	1.00000000 sec
d11	0.03000000 sec
d12	0.00002000 sec

========== CHANNEL f1 ==========

NUC1	13C
P1	5.00 usec
PL1	-6.00 dB
SFO1	75.4752653 MHz

========== CHANNEL f2 ==========

CPDPRG2	waltz16
NUC2	1H
PCPD2	70.00 usec
PL2	-3.00 dB
PL12	13.48 dB
PL13	15.63 dB
SFO2	300.1314860 MHz

F2 - Processing parameters

SI	65536
SF	75.4677313 MHz
WDW	EM
SSB	0
LB	1.00 Hz
GB	0
PC	1.40

1D NMR plot parameters

CX	20.00 cm
CY	84.78 cm
F1P	220.000 ppm
F1	16602.90 Hz
F2P	-10.000 ppm
F2	-754.68 Hz
PPMCM	11.50000 ppm/cm
HZCM	867.87885 Hz/cm

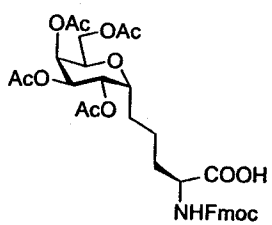

63

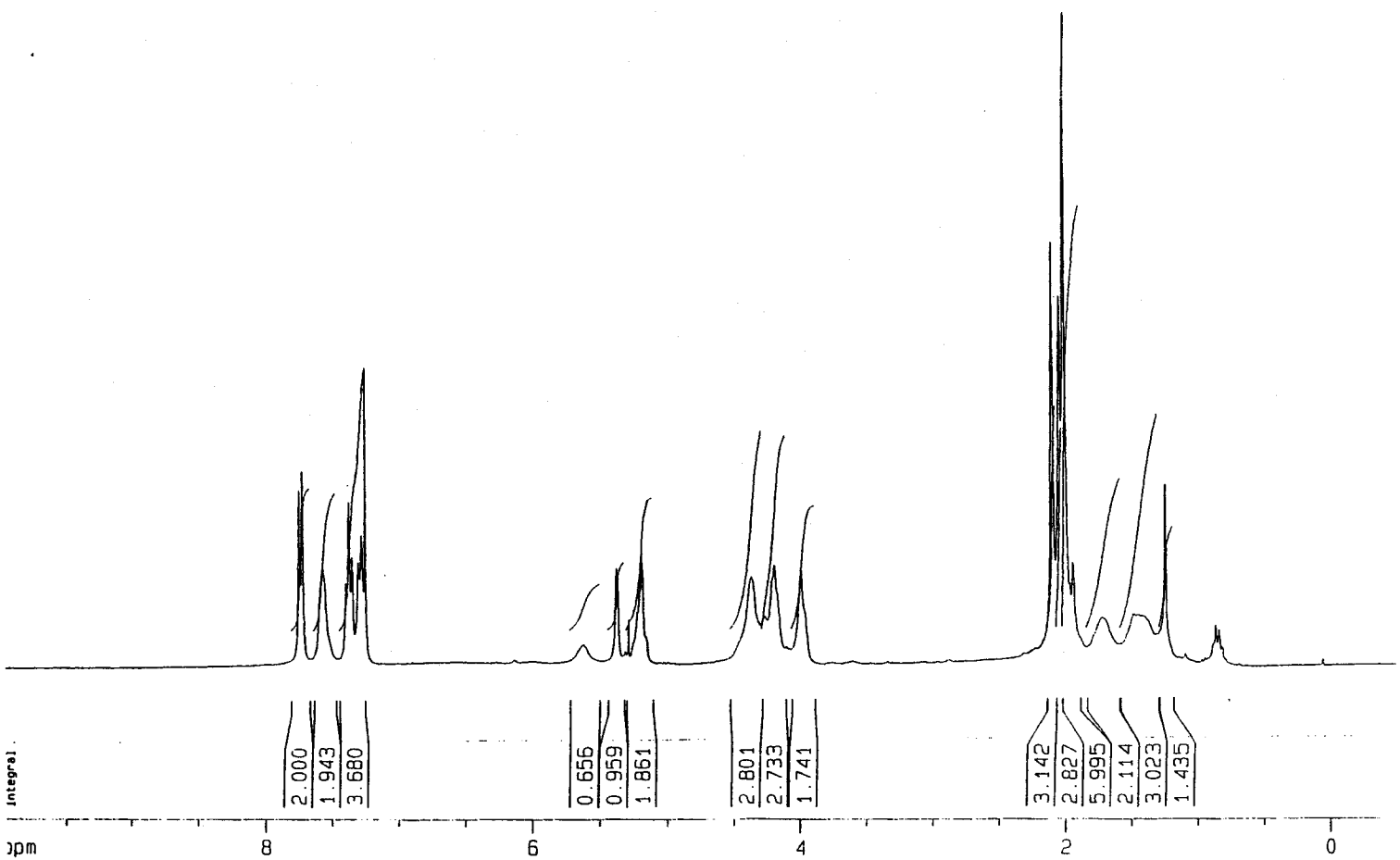

Current Data Parameters

NAME	rbs163later
EXPNO	1
PROCNO	1

F2 - Acquisition Parameters

Date_	20060310
Time	16.06
INSTRUM	spect
PROBHD	5 mm QNP 1H/1
PULPROG	zg30
TD	30720
SOLVENT	CDCl3
NS	31
DS	0
SWH	5081.301 Hz
FIDRES	0.165407 Hz
AQ	3.0228980 sec
RG	181
DW	98.400 usec
DE	6.00 usec
TE	300.0 K
D1	1.00000000 sec

======== CHANNEL f1 ========

NUC1	1H
P1	10.00 usec
PL1	-3.00 dB
SFO1	300.1319477 MHz

F2 - Processing parameters

SI	65536
SF	300.1300092 MHz
WDW	EM
SSB	0
LB	0.10 Hz
GB	0
PC	1.00

1D NMR plot parameters

CX	20.00 cm
CY	9.28 cm
F1P	10.000 ppm
F1	3001.30 Hz
F2P	-0.500 ppm
F2	-150.06 Hz
PPMCM	0.52500 ppm/cm
HZCM	157.56825 Hz/cm

13C with proton decoupling

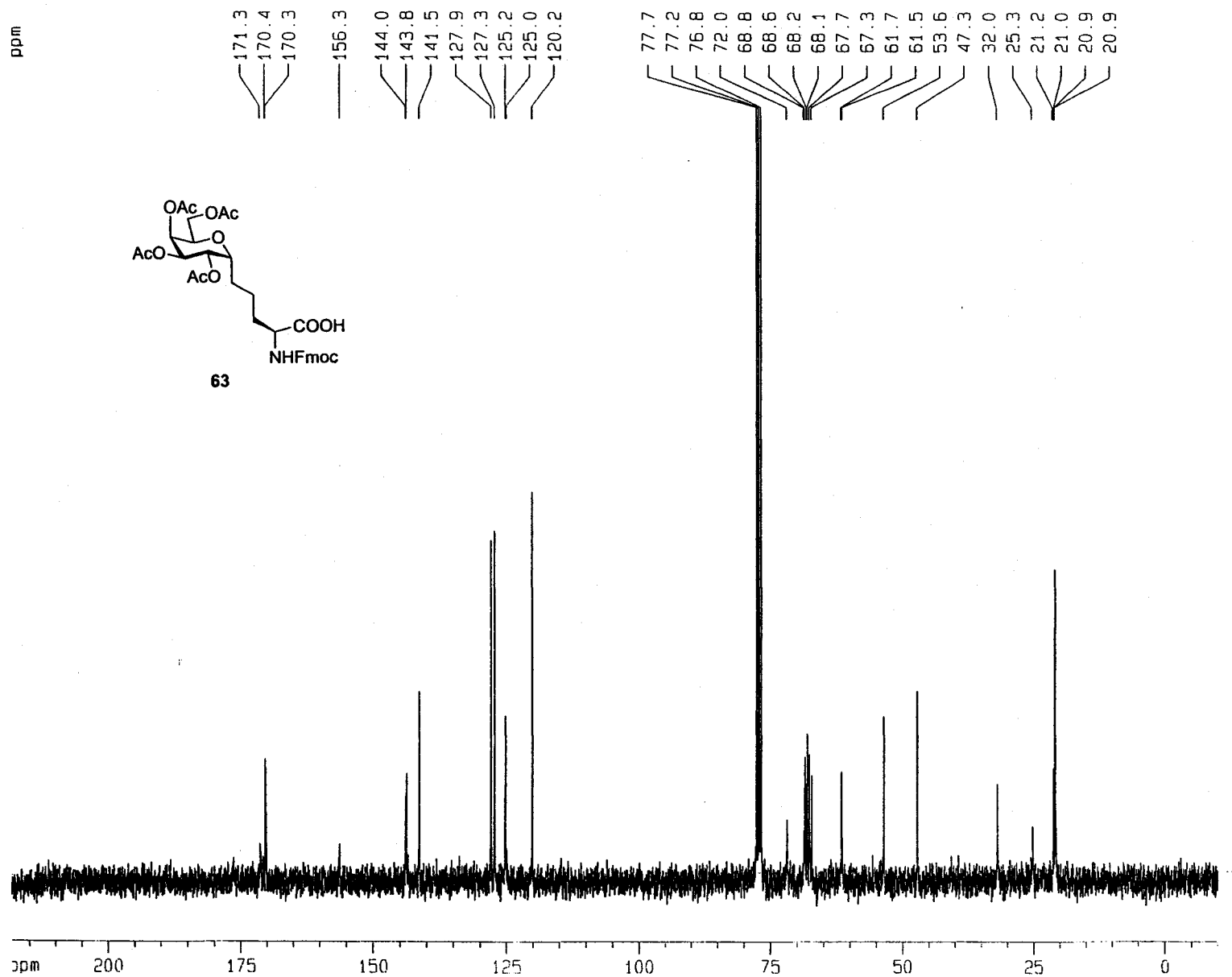

Current Data Parameters

NAME	rbs10629041
EXPNO	2
PROCNO	1

F2 - Acquisition Parameters

Date_	20040629
Time	17.01
INSTRUM	av300
PROBHD	5 mm QNP 1H/1
PULPROG	zgpg30
TD	32768
SOLVENT	CDCl3
NS	702
DS	0
SWH	17985.611 Hz
FIDRES	0.548877 Hz
AQ	0.9110004 sec
RG	4096
DW	27.800 usec
DE	6.00 usec
TE	300.0 K
D1	1.00000000 sec
d11	0.03000000 sec
d12	0.00002000 sec

========== CHANNEL f1 ==========

NUC1	13C
P1	5.00 usec
PL1	-6.00 dB
SFO1	75.4752653 MHz

========== CHANNEL f2 ==========

CPDPRG2	waltz16
NUC2	1H
PCPD2	70.00 usec
PL2	-3.00 dB
PL12	13.48 dB
PL13	15.63 dB
SFO2	300.1314860 MHz

F2 - Processing parameters

SI	65536
SF	75.4677329 MHz
WDW	EM
SSB	0
LB	1.00 Hz
GB	0
PC	1.40

1D NMR plot parameters

CX	20.00 cm
CY	19.07 cm
F1P	220.000 ppm
F1	16602.90 Hz
F2P	-10.000 ppm
F2	-754.68 Hz
PPMCM	11.50000 ppm/cm
HZCM	867.87897 Hz/cm

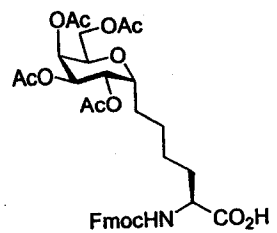

64

Current Data Parameters

NAME	rbs10605041
EXPNO	1
PROCNO	1

F2 - Acquisition Parameters

Date_	20040605
Time	23.52
INSTRUM	av300
PROBHD	5 mm QNP 1H/1
PULPROG	zg30
TD	30720
SOLVENT	CDCl3
NS	61
DS	0
SWH	5081.301 Hz
FIDRES	0.165407 Hz
AQ	3.0228980 sec
RG	456.1
DW	98.400 usec
DE	6.00 usec
TE	300.0 K
D1	1.00000000 sec

========== CHANNEL f1 ==========

NUC1	1H
P1	10.50 usec
PL1	-3.00 dB
SFO1	300.1319477 MHz

F2 - Processing parameters

SI	65536
SF	300.1299964 MHz
WDW	EM
SSB	0
LB	0.10 Hz
GB	0
PC	1.00

1D NMR plot parameters

CX	20.00 cm
CY	10.80 cm
F1P	10.000 ppm
F1	3001.30 Hz
F2P	0.000 ppm
F2	0.00 Hz
PPMCM	0.50000 ppm/cm
HZCM	150.06500 Hz/cm

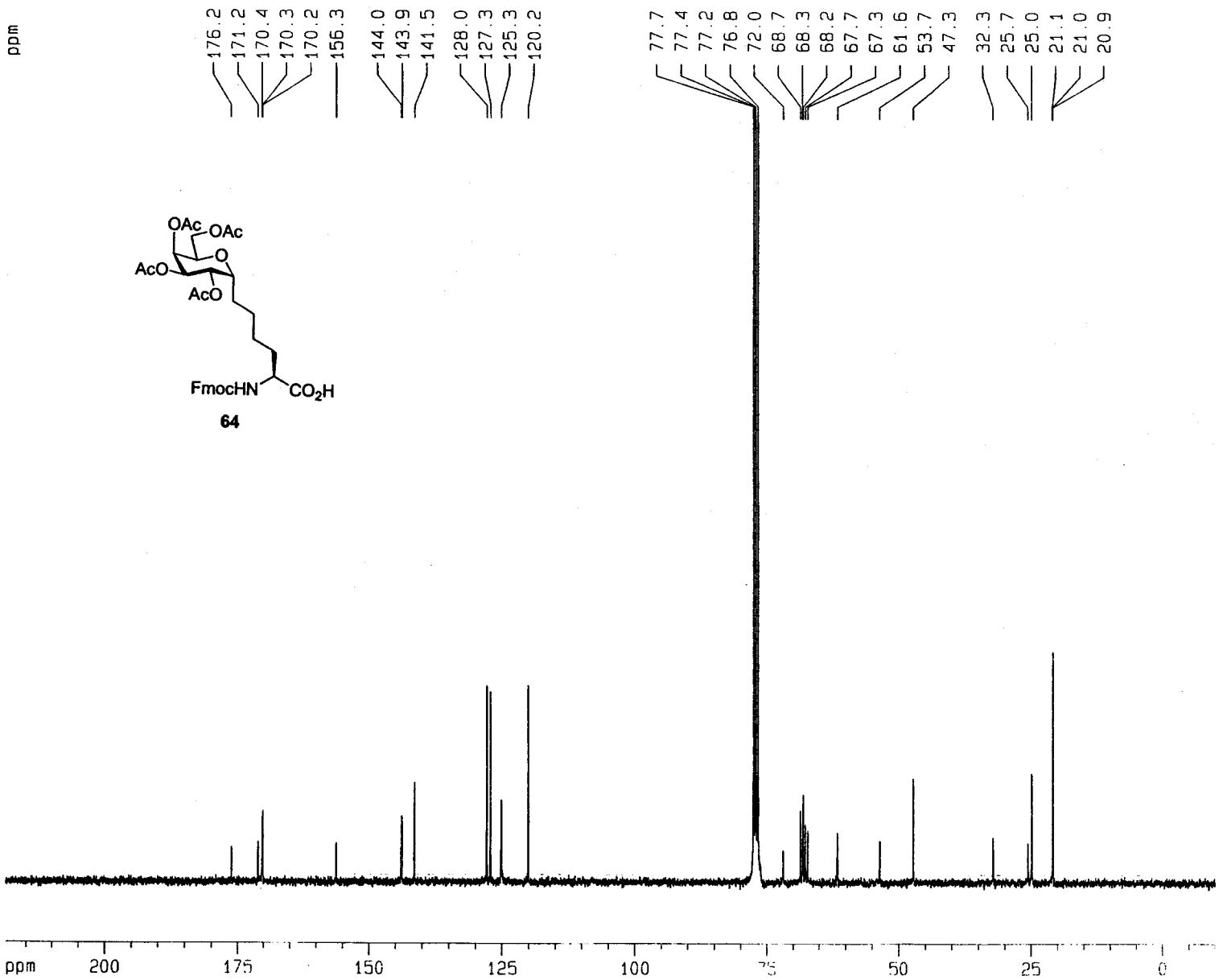

Current Data Parameters

NAME	rbs10605041
EXPNO	2
PROCNO	1

F2 - Acquisition Parameters

Date_	20040606
Time	12.00
INSTRUM	av300
PROBHD	5 mm QNP 1H/1
PULPROG	zgpg30
TD	32768
SOLVENT	CDCl3
NS	22817
DS	0
SWH	17985.611 Hz
FIDRES	0.548877 Hz
AQ	0.9110004 sec
RG	2896.3
DW	27.800 usec
DE	6.00 usec
TE	300.0 K
D1	1.00000000 sec
d11	0.03000000 sec
d12	0.00002000 sec

========== CHANNEL f1 ==========

NUC1	13C
P1	5.00 usec
PL1	-6.00 dB
SFO1	75.4752653 MHz

========== CHANNEL f2 ==========

CPDPRG2	waltz16
NUC2	1H
PCPD2	70.00 usec
PL2	-3.00 dB
PL12	13.48 dB
PL13	15.63 dB
SFO2	300.1314860 MHz

F2 - Processing parameters

SI	65536
SF	75.4677307 MHz
WDW	EM
SSB	0
LB	1.00 Hz
GB	0
PC	1.40

1D NMR plot parameters

CX	20.00 cm
CY	35.96 cm
F1P	220.000 ppm
F1	16602.90 Hz
F2P	-10.000 ppm
F2	-754.68 Hz
PPMCM	11.50000 ppm/cm
HZCM	867.87885 Hz/cm

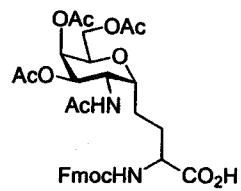

65

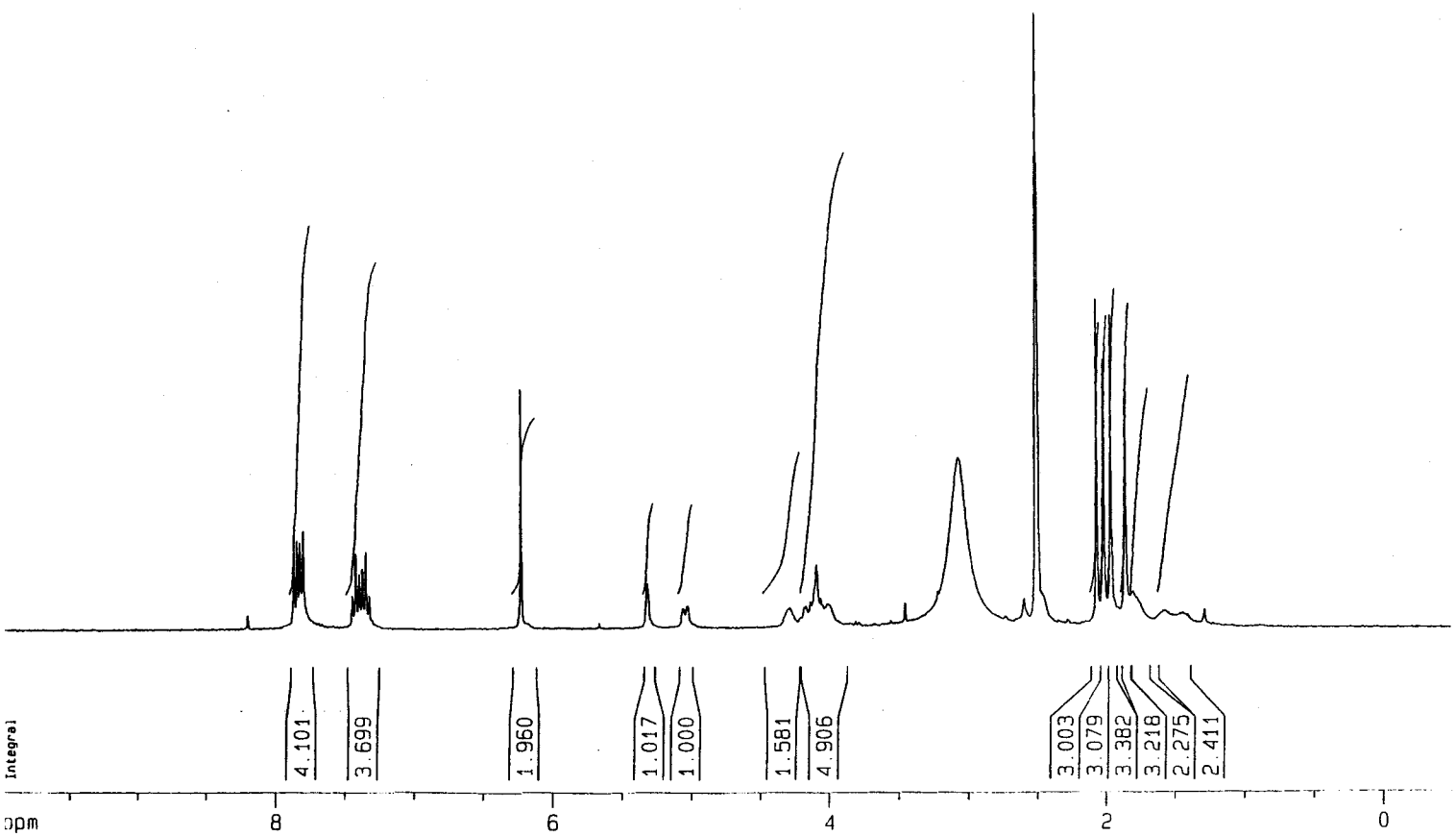


```
Current Data Parameters
NAME          rbs10218051
EXPNO                   2
PROCNO                  1

F2 - Acquisition Parameters
Date_            20050218
Time                14.17
INSTRUM           av300
PROBHD   5 mm QNP  1H/1
PULPROG             zg30
TD                 30720
SOLVENT             DMSO
NS                    99
DS                     0
SWH           5081.301 Hz
FIDRES        0.165407 Hz
AQ            3.0228980 sec
RG                724.1
DW               98.400 usec
DE                6.00 usec
TE                300.0 K
D1           1.00000000 sec

============ CHANNEL f1 =============
NUC1                  1H
P1                16.00 usec
PL1               -3.00 dB
SFO1         300.1319477 MHz

F2 - Processing parameters
SI                 65536
SF           300.1299973 MHz
WDW                   EM
SSB                    0
LB                0.50 Hz
GB                     0
PC                1.00

1D NMR plot parameters
CX                20.00 cm
CY                 8.41 cm
F1P               10.000 ppm
F1              3001.30 Hz
F2P               -0.500 ppm
F2              -150.06 Hz
PPMCM          0.52500 ppm/cm
HZCM          157.56825 Hz/cm
```

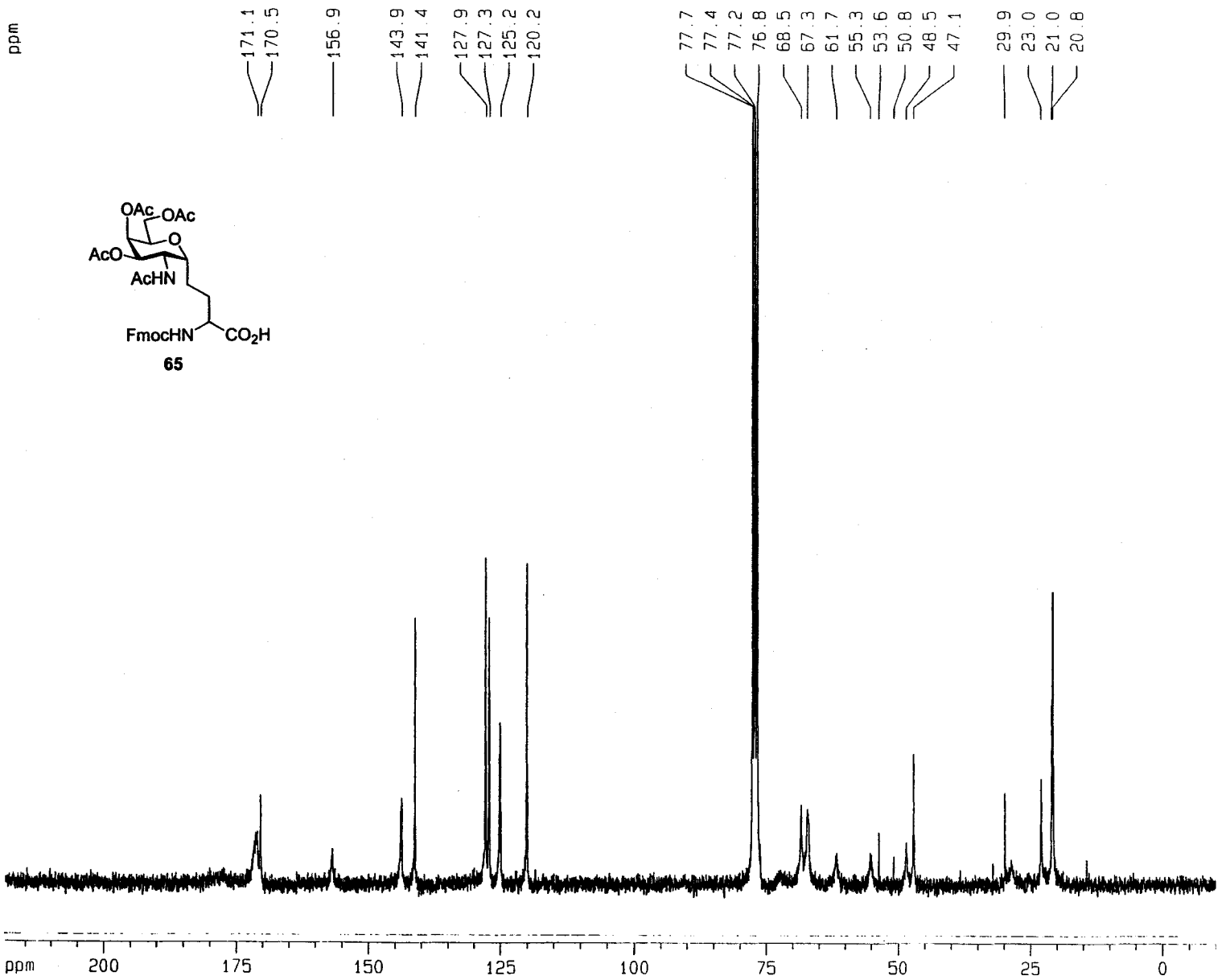

Current Data Parameters

NAME	rbs10207051
EXPNO	2
PROCNO	1

F2 - Acquisition Parameters

Date_	20050207
Time	19.15
INSTRUM	av300
PROBHD	5 mm QNP 1H/1
PULPROG	zgpg30
TD	32768
SOLVENT	CDCl3
NS	24650
DS	0
SWH	17985.611 Hz
FIDRES	0.548877 Hz
AQ	0.9110004 sec
RG	6502
DW	27.800 usec
DE	6.00 usec
TE	300.0 K
D1	1.00000000 sec
d11	0.03000000 sec
d12	0.00002000 sec

========== CHANNEL f1 ==========

NUC1	13C
P1	5.00 usec
PL1	-6.00 dB
SFO1	75.4752653 MHz

========== CHANNEL f2 ==========

CPDPRG2	waltz16
NUC2	1H
PCPD2	70.00 usec
PL2	-3.00 dB
PL12	13.48 dB
PL13	15.63 dB
SFO2	300.1314860 MHz

F2 - Processing parameters

SI	65536
SF	75.4677332 MHz
WDW	EM
SSB	0
LB	1.00 Hz
GB	0
PC	1.40

1D NMR plot parameters

CX	20.00 cm
CY	98.26 cm
F1P	220.000 ppm
F1	16602.90 Hz
F2P	-10.000 ppm
F2	-754.68 Hz
PPMCM	11.50000 ppm/cm
HZCM	867.87897 Hz/cm

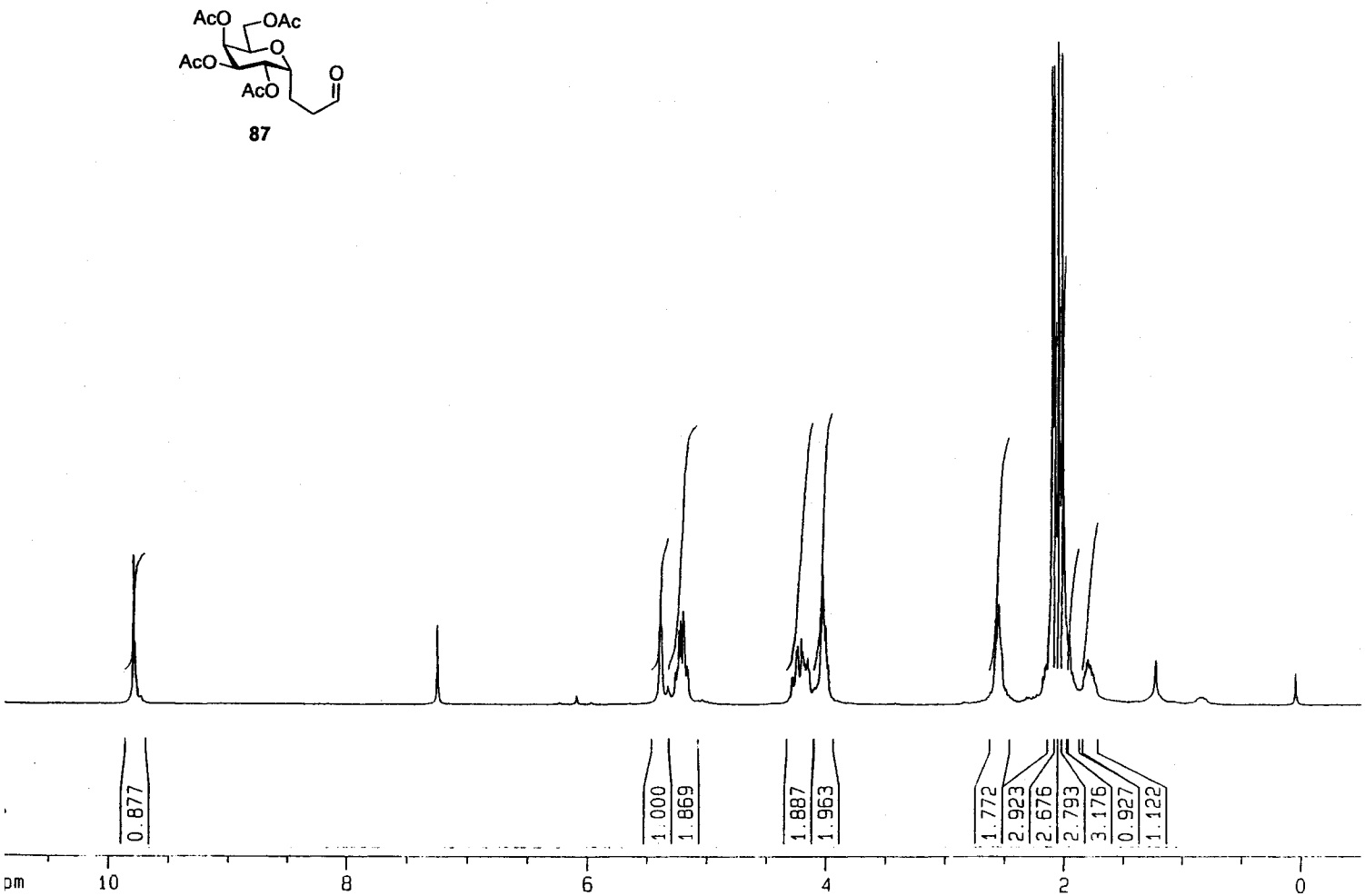


```
Current Data Parameters
NAME                  rbs187
EXPNO                      1
PROCNO                     1

F2 - Acquisition Parameters
Date_              20060224
Time                  15.56
INSTRUM               spect
PROBHD   5 mm QNP  1H/1
PULPROG                zg30
TD                    30720
SOLVENT               CDCl3
NS                       31
DS                        0
SWH               5081.301 Hz
FIDRES            0.165407 Hz
AQ                3.0228980 sec
RG                   228.1
DW                 98.400 usec
DE                   6.00 usec
TE                  300.0 K
D1              1.00000000 sec

======== CHANNEL f1 ========
NUC1                    1H
P1                  10.00 usec
PL1                 -3.00 dB
SFO1           300.1319477 MHz

F2 - Processing parameters
SI                    65536
SF             300.1300089 MHz
WDW                     EM
SSB                      0
LB                    0.10 Hz
GB                       0
PC                    1.00

1D NMR plot parameters
CX                   20.00 cm
CY                    9.62 cm
F1P                 11.000 ppm
F1                3301.43 Hz
F2P                 -0.500 ppm
F2                -150.06 Hz
PPMCM             0.57500 ppm/cm
HZCM            172.57475 Hz/cm
```

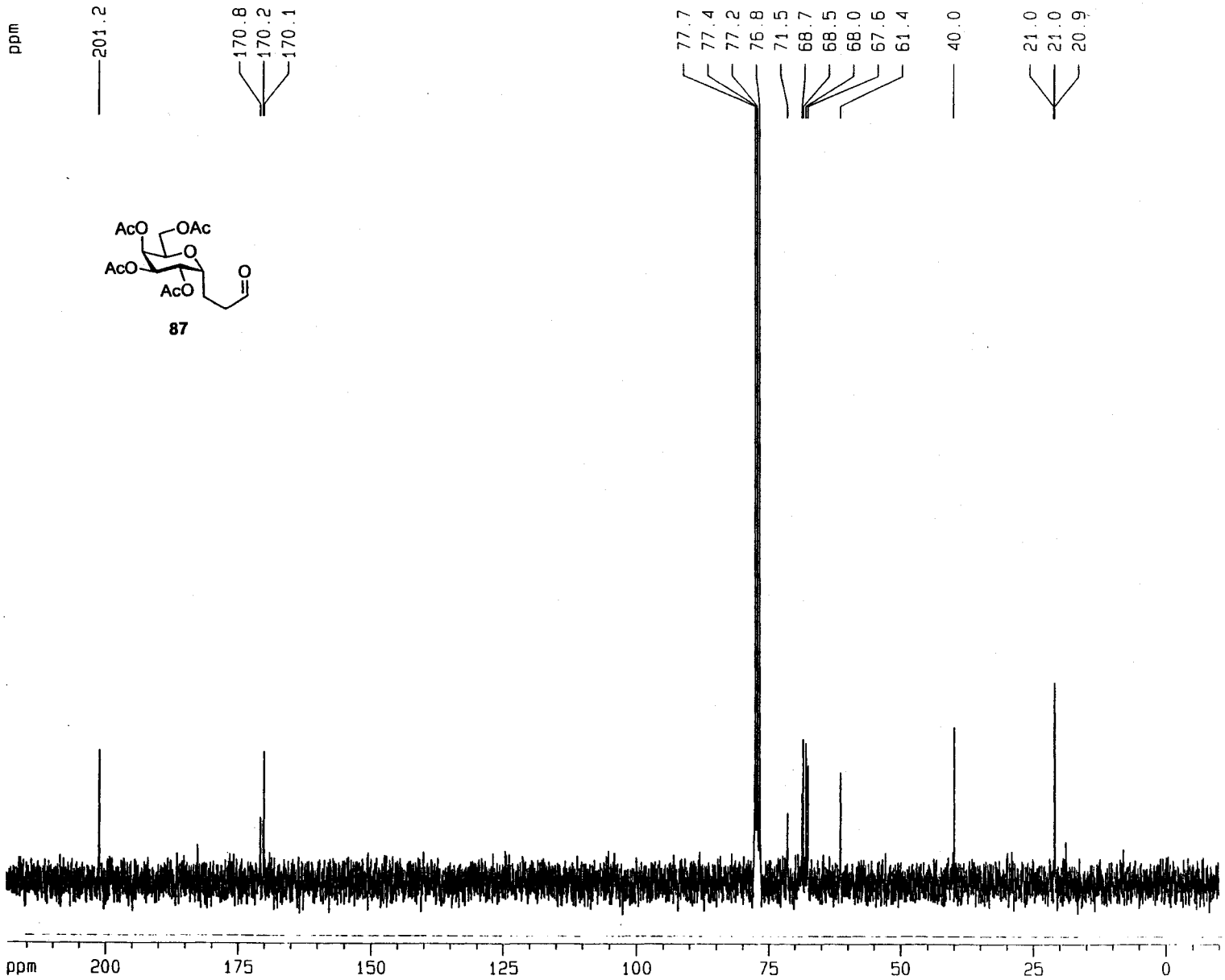

Current Data Parameters
NAME rbs10505043
EXPNO 2
PROCNO 1

F2 - Acquisition Parameters
Date_ 20040505
Time 17.31
INSTRUM av300
PROBHD 5 mm QNP 1H/1
PULPROG zgpg30
TD 32768
SOLVENT CDCl3
NS 872
DS 0
SWH 17985.611 Hz
FIDRES 0.548877 Hz
AQ 0.9110004 sec
RG 3649.1
DW 27.800 usec
DE 6.00 usec
TE 300.0 K
D1 1.00000000 sec
d11 0.03000000 sec
d12 0.00002000 sec

========== CHANNEL f1 ==========
NUC1 13C
P1 5.00 usec
PL1 -6.00 dB
SFO1 75.4752653 MHz

========== CHANNEL f2 ==========
CPDPRG2 waltz16
NUC2 1H
PCPD2 70.00 usec
PL2 -3.00 dB
PL12 13.48 dB
PL13 15.63 dB
SFO2 300.1314860 MHz

F2 - Processing parameters
SI 65536
SF 75.4677307 MHz
WDW EM
SSB 0
LB 1.00 Hz
GB 0
PC 1.40

1D NMR plot parameters
CX 20.00 cm
CY 35.39 cm
F1P 220.000 ppm
F1 16602.90 Hz
F2P -10.000 ppm
F2 -754.68 Hz
PPMCM 11.50000 ppm/cm
HZCM 867.87885 Hz/cm

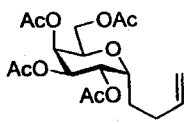

88


```
Current Data Parameters
NAME          rbs10421041
EXPNO                   1
PROCNO                  1

F2 - Acquisition Parameters
Date_           20040421
Time               18.07
INSTRUM          av300
PROBHD   5 mm QNP  1H/1
PULPROG            zg30
TD                30720
SOLVENT           CDCl3
NS                   41
DS                    0
SWH            5081.301 Hz
FIDRES        0.165407 Hz
AQ            3.0228980 sec
RG                  362
DW               98.400 usec
DE                6.00 usec
TE               300.0 K
D1            1.00000000 sec

============ CHANNEL f1 =============
NUC1                1H
P1              10.50 usec
PL1             -3.00 dB
SFO1        300.1319477 MHz

F2 - Processing parameters
SI                65536
SF          300.1299969 MHz
WDW                  EM
SSB                   0
LB                 0.10 Hz
GB                    0
PC                 1.00

1D NMR plot parameters
CX                20.00 cm
CY                 9.95 cm
F1P               10.000 ppm
F1              3001.30 Hz
F2P               -0.500 ppm
F2              -150.06 Hz
PPMCM          0.52500 ppm/cm
HZCM         157.56825 Hz/cm
```

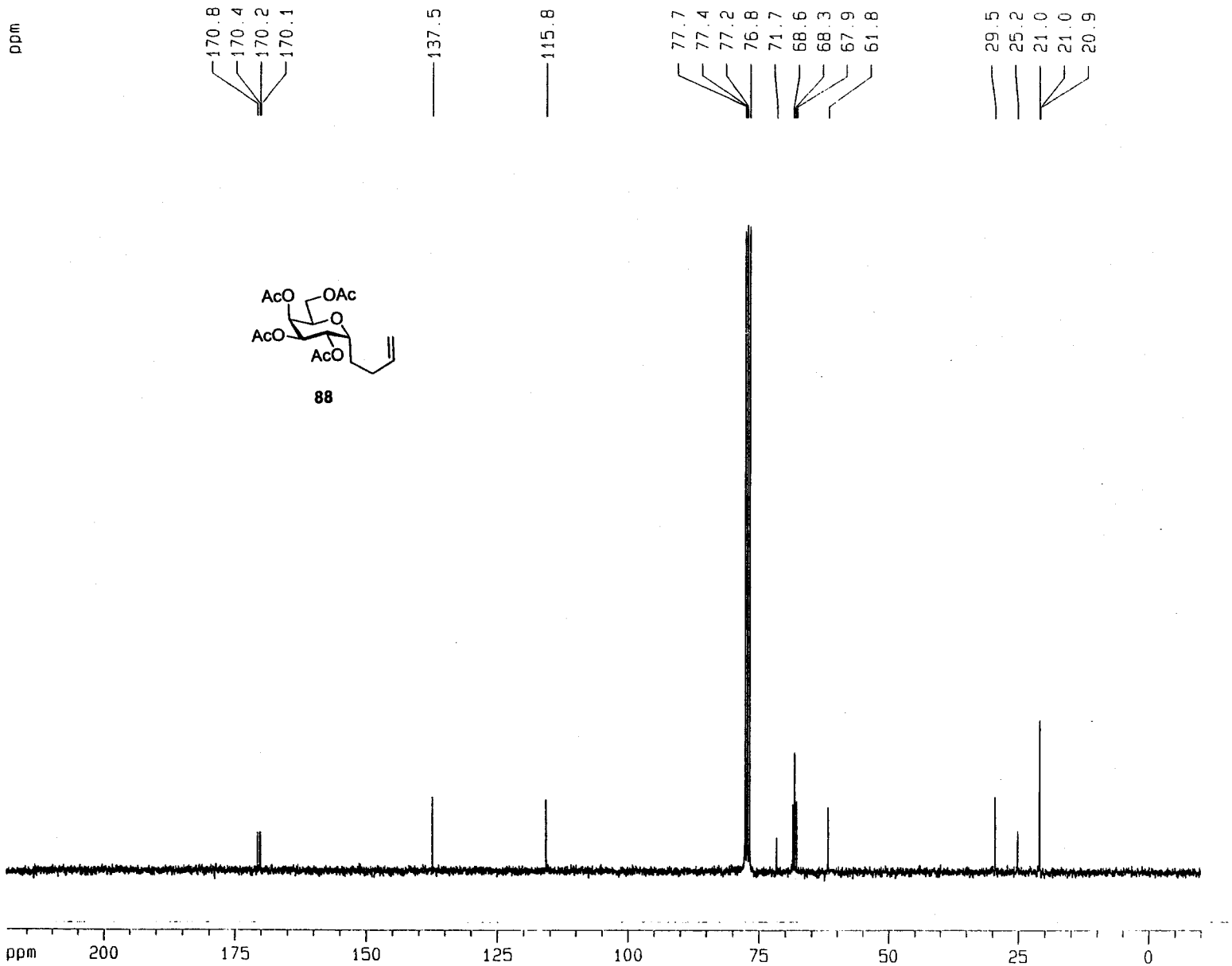

Current Data Parameters
NAME rbs10421041
EXPNO 2
PROCNO 1

F2 - Acquisition Parameters
Date_ 20040421
Time 18 12
INSTRUM av300
PROBHD 5 mm QNP 1H/1
PULPROG zgpg30
TD 32768
SOLVENT CDCl3
NS 1539
DS 0
SWH 17985.611 Hz
FIDRES 0.548877 Hz
AQ 0.9110004 sec
RG 3251
DW 27.800 usec
DE 6.00 usec
TE 300.0 K
D1 1.00000000 sec
d11 0.03000000 sec
d12 0.00002000 sec

========== CHANNEL f1 ==========
NUC1 13C
P1 5.00 usec
PL1 -6.00 dB
SFO1 75.4752653 MHz

========== CHANNEL f2 ==========
CPDPRG2 waltz16
NUC2 1H
PCPD2 70.00 usec
PL2 -3.00 dB
PL12 13.48 dB
PL13 15.63 dB
SFO2 300.1314860 MHz

F2 - Processing parameters
SI 65536
SF 75.4677305 MHz
WDW EM
SSB 0
LB 1.00 Hz
GB 0
PC 1.40

1D NMR plot parameters
CX 20.00 cm
CY 10.84 cm
F1P 220.000 ppm
F1 16602.90 Hz
F2P -10.000 ppm
F2 -754.68 Hz
PPMCM 11.50000 ppm/cm
HZCM 867.87885 Hz/cm

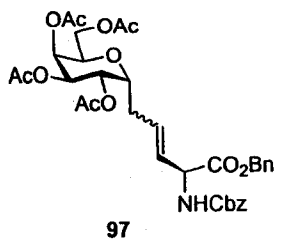

97

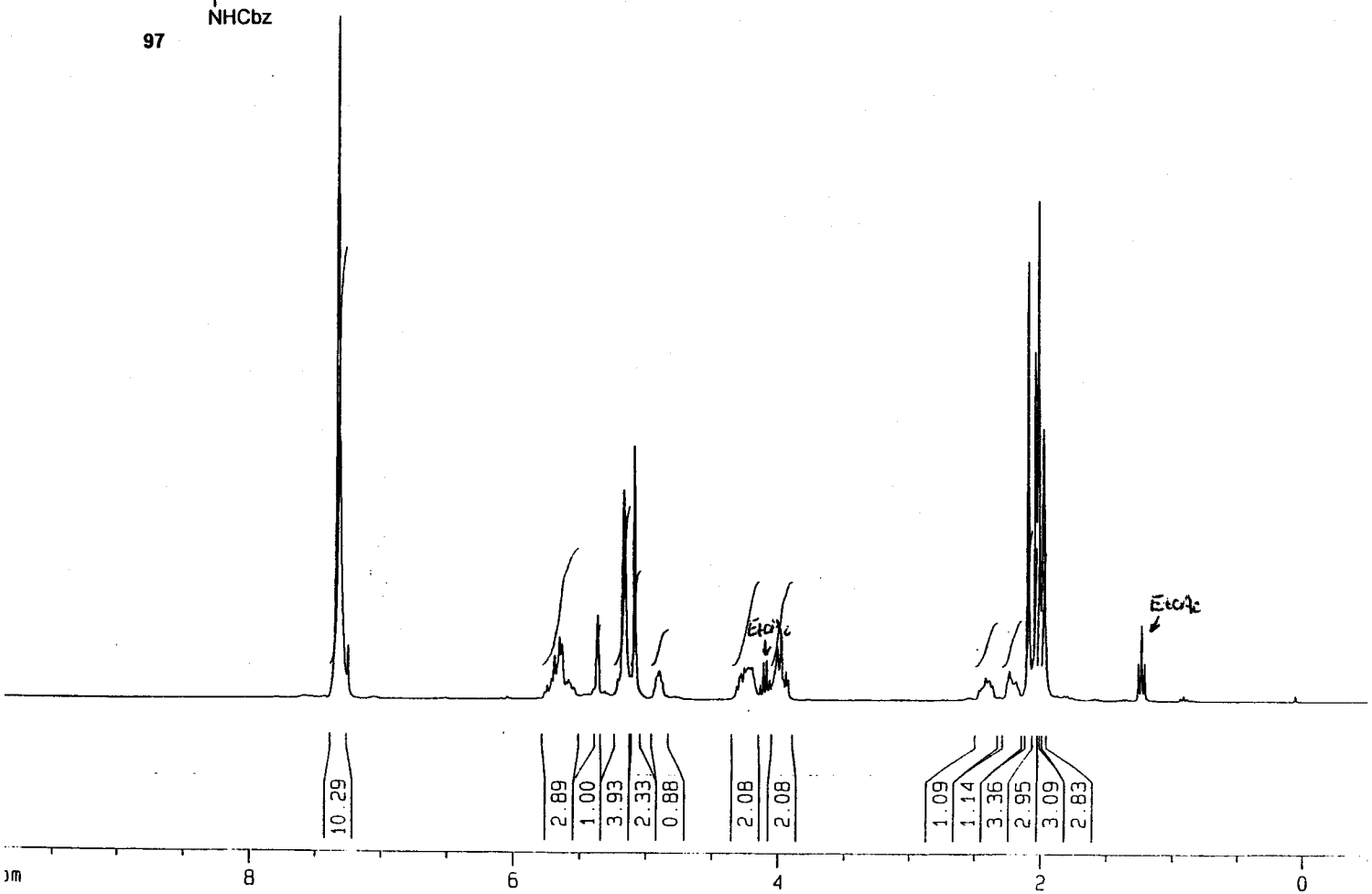


```
Current Data Parameters
NAME         rbs10406041
EXPNO                  1
PROCNO                 1

F2 - Acquisition Parameters
Date_           20040406
Time               15.24
INSTRUM            av300
PROBHD   5 mm QNP  1H/1
PULPROG            zg30
TD                30720
SOLVENT           CDCl3
NS                    21
DS                     0
SWH           5081.301 Hz
FIDRES        0.165407 Hz
AQ           3.0228980 sec
RG                  90.5
DW             98.400 usec
DE              6.00 usec
TE              300.0 K
D1           1.00000000 sec

============ CHANNEL f1 =============
NUC1                1H
P1             10.50 usec
PL1            -3.00 dB
SFO1       300.1319477 MHz

F2 - Processing parameters
SI                 65536
SF         300.1299964 MHz
WDW                   EM
SSB                    0
LB              0.10 Hz
GB                     0
PC                  1.00

1D NMR plot parameters
CX                20.00 cm
CY                 9.82 cm
F1P               10.000 ppm
F1              3001.30 Hz
F2P               -0.500 ppm
F2              -150.06 Hz
PPMCM          0.52500 ppm/cm
HZCM         157.56825 Hz/cm
```

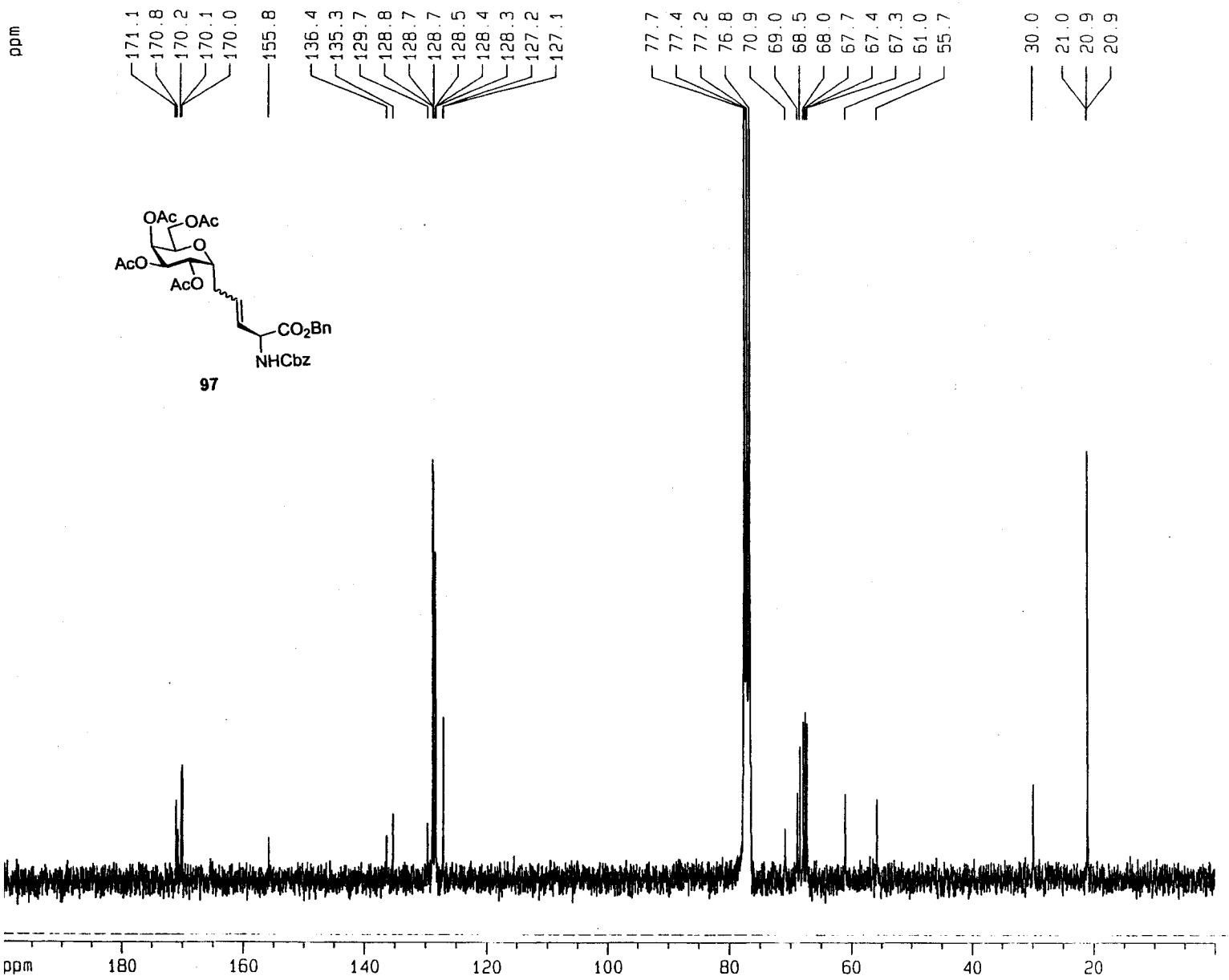

Current Data Parameters

NAME	rbs10607044
EXPNO	1
PROCNO	1

F2 - Acquisition Parameters

Date_	20040608
Time	7.59
INSTRUM	av300
PROBHD	5 mm QNP 1H/1
PULPROG	zgpg30
TD	32768
SOLVENT	CDCl3
NS	21831
DS	0
SWH	17985.611 Hz
FIDRES	0.548877 Hz
AQ	0.9110004 sec
RG	2298.8
DW	27.800 usec
DE	6.00 usec
TE	300.0 K
D1	1.00000000 sec
d11	0.03000000 sec
d12	0.00002000 sec

========== CHANNEL f1 ==========

NUC1	13C
P1	5.00 usec
PL1	-6.00 dB
SFO1	75.4752653 MHz

========== CHANNEL f2 ==========

CPDPRG2	waltz16
NUC2	1H
PCPD2	70.00 usec
PL2	-3.00 dB
PL12	13.48 dB
PL13	15.63 dB
SFO2	300.1314860 MHz

F2 - Processing parameters

SI	65536
SF	75.4677310 MHz
WDW	EM
SSB	0
LB	1.00 Hz
GB	0
PC	1.40

1D NMR plot parameters

CX	20.00 cm
CY	123.55 cm
F1P	200.000 ppm
F1	15093.55 Hz
F2P	0.000 ppm
F2	0.00 Hz
PPMCM	10.00000 ppm/cm
HZCM	754.67725 Hz/cm

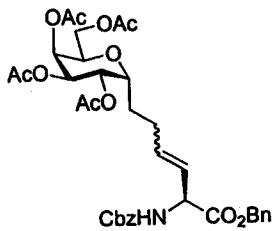

98

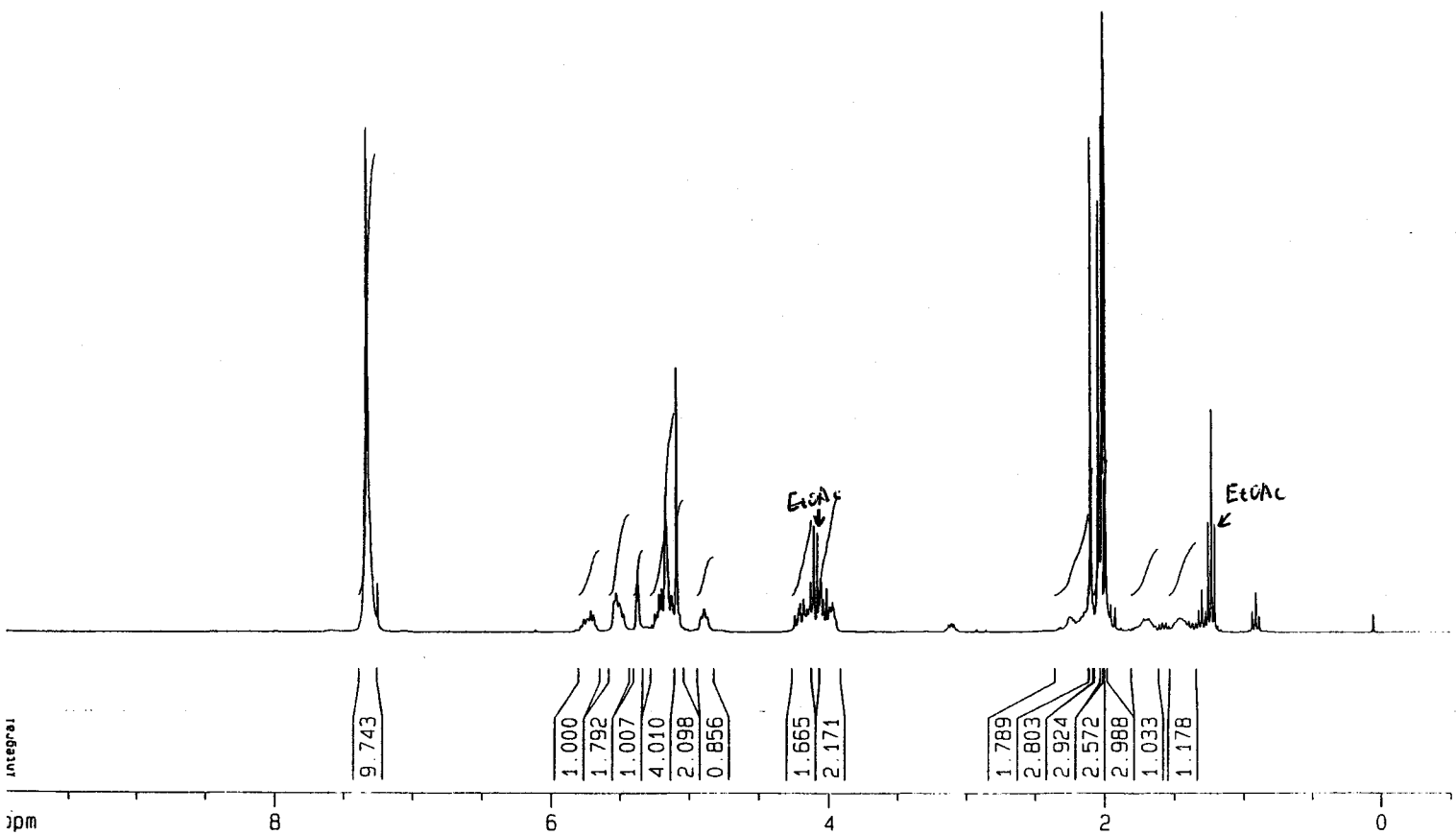


```
Current Data Parameters
NAME                  rbs10513042
EXPNO                           1
PROCNO                          1

F2 - Acquisition Parameters
Date_                    20040513
Time                        19.58
INSTRUM                     av300
PROBHD   5 mm QNP  1H/1
PULPROG                     zg30
TD                         30720
SOLVENT                    CDCl3
NS                             16
DS                              0
SWH                   5081.301 Hz
FIDRES                0.165407 Hz
AQ                    3.0228980 sec
RG                         80.6
DW                    98.400 usec
DE                     6.00 usec
TE                     300.0 K
D1                    1.00000000 sec

============ CHANNEL f1 =============
NUC1                           1H
P1                     10.50 usec
PL1                    -3.00 dB
SFO1                300.1319477 MHz

F2 - Processing parameters
SI                         65536
SF                  300.1299975 MHz
WDW                           EM
SSB                            0
LB                     0.10 Hz
GB                             0
PC                          1.00

1D NMR plot parameters
CX                     20.00 cm
CY                      8.47 cm
F1P                   10.000 ppm
F1                   3001.30 Hz
F2P                   -0.500 ppm
F2                   -150.06 Hz
PPMCM                 0.52500 ppm/cm
HZCM                157.56825 Hz/cm
```

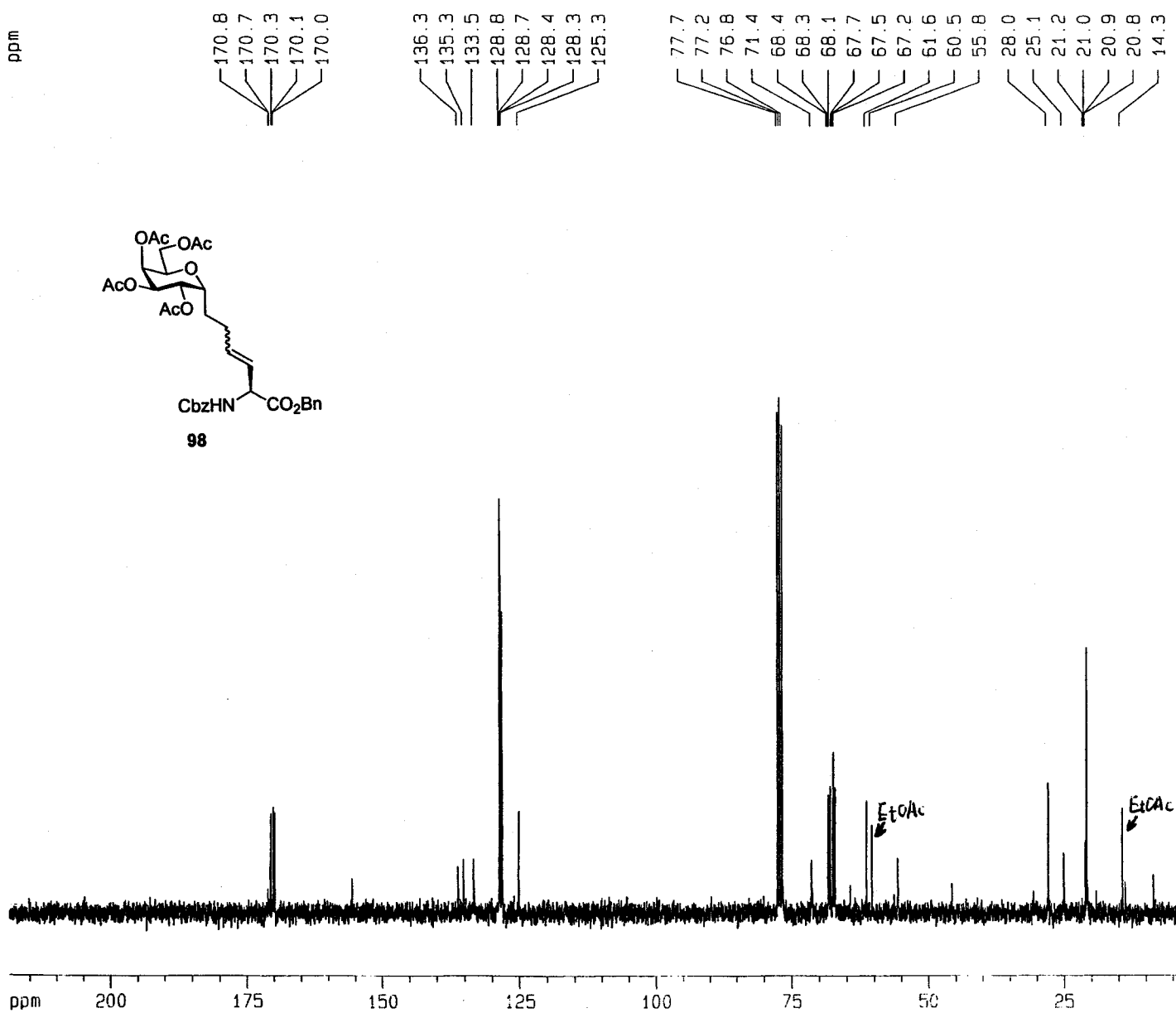

Current Data Parameters

NAME	rbs10513042
EXPNO	2
PROCNO	1

F2 - Acquisition Parameters

Date_	20040513
Time	19.59
INSTRUM	av300
PROBHD	5 mm QNP 1H/1
PULPROG	zgpg30
TD	32768
SOLVENT	CDCl3
NS	193
DS	0
SWH	17985.611 Hz
FIDRES	0.548877 Hz
AQ	0.9110004 sec
RG	2896.3
DW	27.800 usec
DE	6.00 usec
TE	300.0 K
D1	1.00000000 sec
d11	0.03000000 sec
d12	0.00002000 sec

========== CHANNEL f1 ==========

NUC1	13C
P1	5.00 usec
PL1	-6.00 dB
SFO1	75.4752653 MHz

========== CHANNEL f2 ==========

CPDPRG2	waltz16
NUC2	1H
PCPD2	70.00 usec
PL2	-3.00 dB
PL12	13.48 dB
PL13	15.63 dB
SFO2	300.1314860 MHz

F2 - Processing parameters

SI	65536
SF	75.4677362 MHz
WDW	EM
SSB	0
LB	1.00 Hz
GB	0
PC	1.40

1D NMR plot parameters

CX	20.00 cm
CY	8.17 cm
F1P	220.000 ppm
F1	16602.90 Hz
F2P	-10.000 ppm
F2	-754.68 Hz
PPMCM	11.50000 ppm/cm
HZCM	867.87897 Hz/cm

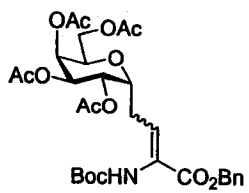

109

Current Data Parameters
NAME rbslACHsubstrate
EXPNO 1
PROCNO 1

F2 - Acquisition Parameters
Date_ 20060315
Time 13.42
INSTRUM spect
PROBHD 5 mm QNP 1H/1
PULPROG zg30
TD 30720
SOLVENT CDCl3
NS 21
DS 0
SWH 5081.301 Hz
FIDRES 0.165407 Hz
AQ 3.0228980 sec
RG 128
DW 98.400 usec
DE 6.00 usec
TE 300.0 K
D1 1.00000000 sec

======== CHANNEL f1 ========
NUC1 1H
P1 10.00 usec
PL1 -3.00 dB
SFO1 300.1319477 MHz

F2 - Processing parameters
SI 65536
SF 300.1300090 MHz
WDW EM
SSB 0
LB 0.10 Hz
GB 0
PC 1.00

1D NMR plot parameters
CX 20.00 cm
CY 10.77 cm
F1P 10.000 ppm
F1 3001.30 Hz
F2P -0.500 ppm
F2 -150.06 Hz
PPMCM 0.52500 ppm/cm
HZCM 157.56825 Hz/cm

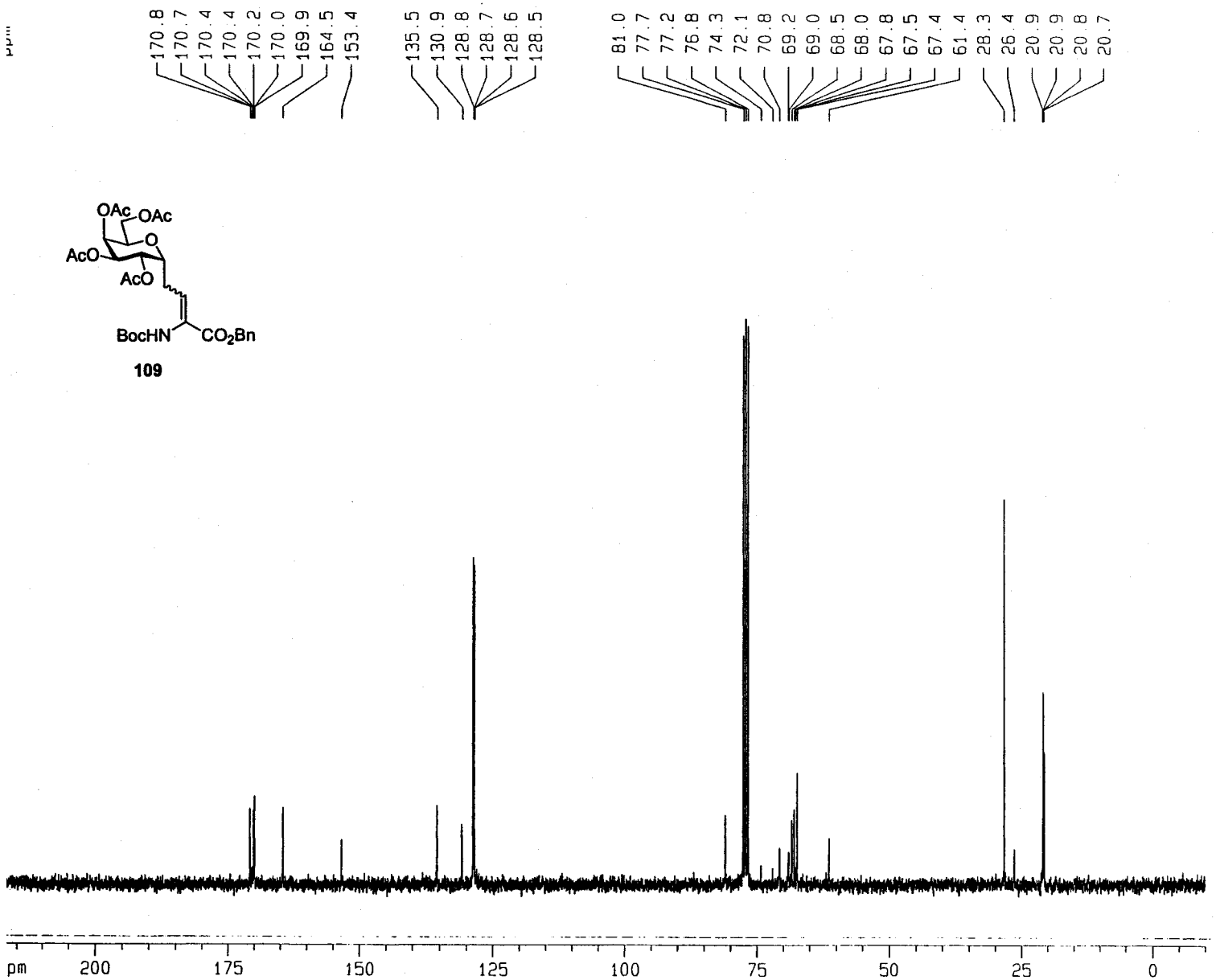

Current Data Parameters
NAME rbs1ACHsubstrate
EXPNO 2
PROCNO 1

F2 - Acquisition Parameters
Date_ 20060315
Time 13.44
INSTRUM spect
PROBHD 5 mm QNP 1H/1
PULPROG zgpg30
TD 32768
SOLVENT CDCl3
NS 732
DS 0
SWH 17985.611 Hz
FIDRES 0.548877 Hz
AQ 0.9110004 sec
RG 3649.1
DW 27.800 usec
DE 6.00 usec
TE 300.0 K
D1 1.00000000 sec
d11 0.03000000 sec
d12 0.00002000 sec

======== CHANNEL f1 ========
NUC1 13C
P1 5.10 usec
PL1 -6.00 dB
SFO1 75.4752653 MHz

======== CHANNEL f2 ========
CPDPRG2 waltz16
NUC2 1H
PCPD2 73.00 usec
PL2 -3.00 dB
PL12 15.00 dB
PL13 120.00 dB
SFO2 300.1314860 MHz

F2 - Processing parameters
SI 65536
SF 75.4677365 MHz
WDW EM
SSB 0
LB 1.00 Hz
GB 0
PC 1.40

1D NMR plot parameters
CX 20.00 cm
CY 9.26 cm
F1P 220.000 ppm
F1 16602.90 Hz
F2P -10.000 ppm
F2 -754.68 Hz
PPMCM 11.50000 ppm/cm
HZCM 867.87897 Hz/cm

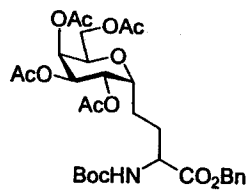

111

Current Data Parameters

NAME	asyhydro_ht
EXPNO	5
PROCNO	1

F2 - Acquisition Parameters

Date	25000000
Time	20.26
PULPROG	zg
SOLVENT	dmso
AQ	4.6530762 sec
FIDRES	0.107456 Hz
DW	500000.0 usec
RG	1024
NUCLEUS	1H
HL1	0 dB
D1	0.0100000 sec
P1	5.6 usec
DE	88.8 usec
SFO1	500.1405972 MHz
SWH	7042.25 Hz
TD	65536
NS	16
DS	0

F2 - Processing parameters

SI	32768
SF	500.1377900 MHz
WDW	EM
SSB	0
LB	0.30 Hz
GB	0
PC	1.00

1D NMR plot parameters

CX	22.00 cm
CY	22.31 cm
F1P	10.000 ppm
F1	5001.38 Hz
F2P	-0.500 ppm
F2	-250.07 Hz
PPMCM	0.47727 ppm/cm
HZCM	238.70212 Hz/cm

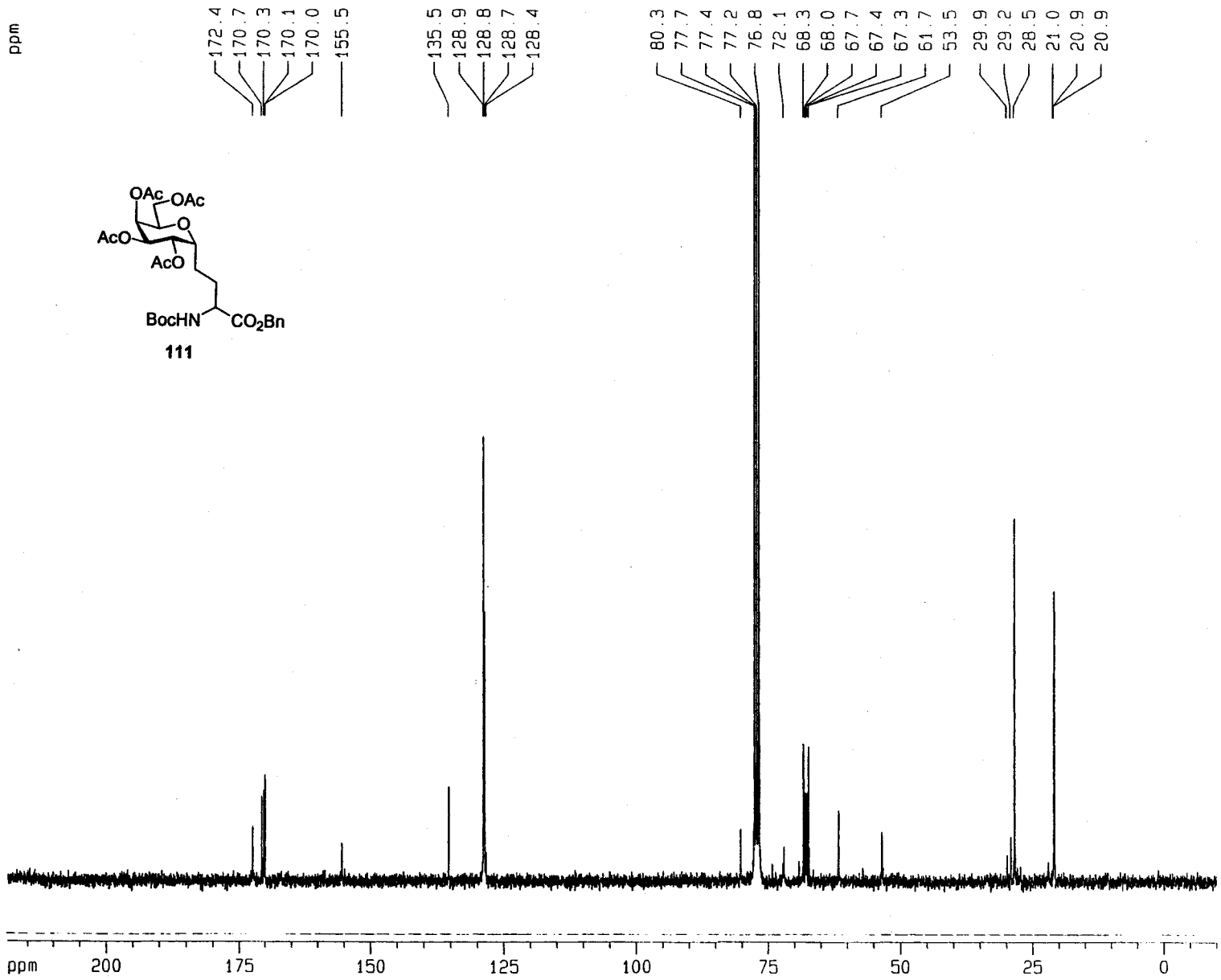

Current Data Parameters

NAME	RBSL111_verynew
EXPNO	2
PROCNO	1

F2 - Acquisition Parameters

Date_	20060318
Time	13.52
INSTRUM	spect
PROBHD	5 mm QNP 1H/1
PULPROG	zgpg30
TD	32768
SOLVENT	CDCl3
NS	6463
DS	0
SWH	17985.611 Hz
FIDRES	0.548877 Hz
AQ	0.9110004 sec
RG	3649.1
DW	27.800 usec
DE	6.00 usec
TE	300.0 K
D1	1.00000000 sec
d11	0.03000000 sec
d12	0.00002000 sec

======== CHANNEL f1 ========

NUC1	13C
P1	5.10 usec
PL1	-6.00 dB
SFO1	75.4752653 MHz

======== CHANNEL f2 ========

CPDPRG2	waltz16
NUC2	1H
PCPD2	73.00 usec
PL2	-3.00 dB
PL12	15.00 dB
PL13	120.00 dB
SFO2	300.1314860 MHz

F2 - Processing parameters

SI	65536
SF	75.4677351 MHz
WDW	EM
SSB	0
LB	1.00 Hz
GB	0
PC	1.40

1D NMR plot parameters

CX	20.00 cm
CY	27.05 cm
F1P	220.000 ppm
F1	16602.90 Hz
F2P	-10.000 ppm
F2	-754.68 Hz
PPMCM	11.50000 ppm/cm
HZCM	867.87885 Hz/cm

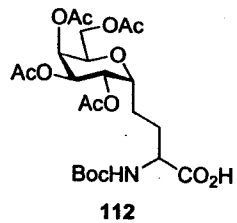

112

Current Data Parameters

NAME	rbsl1005031
EXPNO	1
PROCNO	1

F2 - Acquisition Parameters

Date_	20031005
Time	14.22
INSTRUM	av300
PROBHD	5 mm QNP 1H/1
PULPROG	zg30
TD	30720
SOLVENT	CDCl3
NS	128
DS	0
SWH	5081.301 Hz
FIDRES	0.165407 Hz
AQ	3.0228980 sec
RG	362
DW	98.400 usec
DE	6.00 usec
TE	300.0 K
D1	1.00000000 sec

========== CHANNEL f1 ==========

NUC1	1H
P1	10.50 usec
PL1	-3.00 dB
SFO1	300.1319477 MHz

F2 - Processing parameters

SI	65536
SF	300.1299972 MHz
WDW	EM
SSB	0
LB	0.10 Hz
GB	0
PC	1.00

1D NMR plot parameters

CX	20.00 cm
CY	12.25 cm
F1P	10.000 ppm
F1	3001.30 Hz
F2P	-0.500 ppm
F2	-150.06 Hz
PPMCM	0.52500 ppm/cm
HZCM	157.56825 Hz/cm

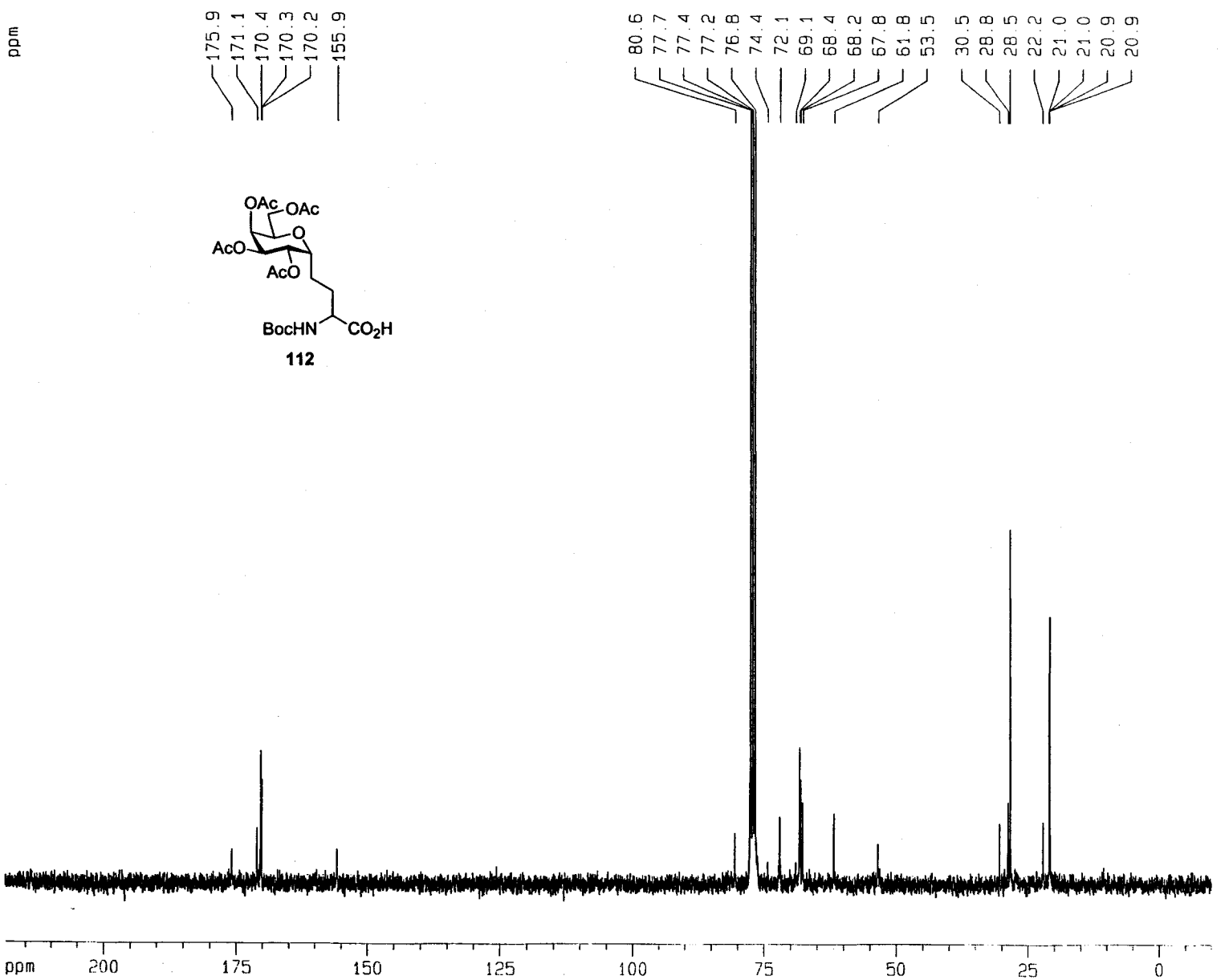

Current Data Parameters

NAME	rbs11005031
EXPNO	2
PROCNO	1

F2 - Acquisition Parameters

Date_	20031005
Time	14.51
INSTRUM	av300
PROBHD	5 mm QNP 1H/1
PULPROG	zgpg30
TD	32768
SOLVENT	CDCl3
NS	6006
DS	0
SWH	17985.611 Hz
FIDRES	0.548877 Hz
AQ	0.9110004 sec
RG	3649.1
DW	27.800 usec
DE	6.00 usec
TE	300.0 K
D1	1.00000000 sec
d11	0.03000000 sec
d12	0.00002000 sec

========== CHANNEL f1 ==========

NUC1	13C
P1	5.00 usec
PL1	-6.00 dB
SFO1	75.4752653 MHz

========== CHANNEL f2 ==========

CPDPRG2	waltz16
NUC2	1H
PCPD2	70.00 usec
PL2	-3.00 dB
PL12	13.48 dB
PL13	15.63 dB
SFO2	300.1314860 MHz

F2 - Processing parameters

SI	65536
SF	75.4677313 MHz
WDW	EM
SSB	0
LB	1.00 Hz
GB	0
PC	1.40

1D NMR plot parameters

CX	20.00 cm
CY	41.16 cm
F1P	220.000 ppm
F1	16602.90 Hz
F2P	-10.000 ppm
F2	-754.68 Hz
PPMCM	11.50000 ppm/cm
HZCM	867.87885 Hz/cm

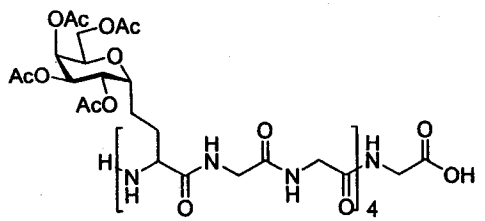

113

Current Data Parameters

NAME	rbs10330041
EXPNO	1
PROCNO	1

F2 - Acquisition Parameters

Date_	20040331
Time	12.00
INSTRUM	AV500WB
PROBHD	5 mm BBI 1H-BB
PULPROG	zg30
TD	65536
SOLVENT	CDCl3
NS	11831
DS	0
SWH	7440.476 Hz
FIDRES	0.113533 Hz
AQ	4.4040694 sec
RG	203.2
DW	67.200 usec
DE	6.00 usec
TE	300.0 K
D1	0.01000000 sec

======== CHANNEL f1 ========

NUC1	1H
P1	10.50 usec
PL1	3.00 dB
SFO1	500.1327766 MHz

F2 - Processing parameters

SI	65536
SF	500.1300150 MHz
WDW	EM
SSB	0
LB	0.00 Hz
GB	0
PC	1.00

1D NMR plot parameters

CX	20.00 cm
CY	20.42 cm
F1P	10.000 ppm
F1	5001.30 Hz
F2P	-0.500 ppm
F2	-250.06 Hz
PPMCM	0.52500 ppm/cm
HZCM	262.56824 Hz/cm

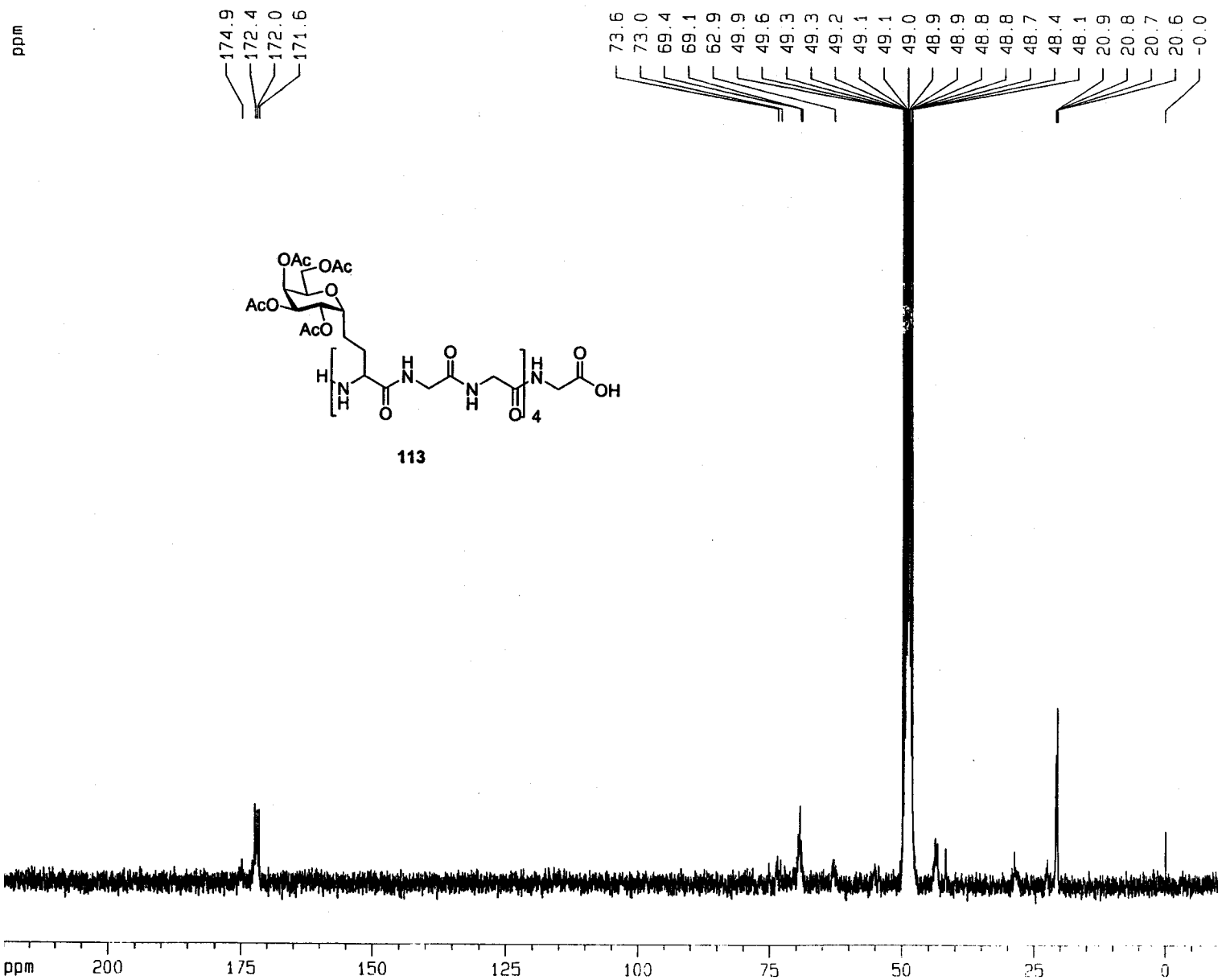

113

Current Data Parameters

NAME	rbs10331041
EXPNO	1
PROCNO	1

F2 - Acquisition Parameters

Date_	20040401
Time	8.39
INSTRUM	av300
PROBHD	5 mm QNP 1H/1
PULPROG	zgpg30
TD	32768
SOLVENT	CDCl3
NS	21578
DS	0
SWH	17985.611 Hz
FIDRES	0.548877 Hz
AQ	0.9110004 sec
RG	3649.1
DW	27.800 usec
DE	6.00 usec
TE	300.0 K
D1	1.00000000 sec
d11	0.03000000 sec
d12	0.00002000 sec

========== CHANNEL f1 ==========

NUC1	13C
P1	5.00 usec
PL1	-6.00 dB
SFO1	75.4752653 MHz

========== CHANNEL f2 ==========

CPDPRG2	waltz16
NUC2	1H
PCPD2	70.00 usec
PL2	-3.00 dB
PL12	13.48 dB
PL13	15.63 dB
SFO2	300.1314860 MHz

F2 - Processing parameters

SI	65536
SF	75.4676429 MHz
WDW	EM
SSB	0
LB	1.00 Hz
GB	0
PC	1.40

1D NMR plot parameters

CX	20.00 cm
CY	334.30 cm
F1P	220.000 ppm
F1	16602.88 Hz
F2P	-10.000 ppm
F2	-754.68 Hz
PPMCM	11.50000 ppm/cm
HZCM	867.87787 Hz/cm

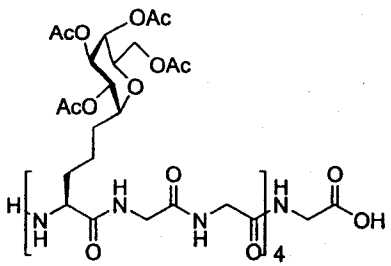

114


```
Current Data Parameters
NAME      rbslpolymer0722
EXPNO                  1
PROCNO                 1

F2 - Acquisition Parameters
Date_           20060312
Time               14.23
INSTRUM            spect
PROBHD   5 mm QNP  1H/1
PULPROG            zg30
TD                30720
SOLVENT           CDCl3
NS                   16
DS                    0
SWH           5081.301 Hz
FIDRES        0.165407 Hz
AQ            3.0228980 sec
RG                  362
DW             98.400 usec
DE              6.00 usec
TE              300.0 K
D1           1.00000000 sec

======== CHANNEL f1 ========
NUC1                1H
P1             10.00 usec
PL1             -3.00 dB
SFO1       300.1319477 MHz

F2 - Processing parameters
SI                65536
SF       300.1300030 MHz
WDW                  EM
SSB                   0
LB             0.10 Hz
GB                    0
PC                 1.00

1D NMR plot parameters
CX               20.00 cm
CY               23.94 cm
F1P           10.000 ppm
F1            3001.30 Hz
F2P           -0.500 ppm
F2            -150.06 Hz
PPMCM         0.52500 ppm/cm
HZCM          157.56825 Hz/cm
```

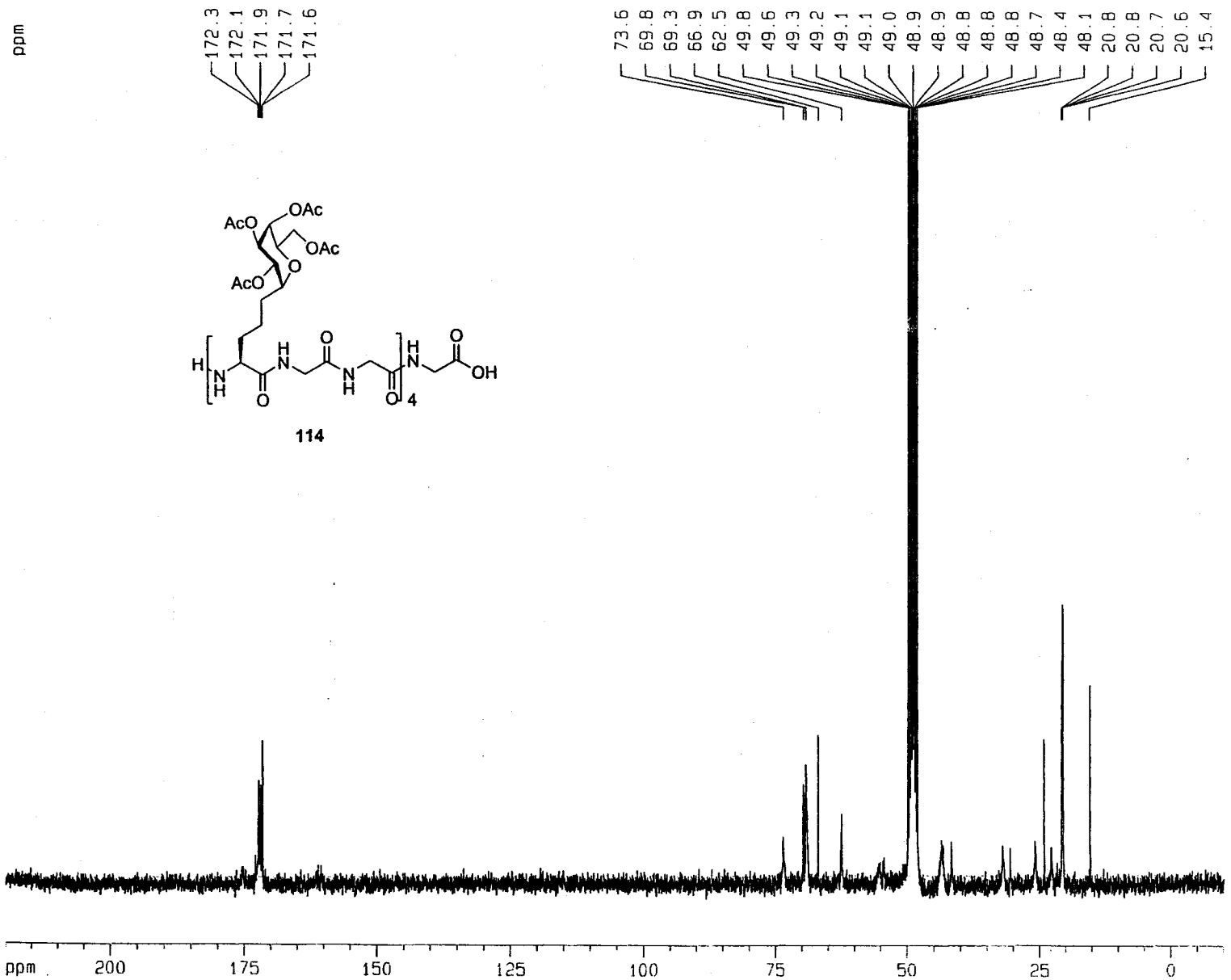

Current Data Parameters

NAME	rbs10728042
EXPNO	2
PROCNO	1

F2 - Acquisition Parameters

Date_	20040728
Time	21.07
INSTRUM	av300
PROBHD	5 mm QNP 1H/1
PULPROG	zgpg30
TD	32768
SOLVENT	CDCl3
NS	20946
DS	0
SWH	17985.611 Hz
FIDRES	0.548877 Hz
AQ	0.9110004 sec
RG	3649.1
DW	27.800 usec
DE	6.00 usec
TE	300.0 K
D1	1.00000000 sec
d11	0.03000000 sec
d12	0.00002000 sec

========== CHANNEL f1 ==========

NUC1	13C
P1	5.00 usec
PL1	-6.00 dB
SFO1	75.4752653 MHz

========== CHANNEL f2 ==========

CPDPRG2	waltz16
NUC2	1H
PCPD2	70.00 usec
PL2	-3.00 dB
PL12	13.48 dB
PL13	15.63 dB
SFO2	300.1314860 MHz

F2 - Processing parameters

SI	65536
SF	75.4676432 MHz
WDW	EM
SSB	0
LB	1.00 Hz
GB	0
PC	1.40

1D NMR plot parameters

CX	20.00 cm
CY	183.81 cm
F1P	220.000 ppm
F1	16602.88 Hz
F2P	-10.000 ppm
F2	-754.68 Hz
PPMCM	11.50000 ppm/cm
HZCM	867.87787 Hz/cm

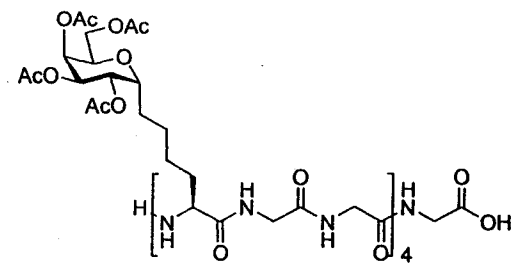

115

Current Data Parameters

NAME	rbslggb0705
EXPNO	1
PROCNO	1

F2 - Acquisition Parameters

Date_	20060312
Time	14.17
INSTRUM	spect
PROBHD	5 mm QNP 1H/1
PULPROG	zg30
TD	30720
SOLVENT	MeOD
NS	27
DS	0
SWH	5081.301 Hz
FIDRES	0.165407 Hz
AQ	3.0228980 sec
RG	512
DW	98.400 usec
DE	6.00 usec
TE	300.0 K
D1	1.00000000 sec

======== CHANNEL f1 ========

NUC1	1H
P1	10.00 usec
PL1	-3.00 dB
SFO1	300.1319477 MHz

F2 - Processing parameters

SI	65536
SF	300.1300032 MHz
WDW	EM
SSB	0
LB	0.10 Hz
GB	0
PC	1.00

1D NMR plot parameters

CX	20.00 cm
CY	52.95 cm
F1P	10.000 ppm
F1	3001.30 Hz
F2P	-0.500 ppm
F2	-150.06 Hz
PPMCM	0.52500 ppm/cm
HZCM	157.56825 Hz/cm

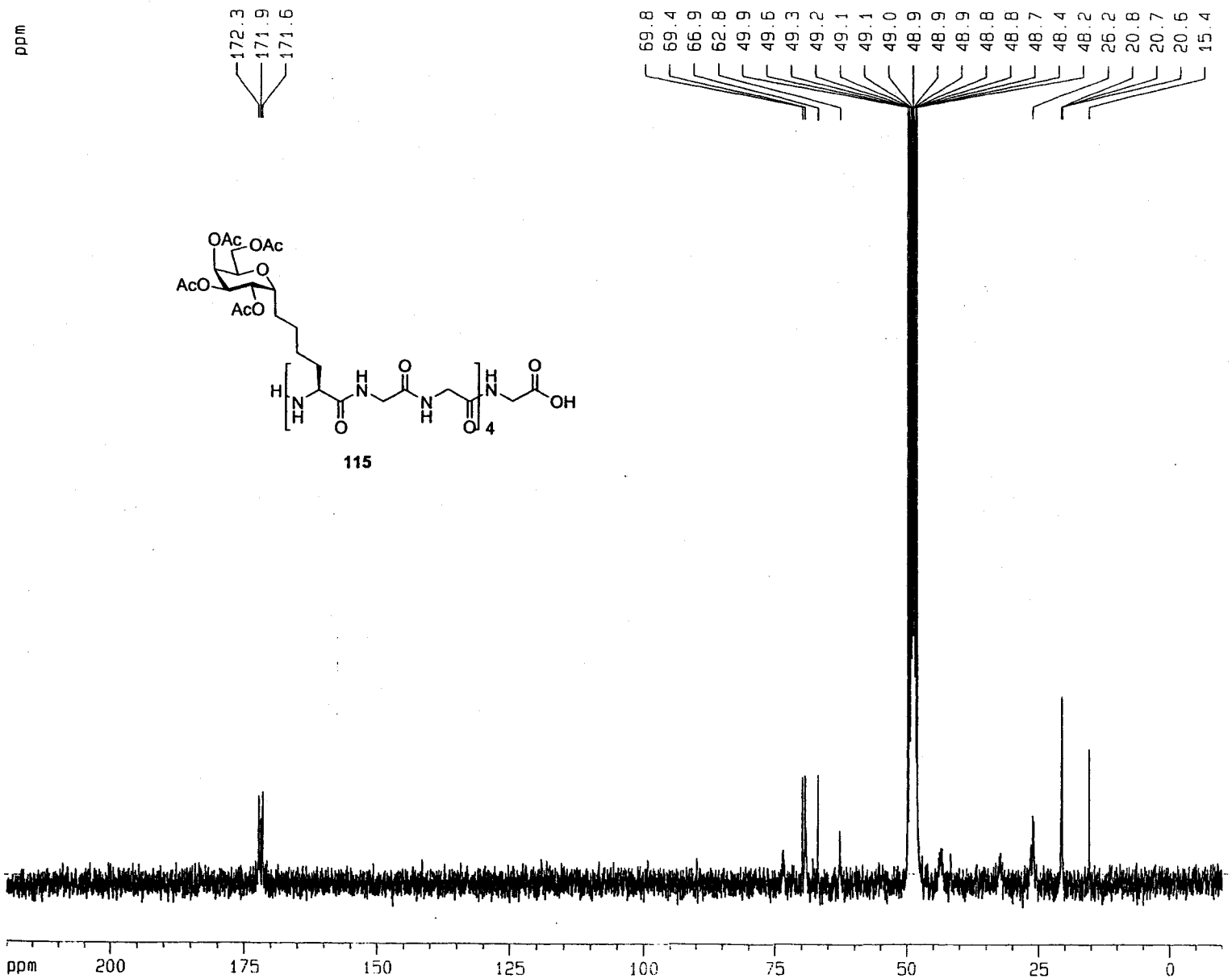

115

```
Current Data Parameters
NAME                  rbs1071104
EXPNO                          2
PROCNO                         1

F2 - Acquisition Parameters
Date_                  20040711
Time                      21.07
INSTRUM                   av300
PROBHD   5 mm QNP  1H/1
PULPROG                 zgpg30
TD                         32768
SOLVENT                   CDCl3
NS                         21492
DS                             0
SWH                17985.611 Hz
FIDRES              0.548877 Hz
AQ                  0.9110004 sec
RG                       5160.6
DW                       27.800 usec
DE                        6.00 usec
TE                       300.0 K
D1                  1.00000000 sec
d11                 0.03000000 sec
d12                 0.00002000 sec

========== CHANNEL f1 ==========
NUC1                        13C
P1                         5.00 usec
PL1                       -6.00 dB
SFO1                75.4752653 MHz

========== CHANNEL f2 ==========
CPDPRG2                 waltz16
NUC2                        1H
PCPD2                     70.00 usec
PL2                       -3.00 dB
PL12                      13.48 dB
PL13                      15.63 dB
SFO2               300.1314860 MHz

F2 - Processing parameters
SI                         65536
SF                  75.4676423 MHz
WDW                           EM
SSB                            0
LB                         1.00 Hz
GB                             0
PC                          1.40

1D NMR plot parameters
CX                        20.00 cm
CY                       366.76 cm
F1P                     220.000 ppm
F1                    16602.88 Hz
F2P                     -10.000 ppm
F2                     -754.68 Hz
PPMCM                  11.50000 ppm/cm
HZCM                 867.87787 Hz/cm
```

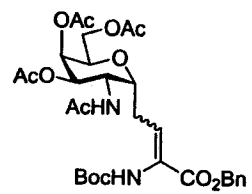

123

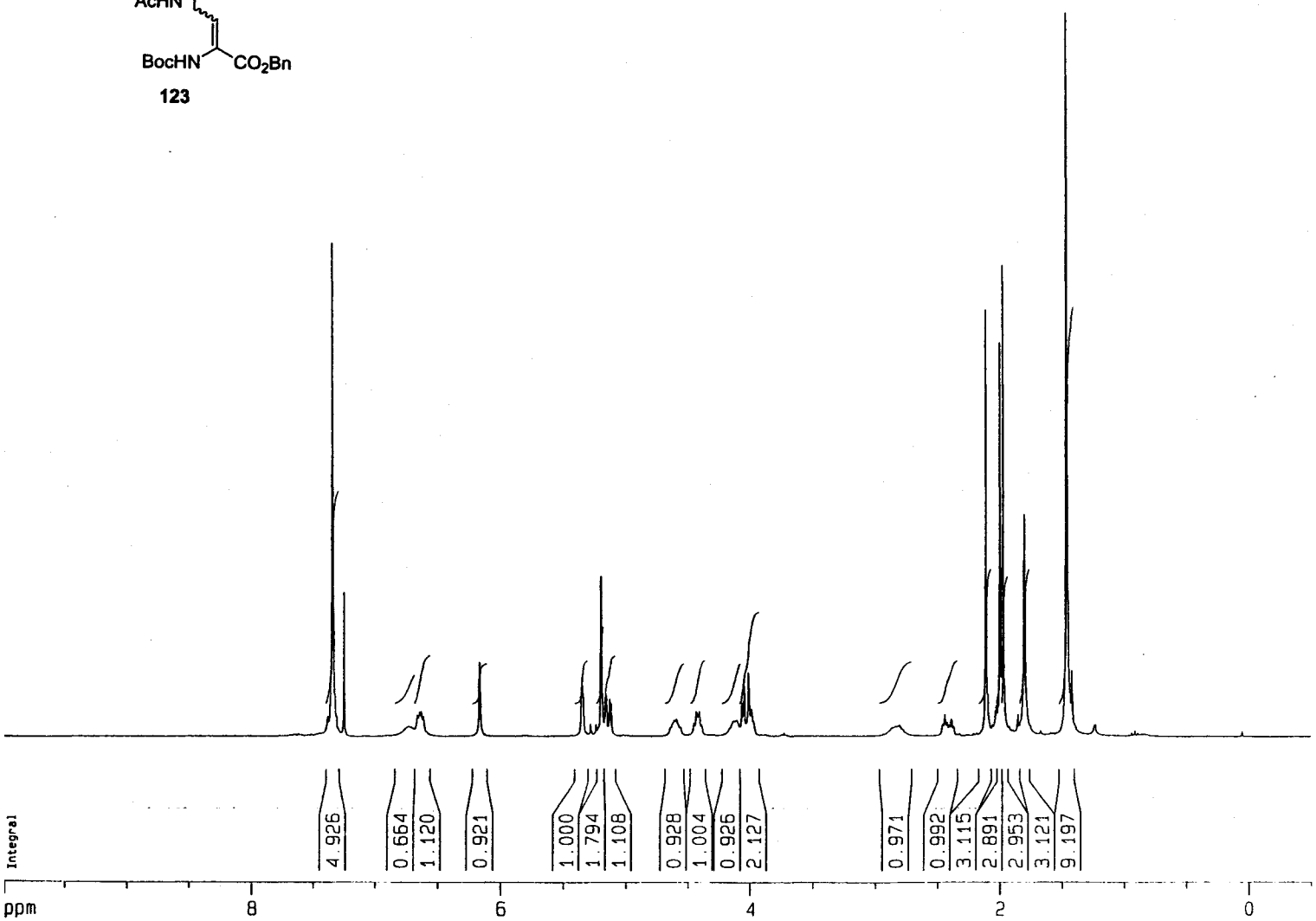

Current Data Parameters

NAME	rbs1123
EXPNO	1
PROCNO	1

F2 - Acquisition Parameters

Date_	20060224
Time	11.04
INSTRUM	spect
PROBHD	5 mm QNP 1H/1
PULPROG	zg30
TD	30720
SOLVENT	CDCl3
NS	28
DS	0
SWH	5081.301 Hz
FIDRES	0.165407 Hz
AQ	3.0228980 sec
RG	287.4
DW	98.400 usec
DE	6.00 usec
TE	300.0 K
D1	1.00000000 sec

======== CHANNEL f1 ========

NUC1	1H
P1	10.00 usec
PL1	-3.00 dB
SFO1	300.1319477 MHz

F2 - Processing parameters

SI	65536
SF	300.1300093 MHz
WDW	EM
SSB	0
LB	0.10 Hz
GB	0
PC	1.00

1D NMR plot parameters

CX	20.00 cm
CY	14.52 cm
F1P	10.000 ppm
F1	3001.30 Hz
F2P	-0.500 ppm
F2	-150.06 Hz
PPMCM	0.52500 ppm/cm
HZCM	157.56825 Hz/cm

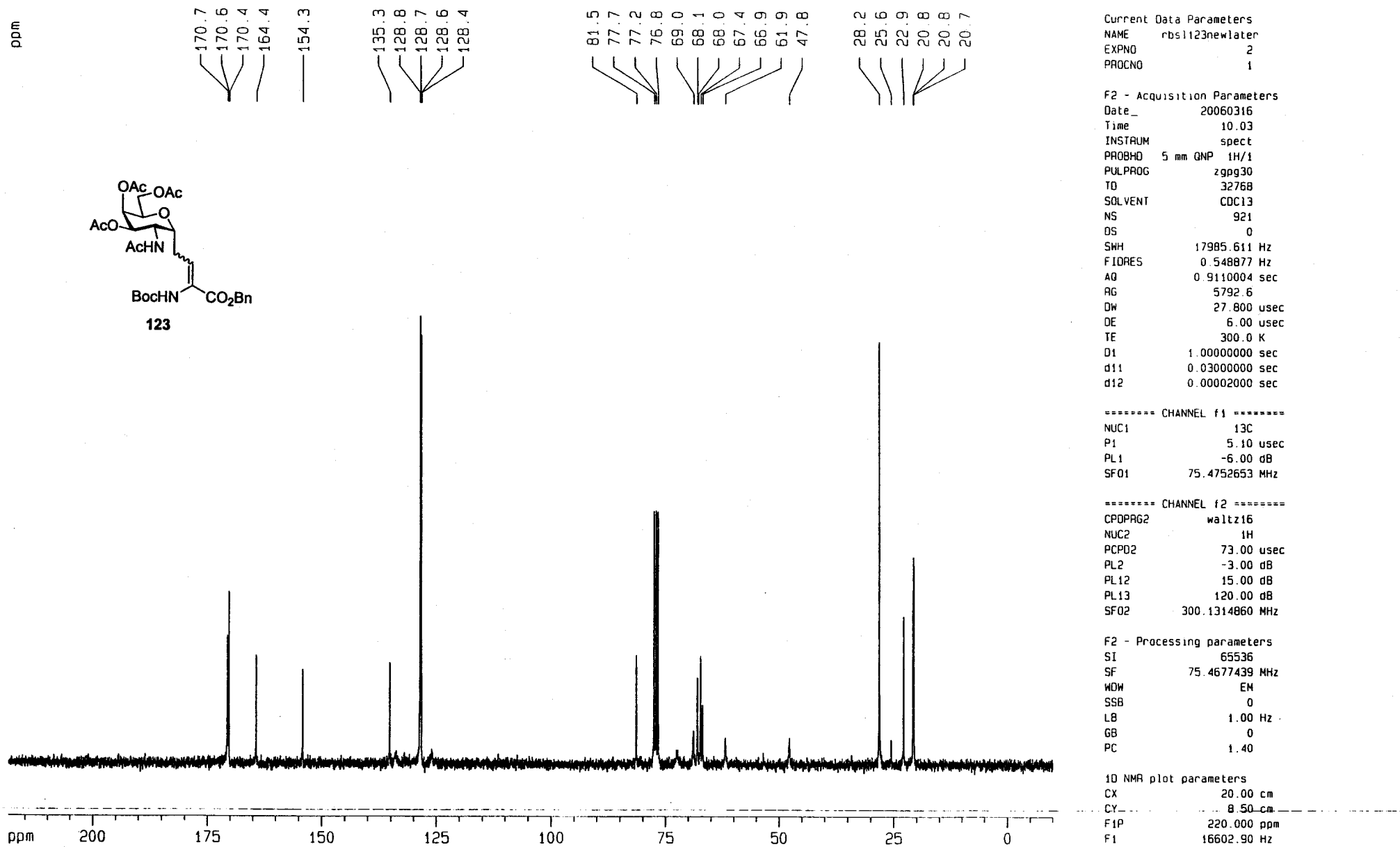

Current Data Parameters

NAME	rbsl123newlater
EXPNO	2
PROCNO	1

F2 - Acquisition Parameters

Date_	20060316
Time	10.03
INSTRUM	spect
PROBHD	5 mm QNP 1H/1
PULPROG	zgpg30
TD	32768
SOLVENT	CDCl3
NS	921
DS	0
SWH	17985.611 Hz
FIDRES	0.548877 Hz
AQ	0.9110004 sec
RG	5792.6
DW	27.800 usec
DE	6.00 usec
TE	300.0 K
D1	1.00000000 sec
d11	0.03000000 sec
d12	0.00002000 sec

======== CHANNEL f1 ========

NUC1	13C
P1	5.10 usec
PL1	-6.00 dB
SFO1	75.4752653 MHz

======== CHANNEL f2 ========

CPDPRG2	waltz16
NUC2	1H
PCPD2	73.00 usec
PL2	-3.00 dB
PL12	15.00 dB
PL13	120.00 dB
SFO2	300.1314860 MHz

F2 - Processing parameters

SI	65536
SF	75.4677439 MHz
WDW	EM
SSB	0
LB	1.00 Hz
GB	0
PC	1.40

1D NMR plot parameters

CX	20.00 cm
CY	8.50 cm
F1P	220.000 ppm
F1	16602.90 Hz
F2P	-10.000 ppm
F2	-754.68 Hz
PPMCM	11.50000 ppm/cm
HZCM	867.87903 Hz/cm

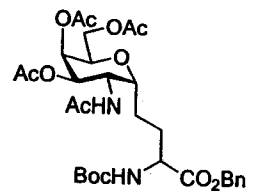

124

Current Data Parameters
NAME suhuai_vt_11jan
EXPNO 1
PROCNO 1

F2 - Acquisition Parameters
Date_ 20050111
Time 8.18
INSTRUM AV500WB
PROBHD 5 mm TBO BB/1H
PULPROG zg30
TD 65536
SOLVENT DMSO
NS 16
DS 0
SWH 7440.476 Hz
FIDRES 0.113533 Hz
AQ 4.4040694 sec
RG 203.2
DW 67.200 usec
DE 6.00 usec
TE 300.0 K
D1 0.01000000 sec

======== CHANNEL f1 ========
NUC1 1H
P1 14.00 usec
PL1 0.00 dB
SFO1 500.1327766 MHz

F2 - Processing parameters
SI 65536
SF 500.1300048 MHz
WDW EM
SSB 0
LB 0.20 Hz
GB 0
PC 1.00

1D NMR plot parameters
CX 20.00 cm
CY 97.36 cm
F1P 10.000 ppm
F1 5001.30 Hz
F2P -0.500 ppm
F2 -250.06 Hz
PPMCM 0.52500 ppm/cm
HZCM 262.56824 Hz/cm

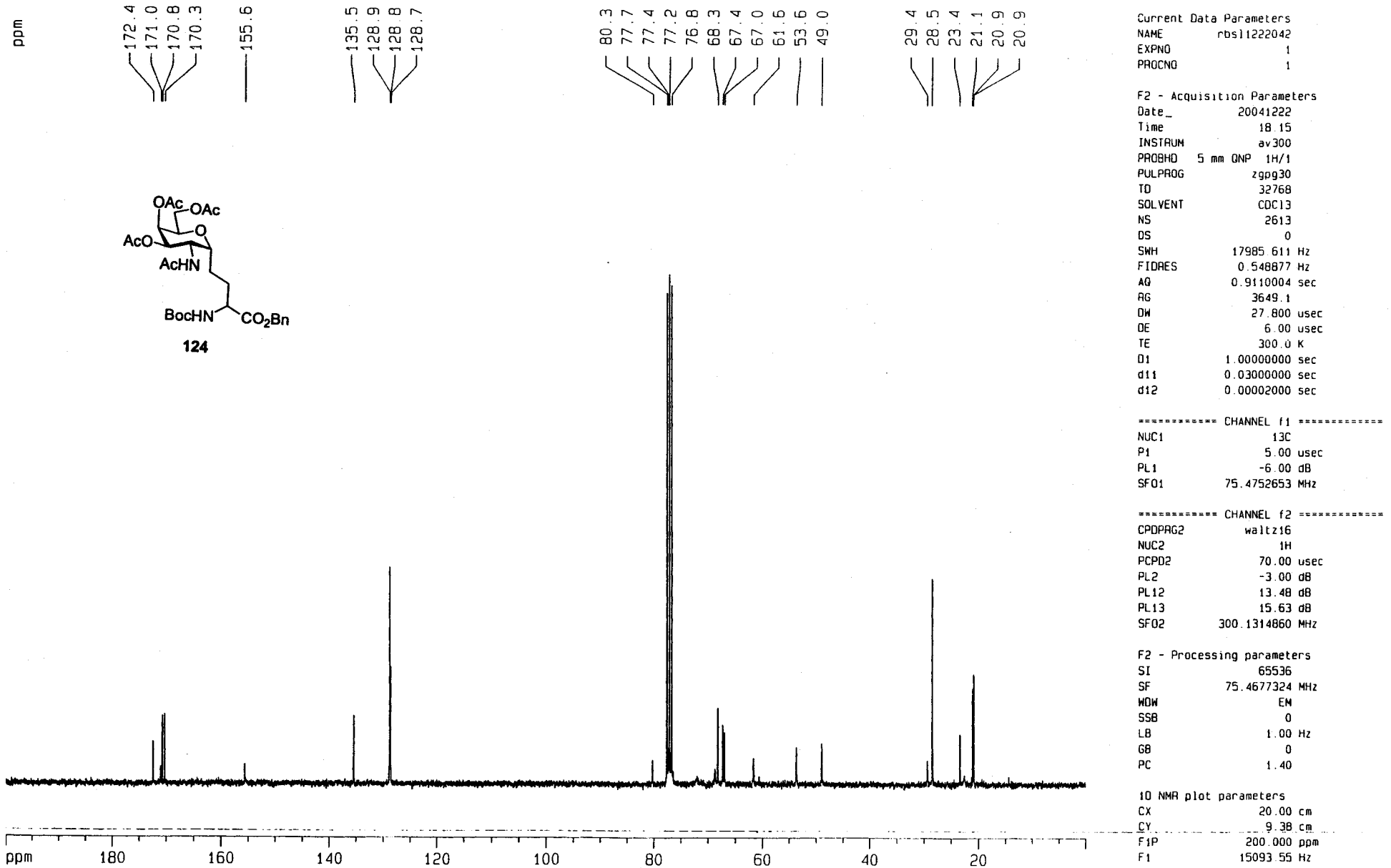

Current Data Parameters

NAME	rbs11222042
EXPNO	1
PROCNO	1

F2 - Acquisition Parameters

Date_	20041222
Time	18.15
INSTRUM	av300
PROBHD	5 mm QNP 1H/1
PULPROG	zgpg30
TD	32768
SOLVENT	CDCl3
NS	2613
DS	0
SWH	17985.611 Hz
FIDRES	0.548877 Hz
AQ	0.9110004 sec
RG	3649.1
DW	27.800 usec
DE	6.00 usec
TE	300.0 K
D1	1.00000000 sec
d11	0.03000000 sec
d12	0.00002000 sec

========== CHANNEL f1 ==========

NUC1	13C
P1	5.00 usec
PL1	-6.00 dB
SFO1	75.4752653 MHz

========== CHANNEL f2 ==========

CPDPRG2	waltz16
NUC2	1H
PCPD2	70.00 usec
PL2	-3.00 dB
PL12	13.48 dB
PL13	15.63 dB
SFO2	300.1314860 MHz

F2 - Processing parameters

SI	65536
SF	75.4677324 MHz
WDW	EM
SSB	0
LB	1.00 Hz
GB	0
PC	1.40

1D NMR plot parameters

CX	20.00 cm
CY	9.38 cm
F1P	200.000 ppm
F1	15093.55 Hz
F2P	0.000 ppm
F2	0.00 Hz
PPMCM	10.00000 ppm/cm
HZCM	754.67737 Hz/cm

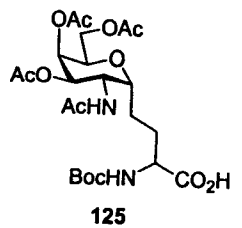

125


```
Current Data Parameters
NAME         rbs10506051
EXPNO                  1
PROCNO                 1

F2 - Acquisition Parameters
Date_          20050506
Time              20.24
INSTRUM           av300
PROBHD   5 mm QNP  1H/1
PULPROG           zg30
TD               30720
SOLVENT          CDCl3
NS                 256
DS                   0
SWH           5081.301 Hz
FIDRES        0.165407 Hz
AQ            3.0228980 sec
RG                574.7
DW               98.400 usec
DE                6.00 usec
TE               300.0 K
D1            1.00000000 sec

============ CHANNEL f1 =============
NUC1                1H
P1                10.50 usec
PL1               -3.00 dB
SFO1         300.1319477 MHz

F2 - Processing parameters
SI                 65536
SF          300.1299972 MHz
WDW                   EM
SSB                    0
LB                0.10 Hz
GB                     0
PC                1.00

1D NMR plot parameters
CX                20.00 cm
CY                20.50 cm
F1P               10.000 ppm
F1              3001.30 Hz
F2P               -0.500 ppm
F2              -150.06 Hz
PPMCM          0.52500 ppm/cm
HZCM          157.56825 Hz/cm
```

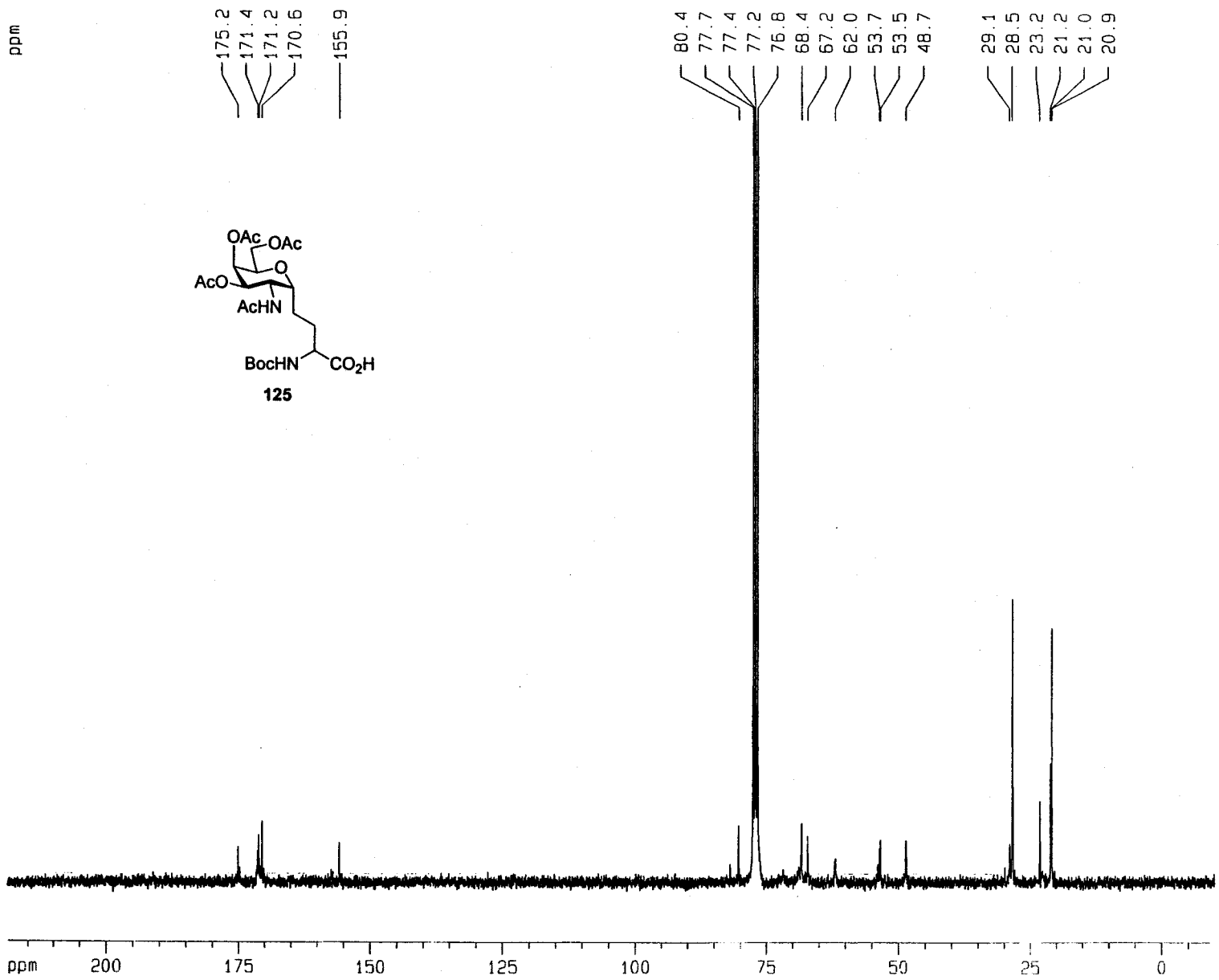

Current Data Parameters

NAME	rbs10509052
EXPNO	1
PROCNO	1

F2 - Acquisition Parameters

Date_	20050509
Time	19.58
INSTRUM	av300
PROBHD	5 mm QNP 1H/1
PULPROG	zgpg30
TD	32768
SOLVENT	CDCl3
NS	24553
DS	0
SWH	17985.611 Hz
FIDRES	0.548877 Hz
AQ	0.9110004 sec
RG	11585.2
DW	27.800 usec
DE	6.00 usec
TE	300.0 K
D1	1.00000000 sec
d11	0.03000000 sec
d12	0.00002000 sec

========== CHANNEL f1 ==========

NUC1	13C
P1	5.00 usec
PL1	-6.00 dB
SFO1	75.4752653 MHz

========== CHANNEL f2 ==========

CPDPRG2	waltz16
NUC2	1H
PCPD2	70.00 usec
PL2	-3.00 dB
PL12	13.48 dB
PL13	15.63 dB
SFO2	300.1314860 MHz

F2 - Processing parameters

SI	65536
SF	75.4677315 MHz
WDW	EM
SSB	0
LB	1.00 Hz
GB	0
PC	1.40

1D NMR plot parameters

CX	20.00 cm
CY	55.57 cm
F1P	220.000 ppm
F1	16602.90 Hz
F2P	-10.000 ppm
F2	-754.68 Hz
PPMCM	11.50000 ppm/cm
HZCM	867.87897 Hz/cm

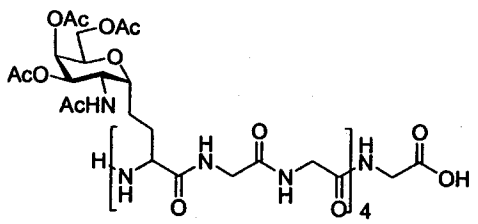

126


```
Current Data Parameters
NAME         rbs10305051
EXPNO                  1
PROCNO                 1

F2 - Acquisition Parameters
Date_          20050305
Time              17.31
INSTRUM           av300
PROBHD   5 mm QNP  1H/1
PULPROG           zg30
TD               30720
SOLVENT          CDCl3
NS                 256
DS                   0
SWH           5081.301 Hz
FIDRES        0.165407 Hz
AQ            3.0228980 sec
RG                287.4
DW               98.400 usec
DE                6.00 usec
TE               300.0 K
D1           1.00000000 sec

============ CHANNEL f1 =============
NUC1                1H
P1               10.50 usec
PL1              -3.00 dB
SFO1        300.1319477 MHz

F2 - Processing parameters
SI                 65536
SF          300.1295263 MHz
WDW                   EM
SSB                    0
LB                0.10 Hz
GB                     0
PC                1.00

1D NMR plot parameters
CX               20.00 cm
CY                9.88 cm
F1P              10.000 ppm
F1             3001.30 Hz
F2P              -0.500 ppm
F2             -150.06 Hz
PPMCM          0.52500 ppm/cm
HZCM          157.56799 Hz/cm
```

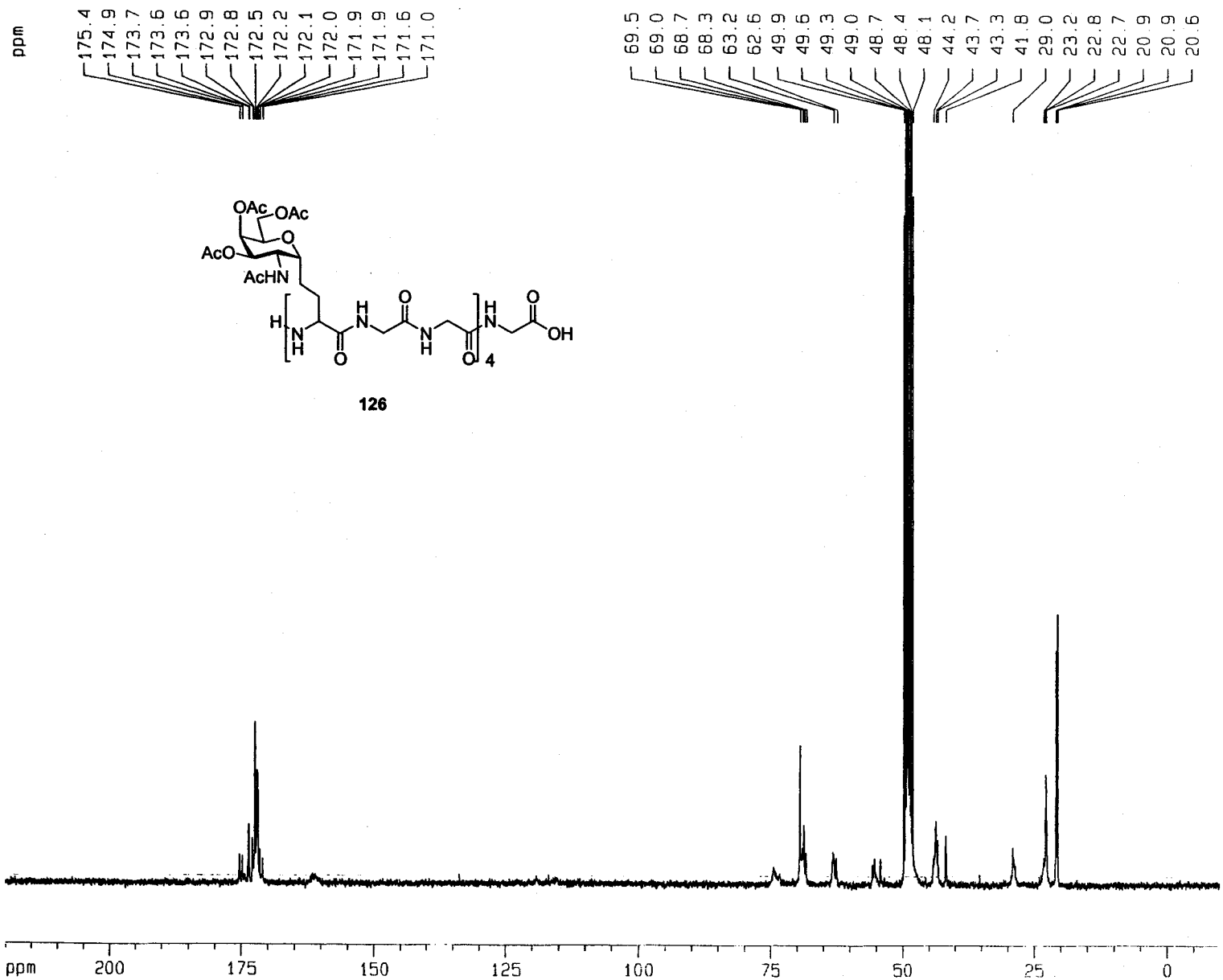

126

```
Current Data Parameters
NAME          rbs10402051
EXPNO                   1
PROCNO                  1

F2 - Acquisition Parameters
Date_           20050402
Time               19.55
INSTRUM            av300
PROBHD   5 mm QNP  1H/1
PULPROG          zgpg30
TD                32768
SOLVENT           CDCl3
NS                28868
DS                    0
SWH           17985.611 Hz
FIDRES        0.548877 Hz
AQ            0.9110004 sec
RG               3649.1
DW               27.800 usec
DE                6.00 usec
TE               300.0 K
D1            1.00000000 sec
d11           0.03000000 sec
d12           0.00002000 sec

============ CHANNEL f1 ============
NUC1                13C
P1                5.00 usec
PL1              -6.00 dB
SFO1         75.4752653 MHz

============ CHANNEL f2 ============
CPDPRG2         waltz16
NUC2                1H
PCPD2            70.00 usec
PL2              -3.00 dB
PL12             13.48 dB
PL13             15.63 dB
SFO2        300.1314860 MHz

F2 - Processing parameters
SI                65536
SF           75.4675235 MHz
WDW                  EM
SSB                   0
LB                 1.00 Hz
GB                    0
PC                 1.40

1D NMR plot parameters
CX                20.00 cm
CY                76.97 cm
F1P              220.000 ppm
F1             16602.85 Hz
F2P              -10.000 ppm
F2              -754.68 Hz
PPMCM          11.50000 ppm/cm
HZCM          867.87646 Hz/cm
```

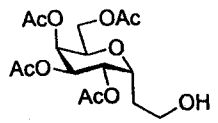

129

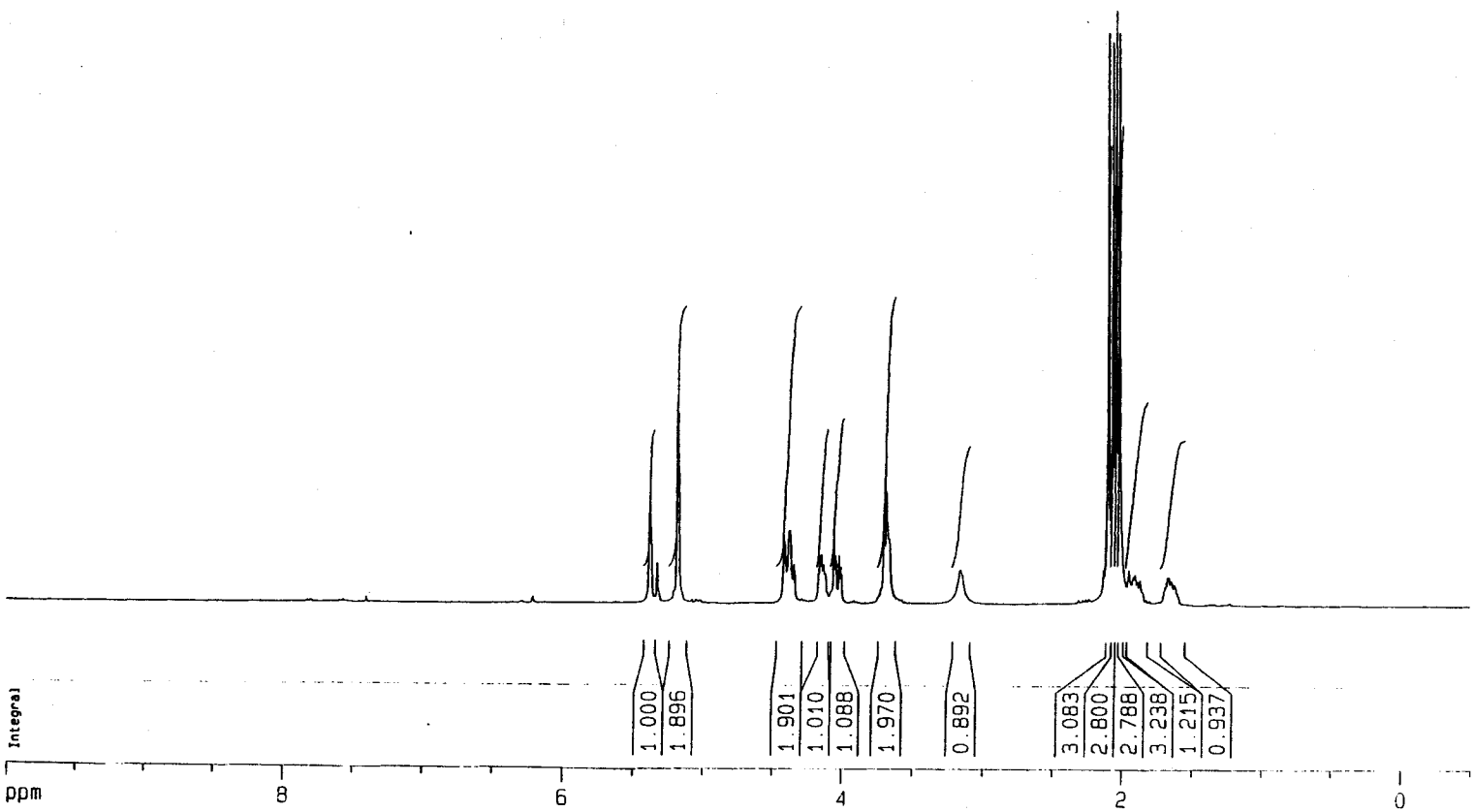


```
Current Data Parameters
NAME                  rbsIgalOH
EXPNO                         1
PROCNO                        1

F2 - Acquisition Parameters
Date_                  20060228
Time                      16.25
INSTRUM                   spect
PROBHD   5 mm QNP  1H/1
PULPROG                   zg30
TD                       30720
SOLVENT                  CDCl3
NS                          16
DS                           0
SWH                5081.301 Hz
FIDRES             0.165407 Hz
AQ                 3.0228980 sec
RG                        20.2
DW                   98.400 usec
DE                    6.00 usec
TE                    300.0 K
D1                 1.00000000 sec

======== CHANNEL f1 ========
NUC1                      1H
P1                   10.00 usec
PL1                   -3.00 dB
SFO1           300.1319477 MHz

F2 - Processing parameters
SI                       65536
SF             300.1299647 MHz
WDW                         EM
SSB                          0
LB                    0.10 Hz
GB                           0
PC                        1.00

1D NMR plot parameters
CX                   20.00 cm
CY                    8.05 cm
F1P                 10.000 ppm
F1                3001.30 Hz
F2P                 -0.500 ppm
F2                -150.06 Hz
PPMCM              0.52500 ppm/cm
HZCM             157.56824 Hz/cm
```

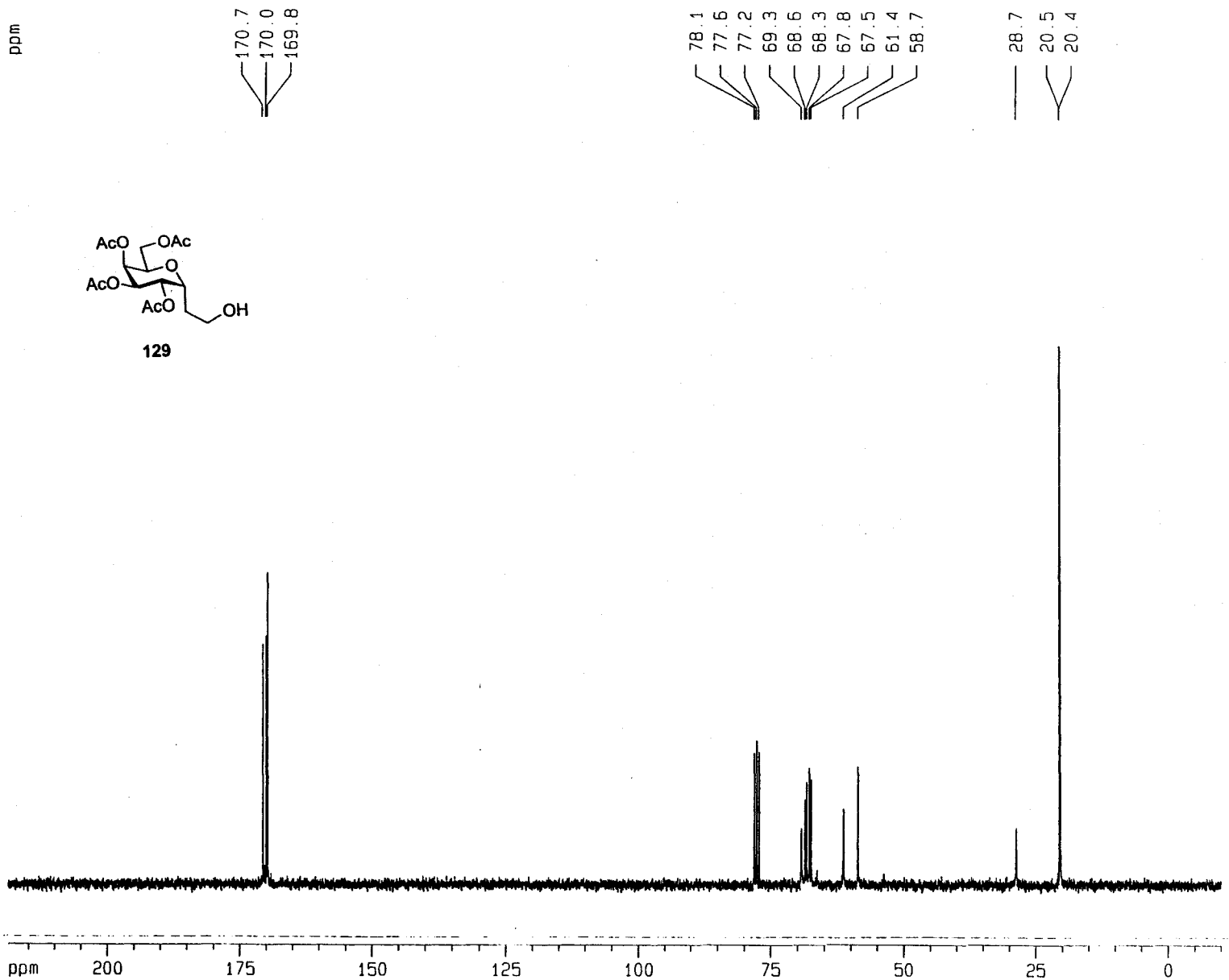

Current Data Parameters

NAME	rbsIgalOH_C
EXPNO	1
PROCNO	1

F2 - Acquisition Parameters

Date_	20060315
Time	13.30
INSTRUM	spect
PROBHD	5 mm QNP 1H/1
PULPROG	zgpg30
TD	32768
SOLVENT	CDCl3
NS	50
DS	0
SWH	17985.611 Hz
FIDRES	0.548877 Hz
AQ	0.9110004 sec
RG	9195.2
DW	27.800 usec
DE	6.00 usec
TE	300.0 K
D1	1.00000000 sec
d11	0.03000000 sec
d12	0.00002000 sec

======== CHANNEL f1 ========

NUC1	13C
P1	5.10 usec
PL1	-6.00 dB
SFO1	75.4752653 MHz

======== CHANNEL f2 ========

CPDPRG2	waltz16
NUC2	1H
PCPD2	73.00 usec
PL2	-3.00 dB
PL12	15.00 dB
PL13	120.00 dB
SFO2	300.1314860 MHz

F2 - Processing parameters

SI	65536
SF	75.4677348 MHz
WDW	EM
SSB	0
LB	1.00 Hz
GB	0
PC	1.40

1D NMR plot parameters

CX	20.00 cm
CY	8.79 cm
F1P	220.000 ppm
F1	16602.90 Hz
F2P	-10.000 ppm
F2	-754.68 Hz
PPMCM	11.50000 ppm/cm
HZCM	867.87897 Hz/cm

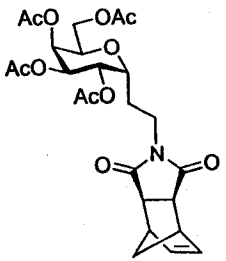

130


```
Current Data Parameters
NAME      rbs1130verynew
EXPNO                  1
PROCNO                 1

F2 - Acquisition Parameters
Date_           20060316
Time               19.10
INSTRUM            spect
PROBHD  5 mm QNP  1H/1
PULPROG            zg30
TD                30720
SOLVENT           CDCl3
NS                   32
DS                    0
SWH          5081.301 Hz
FIDRES       0.165407 Hz
AQ           3.0228980 sec
RG                45.3
DW           98.400 usec
DE            6.00 usec
TE             300.0 K
D1          1.00000000 sec

======== CHANNEL f1 ========
NUC1                  1H
P1           10.00 usec
PL1           -3.00 dB
SFO1     300.1319477 MHz

F2 - Processing parameters
SI                65536
SF     300.1300089 MHz
WDW                  EM
SSB                   0
LB            0.10 Hz
GB                    0
PC                 1.00

1D NMR plot parameters
CX              20.00 cm
CY              10.00 cm
F1P          10.000 ppm
F1           3001.30 Hz
F2P          -0.500 ppm
F2           -150.06 Hz
PPMCM        0.52500 ppm/cm
HZCM       157.56825 Hz/cm
```

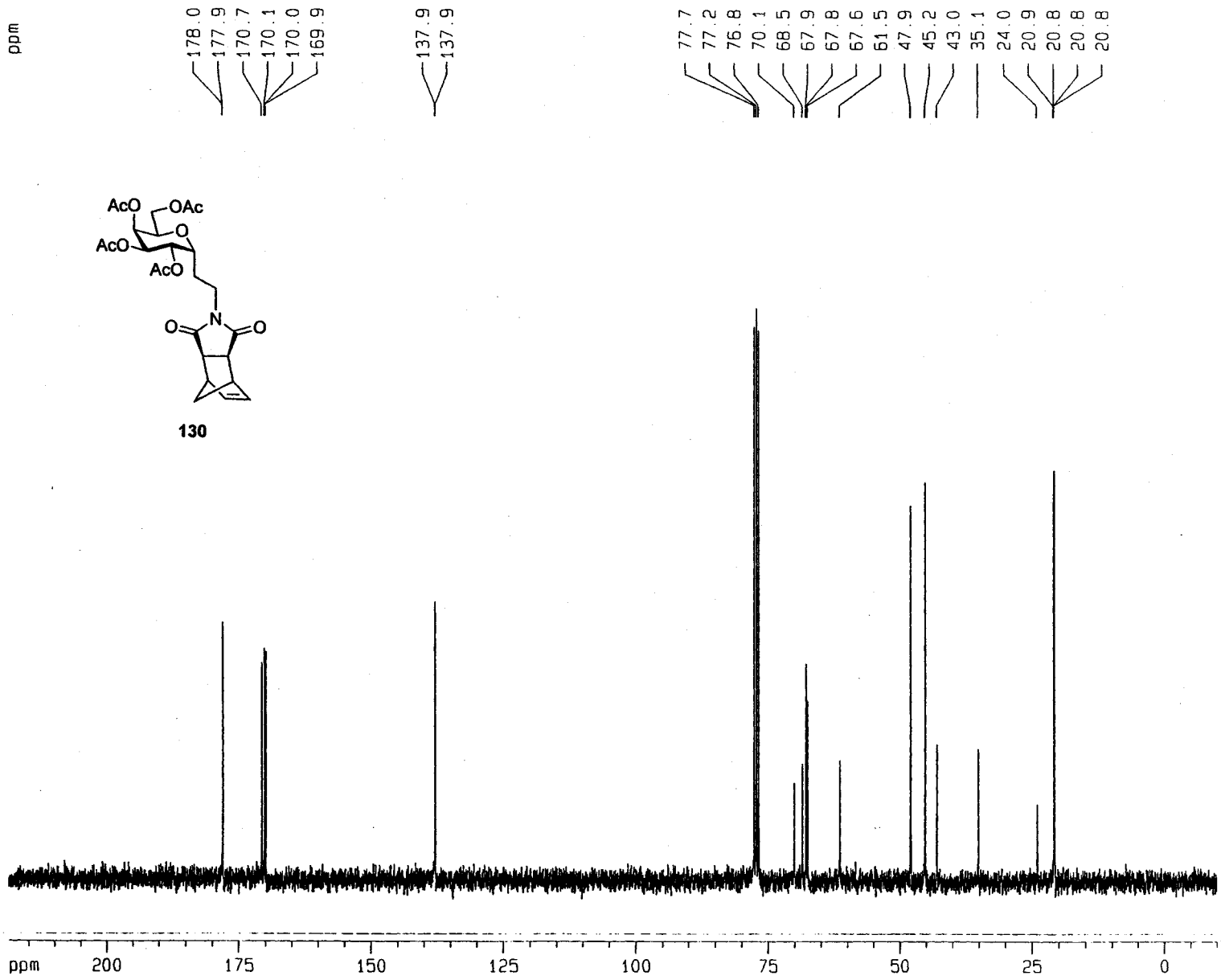

Current Data Parameters

NAME	rbs1130verynew
EXPNO	2
PROCNO	1

F2 - Acquisition Parameters

Date_	20060316
Time	19.13
INSTRUM	spect
PROBHD	5 mm QNP 1H/1
PULPROG	zgpg30
TD	32768
SOLVENT	CDCl3
NS	200
DS	0
SWH	17985.611 Hz
FIDRES	0.548877 Hz
AQ	0.9110004 sec
RG	3649.1
DW	27.800 usec
DE	6.00 usec
TE	300.0 K
D1	1.00000000 sec
d11	0.03000000 sec
d12	0.00002000 sec

======== CHANNEL f1 ========

NUC1	13C
P1	5.10 usec
PL1	-6.00 dB
SFO1	75.4752653 MHz

======== CHANNEL f2 ========

CPDPRG2	waltz16
NUC2	1H
PCPD2	73.00 usec
PL2	-3.00 dB
PL12	15.00 dB
PL13	120.00 dB
SFO2	300.1314860 MHz

F2 - Processing parameters

SI	65536
SF	75.4677406 MHz
WDW	EM
SSB	0
LB	1.00 Hz
GB	0
PC	1.40

1D NMR plot parameters

CX	20.00 cm
CY	9.37 cm
F1P	220.000 ppm
F1	16602.90 Hz
F2P	-10.000 ppm
F2	-754.68 Hz
PPMCM	11.50000 ppm/cm
HZCM	867.87903 Hz/cm

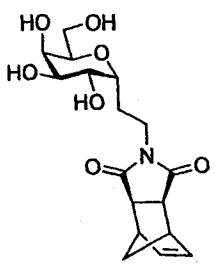

131

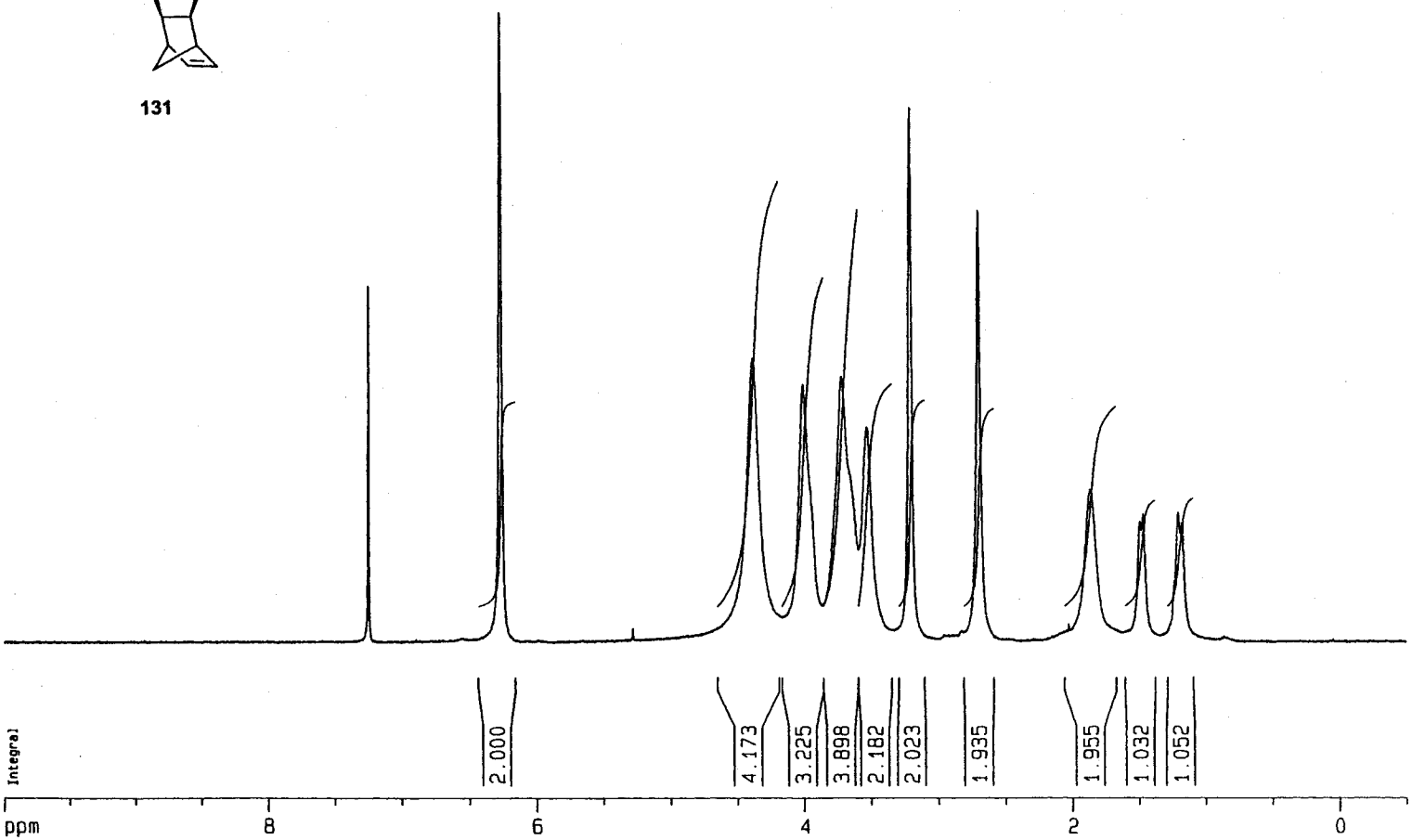


```
Current Data Parameters
NAME          irbslnew131
EXPNO                   1
PROCNO                  1

F2 - Acquisition Parameters
Date_           20060320
Time               10.16
INSTRUM            spect
PROBHD   5 mm QNP  1H/1
PULPROG            zg30
TD                30720
SOLVENT           CDCl3
NS                   16
DS                    0
SWH          5081.301 Hz
FIDRES       0.165407 Hz
AQ           3.0228980 sec
RG                203.2
DW             98.400 usec
DE              6.00 usec
TE             300.0 K
D1          1.00000000 sec

======== CHANNEL f1 ========
NUC1                  1H
P1             10.00 usec
PL1             -3.00 dB
SFO1       300.1319477 MHz

F2 - Processing parameters
SI                 65536
SF         300.1300091 MHz
WDW                   EM
SSB                    0
LB              0.10 Hz
GB                     0
PC                  1.00

1D NMR plot parameters
CX              20.00 cm
CY               8.91 cm
F1P            10.000 ppm
F1            3001.30 Hz
F2P            -0.500 ppm
F2            -150.06 Hz
PPMCM         0.52500 ppm/cm
HZCM        157.56825 Hz/cm
```

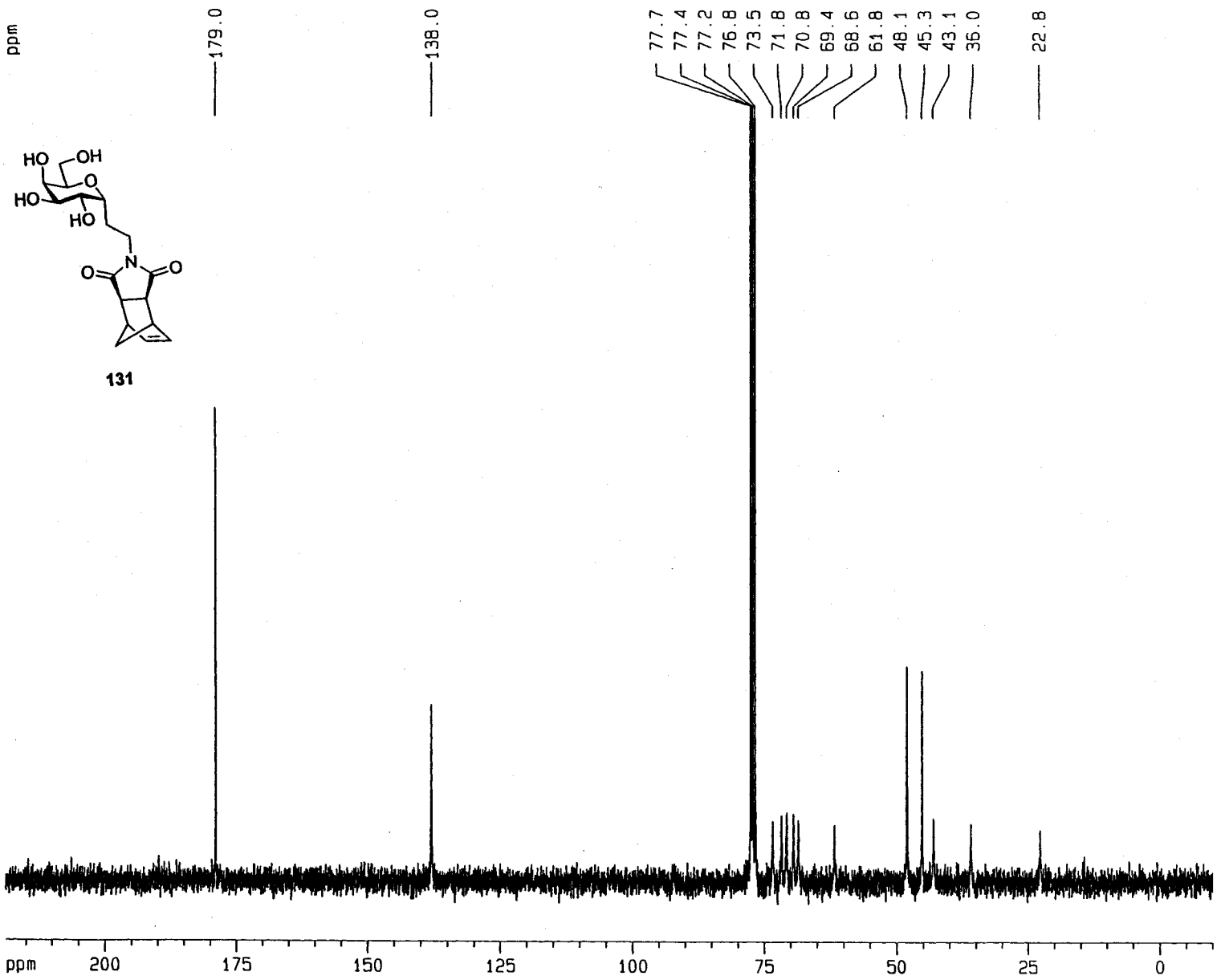

131

Current Data Parameters

NAME	rbs1131verynew
EXPNO	2
PROCNO	1

F2 - Acquisition Parameters

Date_	20060317
Time	14.18
INSTRUM	spect
PROBHD	5 mm QNP 1H/1
PULPROG	zgpg30
TD	32768
SOLVENT	CDCl3
NS	766
DS	0
SWH	17985.611 Hz
FIDRES	0.548877 Hz
AQ	0.9110004 sec
RG	3649.1
DW	27.800 usec
DE	6.00 usec
TE	300.0 K
D1	1.00000000 sec
d11	0.03000000 sec
d12	0.00002000 sec

======== CHANNEL f1 ========

NUC1	13C
P1	5.10 usec
PL1	-6.00 dB
SFO1	75.4752653 MHz

======== CHANNEL f2 ========

CPDPRG2	waltz16
NUC2	1H
PCPD2	73.00 usec
PL2	-3.00 dB
PL12	15.00 dB
PL13	120.00 dB
SFO2	300.1314860 MHz

F2 - Processing parameters

SI	65536
SF	75.4677362 MHz
WDW	EM
SSB	0
LB	1.00 Hz
GB	0
PC	1.40

1D NMR plot parameters

CX	20.00 cm
CY	24.38 cm
F1P	220.000 ppm
F1	16602.90 Hz
F2P	-10.000 ppm
F2	-754.68 Hz
PPMCM	11.50000 ppm/cm
HZCM	867.87897 Hz/cm